Development of novel bio-composite phase change material for passive design interventions in rural households for thermal management

A Thesis

Submitted in Partial Fulfilment of the Requirements for

The Award of the Degree of

DOCTOR OF PHILOSOPHY

By

Urbashi Bordoloi

(Registration number: 206154005)

School of Agro and Rural Technology

Indian Institute of Technology Guwahati

Guwahati-781039, India

July, 2026

DECLARATION

I hereby certify that the information presented in this thesis, entitled '***Development of novel bio-composite phase change material for passive design interventions in rural households for thermal management***', is entirely my own research performed under the supervision of Dr. Pankaj Kalita, Associate Professor, School of Energy Science and Engineering, Indian Institute of Technology Guwahati, India. Any part of this work has not been submitted earlier for the award of any degree, diploma, fellowship, or its equivalent to any University or Institution.

Date: 01.07.2026

Urbashi Bordoloi
Registration number: 206154005
School of Agro and Rural Technology
Indian Institute of Technology Guwahati, India

School of Agro and Rural Technology

INDIAN INSTITUTE OF TECHNOLOGY GUWAHATI

भारतीय प्रौद्योगिकी संस्थान गुवाहाटी, गुवाहाटी- 781039

CERTIFICATE

This is to certify that the work presented in the thesis entitled '***Development of novel bio-composite phase change material for passive design interventions in rural households for thermal management***' submitted by **Urbashi Bordoloi,** a student in the School of Agro and Rural Technology**,** Indian Institute of Technology Guwahati, India for the award of the degree of Doctor of Philosophy has been carried out under my supervision. She has fulfilled all the requirements according to the rules of the institute and the investigations embodied in his thesis have not been submitted previously elsewhere for the award of any other degree or diploma.

Date: 01.07.2026

Dr. Pankaj Kalita
Associate Professor
School of Energy Science and Engineering
Indian Institute of Technology Guwahati
Guwahati – 781039, India

Abstract

In recent times, there has been a shift from traditional vernacular houses to modern architecture in urban and rural areas. To maintain a comfortable thermal environment inside a modern building requires adequate active space heating and cooling systems. The continuously increasing demand for high-quality energy for space heating and cooling, coupled with the associated environmental emissions, necessitates the development and adoption of alternative and more sustainable solutions. In the case of rural areas, the availability and affordability of electricity for thermal management in buildings is another challenge for a country like India. In this regard, low-cost yet effective passive thermal management methods have significant potential to improve the indoor thermal environment and increase operational energy efficiency in the building sector. The present study focuses on developing an affordable material for building envelopes to passively reduce the energy demand for space cooling in hot and humid climates.

The use of organic phase change materials (PCM) in the building envelope can provide high thermal mass and thus can lower the temperature fluctuation inside the building. The leakage issue during phase transition in organic PCM is a critical challenge that requires attention. In the current study, porous biochar for providing shape stability to organic PCM (OM35) has been systematically explored by using three abundant biomasses. Sugarcane bagasse (SCB), water hyacinth (WH), yellow oleander (YO), and their binary and ternary blends have been pyrolyzed at a temperature of 550°C to produce biochar. The biochar has been mixed with OM35 through simple impregnation method for the preparation of seven different form-stable biocomposite PCMs. In addition to exhibiting substantially enhanced leakage resistance relative to pure OM35, the WH-PCM demonstrates a marked improvement in thermal transport properties, with its thermal conductivity increased by 50.5 %. The durability and dependability of the biocomposite PCMs have been studied after completing 500 thermal cycles. The negligible changes in physical, thermal, and chemical properties over the thermal cycles confirm that WH-PCM is a suitable option for use in building envelopes. Subsequently, 50 g of WH-PCM is then inserted into a 20 mm slot located at the center of a clay brick, commonly used in rural construction in India. A controlled study in a developed thermal chamber demonstrates that the WH-PCM-impregnated brick achieves a maximum temperature difference of 7.98 °C across its thickness compared to an identical red clay brick. Following the preliminary results, a (1m × 1m) wall section has been constructed using clay bricks incorporated with WH-PCM. Three wall configurations are studied by varying the placement of the WH-PCM layer in all four directions over one summer month in a hot and humid climate. The optimum results in terms of reduction in inside wall temperature and heat flux are found in the west direction when the WH-PCM layer is applied in the middle of the wall thickness. The maximum peak temperature reduction is found to be 4.66°C compared to the control wall, and the average reduction in daily heat flux is found to be 76%. The compressive strength analysis indicates that the modified brick falls under grade 7.5 of bricks, as per the IS 1077: 1992 standards. With the WH-PCM layer in its optimum position on the brick wall, an experimental cubicle has been constructed, and the interior temperature regulation profile has been studied. The study confirmed that WH-PCM-enhanced walls are beneficial in reducing the overall room temperature during peak summer hours, with a maximum temperature difference of 6°C compared to a reference room of identical dimensions. Based on directional analysis, the application of WH-PCM is recommended for the west and south walls for that particular climate. An Assam-type building is modelled with WH-PCM incorporated walls in the west and south directions for techno-economic analysis. The results showed that with WH-PCM integration, the annual cooling energy load has decreased by 31.5%. Considering the current unit electricity price in India, the PCM-integrated wall assembly achieved a simple payback period of approximately eight years, along with a positive net present value, indicating favourable long-term economic returns. Additionally, the life cycle analysis reveals that using WH-PCM on the south and west walls is environmentally beneficial compared to an identical building with conventional brick walls. PCM intervention in walls results in an approximate 30% reduction in global warming potential. The present study provides a comprehensive analysis and techno-economic comparison, offering critical insights into the optimal preparation of biochar-based PCMs and their cost-effective application in rural housing, as well as the most effective placement and orientation of PCM layers within brick walls to achieve indoor temperature reduction in hot and humid climates.

Acknowledgement

My PhD journey has been immensely enriching, though at times challenging, providing me with invaluable experience. I consider myself fortunate to have received the blessings of God and the unconditional support of numerous individuals throughout my doctoral tenure.

It is a genuine pleasure to express my deep sense of thanks and sincere gratitude to my supervisor, Dr Pankaj Kalita, for his active guidance, help and cooperation throughout my research journey. His systematic and continuous efforts are the main strength to complete my research in the limited time frame.

I would like to express my sincere and heartfelt gratitude to my doctoral committee members, Prof. Sashindra Kumar Kakoty, Prof. Sudip Mitra, and Dr. Ravi K, for their invaluable suggestions, insightful comments, and constructive guidance. Their support has not only shaped my research work in its present form but has also continuously motivated and encouraged me to strive for higher standards in my academic pursuits.

I express my sincere thanks to the Ministry of Education, Government of India, for their invaluable financial assistance for the smooth operation of the research via PMRF research grant. I am also thankful to my PMRF review committee members throughout the tenure for their constructive suggestions which significantly helped in improving the quality of my work.

I am extremely thankful and pay my gratitude to all my faculty members, School of Agro and Rural Technology, IIT Guwahati, for enlightening me with their valuable suggestions at various stages throughout my study period.

I am grateful to all the staff members and teaching assistants of Central Instrumentation Facility, IIT Guwahati and Guwahati Biotech Park for providing me the opportunity to carry out my experiments smoothly during my experimental duration.

I sincerely acknowledge and thank all staff of the School of Agro and Rural Technology and the School of Energy Science and Engineering, IIT Guwahati, for their constant support, cooperation, and assistance throughout my research.

In addition, I would like to thank the School of Agro and Rural Technology, IIT Guwahati, for providing access to the SimaPro software for conducting my LCA studies. In this regard, I would like to express my sincere gratitude to Dr. Dipankar Mandal and Mr. Akash Keot for their valuable assistance during my research work.

I am also extremely thankful to Mr. Kamal Das, Mr. Pankesh Das, Mr. Dipankar Kalita, and Mr. Dharmendra Das for their continuous help during the experimental period. Without their support, I would not have been able to complete this work independently.

I am extremely grateful to Dr. Dudul Das for always being there for me, whenever and wherever I needed guidance and support. His valuable advice and cordial attitude are

the pillars of my inspiration to accomplish my research. I owe my deep sense of gratitude to Dr. Harrison Hihu Muigai, Dr. Samar Das, Dr. Rabindra Kangsha Banik, Dr. Shayaram Basumatary, and Dr. Hirakh Jyoti Das for their unwavering support, ideas and enthusiasm which shapes my present research work. It is my privilege to express my heartfelt gratitude to Mr. Akash Dilip Kamble and Mr. Biraj Das for their constant motivation and genuine encouragement in every possible way throughout my research journey. I would like to take this opportunity to express my sincere thanks to Mr. Bitupan Das for his timely assistance, and encouragement, which greatly facilitated the progress of my research work.

It is my privilege to express my sincere thanks to Ms. Puja Hazarika, Mrs. Priyanka Duarah, Mrs. Vijaya, Dr. Pushpendra Singh, Mr. Mrinmoy Kumar Sarmah, Mr. Manash Jyoti Das, Mr. Debarshi Baruah, Dr. Mebratu Adamu Assegie , Dr. Vikas Thakur, Dr. Deepak Patwa, and Dr. Lepakshi Barbora who constantly motivated and supported me in all ways possible to carry out my work. I also deeply acknowledge Dr. Pranay Kumar Sarkar, Mr. Pankaj Kumar, Ms. Jyoti, Ms. Akshini Anil More, Mr. Abhishek Kumar, Mr. Subham Nath Laskar, Mr. Debangsu Kashyap, Ms. Sudipta Bijoy Sarmah, Mr. Dushyanta Madhav Sharma, Mr. Hirak Basumatary, Mr. Agniprabha Roy, Mr. Monikesh Kakoty, Mr. Shivam Srivastava, Mr. Saurov Choudhury, Mr. Kunuthuru Sivakumar, Mr. Shivam Raj, and Mr. Gaurav Sarmah for their kindness and goodwill in all aspects of my research.

I am thankful to the team of 'Bohagor Duwardolit' for actively involving me in various extra-curricular activities, which helped keep my mind refreshed and provided a welcome balance during my research journey.

Lastly, my research journey would not have been possible without the unwavering support of my dear husband, Mr. Mukunda Madhab Khanikar, who patiently stood by me through moments of self-doubt and emotional challenges throughout this journey. I would like to express my deepest gratitude to my parents, who are my strongest source of strength and encouragement though all stages of my life. Their strong belief in me, unconditional love, and endless sacrifices have shaped not only my academic journey but also the person I am today. I am profoundly grateful to my in-laws, who warmly welcomed me into their family in the midst of my research journey and have provided unwavering support in every possible way. I would like to acknowledge with a great sense of reverence, my gratitude towards all my family members, all my respected seniors and dear friends who always supported me morally.

Finally, my gratitude goes to all who directly or indirectly became a source of support and inspiration for me to accomplish my research successfully.

Urbashi Bordoloi

Contents

Abstract **i**

Acknowledgement **iii**

Contents **v**

Nomenclature **ix**

List of Figures **xiv**

List of Tables **xvii**

Chapter 1 ***Introduction*** **1**

1.1 Motivation *2*

1.2 Latent heat thermal energy storage (LHTES) *4*

1.3 Phase change material(PCM) *4*
1.3.1 Types of PCM 5

1.4 Improvement in organic PCMs *8*
1.4.1 Encapsulation technologies 9

1.5 PCM for building thermal management *12*
1.5.1 Active methods 12
1.5.2 Passive methods 13

1.6 Objectives of the present work *14*

1.7 Organization of thesis *15*

1.8 Summary of the chapter *15*

Chapter 2 ***Literature Review*** **16**

2.1 Introduction *17*

2.2 Form-stable PCM *18*
2.2.1 Bio-based PCM 21

2.3 Thermal cycling stability of PCM *24*

2.4 PCM for building thermal management *25*

2.5 PCM on building envelopes *29*
2.5.1 PCM on the roof and ceiling of buildings 30
2.5.2 PCM on the windows/facade of a building 34
2.5.3 PCM on walls 35

2.6 Techno-economic and environmental assessment analysis *52*
2.6.1 Economic parameters and Carbon emission 52

2.6.2 LCA study 57

2.7 Summary of literature review 59

2.8 Research gaps 60

2.9 Thesis objectives 61

2.10 Summary of the chapter 61

Chapter 3 *Development and characterization of biocomposite PCM* 62

3.1 Introduction 63

3.2 Materials and method for developing biocomposite PCM 63

3.3 Characterization of the biocomposite PCM 64

3.3.1 Leakage test 64

3.3.2 Characterization techniques 65

3.4 Experimental investigation of thermal cycling stability of biocomposite PCMs 66

3.4.1 Development of thermal cycling experimental set-up 66

3.4.2 Thermal cycling test method 68

3.4.3 Characterization of the selected biocomposite PCMs after thermal cycling 68

3.5 Results and discussion on characterization of biocomposite PCM 69

3.5.1 Leakage test results 69

3.5.2 Physical property analysis 71

3.5.3 Morphology and porosity analysis 72

3.5.4 Chemical property analysis 76

3.5.5 Thermal properties (TGA, DTG, DSC and Thermal Conductivity) 81

3.6 Results and Discussion on thermal cycling stability of biocomposite PCM 87

3.6.1 Change in physical appearance 87

3.6.2 Leakage test result after thermal cycling 88

3.6.3 Surface morphology analysis after thermal cycling 90

3.6.4 XRD analysis after thermal cycling 91

3.6.5 FTIR result after thermal cycling 92

3.6.6 DSC result after thermal cycling 93

3.7 Summary of the chapter 96

Chapter 4 *Development and thermal performance analysis of PCM-impregnated brick walls* 97

4.1 Introduction 98

4.2 Development of WH-PCM impregnated walls 98

4.2.1 Development of WH-PCM incorporated bricks for indoor experiment 99

4.2.2 Indoor experimental set-up 100

4.2.3 Outdoor experimental set-up 101

4.2.4 Quality testing of the modified bricks 104

4.2.5 Development of experimental cubicles 105

4.2.6 Experimental design for the thermal performance study 107

4.3 Results and discussion on comparison of the temperature profile in the thermal chamber 108
4.3.1 Autoclaved aerated concrete (AAC) brick 108
4.3.2 PCM-clay brick_1 109
4.3.3 PCM-clay brick_2 109

4.4 Thermal performance test results in outdoor conditions 110
4.4.1 Calibration test 110
4.4.2 Outdoor test results 111
4.4.3 Comparison of peak temperature 119
4.4.4 Thermal amplitude comparison 122
4.4.5 Comparison of the heat flux profiles 123

4.5 Comparison of the quality of normal brick and PCM-incorporated brick 126

4.6 Thermal performance analysis of experimental cubicle 127
4.6.1 Solar irradiance and ambient temperature 127
4.6.2 Comparison of the temperature profile of the experimental cubicles 128
4.6.3 Comparison of the wall-wise temperature profile of the experimental cubicles 130

4.7 Summary of the chapter 133

Chapter 5 *Techno-Economic and Life Cycle Analysis of biocomposite PCM-incorporated building* 135

5.1 Introduction 136

5.2 Numerical Study on the Energy Saving Potential of WH-PCM Walls 136
5.2.1 Climatic background 136
5.2.2 Building Model Description 136
5.2.3 Mathematical formulation 138

5.3 Validation of numerical investigation with experimental study 143

5.4 Energy performance evaluation of the reference and PCM buildings 144

5.5 Economic analysis 145
5.5.1 Static/simple payback period (SPP) 146
5.5.2 Dynamic/discounted payback period (DPP) 146
5.5.3 Net Present Value (NPV) 147

5.6 Life cycle assessment (LCA) 149
5.6.1 Goal and scope definition 149
5.6.2 Life cycle inventory (LCI) 150
5.6.3 Life cycle impact assessment and interpretation 152
5.6.4 Global warming potential (GWP) 154
5.6.5 Cumulative energy and exergy demand 155
5.6.6 ReCiPe 2016 midpoint 156
5.6.7 ReCiPe 2016 endpoint 157
5.6.8 Embodied and operational impact 158

5.7 Summary of the chapter 159

Chapter 6 ***Conclusions and scope for future research*** **160**

6.1 Conclusions and key findings *161*

6.2 Scope for future research *163*

References **165**

Appendix I **186**

List of publications **188**

Nomenclature

Abbreviations

AAC	:	Autoclaved aerated concrete
BET	:	Brunauer-Emmett-Teller
B_1_SW	:	Binary mixture of sugarcane bagasse and water hyacinth
B_2_SY	:	Binary mixture of sugarcane bagasse and yellow oleander
B_3_WY	:	Binary mixture of water hyacinth and yellow oleander
CED	:	Cumulative energy demand
CED_X	:	Cumulative exergy demand
CondFD	:	Conduction Finite Difference Method
DPP	:	Dynamic payback period
DSC	:	Differential scanning calorimetry
DTG	:	Derivative Thermogravimetry
ER	:	Encapsulation ratio
EE	:	Encapsulation efficiency
EC	:	Energy consumption
ECR	:	Energy consumption ratio
FESEM	:	Field emission scanning electron microscopy
FTIR	:	Fourier transformation infrared spectroscopy
GLO	:	Global
GWP	:	Global warming potential
IN	:	India
IPCC	:	International Panel of Climate Change
LCA	:	Life cycle assessment
LCC	:	Life cycle cost
LCI	:	Life cycle inventory
LHTES	:	Latent heat thermal energy storage
NPV	:	Net present value
PCM	:	Phase change material
mPCM	:	Microencapsulated phase change material
MOF	:	Metal organic framework
ROW	:	Rest of world

SCB	:	Sugarcane bagasse
SPP	:	Static payback period
TGA	:	Thermo gravimetric analysis
T_0_SWY	:	Ternary mixture of sugarcane bagasse, water hyacinth and yellow oleander
WH	:	Water hyacinth
XRD	:	X-ray diffractometer
YO	:	Yellow oleander

Notations

A	:	Average net area of the specimen (mm^2)
A_s	:	Area, considering the surface area of the wall and roof (m^2)
c	:	Spatial discretization constant
C_p	:	Specific heat at constant pressure (J/kgK)
C_{ps}	:	Specific heat capacities of the solid state (J/kgK)
C_{pl}	:	Specific heat capacities of the liquid state (J/kgK)
C_1	:	Cost of PCM (USD/kg)
C_2	:	Installation cost of PCM (USD/m^2)
C_r	:	CO_2 emission factor of the carrier
CES	:	Carbon emission savings (kgCO_{2e}/year)
CI	:	Carbon intensity of electricity generation (kg CO_{2e}/kWh)
C_{PCM}	:	Initial cost (INR)
d	:	Discount rate (%)
D	:	Crystallite size (nm)
E	:	Contribution to energy savings by a particular fuel source (kWh)
E_{co}	:	Energy cost (USD)
EF_{el}	:	Electricity emission CO_2 factor
$ES(PCM)$	:	Energy savings obtained from PCM incorporation (kWh)
E_c	:	CO_2 emission during annual cooling energy consumption
$E_{ds,trans}$	:	CO_2 emissions during the transportation stage
$E_{dis,pro}$	:	CO_2 emission during the disposal stage

$E_{dis,tg}$	:	CO_2 emission during the recycling stage
F_0	:	Fourier number
f	:	Melting fraction of PCM (%)
G	:	Operating load capacity of the hoist
h	:	Heat transfer coefficient (W/m^{2}K)
H	:	Enthalpy of PCM (kJ/kg)
H_c	:	Capillary height inside a pore (m)
H_B	:	Building height (m)
ΔH_m	:	Latent heat of fusion of PCM (kJ/kg)
ΔH_s	:	Latent heat of solidification of PCM (kJ/kg)
$\Delta H_m^{Theoritical}$	:	Theoretical enthalpy of biocomposite PCM ((kJ/kg)
$\Delta H_{m,PCM}$	:	Measured enthalpy of PCM (kJ/kg)
i_t	:	Time value of money
I	:	Modified discount rate (%)
i	:	Node that is being modelled
$i+1$	:	Adjacent node to the interior of the construction
$i-1$	:	Adjacent node to the exterior of the construction
j	:	Previous time step (s)
$j+1$	:	New time step (s)
k	:	Thermal conductivity (W/mK)
K	:	Scherrer constant
L_e	:	Transport distance (km)
m	:	Mass of the thermal energy storage material (kg)
m_d	:	Dry weight of brick (kg)
m_w	:	Weight of the wet bricks (kg)
M_t	:	Weight of PCM (kg)
M_c	:	Weight of PCM lifted by hoist (kg)
M_1	:	Initial mass of the biocomposite PCM on filter paper (g)
M_2	:	Final mass of the biocomposite PCM on filter paper after 30 minutes (g)
N	:	Life span of the building (years)

n	:	Number of thermocouples
OM	:	Operation and maintenance cost (USD)
P_{max}	:	Maximum compressive load (N)
Q_c	:	Cooling energy demand (kWh)
r	:	Annual inflation in electricity tariff (%)
R_p	:	Radius of the porous matrix (m)
RP	:	Relative proportion of a particular fuel source (%),
R	:	Thermal resistance (K/W)
S	:	Annual savings (INR/year)
t	:	Time (s)
Δt	:	Time step (s)
T_m	:	Melting temperature of PCM (°C)
T_f	:	Freezing temperature of PCM (°C)
T_{peak}	:	Maximum inside surface temperature of the wall (°C)
T_{min}	:	Minimum inside surface temperature of the wall (°C)
T_0	:	Initial temperature in the solid state of PCM (°C)
T_s	:	Phase-change temperature in the solid state (°C)
T_l	:	Phase-change temperature in the liquid state (°C)
T_f	:	Final temperature in the liquid state of PCM (°C)
T_{sky}	:	Sky temperature (°C)
ΔT	:	Temperature range over which phase change occurs (°C)
ΔT_s	:	Degree of supercooling (°C)
T_i^j	:	Temperature of the node i at time j (K)
u	:	Accuracy of each thermocouple (°C)
$U_{overall}$	:	Overall heat transfer coefficient (W/m^{2}K)
V	:	Volume (m^3/kg)
v	:	Lifting speed of the hoist during PCM installation
x	:	Element thickness (mm)
Δx	:	Finite difference layer thickness (mm)

Greek symbols

α	:	Thermal diffusivity (m^2/s)
β	:	Full width at half maximum (FWHM) of the XRD peak (radians)

ε	:	Surface emissivity
θ_c	:	Contact angle made by the liquid melted PCM with the surface of microspores of the supporting matrix (radians)
λ	:	Wavelength of the X-ray (Å)
θ	:	Bragg angle (º)
ρ	:	Density of PCM (kg/m^3)
σ	:	Stefan–Boltzmann constant (W/m^{2}K^4)
σ_s	:	Surface tension between PCM and encapsulating media (N/m)
ϕ	:	Weight fraction of supporting material
$\phi_{leakage}$	:	Leakage during phase transition of PCM (%)

List of Figures

Fig. 1.1 PCM phase change transition [16] 4
Fig. 1.2 Classification of PCM [17] 6
Fig. 1.3 Melting temperature and enthalpy comparison of different solid-liquid PCM [23] 7
Fig. 1.4 Microencapsulated PCM [23] 9
Fig. 1.5 Microencapsulated PCM [23] 10
Fig. 1.6 Preparation method of shape-stabilized PCM [23] 11
Fig. 1.7 Schematic of a typical active PCM storage tank for building 13
Fig. 1.8 Passive application of PCM in buildings [40] 14
Fig. 2.1 Form stable material preparation method via vacuum impregnation method [51] 19
Fig. 2.2 Diatomite-vermiculite form-stable PCM [58] 20
Fig. 2.3 Steps of biochar-PCM composite preparation [46] 23
Fig. 2.4 (a) Variation of thermal mass according to the thickness of construction materials[80] (b) Energy storage capacity of different materials [81] 26
Fig. 2.5 (a) Test rooms,(b) Indoor temperature profile [88] 27
Fig. 2.6 Schematic view of the proposed models [98] 30
Fig. 2.7 Schematic view of the proposed models [98] 33
Fig. 2.8 PCMs integration measures in windows [119] 34
Fig. 2.9 The working principle of concrete walls incorporating PCMs [132] 37
Fig. 2.10 Six different PCM configuration on burnt clay brick [147] 39
Fig. 2.11 Preparation of PCM concrete bricks 40
Fig. 2.12 Key parameters affecting the economic assessment [191,192] 52
Fig. 2.13 Key parameters affecting the environmental assessment [191,192] 53
Fig. 2.14 Four stages of LCA study [203,204] 57
Fig. 3.1 Methodology for biocomposite preparation 64
Fig. 3.2 Developed thermal cycling chamber 66
Fig. 3.3 Temperature variation inside the chamber w.r.t. time during heating mode 67
Fig. 3.4 Temperature variation inside the chamber w.r.t to time during cooling mode 67
Fig. 3.5 Schematic of thermal cycling test 68
Fig. 3.6 Extent of leakage of the different compositions (a) 4:6 mix, (b) 5:5 mix, (c) 6:4 mix, (d) 7:3 mix, (e) 8:2 mix, (f) 9:1 mix, (g) OM 35 70
Fig. 3.7 The percentage mass loss of different compositions during the leakage test 71
Fig. 3.8 Nitrogen adsorption-desorption isotherms for seven biochars 72
Fig. 3.9 FESEM images of different biochar and their respective composite PCMs, (a) SCB, (b)SCB-PCM, (c)WH, (d) WH-PCM,(e) YO, (f) YO-PCM, (g) B_1_SW, (h) B_1_SW -PCM, (i) B_2_SY, (j) B_2_SY-PCM, (k) B_3_WY, (l) B_3_WY-PCM, (m) T_0_SWY, (n) T_0_SWY -PCM 75

Fig. 3.10 FTIR characteristics curves of biocomposite PCMs, (a) SCB and SCB-PCM, (b) WH and WH-PCM, (c) YO and YO-PCM, (d) B_1_SW and B_1_SW-PCM, (e) B_2_SY and B_2_SY-PCM, (f)B_3_WY and B_3_WY-PCM, (g) T_0_SWY and T_0_SWY-PCM 79

Fig. 3.11 XRD curves of biocomposite PCMs, (a) SCB and SCB-PCM, (b) WH and WH-PCM, (c) YO and YO-PCM, (d) B_1_SW and B_1_SW-PCM, (e) B_2_SY and B_2_SY-PCM, (f)B_3_WY and B_3_WY-PCM, (g) T_0_SWY and T_0_SWY-PCM 80

Fig. 3.12 TGA comparison graphs for OM35 and developed biocomposite PCMs 82

Fig. 3.13 DTG graphs for OM35 and developed biocomposite PCMs 82

Fig. 3.14 DSC curves of different biocomposite PCM 83

Fig. 3.15 Thermal conductivity comparison of PCM (OM 35), SCB-PCM, B_1_SW-PCM, WH-PCM and T_0_SWY PCM 87

Fig. 3.16 Images of PCMs before and after thermal cycling test, (a) OM 35_0 (solid), (b) OM35_200 (solid), (c) OM 35_0 (liquid), (d) OM 35_200 (liquid), (e) WH-PCM_0, (f) WH-PCM_200, (g) T_0-SWY PCM_0, (h) T_0-SWY PCM_200 87

Fig. 3.17 Leakage test on filter paper 88

Fig. 3.18 Comparison of the mass loss of the PCMs during the leakage test 89

Fig. 3.19 FESEM images of (a) WH-PCM_0, (b) WH-PCM_200, (c) T_0_SWY-PCM_0, (d) T_0_SWY-PCM_200, (e) WH-PCM_500, (f) T_0_SWY-PCM_500 90

Fig. 3.20 XRD images of samples of (a) OM35, (b) WH-PCM, (c) T_0_SWY-PCM 91

Fig. 3.21 FTIR graphs of cycled and uncycled PCMs (a) OM35, (b) WH-PCM, (c) T_0_SWY-PCM 93

Fig. 3.22 DSC graph of biocomposite PCMs before and after cycling, (a) W-PCM, (b) T_0_SWY-PCM 94

Fig. 4.1 Methodology of the study of WH-PCM incorporated bricks 98

Fig. 4.2 Preparation of WH-PCM incorporated brick 99

Fig. 4.3 Design of thermal performance test on the single brick in the controlled chamber 100

Fig. 4.4 (a) WH-PCM brick preparation for Case II, (b) WH-PCM brick preparation for Case I and Case III 102

Fig. 4.5 (a) Wall construction on pre-fabricated cast iron frame (Case 0), (b) WH-PCM brick wall construction, (c) Thermocouple and heat flux sensor position on each wall 104

Fig. 4.6 Preparation of clay brick with WH-PCM slot 105

Fig. 4.7 Development of prototype buildings (a) Frame for reference cubicle, (b) Frame for PCM cubicle, (c) Sliding rail provision for PCM cubicle, (d) Interior of the developed PCM cubicle, (e) Reference cubicle outer view, (f) PCM cubicle outer view 106

Fig. 4.8 Experimental cubicle with heat generation unit 107

Fig. 4.9 Temperature profile of different reference and PCM bricks inside the thermal chamber (a) PCM-AAC brick, (b) PCM-clay brick_1, (c) PCM-clay brick_2 108

Fig. 4.10 Calibration test results (a) Exterior surface temperature, (b) Interior surface temperature, (c) Interior heat flux 111

Fig. 4.11 Ambient temperature profile for the experimental period 112

Fig. 4.12 Solar irradiance profile for the experimental period 112

Fig. 4.13 Temperature profile in the east direction (a) Case I, (b) Case II, (c) Case III 113

Fig. 4.14 Temperature profile in the north direction (a) Case I, (b) Case II, (c) Case III 115

Fig. 4.15 Temperature profile in the south direction (a) Case I, (b) Case II, (c) Case III 116

Fig. 4.16 Temperature profile in the west direction (a) Case I, (b) Case II, (c) Case III 117

Fig. 4.17 The thermal resistance and heat flow analysis through WH-PCM walls 120

Fig. 4.18 Heat flux analysis through WH-PCM and reference wall, (a) West wall_Case III, (b) East wall_Case I, (c) North wall_Case II, (d) South wall_Case III, (e) West wall_Case II, (f) North wall_Case I 124

Fig. 4.19 Comparison of quality testing of WH-PCM clay bricks (a) dry density, (b) water absorption test, (c) compressive strength test, (d) efflorescence test of WH-PCM bricks 126

Fig. 4.20 Solar irradiance and temperature profile (a) for the period 8.10.2024 to 8.11.2024, (b) for the period 8.11.2024 to 14.11.2024 128

Fig. 4.21 The interior temperature of both rooms without any applied thermal load 128

Fig. 4.22 The interior temperature of both rooms with applied internal thermal load 130

Fig. 4.23 Interior temperature (a) WH-PCM incorporated walls inside temperature, (b) reference and WH-PCM wall in the south direction, (c) reference and WH-PCM wall in the west direction 131

Fig. 4.24 Interior temperature with internal thermal load (a) WH-PCM walls, (b) reference and WH-PCM wall on south direction, (c) reference and WH-PCM wall on west direction 133

Fig. 5.1 (a) Building model, (b) WH-PCM position on wall, (c) Sun path diagram for the building model, (d) Detailed floor plan of the building model 137

Fig. 5.2 Node depiction for the condFD model [292] 139

Fig. 5.3 Building model for validation, (a) Numerical model, (b) Experimental set-up 143

Fig. 5.4 Validation between experimental and numerical analysis 144

Fig. 5.5 Comparison of annual cooling energy and energy per total building area 145

Fig. 5.6 Comparison of the building sensible cooling load and peak cooling load 145

Fig. 5.7 GWP 20 comparison 155

Fig. 5.8 GWP 100 comparison 155

Fig. 5.9 Cumulative energy and exergy demand (single score) 156

Fig. 5.10 ReCiPe 2016 midpoint categories (with normalization) 157

Fig. 5.11 ReCiPe method midpoint and endpoint categories relation 157

Fig. 5.12 ReCiPe 2016 endpoint categories (single score) 158

Fig. 5.13 Embodied and operational impacts comparison of ReCiPe 2016 endpoint (single score) 159

List of Tables

Table 1.1 Desirable properties of PCM for thermal energy storage 5
Table 1.2 Systematic comparison and applications of different PCMs 8
Table 2.1 Summary of literature review on PCM integration in bricks 43
Table 2.2 Effect of PCM position and thickness on thermal performance of building wall 48
Table 2.3 Main economic parameters involved in PCM usage in buildings 54
Table 2.4 Carbon emission analysis through different stages 55
Table 3.1 Design parameters for thermal cycling chamber 66
Table 3.2 Comparison of the developed and commercial thermal cycling chambers 67
Table 3.3 Accuracy of major testing instruments 69
Table 3.4 The bulk density of the biochar and their respective biocomposite PCMs 71
Table 3.5 BET analysis and comparison of different encapsulation materials 73
Table 3.6 Visible wavelengths and their respective functional groups 77
Table 3.7 Melting point, heat of fusion and specific heat comparison for biocomposite PCM 84
Table 3.8 Average specific heat capacity of the biocomposite PCM 85
Table 3.9 The thermal conductivities of the biochar 86
Table 3.10 Comparison of Crystallite size of OM35 and biocomposite PCMs 92
Table 3.11 DSC results of the uncycled and cycled biocomposite PCMs 94
Table 3.12 Comparison of DSC results with previous studies 95
Table 4.1 Properties of the selected brick [266] 99
Table 4.2 Mean surface temperature and standard deviation for PCM-clay brick_1 101
Table 4.3 Mean surface temperature and standard deviation for PCM-clay brick_2 101
Table 4.4 Matrix of Experimental Conditions for Outdoor Testing 103
Table 4.5 Temperature variation across different experimental period 113
Table 4.6 Comparison of peak temperature reduction 119
Table 4.7 Peak temperature reduction comparison with earlier works 121
Table 4.8 Thermal amplitude values for different directions and WH-PCM positions 122
Table 4.9 Comparison of the present work with published literature 129
Table 5.1 Thermo-physical properties of the construction materials 137
Table 5.2 Properties of WH-PCM 138
Table 5.3 Input parameters for the building model used in the simulation 141
Table 5.4 SPP and DPP values for PCM-integrated buildings under 148
Table 5.5 LCI for 1m^2 normal wall 151
Table 5.6 LCI for 1m^2 WH-PCM wall 151
Table 5.7 LCI for 1 kg of WH-PCM brick manufacturing 151

Table 5.8 LCI for 1 kg of WH-PCM production 151
Table 5.9 LCI for 1 kg of biochar production 152
Table 5.10 Waste disposal mythology of the construction materials 152
Table 5.11 Impact categories description 153

Chapter 1
Introduction

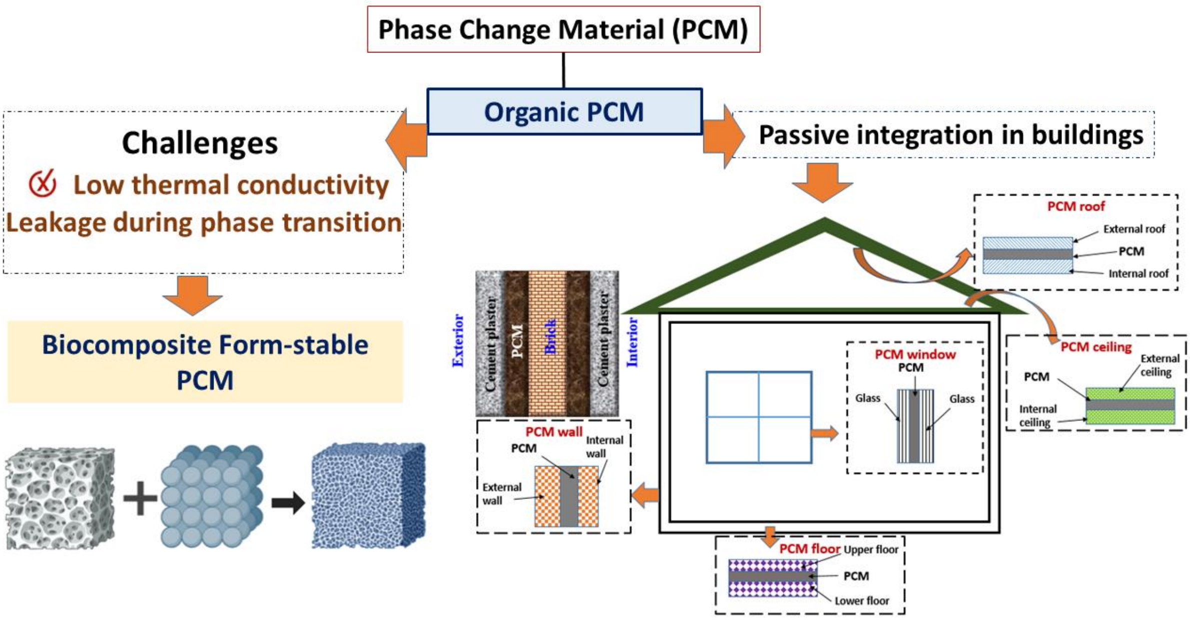

1.1 Motivation
1.2 Latent heat thermal energy storage (LHTES)
1.3 Phase change material (PCM)
1.4 Improvement in organic PCMs
1.5 PCM for building thermal management
1.6 Objectives of the present work
1.7 Organization of thesis
1.8 Summary of the chapter

Outline

1.1 Motivation

The current decade witnesses an exponential rise in global energy demand in the modern building sector. The escalation in heat waves globally, both in frequency and intensity, necessitates longer periods of cooling each day. Space cooling, essential for maintaining indoor thermal comfort amid record-high temperatures, places a growing strain on global electricity demand [1]. It was reported that active space cooling and air conditioning systems consume approximately 16% of the final electricity of the building sector and contribute 3.94% of global greenhouse gas emissions [2]. Despite the fact that this upward trend is essential for human thermal comfort and health, the world is on the verge of a "cold crunch" because of the excessive use of air conditioning systems. In this era of growing energy demand, it is extremely important to focus on energy-efficient solutions for building operations. Effective and sustainable interventions in buildings to meet cooling demand can reduce global energy demand by 12% [3].

China has been leading the growth in energy consumption in the buildings sector, with a yearly rise of 4.8% between 2010 and 2022, followed by India at 1.9% per year [4]. A study on the trend of construction shows that 80% of rural and 97% of urban houses are made of modern construction materials in India by 2018, which fail to provide indoor thermal comfort compared to vernacular buildings [5]. The residential floor area in India is expected to grow more than double in the coming decades, and as a result, space cooling alone is projected to account for nearly 45% of the peak electricity demand by 2050 [6]. Additionally, considering India's climatic zones, the heating requirement for attaining thermal comfort is limited in the country; rather, space cooling is the major demand for human health, well-being, and productivity. Despite having extremely high cooling needs, only 4% of Indian households possessed an air conditioning system by 2016, as people could not afford the high cost related to the procurement and operational costs of the system [2]. Notably, at the global stage, approximately 5 billion households have a substantial requirement for space cooling, yet only one-third of them currently possess an air conditioner [7]. Thus, the world, including India at large, is looking for sustainable and affordable solutions for building cooling demand. Such cooling demand can be attenuated by the implementation of energy-efficient building appliances and thermally efficient building design. Indian Cooling Action Plan (ICAP 2019) has recommended thermal comfort strategies for affordable housing projects under the Eco Niwas Samhita for residential buildings [8]. Integration of passive cooling and efficient envelope strategies can cut future cooling energy use by 20–30% in India. It is estimated that with each 1°C drop in air temperature, the peak cooling demand would be lowered by 2–4% [6].

Passive buildings aim to provide indoor thermal comfort by managing temperature and humidity through efficient design, advanced envelope materials, and balanced ventilation by adhering to the local climatic conditions with minimal utilization of grid-connected electricity [9]. The building envelope serves as a critical mediator of heat transfer between outdoor and indoor environments due to the temperature difference between the indoor and ambient temperatures, reported as more than 60% of total building thermal loads, significantly influencing heating and cooling loads [10]. Enhancing the building envelope with advanced materials through retrofitting and modifications provides an effective means of creating a favorable thermal environment indoors without the need for active energy consumption. Incorporating phase change material (PCM) into the building envelope can serve as a passive cooling strategy by enhancing the thermal mass and thereby modulating heat flow. PCM has been gaining attention in building science because of its characteristics like high heat of fusion, constant operating temperature, high energy density, high durability, corrosion resistance, and non-toxicity [11,12]. If PCM is incorporated into a building system, it can increase thermal comfort, improve building thermal envelope performance and system efficiency, reduce peak power consumption and contribute to the reduction of CO_2 emissions [13]. Besides having the aforementioned favorable characteristics, leakage of liquid PCM, low thermal conductivity and cost remain as challenges [14].

The present study has focused on developing biocomposite PCMs by blending porous biochar with suitable organic PCMs through the simple impregnation method. This biocomposite PCM ensures higher thermal conductivity and shape stability during phase transition than ordinary PCM. The issue of high cost with PCM is also compensated for by the novel PCM, as the raw material is derived from the locally available biomass from rural areas. The biocomposite PCM is incorporated into traditional clay bricks commonly used in rural Indian construction. These enhanced bricks are then assembled to form building walls of an experimental cubicle, enabling improved thermal performance. Walls incorporating biocomposite PCM effectively reduce indoor temperature and limit heat penetration into the tested experimental cubicle, without the need for any active cooling devices. By developing sustainable, biomass-derived biocomposite PCM-integrated building materials, this study takes a step toward achieving SDG 7 (Affordable and Clean Energy), SDG 11 (Sustainable Cities and Communities), and SDG 13 (Climate Action) set by the United Nations for 2030.

1.2 Latent heat thermal energy storage (LHTES)

LHTES is a thermal energy storage method that utilizes the heat absorbed or released during the phase change of a material, enabling the storage and release of large amounts of energy at nearly constant temperature. LHTES is preferable over sensible heat storage because it can provide high energy storage density per unit mass or per unit volume, approximately at the isothermal condition [15].

The latent heat process is mathematically expressed as **Eq. 1.1**.

$$E = m\left[\left\{\int_{T_0}^{T_s} C_{ps}\,dT\right\} + H + \left\{\int_{T_l}^{T_f} C_{pl}\,dT\right\}\right] \tag{1.1}$$

where m is the mass of the thermal energy storage material with the heat of fusion H. The first term represents the sensible heat added to raise the material from the initial temperature T_o to the phase-change temperature T_s in the solid state. The last term is the sensible heat added to raise the material from the phase-change temperature T_l to the final temperature T_f in the liquid phase, C_{ps}, and C_{pl} are the specific heat capacities of the solid and liquid phases, respectively.

1.3 Phase change material(PCM)

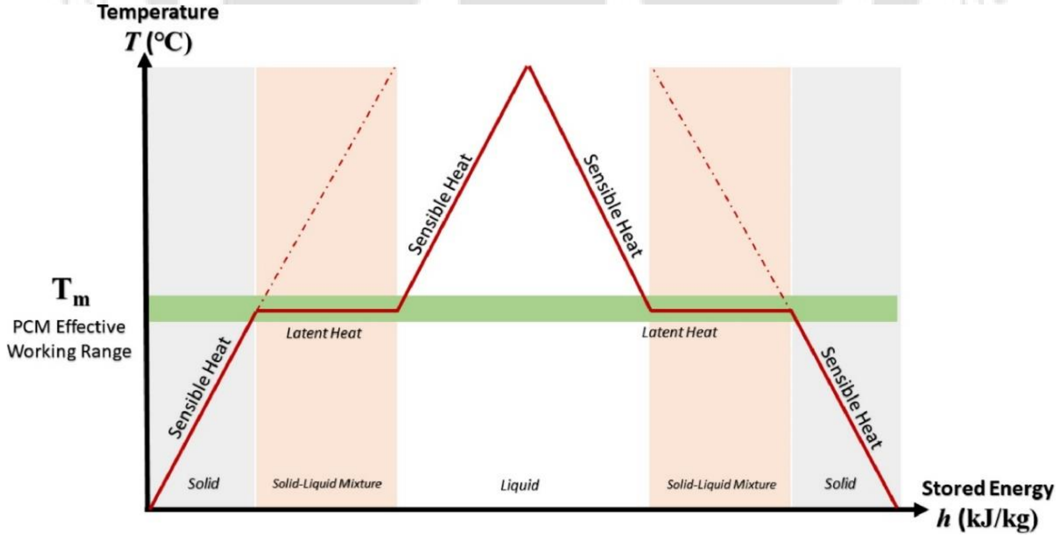

Fig. 1.1 PCM phase change transition [16]

PCM is a substance that absorbs or releases a significant amount of heat as it undergoes a change in its physical state, such as from solid to liquid or vice versa [17]. **Fig.1.1** shows the heat transfer mechanism of the solid-liquid phase change process of PCM. The desirable properties of PCM are listed in **Table 1.1** [18].

Table 1.1 Desirable properties of PCM for thermal energy storage

Characteristics	**Desirable properties**
Thermal properties	Suitable phase transition temperature
	High latent heat of transition
	High thermal conductivity
Physical properties	High density
	Small volume change
	Low vapour pressure
Kinetic properties	Low super-cooling
	Sufficient crystallisation rate
Chemical properties	Long-term stability
	Compatibility with materials of construction
	Reproducible crystallisation without degradation
	No corrosiveness
	No toxicity
	No fire hazard
Economics	Cost effective
	Availability

1.3.1 Types of PCM

PCMs are broadly classified as organic, inorganic and eutectic [16]. The different types of PCM are shown in **Fig. 1.2** and discussed briefly in the subsequent sections.

1.3.1.1 Organic PCM

Organic PCM has the advantages of melting congruently, being chemically and physically stable, and having a high heat of fusion. Its drawbacks are that it is more expensive and flammable, has low thermal conductivity in the solid state, has lower heat storage capacity per unit volume, and has leakage problem during phase transition [13]. The drawbacks are mitigated by using metallic filters, metal-matrix structures, and fin tubes, encapsulation, and preparation of form-stable material using a porous supporting matrix.

Paraffin waxes ($CH_3(CH_2)_nCH_3$) are among the most widely used organic PCMs due to their low cost and moderate thermal storage capacity, typically ranging from 120 to 210 kJ/kg. They are available with melting points between 20°C and 70°C, making them suitable for various low-temperature solar applications. Paraffins are chemically stable, exhibit low vapor pressure in their liquid phase, and do not undergo phase segregation during thermal cycling. However, paraffin suffers from low thermal conductivity (~0.2 W/mK), which limits its heat transfer efficiency. Additionally, they experience significant leakage during phase transitions, which can pose structural challenges [19].

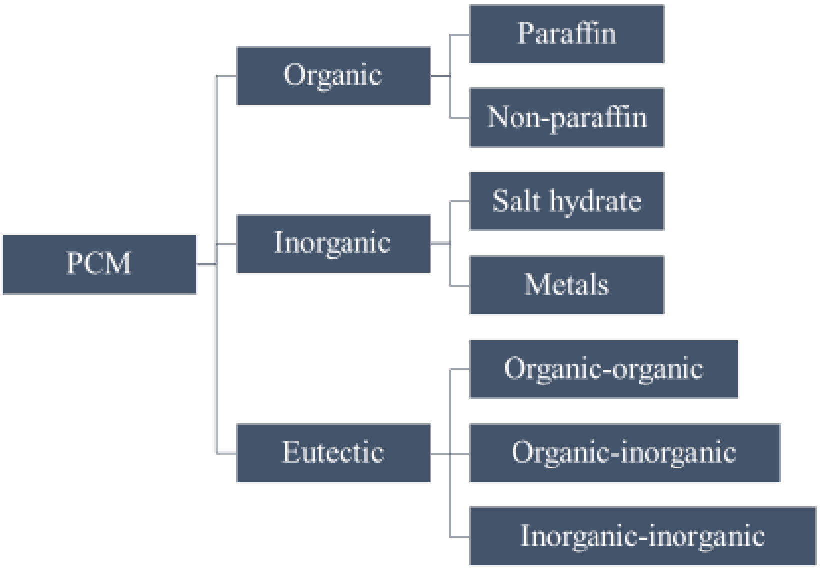

Fig. 1.2 Classification of PCM [17]

Non-paraffin organic PCMs include fatty acids, esters, alcohols, and glycols. These materials offer excellent melting and freezing behavior, high latent heat of fusion, minimal volume change during phase transition, and no supercooling. However, they are approximately three times more expensive than paraffin [20].

1.3.1.2 Inorganic PCM

Inorganic PCMs are advantageous than organic PCMs because they possess double energy storage density, higher thermal conductivity, higher operating temperatures, and lower cost. The disadvantages of inorganic PCMs are that they are corrosive, thus the service life becomes short. Also, inorganic PCMs often suffer from phase segregation and supercooling. Inorganic PCMs can be primarily classified into two groups: salts and salt hydrates, and metals and their alloys [13].

Salt hydrates are typically represented by the formula $A_xB_y.nH_2O$, where n denotes the number of water molecules, and A_xB_y refers to a salt such as a metal carbonate, sulfite, phosphate, nitrite, acetate, or chloride. The bonding in salt hydrates primarily involves ion–dipole interactions, occurring between the ions of the salt and the polar water molecules. In some cases, hydrogen-hydrogen interactions may also be present. The water molecules are loosely bound to the anions, and occasionally to the cations. During a phase change, latent heat is absorbed, causing the salt hydrate to release part or all of its water content, often leading to partial or complete dissolution of the salt [21].

Another category of inorganic PCMs comprises metals and metallic alloys. These inorganic PCMs offer several advantages over salts and salt mixtures. Metallic PCMs possess high thermal conductivity, eliminating the need for additional conductivity-enhancing materials. Furthermore, they offer a high heat of fusion per unit volume, low specific heat, low vapor pressure, and excellent thermal stability and cyclic performance [15].

1.3.1.3 Eutectic PCM

Eutectic PCM refers to the homogeneous mixture of inorganic-inorganic, organic-organic or inorganic-organic PCM. Although an eutectic mixture consists of different melting point PCMs, the resultant melting point is single and usually lower than both the constituents [22]. Upon crystallization, eutectic PCM results in a single crystal. The congruent melting of eutectic PCM makes it very suitable for use in any energy storage applications [15].

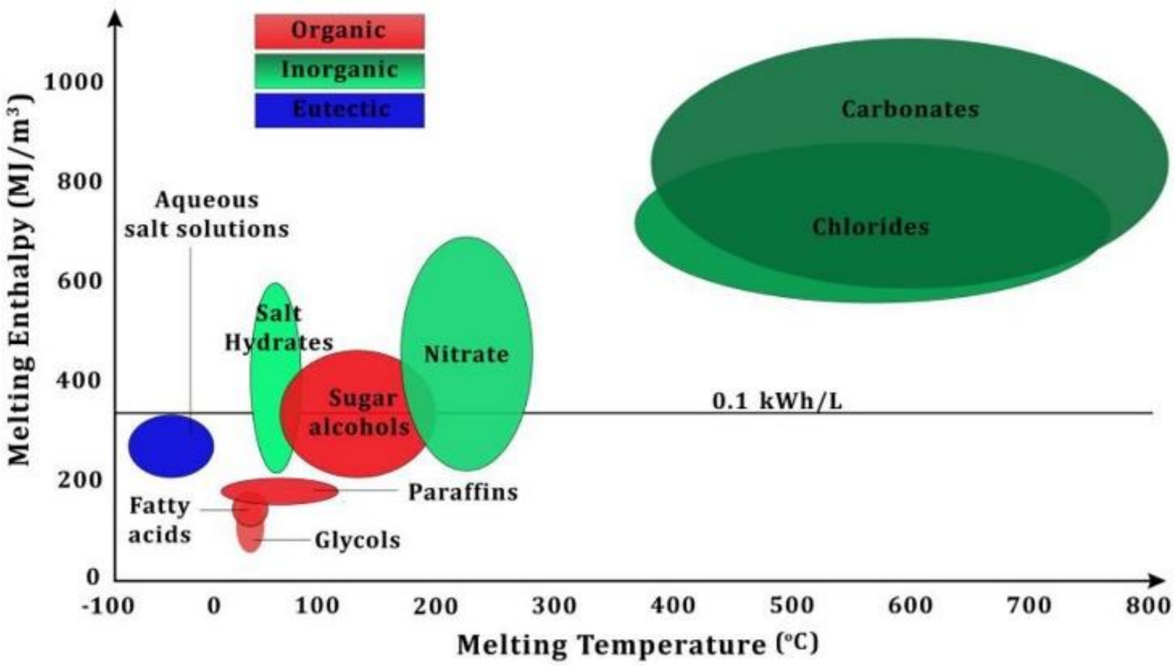

Fig. 1.3 Melting temperature and enthalpy comparison of different solid-liquid PCM [23]

The comparison of the three mentioned PCMs in terms of melting enthalpy and melting temperature is shown in **Fig. 1.3**. According to the comparison, paraffin, glycol and salt hydrates are the most suitable PCMs for building applications, based on their melting point. **Table 1.2** presents a systematic analysis of the different PCMs, showing their respective advantages, key limitations and major applications [19,23–28].

Table 1.2 Systematic comparison and applications of different PCMs

Type	Advantages	Key Limitations	Applications
Organic	Solidifies without sub-cooling Low vapour pressure Congruent melting Chemically stable High heat of fusion Non-toxic Non-reactive Recyclable	Low thermal conductivity Highly flammable	Buildings Textiles Electronic devices Bio-medical Solar PV Food industry
Inorganic	High thermal conductivity Lower volumetric expansion High heat of fusion per unit volume Less costly Non-flammable	High degree of supercooling Lack of thermal stability Incongruent melting Corrosive Chemical instability	Buildings Battery Solar parabolic collector Electric vehicles Water heating and cooling
Eutectics	Sharp melting temperature High thermal storage density No phase segregation congruent phase change	Availability Expensive	Buildings Space applications

1.4 Improvement in organic PCMs

The low thermal conductivity of organic PCMs, along with their tendency to leak during phase transitions, are two major limitations that require fine-tuning for practical applications [29]. Different technologies are being developed to address those problems, so that the use of organic PCM in buildings can be practically possible. The key motive of the modification is to encapsulate the parent organic PCM with some efficient materials so that the shape of the PCM remains intact during the melting process, along with an enhancement in the heat transfer rate. There are mainly three methodologies by which organic PCMs are encapsulated, namely microencapsulation, macroencapsulation and shape-stabilized/form-stable composite preparation [22]. A brief discussion of the different technologies is included in the next subsections.

1.4.1 Encapsulation technologies

1.4.1.1 Microencapsulation of PCM

Microencapsulation refers to the method in which each tiny particle of the PCM is encapsulated with a coating material. The size of microencapsulated PCM varies between µm to mm [23]. A microcapsule of PCM consists of two main components: the core PCM and the polymer or inorganic shell protecting the core, as shown in **Fig. 1.4**.

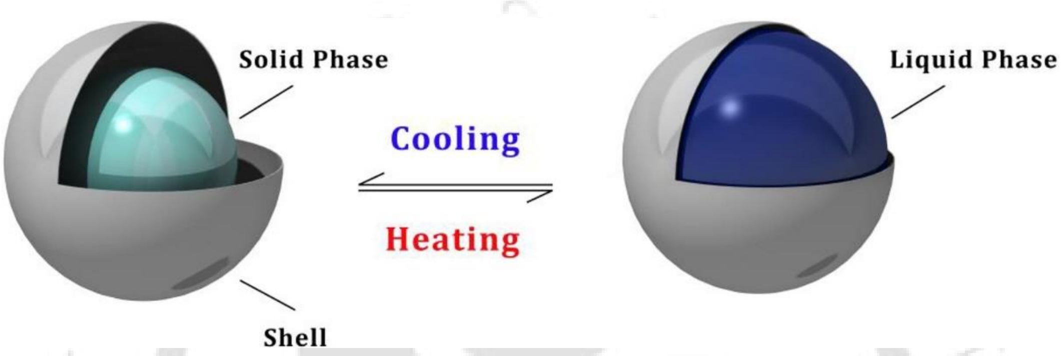

Fig. 1.4 Microencapsulated PCM [23]

Although physical, chemical and physicochemical processes are mostly involved in making microencapsulated PCM, the chemical methods are widely used. The chemical processes are in-situ polymerization, interfacial polymerization, suspension polymerization, and emulsion polymerization. In-situ polymerization is the most efficient method for microencapsulation of organic PCM [30]. This method is beneficial in achieving heat transfer rate, preventing leakage, and improving thermal-mechanical performance. However, the complex and costly fabrication process is one of the drawbacks associated with this technology [27].

Performance Indicators

Encapsulation Ratio (ER): This parameter indicates the effective performance of PCM inside the shell material. The encapsulation ratio is defined as per **Eq. 1.2** [30].

$$ER = \frac{\Delta H_{m,mPCM}}{\Delta H_{m,PCM}} \times 100 \qquad (1.2)$$

where ΔH_m is the latent heat of fusion, and $mPCM$ represents the micro-encapsulated PCM.

For a higher latent heat of fusion, a higher encapsulation ratio is desirable in micro-encapsulated PCM, allowing more core material to be entrapped within the microcapsule.

Encapsulation Efficiency (EE): Encapsulation efficiency measures how effectively core PCM has been encapsulated during the encapsulation process, relative to the theoretical maximum. The mathematical expression for encapsulation efficiency is given by **Eq. 1.3** [30].

$$EE = \frac{\Delta H_{m,mPCM} + \Delta H_{s,mPCM}}{\Delta H_{m,PCM} + \Delta H_{s,PCM}} \quad (1.3)$$

where ΔH_s is the latent heat of solidification. Higher indicates that the microencapsulation process is efficient in entrapping a higher proportion of core PCM.

1.4.1.2 Macroencapsulation of PCM

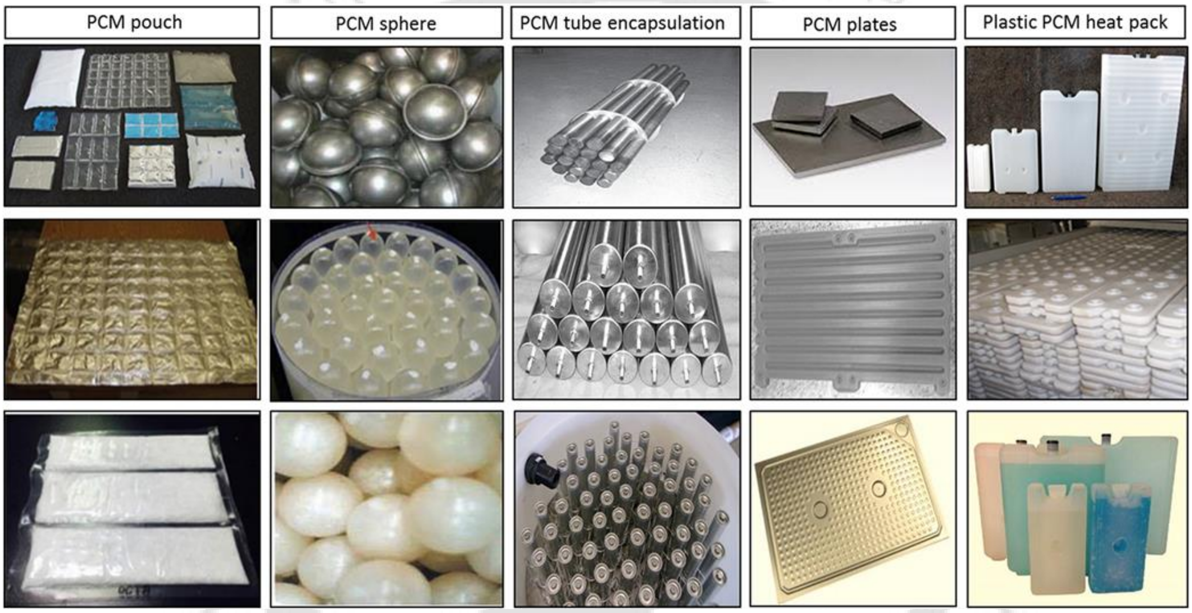

Fig. 1.5 Microencapsulated PCM [23]

This is the most popular method of encapsulation of PCM, as the process is easier and cheaper than the other two available technologies. In contrast to the microencapsulation process, bulk PCM is encapsulated within a container in this method [31]. Vacuum impregnation and autoclave methods are mostly used for the fabrication of this type of PCM. The containers may be in the form of bags, cylinders, panels, plates, tubes, capsules and slabs made of metal and plastic, as shown in **Fig.1.5**. The size of the containers is usually greater than 1 cm. Macroencapsulated PCM can be easily transported and directly incorporated into practical applications because of its easier handling. The thermal conductivity of the shell material plays a crucial role in the heat transfer of macro-encapsulated PCM. Also, the shape of the container affects the rate of melting and solidification in the case of macroencapsulated PCM [32].

1.4.1.3 Form-stable/shape-stabilized composite PCM

In this technology, a composite PCM is formed by mixing the parent PCM within a supporting porous matrix. The porous matrix encapsulates the liquid PCM during the melting process, and thus, leakage is completely prevented through this method [33]. Normally, the interaction between the matrix and the PCM is physical in nature; therefore, the properties of the parent PCM are not affected by this improvisation method. Shape-stabilized PCM are usually fabricated through two methods: two-step impregnation and one-step in situ synthesis technique, as shown in **Fig.1.6**. The two-step impregnation is the primarily used method, involves encapsulating liquid PCMs within the pores of a pre-synthesized support structure. On the contrary, the one-step technique impregnates the PCM into the structure simultaneously with the formation of the porous support, which consists of an interconnected network [23].

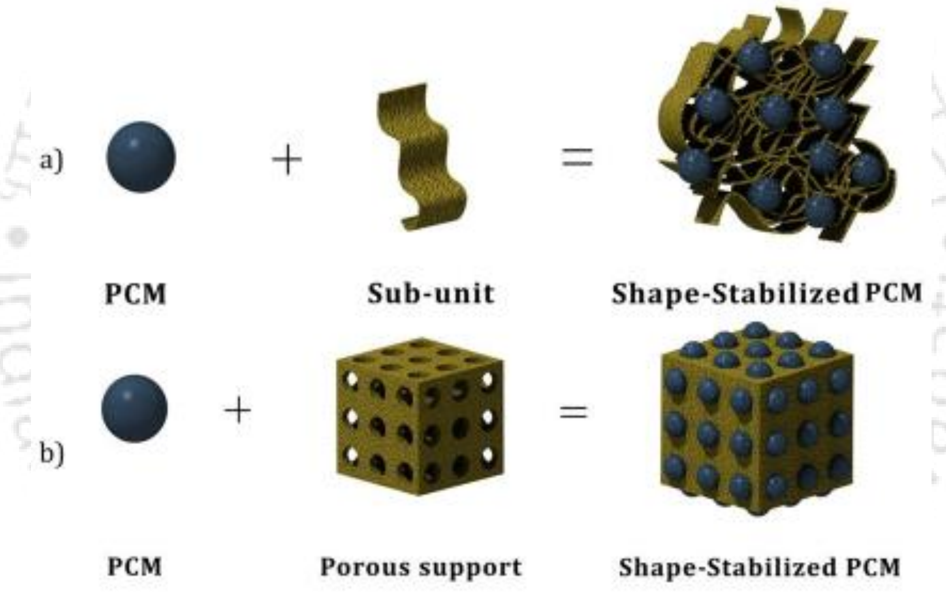

Fig. 1.6 Preparation method of shape-stabilized PCM [23]

The fundamental principle of form-stable PCM formation is the physical confinement of PCM within a porous supporting matrix through capillary action and surface tension force. The capillary force originates from the surface tension between the melted PCM and the walls of the pore structure [34]. For a PCM with density and surface tension σ_s, the capillary height H_c inside a pore radius R_p of the porous matrix is given by **Eq. 1.4**. These capillary and surface tension interactions prevent the PCM from leaking out during melting, ensuring that the composite remains shape-stable throughout thermal cycling.

$$H_c = \frac{2\sigma_s \cos\theta_c}{\rho g R_p} \tag{1.4}$$

Here, θ_c is the contact angle made by the liquid melted PCM with the surface of microspores of the supporting matrix, which is highly influenced by the wettability property of the PCM. A lower contact angle indicates good wettability, ensuring stronger adhesion between the liquid PCM and the supporting matrix.

Among various chemical deposition techniques, such as sol–gel, vacuum impregnation, melt blending, and in-situ polymerization, vacuum impregnation has proven to be the most effective method for developing form-stable composite PCM [22]. By selecting an appropriate supporting matrix, the thermal conductivity can also be enhanced by this method. Selecting the most efficient supporting matrix is the most critical step in this method. Common matrix materials include porous polymers, expanded graphite, silica, carbon nanotubes, metal foams, and fibrous composites [27].

1.5 PCM for building thermal management

Many innovative technologies have been adopted over the years for the integration of PCM for the heating and cooling of buildings. The broad classification can be categorized into two systems - active and passive [35]. In the active method, the involvement of a heat pump, heat pipe, ventilation system and PV system is noticed where the external power source is utilized, and thermal energy generated is stored via PCM. Passive methods involve incorporating PCM directly onto the construction material, such as cement and mortar. Some other method involves the amalgamation of PCM panels to already available building parts like windows, walls and façades [36].

1.5.1 Active methods

The active system involves the use of electricity to run various mechanical and electrical components to achieve building thermal comfort requirements. The use of a heat pump and boiler for the HVAC system is a common technology used for building comfort. This type of system can be relied on both during sunshine and off-sunshine hours. An active system can ensure the complete cycle of PCM charging and discharging. Otherwise, the melting and freezing completely depend on the outdoor temperature.

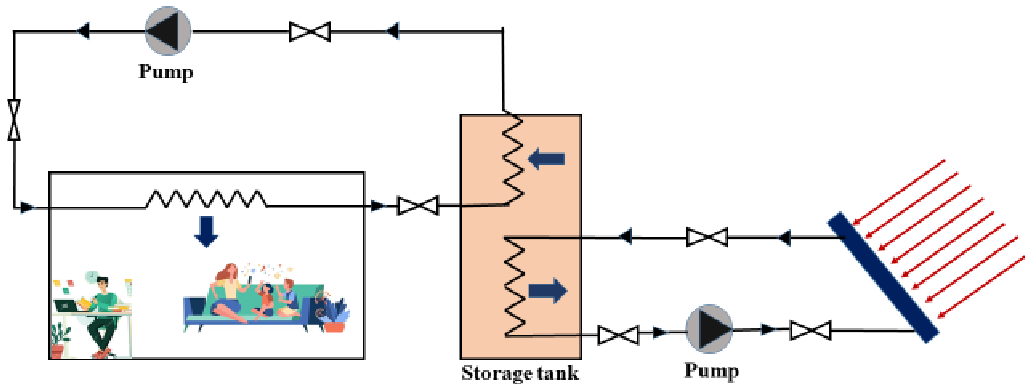

Fig. 1.7 Schematic of a typical active PCM storage tank for building

An efficient heat exchanger system with two PCM storage tanks is a commonly used active thermal energy storage for buildings. The active storage facility is further subdivided into two parts, namely, direct and indirect types. In the case of the direct type active system, the storage media acts as a heat transfer fluid, and for the indirect type, a secondary fluid is circulated through the storage tank for exchanging heat. The various integration methods include integration in the ceiling, floor, wall, suspended ceilings, ventilation system, external solar façade, and solar collectors (solar PV and solar PV/T) [36]. In most of the active TES with buildings, water has been utilized as heat transfer fluid. **Fig.1.7** represents a simple configuration of the active system with PCM storage and a solar collector used for building heating.

1.5.2 Passive methods

Effective passive cooling techniques include the use of materials with low thermal conductivity and advanced properties, employing reflective surfaces and shading strategies, and utilizing sustainable, locally available materials along with low-energy-consuming technologies [37]. The passive building focuses on local climatic conditions, building orientation, the site of the building and building materials. This is the most preferred option as the strategy requires no power input. Numerous innovative building envelope materials have been studied over the past few periods for efficient thermal management. Insulating materials like aerogels, vacuum-insulated panels, foam, mineral wool and fiberglass can provide thermal regulation inside a building [38]. Although insulation material blocks the heat flow across the building envelope, it has little effect on thermal energy storage. In this case, PCM is the best alternative, which can control heat flow by storing excess thermal energy and redistributing the same. Overall, PCMs integrated into building elements can regulate heat transfer, enhance energy efficiency, and reduce indoor temperature [39].

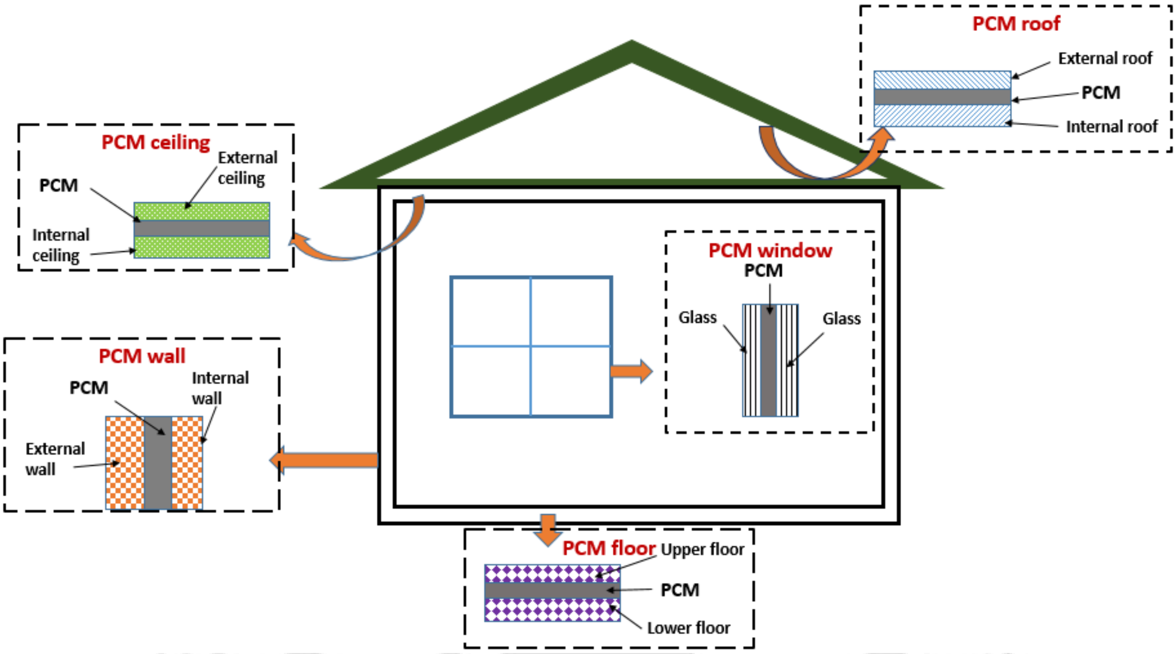

Fig. 1.8 Passive application of PCM in buildings [40]

Passive methods involve incorporating PCM directly onto the construction material, such as cement and mortar, and fabricating the construction with the manufactured material. Some other methods involve the amalgamation of PCM panels with already available building parts like windows, walls, and façades, ceiling, roof, and floor, as shown in **Fig 1.8** The passive methods are also termed free cooling and heating, as the PCM solidifies during the nighttime when the temperature drops and absorb the heat during the daytime, providing cooling inside the building [41].

1.6 Objectives of the present work

The primary aim of the project is to develop novel biocomposite phase change materials for passive design interventions in rural households for thermal management.

The objectives of the present study are listed below.

1) Development of biocomposite phase change material for thermal, chemical, and mechanical stability and its characterization
2) Development of biocomposite phase change materials-filled bricks for optimum thermal management
3) To analyse the thermal performance of biocomposite phase change material-filled brick walls for a hot and humid climate
4) Techno-economic analysis and life cycle assessment of the developed biocomposite phase change material for enhancing energy efficiency in real buildings

1.7 Organization of thesis

This thesis deals with the development of biocomposite PCM for passive design interventions in rural households. The entire thesis has been outlined in six chapters. Chapter 1 presents the motivation, fundamentals of PCM, and their usage in buildings, along with the objectives and outline of the thesis. In Chapter 2, an extensive literature review has been presented on the area of encapsulation technologies for PCM and its integration technologies in buildings. At the end of the chapter, a summary of the literature review, research gaps and objectives of the thesis are outlined. The development of biocomposite PCM, complete characterization and thermal cycling stability of the developed materials have been presented in the Chapter 3. Chapter 4 provides the details of the methods of embedding biocomposite PCM in bricks, and the discussion on the thermal performance tests and PCM-incorporated experimental cubicle is also included. The techno-economic analysis using EnergyPlus software, along with the life cycle analysis (LCA) of the whole building incorporating biocomposite PCM, is presented in Chapter 5. The significant findings of the thesis and the scope of the future research are summarized in Chapter 6.

1.8 Summary of the chapter

The present chapter discusses the need and motivation for the study. The introductory basic concepts are highlighted in the chapter, forming the foundation for all discussions presented in the subsequent chapters. The objectives of the current work, along with the outline of the thesis, are mentioned in this chapter. The detailed methodology to execute the formulated objectives is presented in the next chapter.

Chapter 2
Literature Review

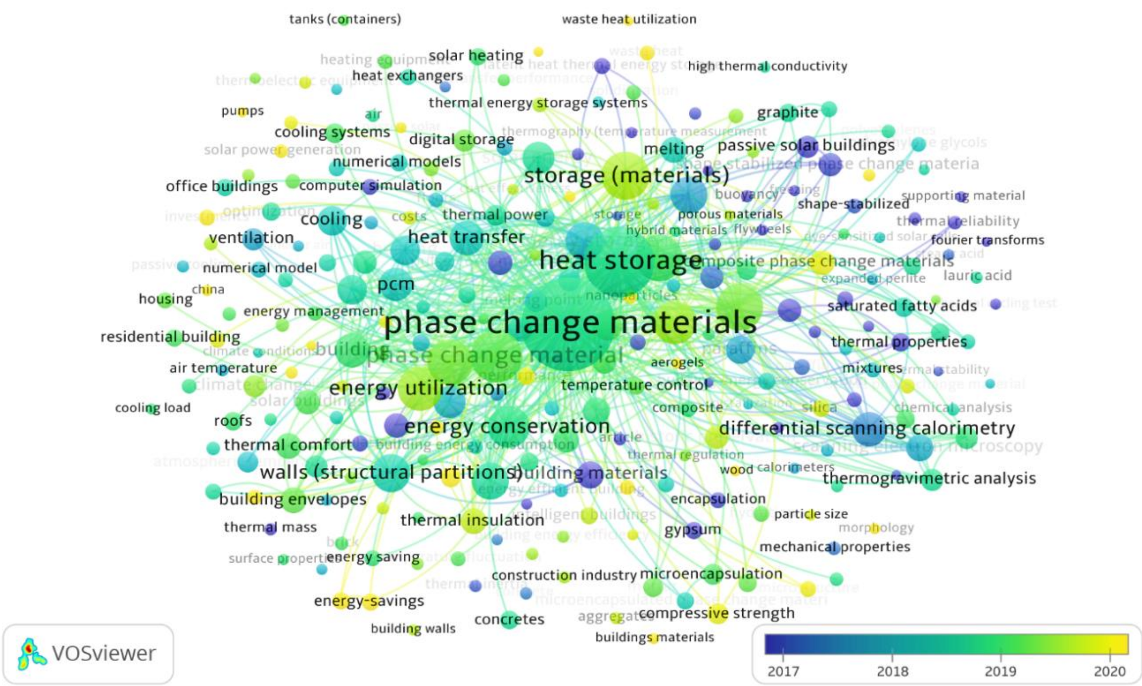

2.1 Introduction
2.2 Form-stable PCM
2.3 Thermal cycling stability of PCM
2.4 PCM for building thermal management
2.5 PCM on building envelopes
2.6 Techno-economic and environmental assessment analysis
2.7 Summary of literature review
2.8 Research gaps
2.9 Thesis objectives
2.10 Summary of the chapter

Outline

2.1 Introduction

The thermal comfort provided with optimized energy consumption is the aim of all energy scientists around the globe. Effective measures should be adopted to create a desired thermal environment inside a building for long-term energy savings, as mentioned in the previous chapter. Different mechanisms have been evaluated, which include building-integrated solar photovoltaic (BIPV) systems, heat pump integration, radiant floor, and passive design of building architecture. The passive design of buildings refers to all energy-efficient and environment-friendly approaches where building design and materials are selected considering the local climatic conditions. The demand for mechanical systems to ensure thermal comfort can be significantly reduced by a well-designed building envelope, lowering the environmental effect. In such circumstances, the application of PCM helps to increase the thermal mass of buildings, thereby reducing temperature fluctuation. PCMs have a high capacity for heat absorption during the melting phase (from solid to liquid), and they also have a high capacity for heat release during the solidification phase (from liquid to solid). The great energy storage capacity of PCMs and their capacity to maintain thermal storage at a steady temperature make their use appealing for a variety of building applications. The selection of appropriate PCM depends on the thermo-physical, kinetic, chemical, economic, and environmental properties, and also the local weather conditions. The most essential thermophysical property involves the melting temperature range, the heat of fusion and thermal conductivity. An inappropriate melting temperature can create difficulties in regulating night time temperatures, and inefficient use during extreme seasons [42]. Out of the three main categories of PCMs, organic PCMs are primarily hydrocarbon-based, comprising long-chain macromolecules rich in carbon and hydrogen, and are the most preferred option in building thermal applications. Organic PCM is less costly, thermally stable with zero supercooling and high heat of fusion, non-corrosive, chemically stable, non-toxic, compatible with building materials, and readily available [43]. Cavity formation in organic PCM during the heat exchange process causes a problem as it increases the thermal resistance. Moreover, the formation of the cavity pushes the mass of PCM surrounding it and causes volumetric expansion, which finally results in leakage of PCM. The low heat conductivity and the problem of liquid leakage during phase transitions have become the two significant shortcomings while using organic PCM in buildings [44]. This chapter provides an extensive description of the various technologies available for PCM encapsulation, along with their applications in different parts of a building. The chapter also presents a summary of the literature review and scope of research.

2.2 Form-stable PCM

To overcome the issues related to low thermal conductivity and leakage during the melting of organic PCM, form-stable PCM has been developed and has received much focus over the parent PCM [45–47]. The form stability is achieved through incorporating PCM into some porous matrix or providing microencapsulation and macroencapsulation.

Shape stabilization of PCM refers to the process where liquid PCM leakage has been prohibited after reaching the melting point of the PCM. The shape stabilized PCM remains in solid state during both melted and solidified conditions. According to a study, there are four primary binding forces through which form stabilization has been achieved: covalent bonding encapsulation force, physical adsorption via capillary, hydrogen bonding and van der Waals force. Physical adsorption, being the most simple and low cost technology is the widely used process for shape stabilization [48]. When liquid PCM is mixed in a porous structure having numerous tiny holes, the liquid PCM rises through capillary action against gravity. After that, the surface tension force between the PCM and the supporting material helps in retaining the PCM within the pores [48]. Here, the main characteristics of the supporting material are the wettability, which means the PCM should be able to wet the surface of the supporting matrix [49]. Also, the supporting matrix should sustain the temperature of the intended operation. The immersion of liquid PCM on porous supporting matrix can be done either in a vacuum or in atmospheric pressure conditions through the impregnation method [50]. Impregnation method is the process of submerging the supporting media into a fluid material carrying active substances [48]. The most commonly used supporting matrices are carbonaceous porous material (traditional carbon material and biochar), minerals and their derivatives (e.g. perlite, diatomite, kaolin, etc.), and polymers [50]. Wan *et al.* [51] manufactured one form-stable PCM by using pinecone biochar as a supporting matrix for palmitic acid (PCM), as shown in **Fig.2.1**. They conducted various characterization tests and concluded that palmitic acid was bonded with biochar due to capillary force and surface tension. No chemical reactions happened between the two materials, and so the chemical properties have not changed from the original PCM. According to their study, the composite with a mass ratio of 6:4 (palmitic acid: pinecone biochar) showed the best stability. The thermal conductivity of the composite material was increased by 43.76% to pure palmitic. Wen *et al.* [52] prepared and studied the thermal properties of a form-stable composite from fatty acid (capric-lauric acid/ diatomite). The composite was made by the vacuum impregnation method. To increase the thermal conductivity, they further added expanded graphite to the composite. They concluded that capric-lauric acid was absorbed by the diatomite holes very effectively without any chemical bonds between the two. They conducted a thermal cycling test and found that the composite has good thermal and chemical stability over 200 cycles of heating and freezing. The addition of expanded graphite increased the thermal conductivity, and 10 wt.% was the most optimized one.

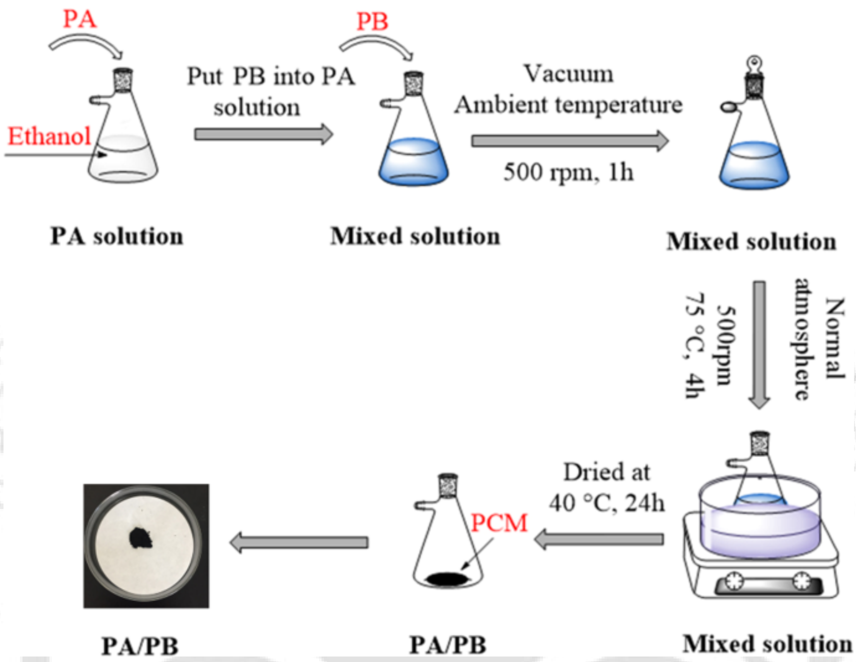

Fig. 2.1 Form stable material preparation method via vacuum impregnation method [51]

Li *et al.* [53] prepared a composite material for thermal energy storage with polyethylene glycol and ZSM-5. The mesoporous ZSM-5 was taken as a supporting material, and the vacuum impregnation method was employed. The thermal conductivity was increased by 200% than the pure polyethylene glycol. Exudation stability test results showed that the doping of PEG could reach up to 50 wt% without any leakage when the composite was undergoing the melting process. Liang *et al.* [54] fabricated a noble PCM using fatty acid and wood flour via the direct impregnation method. Scanning electron microscopy (SEM) images showed that the porous spaces of wood flour are occupied by the fatty acid without leakage. The prepared composite material has high latent heat and a suitable phase change temperature.

Nanomaterials are also used as a supporting matrix for the shape stabilization of PCM. PCM is entrapped in nano-structured materials in three different ways: longitudinal 1D, interfacial 2D, and porous 3D network [55]. The 1D confinement involves electrospinning of the organic PCM into nano-fibres. 2D confinement happens through interfacial interaction, and for a 3D structure, PCM is confined in the porous matrix through the vacuum impregnation method.

Sari *et al.*[56] designed one diatomite- carbon nanotubes and polyethylene glycol (PEG) composite for thermal energy storage. Raw diatomite (RD) and CNT pre-composite were made, and the final composite was made by the vacuum impregnation method. The shape-stabilized composite PCMs successfully confined polyethylene glycol (PEG) without melt leakage, achieving PEG loadings of 42.8, 44.5, and 51.7 wt.% with the incorporation of 0.57, 1.70, and 2.50 wt.% CNTs, respectively. In contrast, PEG absorption in raw diatomite was limited to 41.0 wt.%. The composite had a melting temperature of 7-8^{o} C, latent heat of 51.4-62.9 J/g and thermal conductivity increment up to 93% compared to RD/PEG composite. Metal organic framework (MOF) is another class of emerging supporting matrix that incorporates both organic and inorganic PCM. The suitable properties of MOF as a supporting matrix are ultra-high porosity, higher surface area, and chemical and thermal stability. The main interesting fact of MOF is the adjustable surface properties according to the need, so that the required level of thermal properties of the composite PCM can be achieved [48]. Atinafu *et al.*[57] synthesized shape stabilized PCM using porous nitrogen-doped carbon from the MOF. They reported an improvement of 52% in thermal conductivity and 85% in thermal storage capability with the doped PCMs than the undoped PCM.

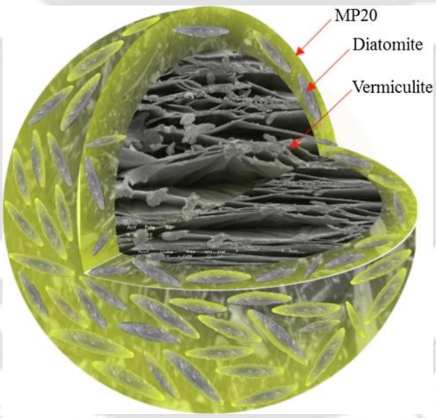

Fig. 2.2 Diatomite-vermiculite form-stable PCM [58]

Form-stable PCM is used in building envelopes mainly as a construction material mixed with cement or mortar, or as a layer in building walls, roofs and ceilings, etc. Hattan *et al.*[59] prepared cement mortar plaster using shape stabilized PCM (PEG 600 with silica fume). Though the prepared plaster proved well for maintaining thermal stability inside the test room, the mechanical strength, density and water absorption capacity of the mortar significantly reduced. Karaipekli *et al.*[60] developed one plaster material by combining pumice, organic PCM and gypsum. The developed PCM-plaster was able to keep the thermal comfort by constantly keeping the indoor temperature at comfort level (20.98 – 23.27^{o} C) over 3000 cycles.

Shi *et al.*[61] used Vermiculite diatomite as a supporting matrix for paraffin and mixed with cement to form a lightweight mortar. They concluded that the mortar could reduce temperature fluctuation up to 3.6°C, but an additional air conditioning system was required for summertime. Hekimoglu *et al.*[62] prepared cementitious composite made up of silica fume/ capric acid-stearic acid, and replaced with normal cementitious mortar. The maximum temperature difference with ordinary cement mortar was found to be 2.48°C and 1.71°C for the heating and cooling stage, respectively. Another work was done by Costa *et al.*[58] to enhance the thermal performance of cementitious mortar by adding form stable diatomite vermiculite paraffin, as shown in **Fig.2.2**. The new PCM maintained a service temperature of 40°C. Hekimoglu *et al.*[63] studied the thermal management properties of a special kind of cement mortar containing fly ash, lauric acid, and myristic acid. Along with satisfactory thermal properties, the composite was strong in terms of mechanical stability, as 28-day compressive and flexural strength were found to be 28.94 MPa and 3.52 MPa, respectively.

It can be inferred from the above section that the shape stability provides an improvement in the thermal performance of organic PCM, which leads to a faster heat transfer rate while used in building envelopes. Most of the supporting matrix used for encapsulation is derived from some synthetic materials like carbon nanotubes, polyethylene glycol and polyethylene etc. The most desirable property of the supporting matrix is its porous nature to encapsulate the melted PCM. The biochar generated through pyrolysis is known for its high porosity and superior surface area. Although some works have been published in this particular area, a more focused study is required for the replacement of synthetic materials with highly porous biochar derived from abundantly available biomass for the development of bio-based energy storage material.

2.2.1 Bio-based PCM

In terms of environmental sustainability, most of the organic PCMs are preferred over inorganic PCMs. But, paraffin, which is the mostly used organic PCM for construction, is derived from petroleum sources, which are non-renewable and non-biodegradable in nature. Therefore, a new category of organic-PCMs has been identified, known as bio-PCM, sourced from renewable biological sources like animal fat, vegetable oil (palm oil, coconut oil, kernel oil), biomass, plant extracts and agricultural wastes[64]. Bio-PCM is advantageous because of the properties like bio-degradability, low embodied carbon, environment-friendly, low flammability and non-toxicity[65]. The use of natural supporting medium for making shape-stabilized composite PCM can be treated as another category of bio PCM [17]. Palm Kernel vegetable oil was also used for preparing composite bio-PCM. The melting temperature and heat of fusion of the hydrogenated Palm Kernel vegetable fat was 26.53°C and 74.35 J/g, respectively. The supporting matrix for composite preparation was also derived from natural resources (natural clay and cellulose fibres). The natural supporting matrix could retain 53% of vegetable fat without leakage. The melting temperature and heat of fusion after composite formation were found to be 27.33 °C and 40.27 J/g, respectively [34].

Organic PCM impregnated with lignocellulosic materials, such as wood and wood derivatives, is a widely used bio-PCM in buildings [66]. Lignocellulose materials offer renewability, lightness, and porosity, enhancing thermal inertia when combined with PCMs. However, their susceptibility to biodegradation and flammability poses key challenges for building applications [66]. The widely used lignocellulosic biomass is waste crop, agricultural waste, waste plant peel, forestry resources, pristine wood, invasive weeds, etc. Palanti *et al*. [67] investigated the resistance to bio deterioration when solid Scots pine wood was impregnated with fatty acid-based bio PCMs. The study concluded three significant findings, which imply that wood impregnated with bio PCM could improve durability against termites. Also, the material inhibited the survival of Hylotrupes bajulus larvae more effectively than conventional wooden building materials, thus extending the service life. Li *et al.* [68] made a composite PCM out of coconut oil and poplar wood fibre to apply to building envelopes. Wood fibres, mostly composed of cellulose (40-50%), possess a large number of hydroxyl groups. Therefore, the wood fibre tends to form intramolecular or intermolecular hydrogen bonds, resulting in a hydrophilic nature and ultimately promoting mould growth. The authors therefore treated the wood fibre with acetic anhydride. Acetic anhydride reacted with the hydroxyl group to form hydrophobic esters, thus preparing the wood fibre ready for use as a construction material. The coconut oil- acetylated wood fibre was mixed with Hexagonal boron nitride to enhance the thermal conductivity. When experimented under artificial climatic chamber on a small sample, the authors reported a reduction in peak temperature (1.88°C) and a delay in peak time (112 min) between the ends of the sample. Linoleic acid and coconut oil were mixed in the ratio of 80:20 and impregnated in both Scots pine softwood and beech hardwood. These two types of wood are extensively used for building construction in European countries. The authors concluded that bio PCM impregnation in wood by a combination of vacuum and pressure was successful with a leakage percentage of 8% and 9% for beech and pine wood, respectively. When used in buildings, the wood material served only as a sensible heat storage medium, but bio PCM impregnation enhanced the heat capacity of the material by around 3 J/g/K [69].

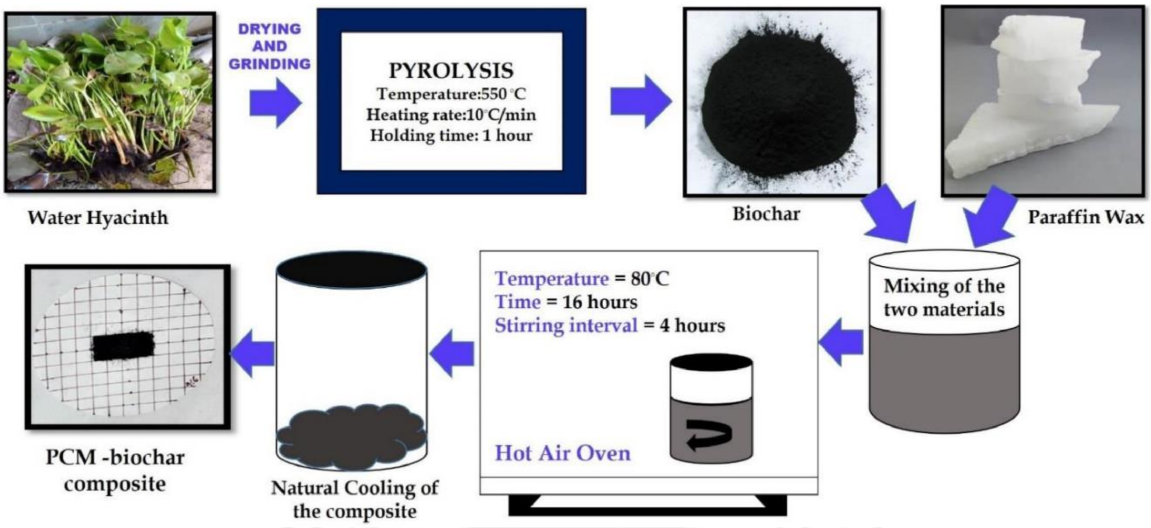

Fig. 2.3 Steps of biochar-PCM composite preparation [46]

Porous carbon is a promising supporting matrix because of its properties like affordability, non-toxicity and highly adsorbent properties. Biomass-based PCM offers numerous advantages, such as structural diversity, which includes layered, fibrous, globular, and 3D structures, and is also excellent for heat transfer due to the carbon network [48]. Among different biomass-based matrices, porous carbon material, known as biochar, is an excellent material for its high porosity, cross-linked 3D structure, and high thermal conductivity, strong corrosion resistance. As the biochar is mesoporous in nature, the confinement of PCM is better than micro- or macro-porous supporting materials. The conversion of biomass to biochar often involves two steps: carbonization of biomass and activation of the produced biochar. Carbonization of lignocellulosic biomass is achieved either by the pyrolysis process or the hydrothermal conversion. To further enhance the surface properties, activation of the produced biochar is performed through physical activation, chemical activation or a combination of both [70]. Jeon *et al.* [71] prepared bio-PCM by mixing rice husk biochar with four different types of bio-PCM, namely, coconut oil, palm oil, palm wax, and soy wax. The highest latent heat of fusion was observed with ricehusk biochar and soy wax mixture, and the value was 83.91 J/g. But, the thermal conductivity value for all the bio-composite PCM was lower than that of the pure PCM, due to the low thermal conductivity of rice husk biochar (thermal conductivity: 0.006 W/mK). Biochar derived from waste material has also been used by researchers to form composite PCM, as shown in **Fig.2.3**. In one study, a cost-effective biochar-PCM composite using biochar derived from invasive aquatic weeds through batch pyrolysis has been discussed. Results show that a 6:4 (wt./wt.%) PCM-to-biochar ratio provides optimal performance with minimal leakage and strong form stability. The porous, carbon-rich structure of biochar also significantly enhances material properties, improving thermal conductivity by up to 13.82 times compared to pure PCM [46].

Although the use of bio-PCM satisfies the environmental concerns, the commercialization of such products on the mass-scale basis is a big challenge to be addressed. However, considering environmental priorities and the potential to boost the rural economy, bio-based PCM should be developed and commercialised.

2.3 Thermal cycling stability of PCM

It is expected that composite PCMs formed by the effective incorporation of PCM into a porous skeleton will give a chemically compatible and thermally stable material. However, the stability and reliability of the selected PCM are very critical issues that must be verified before being applied to the building envelope. The external envelope of a building structure is subjected to continuous changes in environmental factors, including temperature fluctuation, day-night heating and cooling effect, rain and wind, etc. As PCM undergoes a phase change process in each charging and discharging cycle, the properties of PCM may be affected. The cycling stability of PCM is the sustaining of thermal, chemical and physical properties after repeated numbers of melting and freezing cycles [72]. The thermophysical properties of PCM should be intact for long-term use in buildings. The thermal cycling test is a method where simultaneous heating and cooling are externally provided to simulate outdoor conditions. No standard methods for thermal cycling tests have been published till now. It is observed from the literature that Differential Scanning Calorimetry (DSC) is the mostly used analytical method for the analysis of the thermal properties of PCM after the completion of external thermal cycling tests. For performing the thermal cycling experiments, different equipment, including a thermal cycling chamber, thermostatic chamber, thermal bath, oven and electric hot plate, etc., is employed. The heating and cooling of the PCM in the thermal cycling experiment primarily followed the pyramid method, where the PCM is subjected to simultaneous heating and cooling without any isothermal stage in between heating and cooling [72]. Trisnadewi *et al.*[73] experimented with the thermal stability of palm wax, soy wax and paraffin wax for up to 5000 thermal cycles using the thermoelectric heating and cooling device. The authors got degraded values of melting point, freezing point, and heat of fusion for all the waxes and the highest 60% reduction of latent heat of solidification for soy wax was found after 5000 cycles. Shukla *et al.*[74] conducted thermal cycling tests of a few inorganic and organic materials. They recommended that no inorganic material is suitable for thermal storage applications as the properties are deviated after cycling. Paraffin wax was found to be the most stable PCM in terms of melting temperature and latent heat of fusion. Saravanakumar *et al.* [75] tested the effect of 100 thermal cycles on the thermal properties of nano-silica-based PCM. The PCM with 1% nano-silica showed a minimum reduction in terms of melting and freezing points, whereas the plain PCM showed a reduction of 0.87% after 100 thermal cycles. Gowthami *et al.* [76] conducted tests on two form-stable PCMs over 500 thermal cycles. The first PCM consisted of date seed biochar, palmitic acid, and polyethylene glycol, while the second PCM included the same components but used chemically activated date seed biochar. Their results revealed a 3% reduction in latent heat for both PCMs after the thermal cycles, while the melting and freezing temperatures remained unchanged. In another study, 1000 accelerated thermal cycles were performed to form a stable PCM made out of stearyl alcohol with graphitic carbon nitride. The authors demonstrated excellent thermal stability, with negligible variations of 0.1 °C and 0.62 °C in the melting and freezing temperatures, respectively, and changes of only 1% and 0.53% in latent heat after repeated thermal cycling [77]. A similar study was conducted by Gupta *et al.* [78], where they used copper foam as a supporting matrix for the eutectic mixture of Lauric and Myristic Acid. The PCM composites with 35% Boron Nitride and 35% Graphite demonstrated excellent thermal reliability with no significant changes in thermal energy storage parameters after 100 and 500 thermal cycles.

Although some research has been published on thermal cycling, it appears that there is a need for further research into the reliability of different kinds of PCM in terms of physical, chemical and thermal properties. Also, the thermal cycling stability of used PCM on building envelopes after years of experiencing diurnal temperature change has not been studied to date. In this regard, establishing standard test methods will be essential.

2.4 PCM for building thermal management

As mentioned earlier, PCMs offer a reliable means of thermal management in buildings by absorbing, storing, and releasing heat as temperatures fluctuate. **Fig.2.4** illustrates the efficiency of PCM over other commonly used construction materials for passive cooling in buildings. It is evident from **Fig.2.4 (a)** that for the same thermal mass of the building materials, the thickness that PCM requires is significantly thinner, which saves the construction material cost. Also, as shown in **Fig.2.4 (b)**, PCM exhibits the highest thermal energy storage capacity compared to conventional construction materials, making it effective for enhancing the thermal performance of building envelopes [79].

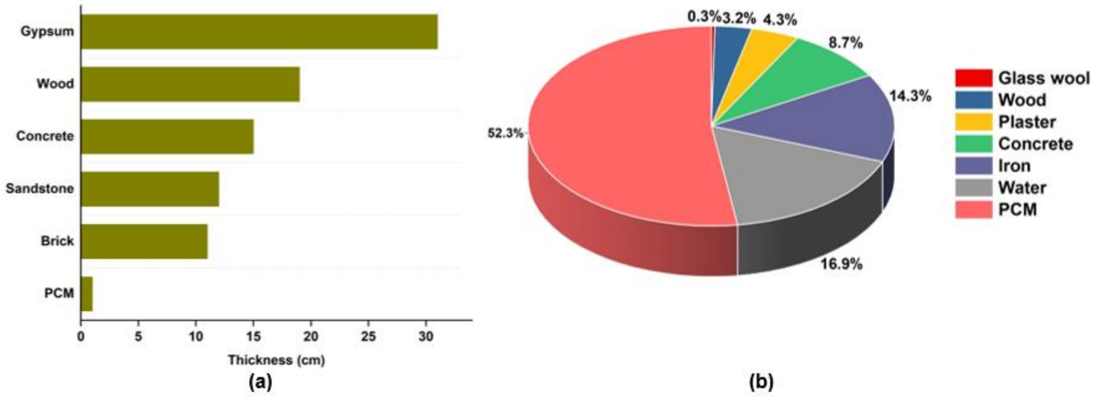

Fig. 2.4 (a) Variation of thermal mass according to the thickness of construction materials[80] (b) Energy storage capacity of different materials [81]

PCMs are integrated directly into building structures through methods like direct incorporation, impregnation of PCM through immersion and imbibing, direct immersion, microencapsulation, macroencapsulation, and shape-stabilization. Direct incorporation involves mixing PCM into construction materials, offering economic advantages despite potential issues like leakage and altered mechanical properties. Direct immersion utilizes construction materials with specific properties, dipping them into a liquid PCM bath. Although direct incorporation involves a simple and less expensive procedure, leakage of PCM can be a major challenge in this type of construction [82]. Microencapsulation involves incorporating PCMs into construction materials. Microencapsulation, preferred for large-scale applications, overcomes leakage problems and enhances thermal cycling but requires non-corrosive and thermally conductive encapsulation. Macroencapsulation is the most widely used methodology for PCM incorporation in buildings, but it results in a low heat transfer rate due to the reduction in the surface-to-volume ratio [82]. Shape-stabilized PCM, formed by cooling liquid PCM mixed with a porous supporting material, provides leakage-free solutions [83,84]. Shape stabilisation gives a higher heat transfer rate and a reduction of material cost as compared to macroencapsulation technology [82]. In the subsequent sections, different experimental and numerical works are discussed briefly, where PCM application results in successful thermal management of buildings.

Wang *et al.* [85] investigated the impact of employing PCM in a full-scale room throughout the year for Shanghai, China. Portland cement, yellow sand, and shape-stabilized PCMs were used to make bricks which had respective mass ratios of 37.5%, 22.5%,40%, respectively. The bricks were applied on the external wall of the full-scale room and tested for three seasons, i.e., summer, mid-season and winter. For the summer season, a maximum temperature reduction of 0.2^{o}C was found accompanied by a delay period of 1-2 hour and, a reduction of 24.32% cooling load. Rathore *et al.* [86] developed two cubicles with dimensions of (1.12×1.12×1.12) m^3, one with PCM (OM37) encapsulated and the other one without PCM. Microencapsulated PCM was integrated into the walls and roofs. The material used for making micro-capsules of PCM is aluminium alloy 8011 of 0.5mm thickness, 16.7mm diameter, and 900mm length. The experimental cubicle with micro-PCM has achieved a peak temperature and cooling load reduction of 59.79% and 38.76%, respectively. Nghana *et al*.[87] performed a study with bio PCM on a building and compared the results with a reference building. In the experimental study, both buildings were located side by side and monitored for the month of September. For the period of testing, it was found that the bio PCM decreased the peak indoor air temperature by up to 0.6°C. In conclusion, it was found that with PCM, the interior wall surface temperatures were lower, thereby reducing the potential for heat loss across the exterior wall by 63%. Yasiri *et al*. [88] experimentally evaluated PCM (macroencapsulated paraffin wax) integrated walls and roofs under non-ventilated conditions in summer hot days, as shown in **Fig.2.5 (a).** PCM-integrated building envelopes have demonstrated indoor temperature stabilization (**Fig.2.5 (b)**), achieving an average temperature reduction of up to 2°C and a heat gain reduction of 56 W.

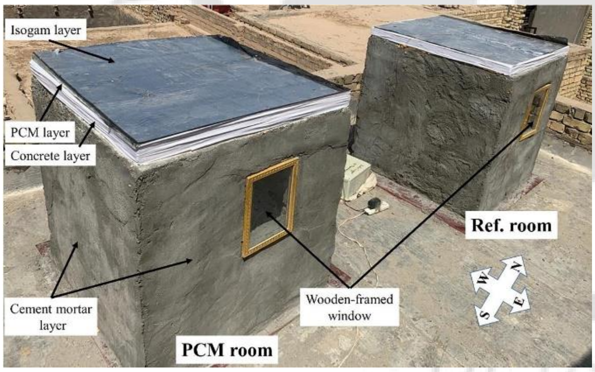

(a)

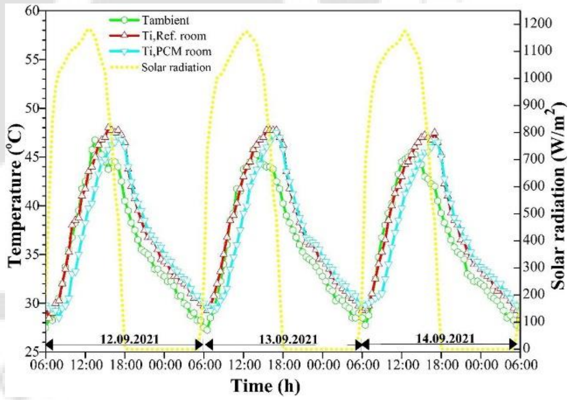

(b)

Fig. 2.5 (a) Test rooms,(b) Indoor temperature profile [88]

Marani *et al*.[89] performed a parametric study on macroencapsulated PCM with concrete panels in three different climatic conditions and reported an interior surface temperature reduction up to 5.4^{o}C. Shahcheraghian *et al.*[90] used hydrated salt for building an exterior wall to improve the indoor temperature stability of a 1 m^3 cubicle. The PCM enhanced cubicle showed reductions of 1.5 °C in average temperature and 2.3 °C in peak indoor temperature during summer conditions. Additionally, the heat gain was reduced by 44% when PCM was installed on the eastern wall. In another experimental study, Yasiri *et al*. [91] built a cubicle similar to the one previously described and compared its hourly temperature profiles and heat gain with an identical non-conditioned cubicle. The PCM-integrated cubicle showed significant improvements in indoor temperature reduction (approximately 4°C) compared to the reference cubicle. PCM performance varied with wall orientation, and the highest effectiveness was shown for east-facing walls and the roof during morning hours, while west-facing walls were most effective in the afternoon.

Given that retrofitting full-scale buildings with PCMs and assessing their energy performance is often economically challenging, numerical simulations provide a reliable framework for performance assessment. Numerous studies have been published utilising simulation software such as EnergyPlus, TRNSYS, Autodesk Insight, eQUEST, OpenStudio, and DesignBuilder. The complexity of the study of heat transfer of PCM-incorporated buildings is more than that of conventional buildings. The envelopes of conventional buildings are made up of materials with constant properties, but the addition of PCM results in dynamic heat storage and release, along with phase transition. The melting and solidification result in non-linear heat transfer involving moving boundaries. At the same time, modelling the building with PCM, the building element is treated as a one-dimensional unsteady convective heat transfer system without internal heat generation to describe the PCM thermal behaviour [92]. The 1D transient heat conduction equation is represented in **Eq. 2.1**, which is modified as **Eq. 2.2** to accommodate the phase transition behaviour of PCM. f is the melting fraction, in **Eq. 2.2**, which varies from 0 to 1 as per the **Eq. 2.3** [92].

$$\frac{\partial T}{\partial t} = \alpha \frac{\partial^2 T}{\partial x^2} \tag{2.1}$$

$$\frac{\partial T}{\partial t} = \alpha \frac{\partial^2 T}{\partial x^2} - \frac{\Delta H_m}{C_p}\frac{\partial f}{\partial t} \tag{2.2}$$

$$f = \begin{cases} 0 & if \quad T \le T_s \\ \dfrac{T - T_s}{T_l - T_s} & if \quad T_s < T < T_l \\ 1 & if \quad T > T_l \end{cases} \tag{2.3}$$

where T , ΔH_m, α , t, and represent temperature $\left({}^oC\right)$, latent heat of fusion (J/g), thermal diffusivity m^2/s , time (s), and element thickness (mm), respectively. The subscripts *s* and *l* represent the solid and liquid phases of PCM.

Arumugam *et al.*[92] modelled an office building in five different climatic conditions of India to theoretically determine the optimal position for the PCM layer for reducing cooling demand using DesignBuilder software. The authors stated that PCM on the outer surface of the wall, irrespective of the location, yielded a comfortable indoor environment, along with a reduction in cooling demand. A maximum cooling load reduction of 64% was reported for the summer conditions of Bangalore city. Application of PCM on the roof and walls of a building resulted in reduced summer heat gains by 12.6%–36.2%, and 10.4%–26.6%, respectively, for a residential building in Delhi. It has been observed that the thermal performance was independent of the melting temperature of PCM, but the enhancement in the latent heat of fusion led to an increase in the overall heat gain. Integrating PCM in buildings could reduce city-wide electricity demand by 80–224 GWh and lower CO_2 emissions by 66–184 kt annually [92]. Rai [93] conducted a simulation study analyzing the thermal performance of various one-dimensional wall configurations incorporating PCMs and insulation under 16 outdoor sol-air temperature profiles using EnergyPlus software. The study showed that PCM integration in insulated walls did not reduce total daily cooling loads, but helped manage peak loads by flattening hourly heat gain fluctuations. Optimal performance was achieved when the PCM was placed on the inner side, shielded from outdoor heat, with a melting point near the indoor set temperature.

The above literature analysis indicates that experimental investigations have mainly focused on temperature regulation and heat gain/ loss assessment rather than energy load calculations. Numerical study shows the potential of detailed energy analysis in a real-scale building after the implementation of a PCM layer. Additionally, the PCM integration through the building envelope is the predominant passive cooling strategy. Therefore, the following sections outline the available technologies for PCM integration into the building envelope and discuss their impacts in detail.

2.5 PCM on building envelopes

Enhancing the thermal mass of a building is achievable through modifications to the materials and design of its envelope, leading to reduced electricity consumption for space heating or cooling. As the surface area of walls constitutes the major portion of any building envelope, there is considerable potential for enhancement in this specific domain. The R-value, which represents the thermal resistance of any building envelope, is a predominant factor that controls the heat flux of any building [94]. Enhancement of R-value by installing a layer on the external envelope is encouraged for a steady indoor thermal environment [95]. Different thermophysical properties, specifically thermal energy storage and thermal conductivity, are the major determining parameters of selecting materials for the alteration of properties of the building envelope [10,22]. The building wall is mostly modified by the integration of insulating materials like expanded polystyrene, mineral wool, perlite, Polystyrene, aerogel, or with PCMs [96,97]. PCMs integrated into building elements like walls, roofs, floors, ceilings, and windows can regulate heat transfer, enhance energy efficiency, and reduce energy consumption. In the following subsection, the integration of PCMs into building roofs, windows, and walls is discussed extensively.

2.5.1 PCM on the roof and ceiling of buildings

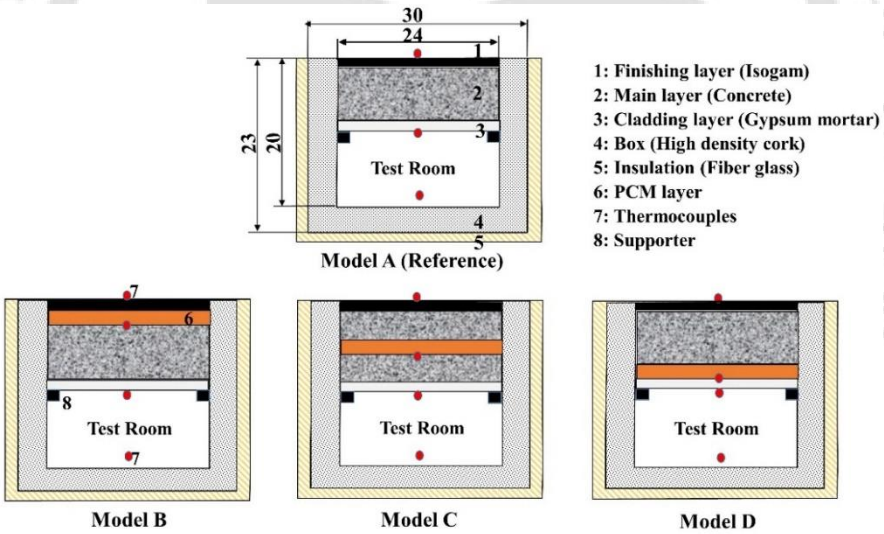

Fig. 2.6 Schematic view of the proposed models [98]

The roof of any building receives more than 1000 W/m^2 direct solar radiation in clear sky conditions. Out of all the received solar irradiation, 20-95% is absorbed by the roof materials, resulting in a higher temperature of the roof than the other walls of buildings [99]. Due to the higher temperature difference between the room and the roof, the application of PCM can reduce the high heat transfer from the roof to the room [100]. Many researchers around the globe have tried to develop numerous innovative designs related to PCM-incorporated rooftops of buildings [101–103].

Yasiri *et al.* [98] performed an extensive study on the optimum position of macroencapsulated PCM roofs under hot climatic conditions. Four models have been developed, as shown in **Fig. 2.6**. The reference room (model A) consists of three layers, namely isogam, concrete and gypsum mortar. Models B, C and D represent additional layers of PCM at different positions. The experiments resulted in a maximum reduction of room temperature of 9°C by model B. Positions of PCM layers close to the interior were not recommended for non-conditioned buildings. Beemkumar *et al.* [104] experimentally controlled the temperature fluctuation by PCM on the roof and reported that the building peak temperature rise was reduced by 1-2°C. Pasupathy *et al.* [105] studied both numerically and experimentally the thermal management of buildings by incorporating PCM on the rooftop. They observed that the temperature is maintained constantly at 27°C for the month of January in Chennai, India. The failure to select an appropriate PCM layer thickness led to uneven temperature fluctuation in a day due to insufficient solidification and melting of PCM [106]. In another work, roofing materials were improvised by adding four different types of PCM by Mano *et al.* [107]. The maximum reduction compared to the reference sheet was obtained as 2.8% for the PCM with a melting temperature of 59°C when the outer roof was maintained at 50°C. Ceilings with PCM as an option for providing thermal comfort to retrofitting houses were investigated, and it was found that the number of hours of thermal discomfort was reduced by 34%. Improvements were recommended because the mentioned passive integration effectiveness was lower than that of the lab-scale experiments for a real building [108].

Different theoretical analyses [109–111] have been done, and the experimental results have been validated by confirming the energy-saving potential of the modified roof with PCM layers. Li *et al.* [112] developed a mathematical model to compare the thermal performance of PCM-incorporated roofs with conventional roofs. The governing equation for the 3D unsteady energy equation for the non-PCM layer in the building roof is given by **Eq. 2.4**.

$$\rho_i C_{P,i} \frac{\partial T}{\partial \tau} = k_i \left(\frac{\partial^2 T}{\partial x^2} + \frac{\partial^2 T}{\partial y^2} + \frac{\partial^2 T}{\partial z^2} \right) \tag{2.4}$$

where T, ρ, k and are temperature (K), density, thermal conductivity and specific heat of the layer (i) of the roof, respectively. The energy equation for the PCM layer, as shown by **Eq. 2.5**, was formulated based on the enthalpy porosity technique, where the mushy region of PCM was treated as a porous medium.

$$\rho_j \frac{\partial H}{\partial \tau} = k_j \left(\frac{\partial^2 T}{\partial x^2} + \frac{\partial^2 T}{\partial y^2} + \frac{\partial^2 T}{\partial z^2} \right) \tag{2.5}$$

where H is the enthalpy of the PCM layer j which is determined by using the governing **Eq. 2.6**, as a sum of sensible enthalpy and latent heat.

$$H = H_{ref} + \int_{T_{ref}}^{T} C_{p,j} dT + f \Delta H_m \tag{2.6}$$

where H_{ref} is the reference enthalpy at reference temperature T_{ref}. f and ΔH_m represented the liquid fraction and latent heat of PCM, respectively.

The liquid fraction of the PCM layer is defined as per **Eq.2.7.**

$$f = \begin{cases} 0, & if\ T \langle T_F\ (solid) \\ 1, & if\ T \geq T_F\ (liquid) \end{cases} \tag{2.7}$$

where F represents the fusion of PCM.

In this model, the authors set the boundary conditions of heat transfer as per **Eqs. 2.8** and **2.9**, for the outer surface exposed to solar radiation and the inner surface near the indoor environment, respectively.

$$-k \frac{\partial T}{\partial n} = h_{out}\left(T_{eq} - T_{out}\right) - \varepsilon\sigma\left(T_{sky}^4 - T_{out}^4\right) \tag{2.8}$$

$$-k_{co} \frac{\partial T}{\partial n} = h_{in}\left(T_{co} - T_{in}\right) \tag{2.9}$$

where h_{out}, T_{out} and T_{eq} is the convective heat transfer coefficient of the exterior layer $\left(W/m^2 K\right)$, temperature of the exterior layer (K), and equivalent temperature (K), respectively. ε is the surface emissivity. σ is the Stefan–Boltzmann constant. T_{sky} is the sky temperature (K), which is approximately equal to $(T_a - 285)$.

The equivalent temperature T_{eq} is expressed as **Eq. 2.10.**

$$T_{eq} = T_a + \frac{\alpha Q_{sol}}{h_{out}} - 3.8 \tag{2.10}$$

where subscript co and in represented reinforced concrete of the roof and the indoor environment, respectively. h_{in}, T_{co} and T_{in} is the convective heat transfer coefficient $(W/m^2 K)$, temperature of the inner surface layer (K), and indoor temperature (K), respectively.

Yu *et al.*[113] performed a simulation study of the dynamic thermal performance of a ventilated roof with shape-stabilized PCM for Wuhan, China. Their results showed the optimum parameters as PCM melting temperature range of 35-38°C, thickness of 30-40 mm and ventilation rate of 2.4-2.5 m/sec. Bhamare *et al.*[114] developed a numerical model for roofing technology with PCM. They reported that the PCM layer with an inclination angle of 2 ° (**Fig. 2.7**) to the roof material showed the best result in terms of thermal performance.

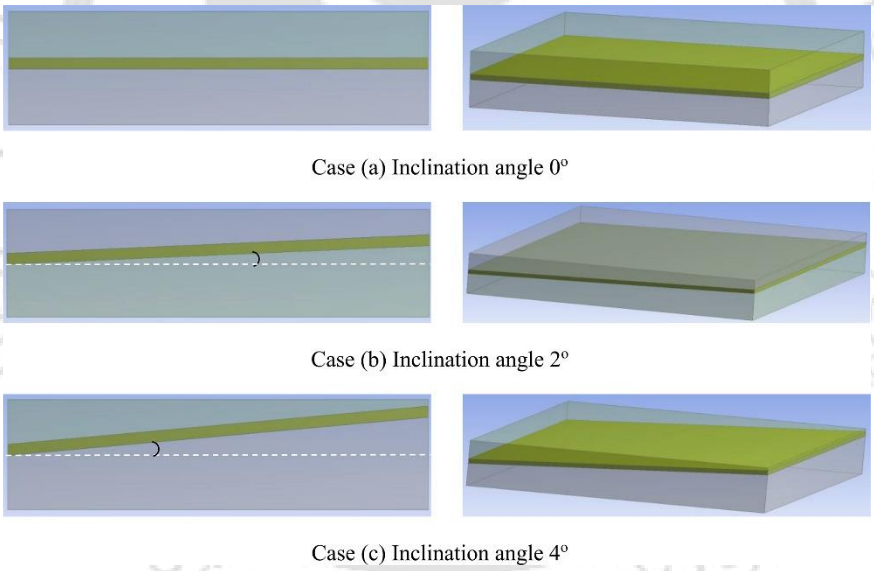

Fig. 2.7 Schematic view of the proposed models [98]

The thermal mass of roof materials increased with PCM integration and is thus capable of reducing the heat gain of the building by absorbing the heat of fusion during the melting process [115]. The suitable melting temperature for comfort, proper orientation, thickness, and position of the PCM layer are some of the important points to consider before integration. It is quite difficult to select a PCM that would be suitable for all weather conditions, so double layers of PCM were suggested [116].

2.5.2 PCM on the windows/facade of a building

Windows are crucial for a building's thermal behavior, affecting energy efficiency and indoor comfort by allowing heat gain and loss. Well-designed, insulated windows enhance energy performance and occupant well-being. PCM window systems can capture and regulate radiation, impacting indoor thermal behavior. The window-to-wall ratio significantly influences natural ventilation, solar radiation penetration, and heating/cooling loads, making windows a key element in building envelopes [117]. When PCM is integrated with a transparent window system, normally, NIR (near infrared) radiations are absorbed, and the visible lights are transmitted inside buildings. This phenomenon can be achieved because some PCM, for example, paraffin wax, possess high optical properties [118]. PCM can be integrated in windows in different ways, as shown in **Fig.2.8,** including window cavity between glazing pane, window blinds, and frames.

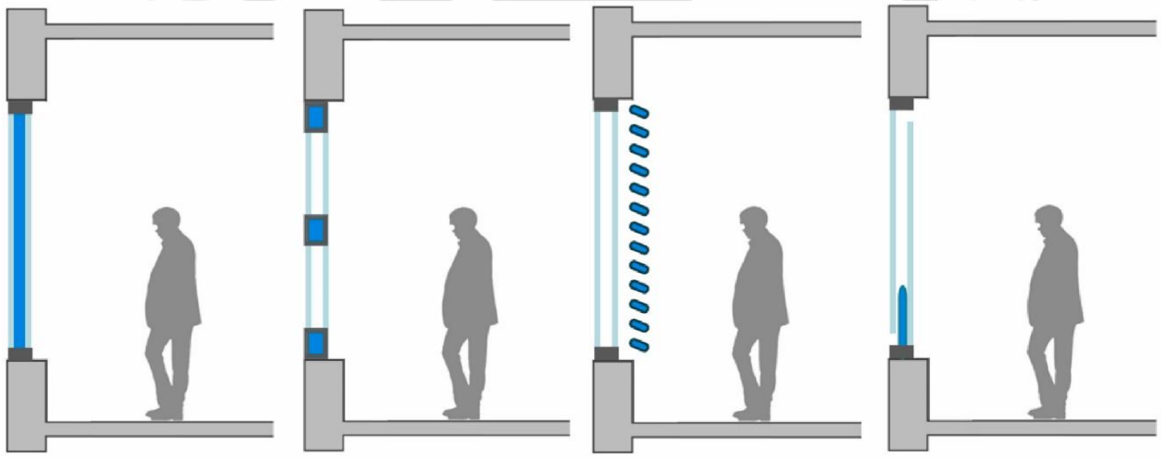

(a) Integration to window cavity | (b) Integration to frames | (c) Integration to sunshade components | (d) Integration to air vent heat-exchanger

Fig. 2.8 PCMs integration measures in windows [119]

To decrease the cooling load of summer and to increase the thermal resistance of the window, a double-glazed window (17 mm thickness) was filled with paraffin wax of melting temperature of 41°C and was compared with a traditional single glass window (6 mm thickness). The authors reported that the maximum temperature reduction was 8°C on the ground floor compared to the traditional glass window. The window frame also needs attention to reduce energy consumption during the cooling season. This type of work was done by Jiang *et al.*[120] where they compared thermal performance results among single-panel glass and three types of multilayer glass windows. Triple-pane glass with PCM frame gave the best results for their test climate in China. Li *et al.*[121] analyzed a novel laminated microencapsulated PCM blind system for a double skin façade to reduce overheating problems in warm seasons. The PCM blind was able to keep the temperature at that of the ambient in the summertime and performed better than the aluminium blind.

The modification of the window is an effective retrofitting solution for rural areas in extremely cold seasonal areas because of its easy installation, low operating cost, flexibility of operation, and easy maintenance. Integrating PCMs within windows does not consume additional space within the building, making it a space-efficient solution compared to other options. On the other hand, the low surface area of windows, compared to larger surfaces like walls or ceilings, limits the overall heat storage capacity of PCM. Also, the thermal comfort provided by the PCM window will largely depend on the wall-to-window ratio of a building, and only localized control of temperature may be achieved if the ratio is very high.

2.5.3 PCM on walls

In this section, three classifications of PCM integration on walls have been described separately. The first section discusses the PCM integration on inner walls, popularly known as wallboard or Gypsum board. The second section discusses PCM integration in concrete walls as an additional layer or within the construction material. The third section comprises the PCM integration techniques with bricks, which are later used for wall construction.

2.5.3.1 PCM on Wallboard

Diverse types of numerical and experimental analyses have been performed over the years on PCM wallboard performance for the thermal management of buildings [122,123]. Heat transfer in PCM-integrated wallboards is nonlinear, leading to a varied temperature distribution. A longer phase transition period can enhance thermal comfort as PCM changes phase within a narrow temperature range. Internal PCM walls can achieve more energy savings by charging when indoor temperatures exceed comfort levels and discharging when they fall below. PCM internal wallboard is more energy efficient than PCM external wallboard, and for that, increasing the heat of fusion is recommended [124]. Baetens *et al.* [125] identified three manufacturing methods for PCM wallboard. The first method involves incorporating PCM pallets during manufacturing. The second method is impregnation of PCM into wallboard panels, and the third is industrial manufacturing where PCM is mixed with gypsum slurry.

PCM impregnation during manufacturing via absorption was recommended for enhanced heat storage capacity.

Biswas *et al.*[126] tested a nano-PCM-based Gypsum wallboard (1.3 cm thick) under varying weather conditions in a natural exposure facility in cold climatic conditions. They manufactured nano-PCM with expanded graphite mixed with gypsum powder by 20% by weight and later cast it at room temperature to make the wallboard. The heat gain difference of 23.49% between gypsum wallboard and nano-PCM wallboard was obtained when the room temperature set points were 20-23.3^{o}C. Kong *et al.* [127] developed a composite PCM (60 wt.% % of Paraffin and 40 wt.% of Expanded perlite) with acrylate copolymer emulsion to provide extra protection for liquid leakage of PCM. The composite PCM board is incorporated both into the walls and the plate-type heat accumulator, and then installed into a prototype building of 1m^3 size. During the test period, buildings equipped with both passive and active systems experienced daytime temperatures of approximately 1°C cooler and night-time temperatures of 2.15°C warmer compared to buildings with only an active heating system. Lee *et al.* [128] developed a novel concept named plug and ply wall (PPW), which enables faster installation, dismantling and flexibility for different wall constructions in real climatic conditions. The authors tested PCM thermal board with molecular encapsulated paraffin of melting temperature 20.6^{o}C and found average daily heat transfer reductions of 27.4% and 10.5% for south and west-facing walls, respectively. Barzin *et al.*[129] performed experiments with PT20 PCM-impregnated gypsum board for a test hut in New Zealand (Auckland). At first, an AC unit was provided to discharge the PCM at night; after that, night ventilation using outdoor air was supplied for PCM solidification. A weekly electricity savings of 73% was observed when night ventilation was used for PCM discharging. However, the authors recommended this type of arrangement for office buildings rather than residential buildings, where comfortable temperatures had to be maintained for office hours only.

Lightweight steel construction is another emerging building construction technology in recent years because of its recyclability and reuse. The main drawback of lightweight steel construction is the low thermal mass and thermal inertia [130]. To mitigate this issue, PCM-incorporated drywall is a good option, with optimisation of the thermal properties of the PCM. Soares *et al.*[131] optimized multiple dimensions of PCM drywall for steel constructions for different climatic conditions using dynamic energy simulation. The authors considered seven different climatic conditions of European cities located in Spain, Portugal, Italy, France, Romania, Poland, and Sweden. An optimum thickness of 4 cm of PCM drywall was found to be suitable for all the considered climatic conditions. They gave the conclusion that PCM drywall was mostly suited for the Mediterranean climate (hot/ warm summer and mild winter).

PCM wallboard offers ease of installation compared to other PCM techniques. PCM-impregnated gypsum wallboard is resistant to fire due to its chemical composition. It absorbs heat by releasing bound water as steam, limiting temperature rise. With low thermal conductivity and non-combustibility, gypsum aids in fire prevention and structural protection. Ideal for lightweight construction, the system warrants further analysis for durability and cost-effectiveness, given the flexibility of wallboard replacement over time. Before installing PCM wallboards, the thickness, orientation, and position of the wallboard should be optimized along with the proper discharging process so that released heat does not flow to the interior of buildings, causing thermal discomfort.

2.5.3.2 PCM applied to concrete walls

The concept of PCM-integrated concrete involves incorporating PCMs into concrete to achieve enhanced thermal management properties, as shown in **Fig.2.9.** The methods of PCM incorporation in concrete can be primarily divided into two parts: direct and indirect methods. In the direct method, PCM powder or granules are directly mixed with concrete. Though this process is simple, it leads to severe concern regarding leakage of PCM, structural and thermal properties of PCM [132]. The indirect method involves encapsulating the PCM, as described in **Section 1.4.1**, and then incorporating it into concrete.

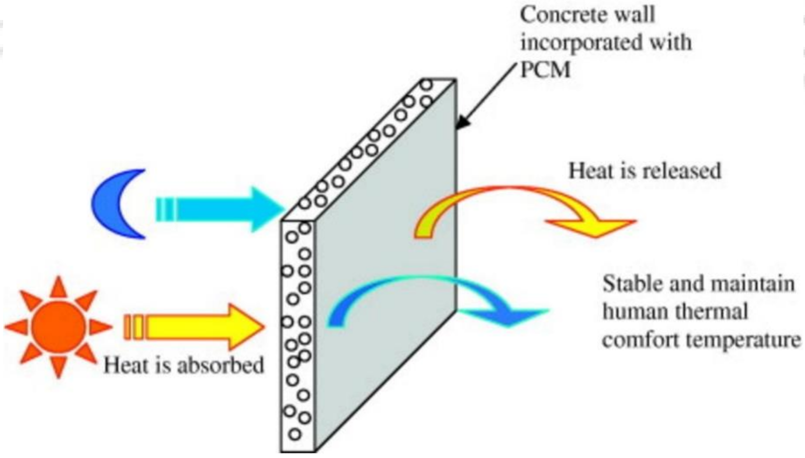

Fig. 2.9 The working principle of concrete walls incorporating PCMs [132]

Shi *et al.*[133] experimentally assessed the effect of position on macroencapsulated PCM on concrete walls for regulating indoor temperature and relative humidity. PCM was encapsulated with concrete in different positions, namely, externally bonded, laminated within, and internally bonded. The macro-encapsulation was done with a stainless steel box. It was found that PCM laminated within the concrete showed the maximum temperature reduction of 4^{o}C. This work proved that when PCM was inserted inside the wall, the best results in terms of temperature reduction could be obtained, but the inclusion of a stainless steel box was not a practical solution in terms of cost. Zeng *et al.*[134] fabricated a wall of size (800mm x 800mm) with shape-stabilized PCM consisting of paraffin, HDPE particle and expanded graphite powder. The prefabricated walls with four different thicknesses (10mm,20mm,30mm and 40mm) were compared against a common concrete wall. It was found that 30 mm thick shape-stabilized PCM wall with thermal conductivity of 0.2 W/mK was able to optimized energy saving by 35.83%. Castell *et al.* [135] performed a comparative study between five cubicles made up of only concrete, one with Polyurethane insulation and another two with two different PCM (RT-27 and SP-25 A8). A heat pump was employed for cooling purposes, and it was reported that the use of PCM reduced electrical energy consumption by about 15%. A peak temperature drop of 1^{o}C has been obtained with smoother temperature fluctuation throughout the day for the PCM rooms compared to the concrete room. Figueiredo *et al.* [136] evaluated the thermal performance of concrete incorporating PCM (Micronal DS5001) for the reduction of energy demand in buildings. The loss of strength of concrete incorporating PCM was 68% in compression and 51% in bending, with a slight increase in thermal behavior. In a study where PCM was encapsulated in a foamed concrete panel and installed on the exterior surface of a test room, a reduction of 9.75 °C in the interior temperature was achieved. The extra insulation provided by the air cavity with ventilation along the PCM concrete panel was beneficial in decreasing the overheating by 54% compared to the reference cell [137]. The same authors also concluded that increasing the thickness of the PCM-enhanced concrete panel to a certain extent and an appropriate phase transition temperature resulted in energy efficiency of buildings. Ten panel thicknesses (0.5–5 cm) were tested, where 3 cm was identified as the optimum thickness for maximum cooling load reduction of 25.1%. Thicker panels store more heat and reduce daytime heat gain but release more latent heat during solidification at night, which raises the minimum indoor temperature and increases the cooling load [138].

M'ziane *et al.*[139] studied the transient behavior of a plaster wall containing microencapsulated PCM using a finite differential method. The authors considered a 1D transient phase change with conduction. The conduction-controlled phase change enthalpy equation is the same as presented in **Eq.2.1**. The general enthalpy formula for the non-linear relation of phase transition considering the sensible and latent heat is also the same as described in **Eq. 2.2.** The authors validated the enthalpy model with analytical data and found that increasing the thickness of PCM plaster wall was beneficial for thermal comfort maintenance up to a certain value; exceeding which had no positive effect on thermal comfort.

The aforementioned investigations demonstrate that the internal temperature can be decreased passively by including PCM; however, the correct insertion technique needs to be adjusted for real-world uses. Along with that, the strength of concrete after PCM installation is another area to be investigated properly.

2.5.3.3 PCM integrated bricks

Bricks are the preferred construction material in terms of thermal behavior because of their high heat capacity and high thermal mass performance [37]. The red clay brick can maintain the indoor temperature fluctuation to a great extent, and the incorporation of PCM with brick may result in significant changes in the stabilization of indoor temperature. Lots of researchers around the globe have shown interest in PCM building blocks as a passive technology for attaining thermal comfort [140–145]. PCM needs to be encapsulated in some way before applying it directly to the buildings to prohibit leakage while melting from solid to liquid. Saxena *et al.* [146] found that proper differential scanning calorimetry (DSC) analysis is important for selecting PCM before embedding it into bricks.

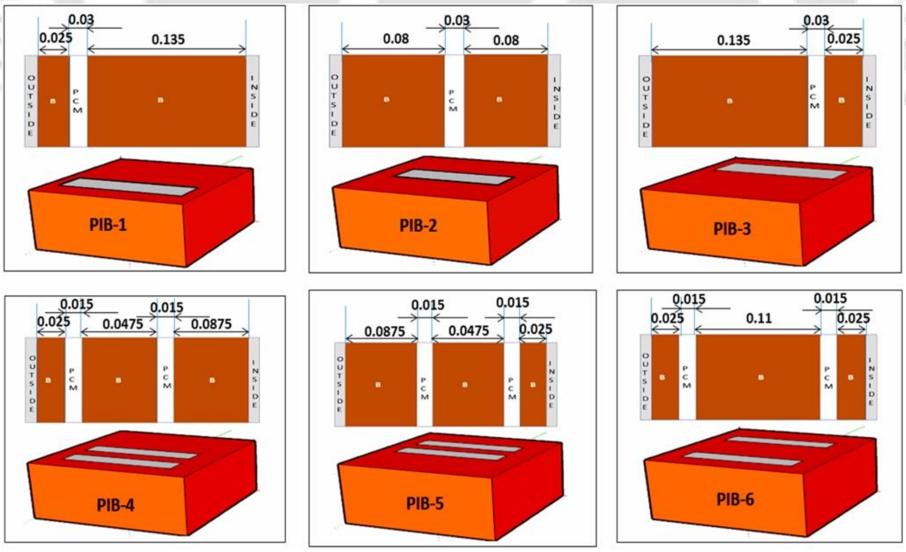

Fig. 2.10 Six different PCM configuration on burnt clay brick [147]

The application of PCM on bricks showed potential in maintaining a comfortable thermal environment, with an indoor temperature reduction of up to 6°C and a delay time of 4 hours. Also, the building energy consumption reduced by 3.12 %–56 % with the modifications of existing bricks compared to normal bricks [148]. Shaik *et al*.[147] studied the impact of different configurations of PCM (**Fig.2.10**) on burnt clay bricks to assess the cost-saving potential of air conditioning in buildings. Out of six different PCMs, OM29, with the configuration of PCM on the outside of the brick, showed the best results in terms of annual energy cost savings, carbon emission, and payback period. Also, their study explained that a higher latent heat of the PCM led to lower energy consumption of the air-conditioning system. Abbas *et al*.[149] conducted a study involving experimental and numerical analysis of using PCM capsules as insulation in hollow bricks for walls. The results demonstrated that PCM encapsulation significantly reduces room temperature fluctuations, lowers the inner surface temperature by about 4.7°C, and increases the time lag by 2 hours compared to untreated walls. Hamidi *et al*.[150] studied the effect of PCM on hollow brick walls in Mediterranean climates. The authors found that PCMs with a 26°C melting temperature can save up to 56% of energy for cooling in the North-East Mediterranean climate.

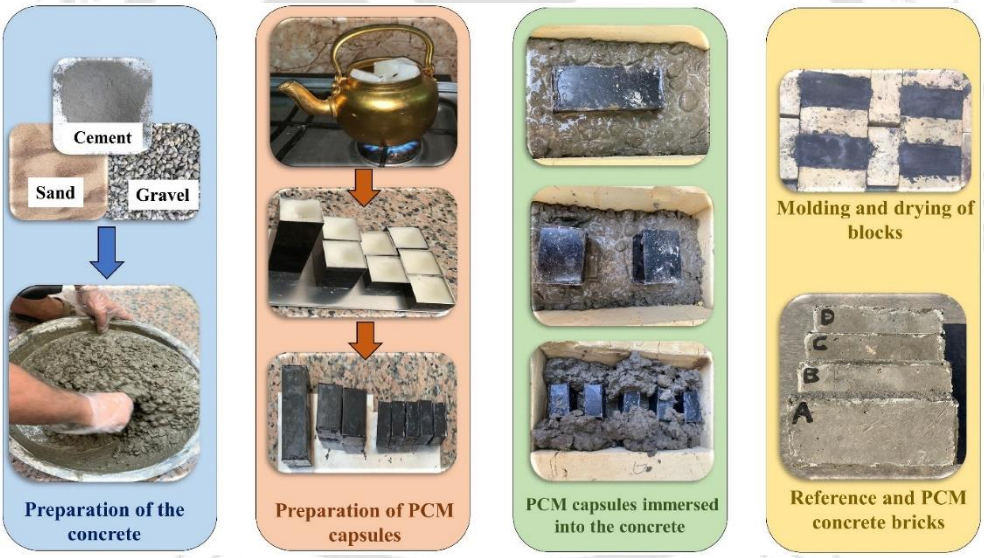

Fig. 2.11 Preparation of PCM concrete bricks

Saxena *et al*.[151] developed slotted PCM red bricks using Eicosane and OM35 and experimented on their temperature and heat flux profile under real conditions of peak summer in Delhi, India. The authors reported a temperature reduction of upto 10°C with PCM-incorporated bricks, where the thickness of PCM was 12 mm. Another study [143] by the same authors stated that a temperature reduction of up to 9.5°C and 6°C was obtained by dual and single PCM layer, respectively, within the brick. They recommended an auxiliary setup other than fins for night cooling of the PCM before increasing the thickness of the PCM layer. Yasiri *et al.* [152] produced four concrete bricks incorporating 1, 2, and 5 PCM capsules. The paraffin was melted, filled into aluminium capsules, solidified, and sealed with a 1 mm thick aluminium cap. Finally, PCM capsules were immersed carefully inside the concrete and left to dry naturally. The preparation method is shown in **Fig.2.11.** The thermal performance, expressed in terms of PTR (peak inner temperature reduction), HTRc (conductive heat transfer reduction), and TD (time delay), was evaluated to compare the PCM-integrated bricks with the reference brick. It was found that the PCM of high melting temperature can significantly improve the thermal performance of concrete bricks under maximum outdoor temperatures. An increase in the encapsulation area leads to greater temperature reduction, enhanced heat transfer mitigation, and longer heat delay time. The best PTR and HTRc were calculated for the brick with 5 numbers of PCM capsules as 156.5 % and 61 %, respectively.

Alawadhi [140] experimentally investigated a brick with cylindrical holes filled with PCM as a method for reducing the heat gain in buildings during working hours (7 am to 5 pm). Three PCMs were used: n-octadecane, n-eicosane, and P116. Out of these three, n-eicosane showed the best result as it reduced heat flux up to 24.2%. The location of PCM cylinders was also studied at a position of H/2, H/3, where the H/2 position(centreline) showed the best result with a heat reduction of 17.55% and other positions were not preferred because they could weaken the strength of the brick. The number of cylinders to be used has also been studied, and the reduction of heat flux was obtained as 11.5%, 17.9%, and 24.25% for using 1,2 and 3 cylinders, respectively.

The innovation of lightweight autoclaved aerated concrete (AAC) bricks is bringing remarkable changes in construction science as the bricks are cost-effective, environment-friendly, energy efficient, less dense, non-toxic, and more durable than traditional red bricks [153]. The AAC bricks can sustain the physical and mechanical properties (appearance, weight, and compressive strength) up to a temperature of 500^{o}C [154]. AAC brick is a green construction material, as the raw materials involved in this brick are 60-65% flyash, which is a waste generated from coal thermal power plants. As AAC bricks possess a higher strength-to-weight ratio, the dead load of the structure gets reduced, thus providing construction economy [155]. The low thermal conductivity of AAC bricks helps to maintain the inside thermal comfort of buildings, which in turn can save the electrical load for space cooling. There have been a few experiments where the thermal performance of AAC bricks has been further improved by using PCM. A study was performed by Punlek *et al.*[156] where the researcher performed experiments on PCM-coated AAC walls to examine the thermal effectiveness. The maximum temperature difference of 2°C was observed for the east wall between the tested AAC house and PCM coated house. The PCM-coated house was able to maintain the temperature below ambient temperature for 2 hours and 30 minutes longer than the reference house. Further, a savings of 25% of cooling load consumption was observed with a PCM-coated house, which is significant.

Table 2.1 summarize different works on PCM integration into bricks, highlighting the potential of temperature and heat flux regulation. Among the available PCM types, organic PCMs and inorganic hydrated salts are the most suitable options. The melting point is the key parameter that controls the heat transfer mechanism of PCM when incorporated into bricks. Improper selection of the melting point resulted in insufficient cooling and failure of temperature regulation. Also, a higher heat of fusion of PCM leads to dampening the heat flow, and thus is efficient for temperature maintenance within the comfort limit.

A study conducted by Gao *et al.*[148] revealed that although the research on the incorporation of PCM for building thermal management has been increasing over the last few years, the application of PCM for bricks still needs attention. As bricks are the main construction material for all heavyweight buildings, PCM modification in bricks can be a permanent solution in all aspects. Once built, bricks cannot be replaced, so the utmost test is a must for their durability and strength. Furthermore, a study highlighted the need for further research into optimizing PCM properties and addressing challenges such as risk of leakage, seasonal adaptability, flammability, and mechanical strength in building applications [157].

Table 2.1 Summary of literature review on PCM integration in bricks

Author name	**Objective of the study**	**Nature of the study**	**PCM used**	**Performance in terms of temperature regulation**	**Important findings**
Saxena *et al.*[146]	Thermal analysis of PCM incorporated bricks for Delhi, India	Experimental	Eicosane, OM35	4.5°C to 7°C temperature reduction	Reduction of heat flow of 8% and 12% for Eicosane and OM35, respectively, was found.
Mahdaoui *et al.* [158]	Thermal behavior analysis of PCM impregnating bricks under summer climatic conditions of Morocco	Numerical simulation	n- Nonadecane	Not mentioned	16 % PCM mass was optimized for an indoor temperature of 27.5°C for summer conditions PCM with melting temperature 32°C showed the best thermal performance
Younsi *et al.* [159]	Analysis of thermal performance for hybrid brick walls embedding PCM	Numerical simulation	Micro encapsulated PCM	2.7°C peak temperature reduction	Resulted in an 83% heat flux reduction when an additional insulation layer was added with PCM
Gao *et al.* [160]	Analysis of the thermal behavior of hollow bricks with PCM	Experimental+ Numerical	PCM with melting temperature 18°C–23°C	Temperature reduction was not mentioned; the highest delay time was 9.83 hours.	Inner cavities for PCM insertion were better for thermal performance Reduced peak heat flux by 26.07 W/m^2, but failed to reduce average heat flux

Dabiri *et al.*[161]	Latent and sensible heat analysis of PCM incorporated brick and cold and hot climatic conditions of Tehran, Iran	Numerical analysis	RT 35	Winter temperature: 19°C to 26°C, Summer temperature: 23°C to 32°C	In summer, 71% of the heat storage happened as latent heat, and in winter, 72% happened due to sensible heat
Li *et al.* [162]	Thermal performance analysis of PCM-based brick wall on mid-season and summer days	Experimental	Shape stabilized PCM (GH 20)	1°C peak temperature reduction with 2-3 hours delay (mid-season)	In mid-season days (March 29-April 30), the PCM was in a melting temperature range, providing minimum interior temperature fluctuation; but in summer, the PCM remained in a liquid state with no phase transition
Principi *et al.*[163]	Thermal analysis of hollow bricks with PCM and low emissivity coating	Experimental+ theoretical	Sodium sulfate decahydrate	Not mentioned	PCM led to a delay of about 6 h in the heat flux peak with a reduction of 25%
Kong *et al.*[164]	Performance analysis of the use of PCM on perforated bricks for cooling storage	Experimental	Capric acid	2.2°C overall temperature reduction	PCM panel on outside of the test room was 1°C and PCM panel on inside of the room was 2°C cooler than the reference room. Thermal lag of 2-3 hours has been noticed.
Chelliah *et al.* [165]	Analysis of terracotta bricks integrated with PCM for hot, dry and composite climatic conditions for India	Experimental + Theoretical	Organic PCM (OM 18, OM 29, OM 32, OM 37), Hydrated salt (HS 22)	Not mentioned	OM 32 was the most suitable option considering the thermoeconomic behavior

2.5.3.4 Key parameters affecting thermal management on walls

The key parameters that influence the functioning of PCM in building envelopes include melting temperature, PCM quantity and thickness, and PCM position [39]. A study conducted by Li *et al.*[162] aimed to evaluate the thermal performance of a west wall embedded with shape-stabilized PCMs, with a phase change range of 15.80–22.28 °C. The lower melting temperature range of the PCM degraded the thermal performance during the summer season, as the phase transition did not happen, and the cooling load was increased by up to 43.23%. The authors recommended PCMs with higher melting points (28–33 °C) for better thermal performance. A review study analyzed that when PCM is applied to bricks, with the combination of insulation or ventilation systems, it could increase the thermal lag by about 4 hours and significantly improve indoor thermal comfort by lowering wall and indoor temperatures. The authors recommended that PCMs should have phase change temperatures near ambient levels for optimal thermal performance and use thin-layer encapsulation for better heat transfer [166]. A study conducted by Wang *et al*. [167] using EnergyPlus concluded that the PCM melting temperature range of 22-26^{o}C was suitable for both winter and summer seasons, but the optimization of melting temperature is purely seasonal. During the summer, the east and west walls exhibit the greatest energy-saving efficacy, with the east wall model achieving a remarkable 27.78%, while in winter, the highest efficiency is observed in the south wall model with PCM22. Another simulation analysis based on EnergyPlus by the same researchers revealed that 30 mm PCM thickness with a melting point of 20^{o}C could save 20% electricity needed for air conditioning systems for buildings in Shanghai. However, the passive PCM-enhanced wallboard could not be satisfactory in the summer season due to insufficient solidification during the night [168].

A study conducted by Qu *et al.*[169] presented that the type of building envelope on which PCM was applied was the most influential factor according to multi-factor simulation analysis, followed by PCM layer layout, PCM type and PCM layer thickness. Their study confirmed that PCM should be applied to the part of the building envelope that receives the maximum solar radiation. Anter *et al*. [170] found that paraffin (RT-35HC) was able to reduce temperature and cooling energy by 3.4^{o}C and 66%, respectively, when placed with a thickness of 1.5 cm each, both from the inner and the outer sides of the wall. In the study conducted by Saeed *et al*. [171], an analytical and transient model was used to determine the temperature reduction with PCM (n-Eicosane, P116) bricks. The dimensions of the studied brick were 15 cm × 15 cm with a height of 10 cm. PCM holes were made with a dimension of 3cm×3cm. Increasing the number of holes enables higher PCM incorporation in the wall, thereby improving temperature regulation. The melting process completion time depends on the PCM type, the climate and the location. N-Eicosane completed the melting process faster than P116. N-Eicosane with four holes reduced the temperature by 53% as compared to a brick without PCM. Haghshenaskashani *et al.* [172] numerically studied a two-dimensional model for simulating and analyzing PCM (n- Octadecane) in order to minimize energy consumption in buildings. The authors got a temperature reduction of up to 32% with three holes of size (6 x 3 cm) for a brick size of 25×15×15 cm. The same work also reported that the location of PCM materials should be near the outdoor position for better performance.

Chihab *et al.* [173] examined the effect of four PCM filling rates (0%, 33.33%, 66.66%, and 100%) in the holes of clay bricks. The positions of holes in the brick are at h/2, h/3, and 2h/3The results showed that filling the central cavities with a PCM (melting temperature of 32 °C), combined with low-emissivity coating or insulation in the inner and outer cavities, provides the greatest enhancement in the thermal inertia of hollow clay brick walls. T. Mukram *et al.*[174] conducted a comparative experimental study on bricks integrated with macroencapsulated and microencapsulated PCM for cooling applications. The study used HS29 for macroencapsulation (placed at the center of the brick) and ME29P for microencapsulation (applied to the outer wall surface). The results showed that the centrally encapsulated PCM brick performed better during the heating cycle, while the microencapsulated PCM brick demonstrated improved performance during night-time cooling. Tuncbilek *et al.* [175] performed a numerical simulation study to evaluate the seasonal and annual performance of PCM-integrated bricks for the Marmara region of Turkey. The results indicated that positioning the PCM near the interior surface of the wall led to the highest energy savings. The impact was found to be more significant during the heating season compared to other periods of the year. Arumugam *et al.* [176] systematically reviewed the potential of different passive technologies, such as PCM, insulation, and natural ventilation techniques, in different climatic regions based on the Koppen-Geiger climatic classifications. PCM integration on the outer surface of the building for tropical and arid climates and at the middle or innermost layer for temperate and cold climates was recommended based on their study. Jin *et al.* [177] investigated the influence of salt hydrate PCM phase states (solid, partially melted, and fully melted) on the thermal performance of building walls. Their results showed that the PCM layer located after one insulation layer from the indoor environment was the optimum location for PCM layer installation. Their findings also confirmed that the optimum position was affected by both PCM properties and environmental conditions.

Table 2.2 represents recent studies examining the impact of PCM position and thickness on wall thermal performance and building energy savings. In most of the numerical studies, PCM is inserted as a separate layer between the brick and concrete, as it is the easiest method for analysis. For experimental investigations, PCM is incorporated into cavities located either in the brick units or in the wall assembly. Macroencapsulation of PCM is the most commonly used integration technique due to its ease of implementation in practical applications. The incorporation of the PCM layer is preferred at the outside of the brick in buildings for the proper utilization of the latent heat with the absorption of solar radiation during the day time. The PCM incorporation in the middle of the thickness of the brick provides optimum value both for mechanical strength and thermal performance. The effect of the thickness of PCM is very significant both for annual energy demand and economic benefits. A thicker PCM can reduce the heat flow up to a certain limit, after which the effect diminishes. Sometimes, rather than having a single layer of PCM, multiple layers on the walls can make the thermal performance better.

Table 2.2 Effect of PCM position and thickness on thermal performance of building wall

Reference	Type of work	Type of PCM	Component of the wall	Method for integration	PCM thickness (cm)	PCM position	Thermal performance		Energy savings	Key observations
							Temperature reduction (%)	Heat flux reduction (%)		
Li et al. [178]	Numerical	Enerciel 22	Separate the PCM layer between the brick and plaster	Not specified	1	Interior	Overall reduction of temperature fluctuation (specific value not given)	15.6	Not mentioned	▪ PCM with melting point closer to room temperature, with low thermal conductivity and positioned near the exterior surface provides better heat transfer reduction ▪ Thicker PCM reduces heat transfer more, but the benefit decreases as thickness increases
						Exterior		16.95		
					2	Interior		29.2		
						Exterior		30.2		
					4	Interior		46.82		
						Exterior		47.58		
Anter *et al.* [179]	Numerical	Paraffin (RT35 HC)	PCM layer between brick and mortar	Not specified	1		5.79		66 (when 3 cm PCM split as 1.5 cm from inside and 1.5 cm from outside	▪ PCM position close to exterior wall gives better results in terms of heat flux reduction
					2		13.4			
					3 (best)	Outer	18.84	77.33		
						Inner	13.91	57.33		
						Both inner and outer	21.15	64		
					4		19.42			
					6		20.86			
					8		20.86			

Liu et al. [180]	Numerical	Not mentioned	A layer in lightweight wallboard	Not specified		Inner	3.04	52.8		▪ PCM mainly acts as a thermal regulating medium rather than as an insulator ▪ Energy savings are not proportional to thickness, and thus increasing thickness is not efficient beyond a limit
					0.5	Middle	1.81	51.9		
					1 (best)	(Best)	3.65	63.4		
					1.5		5.4	66.82		
					2		7.24	69.56		
						Outer	3.07	53.2		
Arıcı et al. [181]	Numerical	Paraffin	A layer between concrete and plaster	Not specified	0.1 cm to 2 cm	Inner Outer	Not quantified	35-99%	Not directly mentioned	▪ The benefits of the PCM layer are possible up to a thickness of 12 mm, after which it decreases ▪ PCM layer near the interior wall is the best location for cooling conditions
Sahili et al. [182]	Numerical	Paraffin	A layer between brick and either mortar or gypsum plasterboard	Not specified	1.5	Inner Outer	Direct value not mentioned	Not given	13.77 12.59	▪ Multiple layers of PCM on walls are more efficient compared to a single-layer PCM in energy consumption reduction ▪ PCM placed near the interior showed the most cooling energy savings ▪ The south wall with PCM showed more energy efficiency

Sun et al. [183]	Numerical	Not specified	A wall layer sandwiched between insulation	Macro-encapsulation with polymer sheet	0.7	Near the interior	Not mentioned	65.83	Not mentioned	▪ When the indoor air is warmer, the PCM works best near the indoor surface ▪ Peak heat flux reduction increased with PCM thickness until an optimum, then declined
Shi et al. the [184]	Numerical	Inorganic-eutectic	Layer on wall	Macro-encapsulation	0.1 0.2 0.3	Not given	44.8 35.6 35.1	Not mentioned		▪ Applying PCM can effectively extend the thermal comfort duration from 26.7% to 94.1%
Jamal et al. [185]	Numerical	n-Eicosane	Brick cavities	Macro-encapsulated PCM in a plastic container		Inner Outer	Not mentioned Not mentioned	5.97 31.91	9 21	▪ The melting temperature of PCM has significant influence on thermal performance, which selection is based on local climatic conditions
Li et al.[186]	Experi-mental	Paraffin	As a wall layer between hemp concrete	Macro-encapsulated with a thin aluminium shield	2.12	Exterior Interior	-4.6 3.7	73 9	98.1 84.3	▪ The results were obtained using a combined PCM–air layer integration, rather than PCM alone ▪ Proposed a dynamic configuration, where the PCM layer can be repositioned along with the air layer, which adjusts the thermal resistance and temperature gradient between indoors and outdoors

Rathore et al. [187]	Experi-mental	Paraffin (OM37)	Horizontally placed tubes in the center of the concrete wall	Macro-encapsulation with aluminium alloy tubes	1.57	Middle	9.18	41.31	38.76	▪ Night ventilation was recommended for proper discharging of PCM; otherwise minimum indoor temperature at night was higher
Wang et al. [188]	Experi-mental	Shape-stabilized Paraffin	Bricks	SSPCM mixed with portland cement, yellow sand, and made in wooden moulds	12	Whole wall	Not directly mentioned	~26	24.32	▪ Reduced max interior wall temperature by ~0.2 °C with a time delay of 1-2 h
Gounni et al. [189]	Experi-mental	Paraffin	Cavity in walls	Composite PCM (polyethylene+ paraffin) as a flexible PCM panel	0.5	Inner	9.81	Not mentioned		▪ Influence of PCM on reduction of surface temperature was more effective when placed on the interior side of the wall ▪ For greater peak heat flux reduction, PCM should be positioned close to the heat source and distributed within the wall
						Outer	0.25	Not mentioned		
					1		Not mentioned	20.4	Not mentioned	
					1.5	Outside		26.6		
						Middle		29.2		
						Inside		26.3		
					2			31.8		

2.6 Techno-economic and environmental assessment analysis

The technical assessment of PCM usage in buildings primarily involves the study pertaining to thermal properties, integration technologies, compatibility, safety, and durability [190]. The published work on technical assessment studies has already been extensively discussed in the previous sections of this chapter. In this subsection, the focus area would be the economic and environmental analysis related to PCM integration in buildings. The economic assessment mainly concentrated on initial cost, operational cost savings, maintenance cost, payback period and lifecycle cost. Accordingly, the environmental analysis covers the study like net environmental benefits, resource use, embodied energy, greenhouse gas emission, and end of life [190]. The commonly used tools for assessing the techno-economic-environmental performance of PCM-integrated buildings include Life Cycle Assessment, energy simulation modelling, Life Cycle Cost Analysis, and Cost–Benefit Analysis [190].

2.6.1 Economic parameters and Carbon emission

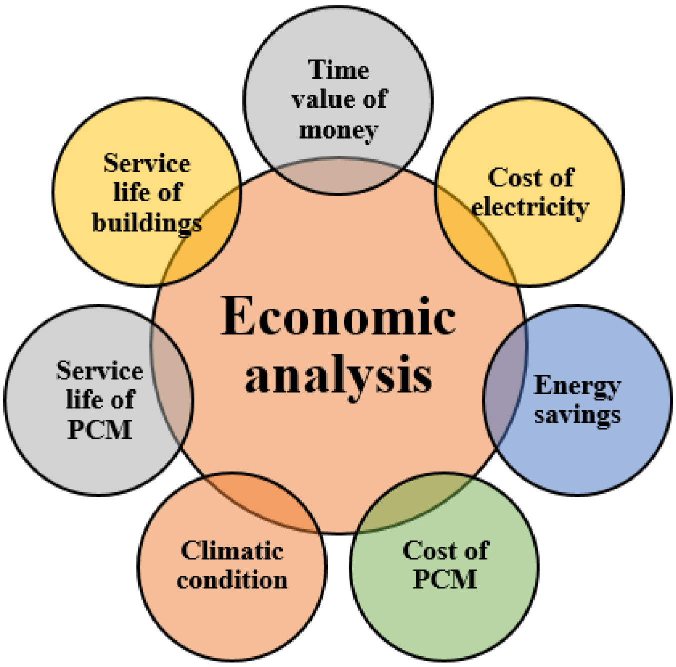

Fig. 2.12 Key parameters affecting the economic assessment [191,192]

Ahmad *et al.*[193] conducted a study to estimate the impact of PCM envelope on the energy, economic, and environmental performance of a residential mid-rise apartment building, considering 50 years of lifespan. The authors concluded several points in terms of the economic and environmental feasibility of the system. The first one is that the economic viability of

PCM-integrated buildings primarily depends on two key factors: the local electricity cost and the amount of energy savings achievable in a given city. The second conclusion is that compared to regions that rely heavily on renewable energy, cities or countries dependent on fossil fuels for electricity generation can achieve larger carbon-emission reductions for each unit of energy saved. The key elements that effect the economic feasibility and carbon emission of using PCM in buildings are highlighted in **Fig.2.12** and **Fig.2.13** respectively.

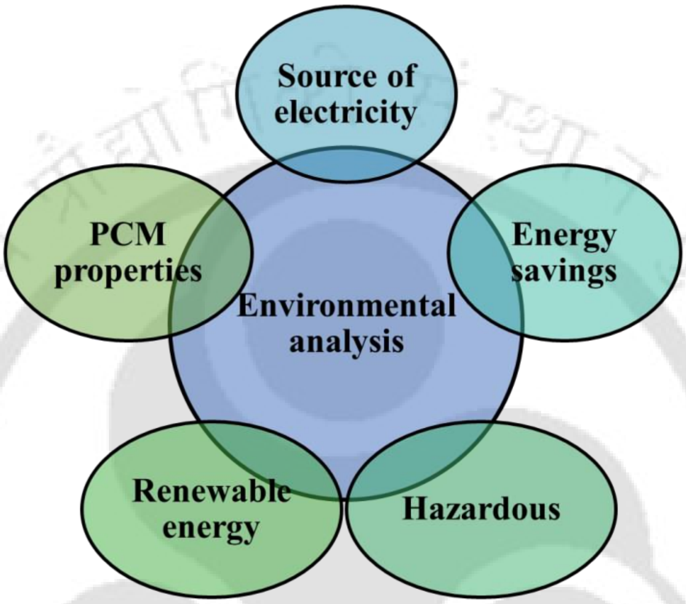

Fig. 2.13 Key parameters affecting the environmental assessment [191,192]

Some of the widely used economic parameters in the field of PCM integration in buildings are discussed in **Table 2.3**.

Agarwal *et al.*[192] analysed energy and economic performance of PCM integrated bricks for composite climatic conditions of India. Their results showed that the payback period is not feasible (ranging from 181 to 10,000 years), because PCM materials are very expensive (lab-grade), making the initial cost huge. Similar conclusions were reported from a study based on EnergyPlus analysis for a PCM-integrated multi-story building in five different regions of China [194]. A study conducted by Raheim *et al.* [195] also stated the same conclusion that although a thicker PCM layer was useful for energy saving in buildings, the corresponding payback period reached up to 57.6 years. They suggested adding an insulating layer along with a 1 cm PCM layer to the building envelope for both energy saving and cost benefit.

Table 2.3 Main economic parameters involved in PCM usage in buildings

Economic parameter	Definition	Formula
Static payback period (SPP) [196]	Time required for the initial investment needed for PCM integration in buildings to be recovered through the annual energy saving cost	$SPP = \frac{CPCM}{S} = \frac{\text{Total cost of PCM}}{\text{Energy savings} \times \text{Electricity cost}}$ $CPCM = (V \times \rho \times C_1) + (A \times C_2)$ $V = \text{volume } (m^3/kg)$ $C_1 = \text{cost}(\text{USD/kg})$ $A_s = \text{area } (m^2)$, the surface area of wall and roof $C_2 = \text{installation cost of PCM } (USD/m^2)$
Dynamic payback period (DPP) [197], [198]	Same as SPP, but DPP considers the time value of money	$DPP = \frac{\ln\left(\frac{S}{S - C_{PCM} \times I}\right)}{\ln(1+I)}$ $I = \frac{(1+i)}{(1+r)} - 1$ I = modified discount rate i_t = time value of money r = annual inflation in electricity tariff
Net Present Value (NPV) [198]	The difference between the present value of benefits and costs over the lifespan of the building	$NPV = \frac{S\{(1+I)^n - 1\}}{i\{(1+I)^n\}}$ N = life span of the building
Life cycle cost (LCC) [199]	Includes total cost over the entire lifespan from PCM manufacturing to operation cost	$LCC = IC + \left(\frac{1-(1+d)^{-n}}{d}\right)(EC_o + OM)$ IC = the initial investment cost for buiding materials EC_o = energy cost OM = operating and maintenance cost d = discount rate

Several economic analyses have been published in which EnergyPlus was used to compute the energy performance of buildings, and the resulting outputs were then used to determine the associated economic parameters. One such study confirmed that the most sensitive parameter for economic benefits is the thickness of the PCM layer and the density of the PCM, whereas thermal properties had the least effect on long-term economic benefits [197]. M'hamdi *et al.*[200] evaluates the energy, environmental, and economic performance of integrating PCM into different building envelopes across North African climates through EnergyPlus analysis. The environmental and economic analyses showed that, when applied optimally, PCM integration reduced energy costs by up to 10% and CO_2 emissions were lowered by 707 kg/year. The corresponding payback period ranges from 7 to 43 years for different climatic conditions, with an average of approximately 23 years.

Table 2.4 Carbon emission analysis through different stages

Stages	**Formula**	**Parameters used**
Manufacturing	Not mentioned	Not mentioned
Transportation	$E_{trans} = M_t LeC$	M_t = Weight of PCM Le = Transport distance C = CO_2 emission factor of the carrier
Construction	$E_{pro} = EF_{el} \frac{2H_B M_c}{3600VC}$	EF_{el} = Electricity emission CO_2 factor M_c = Weight of PCM lifted by hoist H_B = Building height v = lifting spped of hoist during PCM installati on G = Operating load capacity of hoist
Operation (considering only cooling energy)	$E_c = \frac{Q_c}{COP} \frac{EF_{el}}{(3.6\times10^6)}$	E_c = CO_2 emisssion due to annual cooling energy consumption Q_c = Cooling energy demand
Demolition	$E_{demol} = 0.9E_{pro}$	
Phase change layer disposal	$E_{dis} = E_{dis,trans} + E_{dis,pro} - E_{dis,tg}$	$E_{ds,trans}$ = CO_2 emission during transportation stage $E_{dis,pro}$ = CO_2 emission during disposal stage $E_{dis,tg}$ = CO_2 emission during recycling stage

Ji *et al.*[201] presented a study on the synthesis of PCMs suitable for energy saving and carbon reduction in building envelopes for a building lifespan of 30 years. Their study resulted in a reduction of CO_2 emission by 29.9 kg/m^2 after 30 years of using PCM-incorporated envelopes.

Zhang *et al.*[202] systematically analysed the different stages of carbon emission analysis, from the production phase to the recycling phase. The assessment adopts a cradle-to-cradle life cycle approach to evaluate the carbon intensity of PCM-integrated walls, covering manufacturing, transportation, construction, operation, demolition, and disposal stages, as mentioned in **Table 2.4**. No formula was mentioned for the manufacturing phase CO_2 emissions. Transportation emissions related to PCM transportation from the manufacturing site to the construction site. In the construction stage, emissions are simplified to include only hoisting electricity consumption. Operational emissions arise from heating and cooling energy demands over the service life of the PCM wall, which is again elaborated in the subsequent sections.

Abilkhassenova *et al.*[196] also evaluated the energy, environment and economic performance of PCM-integrated buildings. The environmental impact assessment was done by the reduction in CO_2 emissions due to PCM, and considered the carbon intensity of electricity generation from various fuel sources. **Eqs. 2.11-2.13** represent the energy contribution of each fuel source and carbon emissions savings.

$$E_i^{/} = RP_i \times ES\left(\mathrm{PCM}\right) \tag{2.11}$$

where E is the contribution to energy savings by a particular fuel source (kWh), RP is the relative proportion of a particular fuel source (%), $ES(PCM)$ is the energy savings obtained from PCM incorporation (kWh), and i is the particular fuel source.

$$E_n^{/} = RP_n \times ES\left(\mathrm{PCM}\right) \tag{2.12}$$

Here, *n* is the nth number of fuel sources.

$$CES = \sum_{i=1}^{n} E_i^{/} \times CI_i \tag{2.13}$$

Here, CES is the carbon emission savings $\left(kgCO_{2e}/year\right)$, and CI is the Carbon intensity of electricity generation $\left(kgCO_{2e}/year\right)$.

In conclusion, the economic feasibility of PCM-integrated buildings remains uncertain and highly dependent on multiple factors, highlighting the need for detailed financial evaluations. Future studies should prioritize low-cost PCM development, adopt dynamic payback approaches, optimize PCM use for different climates, incorporate electricity tariffs and service life, and apply comprehensive life cycle cost analysis.

2.6.2 LCA study

LCA is considered the most effective tool to analyse the environmental impact of any product. LCA study normally involves all the stages covering a product life cycle, i.e., raw material extraction, manufacturing process, transportation, maintenance and disposal or recycling [203]. The four main stages of LCA have been outlined in **Fig.2.14**. The goal of the LCA study highlights the reasons for conducting the LCA. The scope basically outlines the assumptions, methodological choices, functional unit, and system boundary of the study. The life cycle inventory involves the specific data collection pertaining to the study. The result interpretation reflects the conclusion and recommendation based on the selected goal and scope [204].

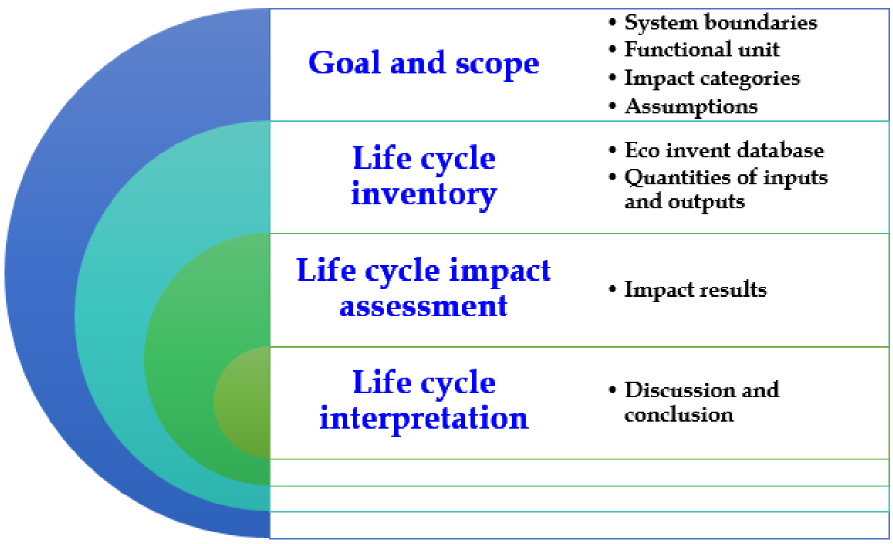

Fig. 2.14 Four stages of LCA study [203,204]

Three types of LCA studies are generally reported. Cradle to grave analysis involves raw material extraction to production, use, and end-of-life. Cradle to gate analysis includes only raw material extraction, processing, and manufacturing. Cradle to cradle is similar to cradle to grave, but the product is put for recycling in this analysis [205].

Fabiani *et al.*[206] tested palm oil as an alternative to the petroleum organic PCM, and performed the LCA according to the international standards of the ISO 14,040 series. The cradle to gate method was applied in the study, as no data were available for using palm oil in building thermal management. The results from ReCipe and IPCC analysis showed that raw palm oil had 5 and 10 times more impact, respectively, in terms of ecosystem and human health, compared to paraffin. This occurred due to the significant environmental impact of palm oil cultivation. Menou *et al.*[207] compared the environmental effect of replacing salt hydrate and paraffin with ester for the walls in a house-shaped experimental cubicle. Adding PCM increases the environmental impact during the manufacturing phase of the building, with esters causing a lower increase than paraffin, by about 6.1% for esters and 18.5% for paraffin. Antypa *et al.* [208] developed a compact storage module by encapsulating salt hydrate in an aluminium case. The authors analysed the hotspots that had a significant impact on the environment. Cradle to gate boundary approach was employed in the study. The manufacturing stage of macroencapsulated PCM contributed 5.81 kg CO_2 eq., and aluminium recycling had the highest impact above all. The authors concluded that if the recycled aluminium was replaced with new scrap and post-consumer scrap aluminium, the impact could be reduced by 46%. Castell *et al.* [209] developed and conducted LCA on two experimental cubicles, one with alveolar bricks and the other with macroencapsulated PCM. The primary goal of their study was to check whether the environmental impact caused by PCM manufacturing could be compensated for by the energy savings during the operational phase. When manufacturing and operational stages were combined, the PCM cubicle reduced the total environmental impact by 33.8% (ReCiPe 2016) and 34.5% (IPCC 2013 GWP100) compared to the reference cubicle. In another study, Vega *et al.*[204] assesses the environmental impact of incorporating PCMs into the envelopes of a lightweight building with dimensions of (2.5 × 2.5 × 2.43) m^3. A cradle to grave analysis was performed during the study, including manufacturing, operational phase and environmental payback period. The environmental payback period for their study was defined as the time when the environmental impact was equal for both the PCM and the reference building. Integrating PCM into the wall and roof of the lightweight building resulted in an 84.4% decrease in environmental impact over 20 years of lifetime. Also, the PCM integrated building reduced the environmental payback period by more than 15%.

In terms of environmental sustainability, PCM integration in buildings is a promising strategy. PCM mainly decreases the peak cooling load during the operational stage of the building, which in turn reduces related carbon emissions. The manufacturing of PCMs and their available incorporation technologies generally impose a higher environmental burden than conventional construction materials; however, when assessed over the entire building lifespan, the overall environmental impact is reduced. Current research indicates that bio-based PCMs with enhanced thermal properties represent the most sustainable pathways. Recycling of PCM is another scope of research to enhance the environmental profitability. Further detailed studies are needed to quantify environmental benefits regarding PCM usage in buildings.

2.7 Summary of literature review

Many existing modern buildings exhibit poor thermal performance, limited energy efficiency potential, and inadequate thermal insulation. PCM incorporation in such buildings can efficiently control the indoor thermal conditions with reduced energy demand. Numerous published works on that particular area have been reviewed in the above sections. The critical observations from the review work has been summarized below.

1) Organic PCMs are the most widely used PCM category for passive thermal management in buildings, followed by inorganic hydrated salts. Leakage of organic PCM is a very serious concern regarding building use, as leakage effects the structural integrity of the construction.
2) Physical and vacuum impregnation methods are the simplest, least expensive, and most widely used techniques for preparing form-stable PCMs.
3) Macroencapsulation technology is the most commonly used method for PCM incorporation in buildings. Considering the cost and heat transfer mechanism, this method is not efficient. Form-stable PCM composite is reported to be the best alternative.
4) As the performance of PCM is highly dependent on the diurnal temperature fluctuation for building applications, the passive system sometimes fails to complete the discharging process. In such cases, night ventilation or free cooling of the building is recommended by many researchers.
5) Single PCM with one melting temperature range sometimes is not useful for attaining thermal management, due to dynamic seasonal variation. An eutectic mixture of more than one PCM and other composite PCM with multiple panels should be incorporated in such cases.
6) In most published numerical studies on PCM applications in buildings, the PCM layer is modelled as a separate layer inserted between construction materials. In contrast, most experimental studies employ cavities, holes, or slots within bricks or concrete for PCM insertion.
7) The governing equation of PCM modelling in buildings is based on the basic transient heat conduction equation. To incorporate the phase change process of PCM, the basic

equation is modified using the enthalpy method. This process is observed to be followed predominantly in all the published literature.

8) PCM thickness, position and melting point are the three main selection criteria for PCM in building applications. The melting point should be selected based on the ambient temperature or human comfort range. Increasing PCM thickness improves thermal performance up to a certain limit, beyond which the performance degrades. The PCM position on the wall depends on the heating and cooling needs of the building, and it varies according to the climatic conditions and altitude.

2.8 Research gaps

Based on the rigorous literature review, the following research gaps have been identified regarding thermal management in buildings using PCM.

1) No literature has been found mentioning the appropriate and reliable method for the evaluation of the durability study of PCM before applying it in buildings. The studies related to long-term chemical, thermal, and mechanical stability of PCMs over thousands of thermal cycles are limited.
2) No published work has been found that utilizes biocomposite PCM as a building material for thermal management. Standard experimental test methods for evaluating the thermal performance, mechanical strength, bulk density, corrosion resistance, water absorptivity, fire resistance, and hygroscopicity of biocomposite PCM are not found in the open literature.
3) Extensive experimental work on PCM-integrated building envelopes is very limited. However, it has been noticed that numerical research in this area is dominating, which implies a tremendous scope for experimental study.
4) The study related to optimization of the PCM integrated building envelope by climatic conditions, specifically for the Indian climate, has not been found.
5) Very few experimental works comprehensively discuss the complete PCM charging and discharging cycle; while daytime melting has been widely investigated, the nighttime solidification process remains largely unexplored.
6) A comprehensive economic and environmental assessment study of a practical PCM-integrated building is not found in the published literature.

2.9 Thesis objectives

Based on the research gaps, the following objectives are formulated for the present study.

1) Development of biocomposite phase change material for thermal, chemical, and mechanical stability and its characterization
2) Development of biocomposite phase change materials-filled bricks for optimum thermal management
3) To analyse the thermal performance of biocomposite phase change material-filled brick walls for a hot and humid climate
4) Techno-economic analysis and life cycle assessment of the developed biocomposite phase change material for enhancing energy efficiency in real buildings

2.10 Summary of the chapter

In this chapter, a detailed literature review on form-stable PCM, bio-PCM, and thermal management of PCM in buildings has been discussed. Based on the review, it has been observed that bio-based PCM is highly encouraged in building applications for passive cooling; however, more studies are required on the preparation and detailed analysis in order to evaluate its sustainability. Focused studies on building envelopes have shown that applying PCM in walls yields the best results in terms of heat transfer reduction and temperature attenuation. Additionally, the effect of PCM position and thickness on the wall is a crucial parameter that varies with climatic conditions. Based on the review of literature, a summary of research gaps has been identified and reported. Considering the research gaps, importance, relevance, resources and strength, objectives of the thesis have been formulated. To address these objectives, methodologies are formulated and presented in the next chapter.

Chapter 3
Development and characterization of biocomposite PCM

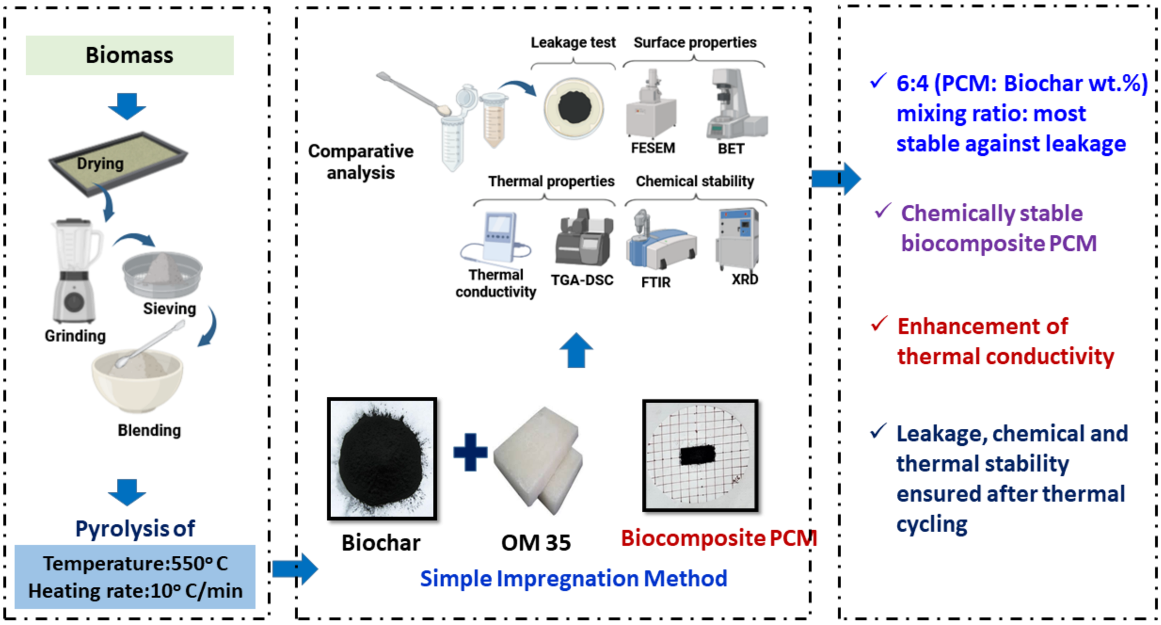

Outline

3.1 Introduction
3.2 Materials and method for developing biocomposite PCM
3.3 Characterization of the biocomposite PCM
3.4 Experimental investigation of thermal cycling stability of biocomposite PCMs
3.5 Results and discussion on characterization of biocomposite PCM
3.6 Results and Discussion on thermal cycling stability of biocomposite PCM
3.7 Summary of the chapter

3.1 Introduction

This chapter discusses the characteristics and applicability of eco-friendly and cost-effective biochar having high porosity for encapsulating organic PCM for building applications. The comparative analyses of the developed biocomposite PCMs have been conducted using four major characterization techniques such as leakage stability, chemical properties, thermal properties, and thermal cycling stability. The performed morphological, structural, chemical and thermal studies are also highlighted in the chapter.

3.2 Materials and method for developing biocomposite PCM

In the present study, biochar produced from water hyacinth (WH), yellow oleander (YO) and sugarcane bagasse (SCB) through the pyrolysis process has been used as an encapsulation material for the biocomposite PCM preparation. The selection of biomasses depends on the fact that WH plant adversely affects the aquatic lives of water bodies in rural areas; SCB is an agricultural waste, and YO is abundantly available in the locality. WH plant, YO plant (stem and leaves) and SCB wastes are collected from the locality of the IIT Guwahati campus (26.18^{o}N, 91.69^{o}E). After being cleaned, the collected biomass is oven-dried for 24 hours in a hot air oven (Make: Hamco, Model: 105 series) at a temperature of 105±2°C. The dried biomass is then ground to make a powder sample of particle size around 500 µm. The binary blend is produced by mixing two biomass (50:50 wt.%: wt.%), and the ternary mixture is produced by combining three biomass prior to pyrolysis in equal proportions (33 wt.% of each biomass). The pyrolysis is done at a temperature of 550°C with a heating rate of 10°C/min for a retention time of 1 hour, with the supply of Argon gas to provide an inert atmosphere. The same pyrolytic conditions are applied for all the co-pyrolysis processes to make the binary and ternary blends.

The PCM selected for making composite is organic material (OM35), having a nominal melting temperature range of 35-39^{o}C and thermal cycles up to 2000 cycles [210]. The organic PCM is purchased from Pluss Advanced Technologies, India [211]. The PCM-biochar composite material is prepared via the direct impregnation method. The PCM and the biochar are put in a glass beaker and sealed in the mouth of the beaker with aluminium foil. The glass beaker is then kept in a hot air oven for 16 hours at a set temperature of 50^{o}C so that proper melting of PCM can be ensured. The PCM–biochar mixture is stirred at an interval of 4 hours to achieve the desired homogeneity. After 16 hours, the samples are taken out from the oven, cooled to room temperature by natural air cooling, and packed in air-tight pouches for further analysis.

The stages of biocomposite PCM preparation are shown in **Fig. 3.1.**

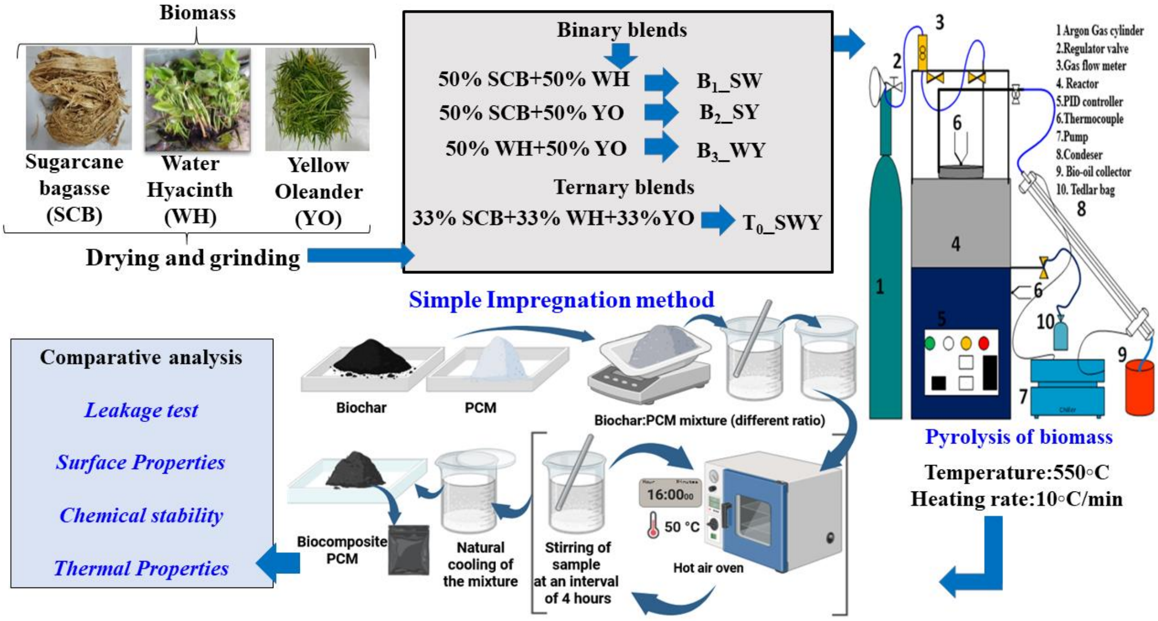

Fig. 3.1 Methodology for biocomposite preparation

3.3 Characterization of the biocomposite PCM

3.3.1 Leakage test

The leakage test is performed to check the best biochar to PCM mixture ratio out of six different blends of biochar and PCM. The mixture ratios selected for testing are 4:6, 5:5, 6:4, 7:3, 8:2 and 9:1 (wt.% of PCM: wt.% of biochar). The leakage test for all the biocomposite PCM samples is carried out by using cellulose filter paper (Whatman grade 1) of 11-micron size and 12.5 cm diameter. Gridlines have been drawn on each filter paper, which divides the circular filter paper into squares of 1 cm^2. The samples are placed at the center covering 8 cm^2 of the filter paper for the initial phase. Then the samples are kept in a hot air oven for 30 minutes at 40°C and observed for any leakage of the PCM material from the initial stage. A sample weight of 1.5 g is kept constant for every mixture composition. The mass loss percentage of each composition mixture has been calculated after 30 minutes with an analytical weighing balance (Make: Contech, Model: CAI-234). The mass loss percentage is obtained through the following **Eq. 3.1** [212].

$$\phi_{leakage}(wt.\%) = \frac{M_1 - M_2}{M_1} \times 100\% \quad (3.1)$$

where M_1 is the initial mass of the biocomposite PCM on filter paper, M_2 is the final mass of the biocomposite PCM on filter paper after 30 minutes.

The leakage of the PCM from the biochar matrix during melting is observed through visual inspection on the filter paper. The sample composition (PCM: biochar) with minimum leakage is selected for further characterization.

3.3.2 Characterization techniques

The bulk densities of the biochar and biocomposite PCM have been determined according to ASTM D1622-08 [213]. The surface morphologies of the materials are analyzed using Field Emission Scanning Electron Microscope (FESEM) (Make: Zeiss, Model: Sigma). The surface area, pore volume and pore size of all the biochar is determined through BET surface area analyzer (Make: M/s Micromeritics, U.S.A, Model No: Tristar II). Crystallinity and phase change identification are analyzed using X-ray powder diffraction (XRD) (Make: Bruker, Netherlands, Model No: D8 Advance). The XRD measurements are done using Cu Kα (λ = 0.05°/s, 1.54 Å) radiation. A step size of 0.05° in the two-theta degree range of 10° to 70° is employed while scanning the samples. Functional groups are identified by a Fourier transform infrared spectrometer (FTIR) (Make: PerkinElmer, Singapore, Model: LS 45). The scanning range is from 4000 cm^{-1} to 500 cm^{-1}. The thermal conductivity is measured using the KD2 Pro thermal conductivity meter, which has a needle length of 10 cm and a diameter of 2.4 mm, with a measurement range of 0.02 to 2.00 W/mK. For each sample, 110 g PCM-biocomposite is taken in an acrylic container of diameter 60 mm and height of 55 mm, and compacted in three-layers by applying a static load of 0.1 kN using a proving ring and loading frame so that uniformity of each sample can be maintained [214]. The thermal conductivity of biochar is determined using a KD2 Pro dual-needle SH-1 sensor, with a needle length of 30 mm, a diameter of 1.3 mm, and a probe spacing of 6 mm. 60 g of each biochar sample is taken in an acrylic mould of 60 mm diameter and compacted as the same way like the biocomposite PCM. Thermal stability is determined using a high-temperature Thermo Gravimetric (TG) System (Make: Netzsch, Model: STA449F3A00) at a heating rate of 10°C/min from 30^o to 500°C using Nitrogen. The Differential Scanning Calorimetry (DSC) experiments are performed using Mettler Toledo DSC 3 instrument at a heating rate of 10°C /min for a temperature range of 25-95°C. Pure nitrogen gas is used for purging during the DSC analysis. The heat flow rate with change in temperature is obtained for the samples in the endothermic mode during the DSC analysis.

3.4 Experimental investigation of thermal cycling stability of biocomposite PCMs

The thermal cycling test involves an investigation into the stability of PCMs by comparing the physical, chemical, and thermal properties. The material selected for the thermal cycling test is WH-PCM, T_0_SWY-PCM, and the parent PCM (OM35). The study introduces a cost-effective thermal cycling chamber as a novel development and employs various characterization techniques to assess the properties of the PCMs before and after thermal cycles.

3.4.1 Development of thermal cycling experimental set-up

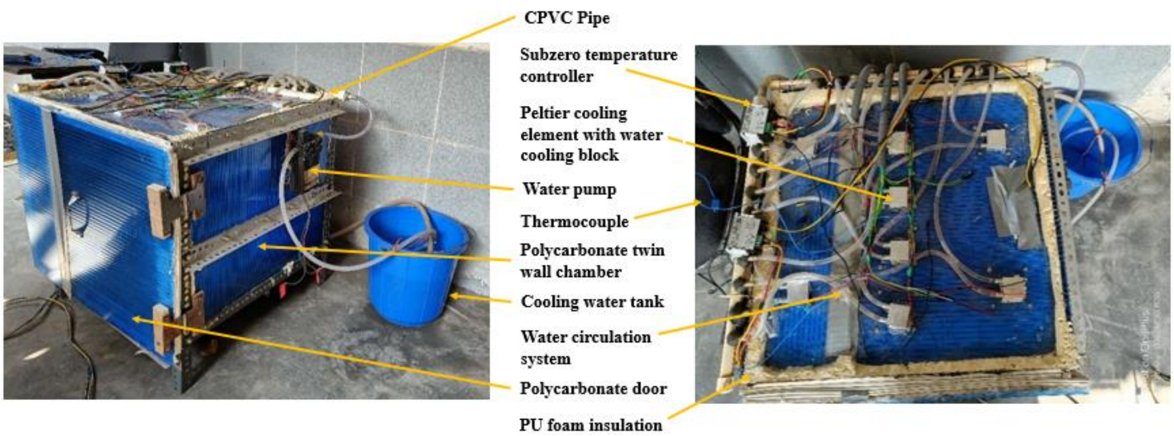

Fig. 3.2 Developed thermal cycling chamber

Table 3.1 Design parameters for thermal cycling chamber

Chamber dimensions (Inner)	:	✓ 500 mm × 600 mm × 600 mm (H × W × D)
Cabinet walls	:	✓ Polycarbonate twin-wall sheet (10 mm thickness)
Door	:	✓ Polycarbonate twin-wall sheet (10 mm thickness) with magnetic and rubber sealant
Insulation	:	✓ 3 cm glass wool (thermal conductivity: 0.040 W/mK)
Heating element	:	✓ One incandescent bulb (150 W)
Cooling system	:	✓ Peltier cooling element: 8 numbers (Model no. 12706, 12 V) ✓ Water cooling block: 8 numbers (40 mm x 40 mm x 12 mm) ✓ Aluminum heat sink radiator: 8 numbers (40 mm x 40 mm x 20 mm) ✓ DC water pump and Fan (12 V) ✓ Pipe (CPVC ¾ and silicon 10 mm thickness) and connector
Temperature controller	:	✓ Sub-zero temperature controller (Model no. SZ7529T)

Thermal cycling chambers are used to observe the effects of temperatures on a product or material in varying temperature ranges. Though commercial thermal cycling chambers are available in the market, the high installation cost is a big challenge that needs the attention of the scientific community. The current study describes the design and development of a simple, inexpensive and light-weight thermal cycling chamber to simulate natural climatic conditions and perform tests involving simultaneous heating and cooling, as shown in **Fig.3.2.** The key design parameters of the thermal cycling chambers are listed in **Table 3.1.** The detailed design procedure and calculations are presented in **Appendix I.**

3.4.1.1 Heating and cooling rate in the thermal cycling chamber

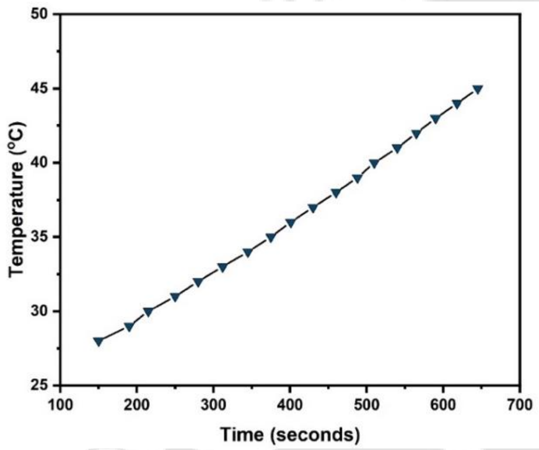

Fig. 3.3 Temperature variation inside the chamber w.r.t. time during heating mode

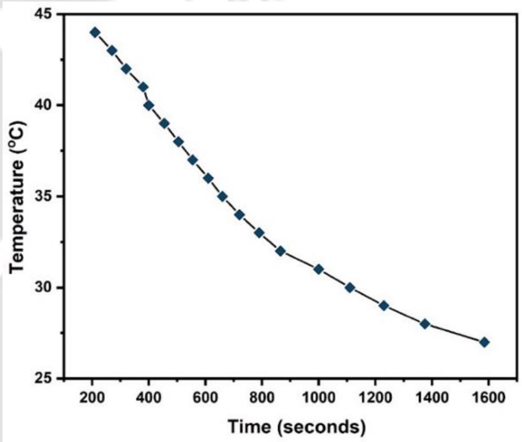

Fig. 3.4 Temperature variation inside the chamber w.r.t to time during cooling mode

Fig.3.3 and Fig.3.4 represent the temperature variation inside the thermal cycling chamber during the heating and cooling modes. The heating rate inside the chamber is 1.6^{o} C/min. The cooling rate inside the chamber is 0.6^{o} C/min. **Table 3.2** shows the comparison of the main parameters of the developed chamber with a commercial chamber. The cost of the chamber is significantly reduced with a comparable heating and cooling rate.

Table 3.2 Comparison of the developed and commercial thermal cycling chambers

	Developed thermal cycling Chamber	**Climate thermal chamber (STERICOX™)**[215]
Inner dimensions (H×W×D)	$500\,mm \times 600\,mm \times 600\,mm$	$850\,mm \times 600\,mm \times 800\,mm$
Temperature Range (^{o}C)	25 to 50	-20 to 150
Heating rate (^{o}C/min)	1.6	2.0-4.0
Cooling rate (^{o}C/min)	0.6	0.7-1.0
Cost of the product (INR)	65,000 (manufacturing cost)	12,65,000.00 (market price)

3.4.2 Thermal cycling test method

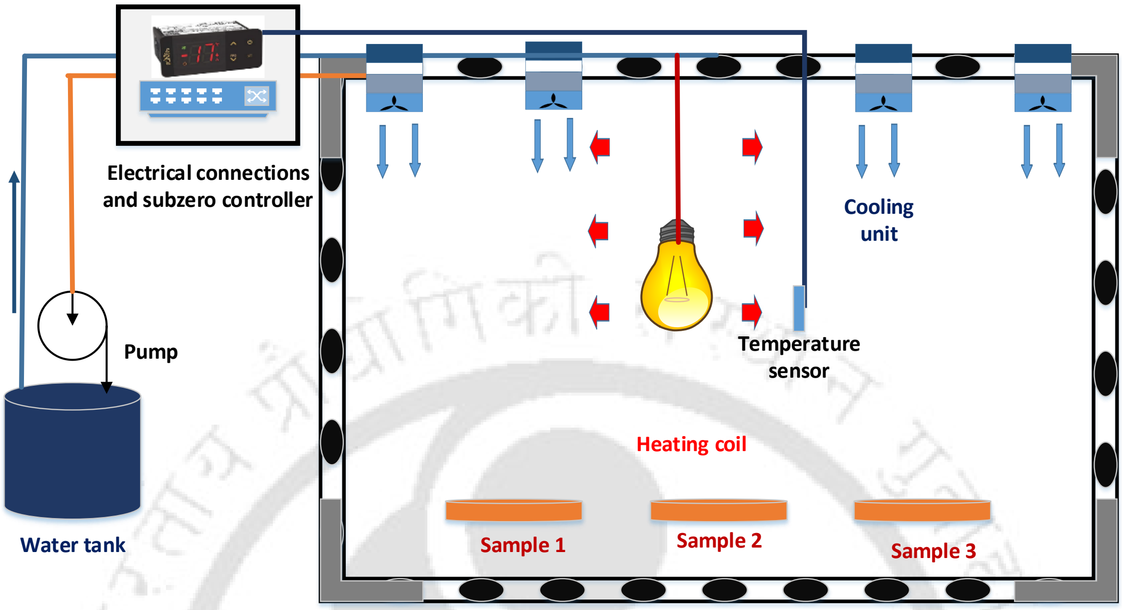

Fig. 3.5 Schematic of thermal cycling test

In the experimental procedure, each PCM, weighing approximately 25 g, is placed on a glass plate within a thermally insulated chamber, as shown in **Fig.3.5**. The PCM undergoes a cycle where it is heated above its melting point and then cooled below the solidification temperature. This process constitutes one cycle, with the chamber temperature maintained between 25-45°C. Immediate cooling follows complete melting, and each charging and discharging cycle lasts for 180 minutes. The experiments encompass 500 cycles, and samples are extracted after the 50^{th}, 100^{th}, 150^{th}, 200^{th} and 500^{th} cycles for future analysis. The PCMs are labelled as WH-PCM_0, T_0_SWY-PCM_0, WH-PCM_500, and T_0_SWY-PCM_500, indicating the number of completed cycles for each respective PCM.

3.4.3 Characterization of the selected biocomposite PCMs after thermal cycling

The procedure for the leakage test and characterization is already described in previous **Sections 3.3.1** and **3.3.2**. The leakage stability of the PCMs is performed on filter paper (Whatman grade 1) of 11-µm size and 125 mm diameter. The surface morphologies of the materials are analyzed using Field Emission Scanning Electron Microscope (FESEM) (Make: Zeiss, Model: Sigma 300). The crystallinity of the materials has been investigated through a

9KW Powder X-ray diffraction (XRD) System (Make: Rigaku Technologies, JAPAN, Model: Smartlab). The Fourier Transform Infrared (FTIR) spectra to know the functional groups of the material are obtained through an IR Spectrophotometer (Make/model: Thermo Fisher Thermo Nicolet iS10). The different thermal properties are measured through differential scanning calorimeter (DSC) analysis (Make: TA Instruments, Model: DSC 25) with a heating rate of 10^{o}C/min. The accuracy analysis of the major instruments has been added in **Table 3.3.**

Table 3.3 Accuracy of major testing instruments

Instrument Name	**Accuracy of the instrument**
Hot air oven	±0.2^{o}C
Weighing balance	±0.001 g
Thermal cycling chamber	±0.25^{o}C
X-Ray Diffractometer	±0.00004^{o}
Differential Scanning Calorimeter	Temperature: ±0.1^{o}C, enthalpy: ±0.1%

3.5 Results and discussion on characterization of biocomposite PCM

3.5.1 Leakage test results

The leakage test determines the percentage of shape stability of pure PCM obtained after the composite formation, which is very important for the practical applicability of the composite PCM. **Figures 3.6 and 3.7** show the leakage test photographs of the area covered by different compositions and the mass loss of each composition, respectively. No leakage can be visualized with compositions 4:6 and 5:5. For the mentioned compositions, the mass of biochar is more compared to PCM, so the mass of PCM is insufficient to be dispersed into the biochar matrix. The composite formation is incomplete for the compositions 4:6 and 5:5. A very small amount of liquid traces can be observed with the 6:4 compositions, with a mass loss of 9.75%. Minimum leakage is observed with the 6:4 composition because the porous biochar protected the melting of PCM through capillary action and surface tension force [216].

Initial state | **Leakage after 15 minutes** | **Leakage after 30 minutes** | **Initial state** | **Leakage after 15 minutes** | **Leakage after 30 minutes**

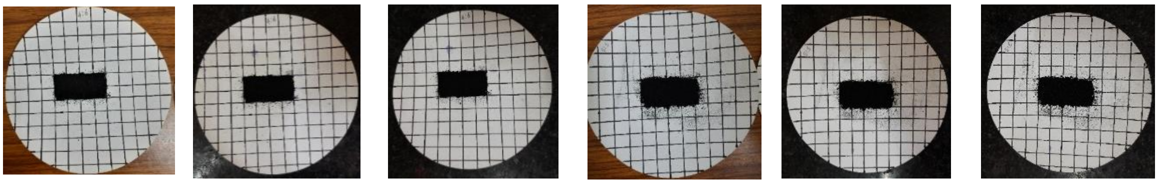

(a) 4:6 composition (b) 5:5 composition

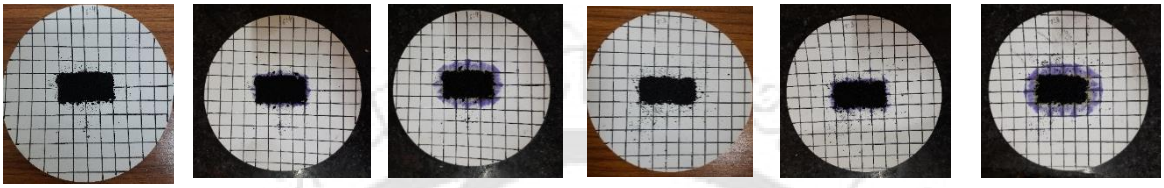

(c) 6:4 composition (d) 7:3 composition

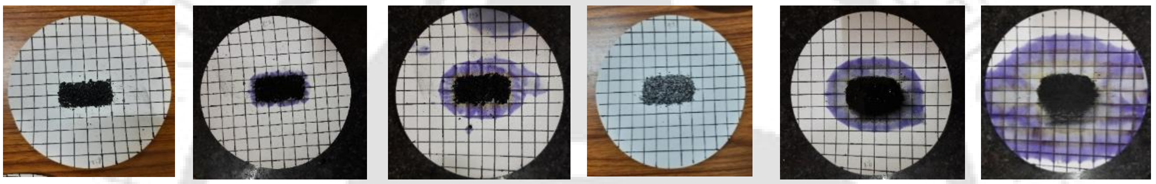

(e) 8:2 composition (f) 9:1 composition

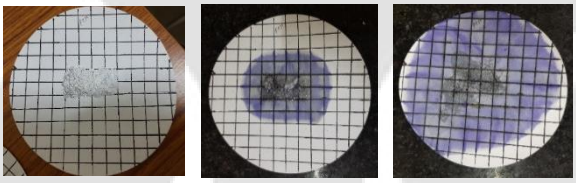

(g) OM 35

Fig. 3.6 Extent of leakage of the different compositions (a) 4:6 mix, (b) 5:5 mix, (c) 6:4 mix, (d) 7:3 mix, (e) 8:2 mix, (f) 9:1 mix, (g) OM 35

The different organic surface functional groups (E.g., Ketones, Hydroxyl, and Pyridine) present in the biochar form hydrogen bonding and van der Waals forces with OM35 and thus prevent excessive leakage [217,218]. The other three samples with higher PCM content (7:3, 8:2, 9:1) showed a noticeable amount of leakage. The composition 9:1 saturated almost the entire filter paper with liquid PCM traces, and the highest mass loss is observed with that particular composition. This is due to the fact that the amount of OM35 is excessive compared to biochar, and so the biochar is unable to encapsulate the PCM in the pores. As composition 6:4 is best in terms of formation stability on filter paper and negligible mass loss, it is selected for further experimentation for all the biocomposite PCM.

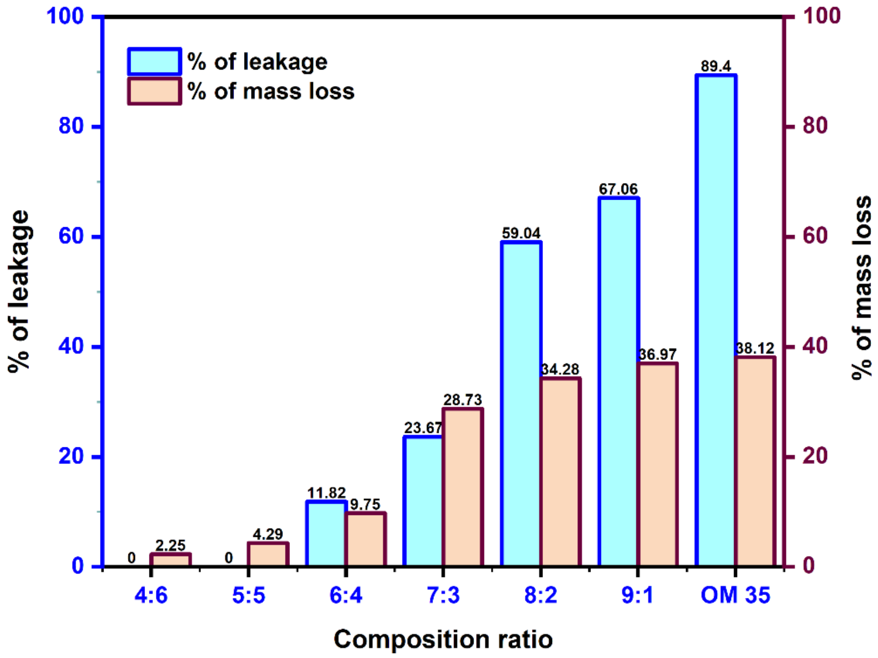

Fig. 3.7 The percentage mass loss of different compositions during the leakage test

3.5.2 Physical property analysis

3.5.2.1 Bulk density analysis

Table 3.4 The bulk density of the biochar and their respective biocomposite PCMs

Encapsulation material	Density (kg/m^3)	PCM	Density (kg/m^3)
SCB biochar	119.497±0.004	SCB- PCM	425.506±0.015
WH biochar	152.300 ±0.007	WH- PCM	510.215±0.004
YO biochar	240.193±0.008	YO -PCM	580.196±0.004
B_1_SW biochar	139.596±0.011	B_1_SW-PCM	440.293±0.004
B_2_SY biochar	183.170±0.007	B_2_SY-PCM	364.156±0.004
B_3_WY biochar	146.039±0.001	B_3_WY-PCM	371.493±0.008
T_0_SWY biochar	197.503±0.004	T_0_SWY- PCM	440.320±0.012

Table 3.4 shows the apparent bulk density of both the encapsulating material and its respective biocomposite PCM. Higher bulk density indicates higher volumetric energy storage densities for a specified space, and YO-PCM showed the highest bulk density among all the composite PCMs. The increased bulk densities of the biocomposite PCM compared to those of their respective biochar show that PCM is entrapped in the pores of the biochar matrix during composite formation.

The mesoporous structure of biochar is highly appreciated as a scaffold material, as the microporous structure negatively affects the thermal storage capacity of PCM, and the macroporous structure provides less capillary force. Moreover, the active hydroxyl group present in biochar enhances the sorption capability of the PCM. It is expected that biochar-based carbon material will increase the loading ratio of PCM, thereby increasing the thermal properties of composite PCM [219].

3.5.3 Morphology and porosity analysis

3.5.3.1 BET analysis

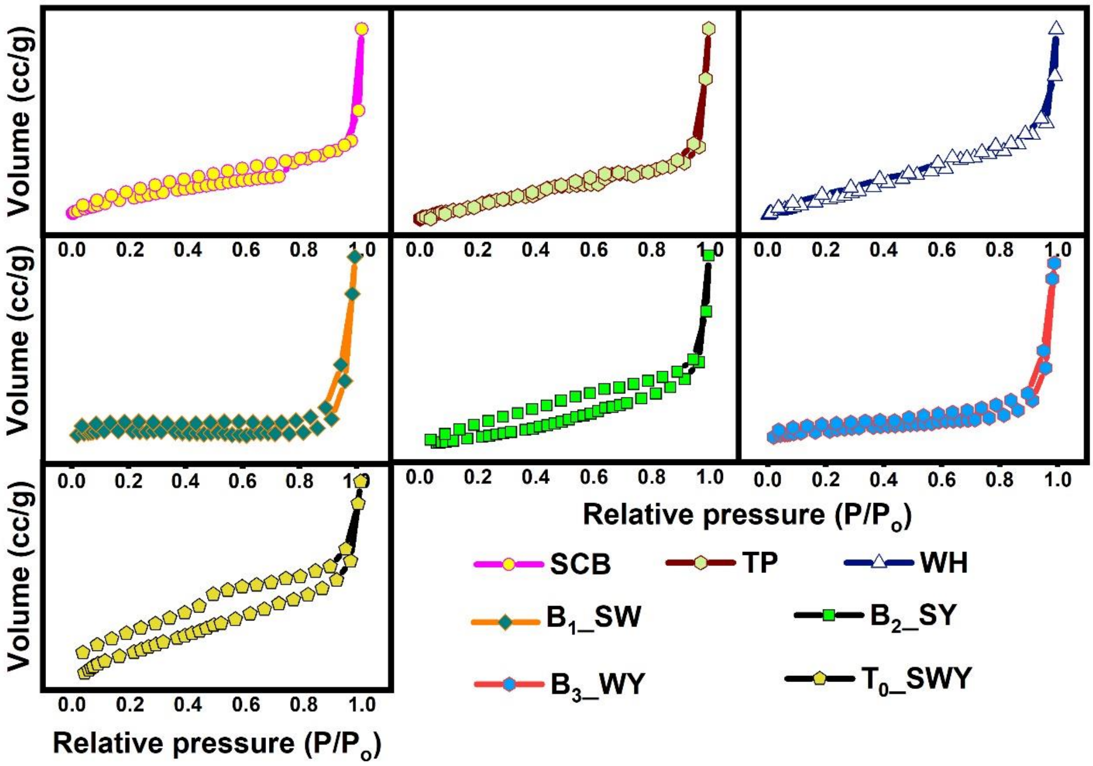

Fig. 3.8 Nitrogen adsorption-desorption isotherms for seven biochars

The biomass-based porous carbon with a high specific surface area used as an encapsulating scaffold is capable of absorbing a large amount of PCM. The N_2 adsorption and desorption experiment investigated the BET-specific surface area and pore-size distribution of the prepared composite. The isotherms, as shown in **Fig.3.8,** can be categorized under type II/IV isotherm, confirming the presence of wide mesopores; the highest adsorption value is found at a relative pressure (P/P_o) of 0.95-1.0 [220]. The mesoporous structure is the most preferred option as an encapsulating medium because the presence of too small pores (microporous) results in molecular motion hindrance, thus hampering desired thermal performance, and too large (macrospores) pores cannot offer liquid stability of molten PCM [221].

Table 3.5 BET analysis and comparison of different encapsulation materials

Encapsulation material name	**S_{BET} (m^2/g)**	**Pore Volume (cm^3/g)**	**Pore size (nm)**	**References**
SCB	17.78	0.025	12.86	This study
YO	14.37	0.018	13.62	This study
WH	14.00	0.042	11.92	This study
B_1_SW	1.80	0.020	28.14	This study
B_2_SY	4.99	0.019	3.71	This study
B_3_WY	2.54	0.015	3.71	This study
T_0_SWY	16.09	0.039	3.18	This study
Rice husk	8.57	0.015	3.84	[222]
Miscanthus Straw	37.20	Not given	Not given	
Oilseed Rape	77.60	0.23	1.5-16.81	[220]
Sewage Sludge	7.40	0.03	1.5-16.8	
Raw diatomite	19.06		2.50	
Purifieddiatom frustules	35.05	Not given	3.11	
sintereddiatom frustules	228.28		14.52	[223]
Natural Sepiolite 1	18.91		18.95	
Natural Sepiolite 2	10.89		10.79	
Natural Sepiolite 3	63.52	Not given	19.81	[224]
Treated Sepiolite 1	20.37		16.46	
Treated Sepiolite 2	15.18		8.15	
Treated Sepiolite 3	105.35		14.95	

Table 3.5 compares the pore size values of different encapsulating media, and the developed biochars show a similar pore size distribution as found in the literature. All the pores are in the mesoporous range (2-50 nm) because of the wider opening of the feedstock due to the powdered particle size of all the biomasses. The tubular structure of lignocellulosic biochar makes it richer in microporosity, thus a suitable candidate for the impregnation method [225]. At 550^{o}C, dehydration of cell structure happens, contributing to the small pores. The study also revealed that at a heating rate of 10^{o}C/min, the volatile matter is released from the surface of

biomass, and thus, an open fiber structure is formed, and cavities within biochar can be seen [226]. The highest surface area is found in the T_0_SWY-PCM sample because of the presence of a comparatively smaller pore size among the seven samples. The pore size of blended biochars (except B_1_SW) results in a smaller pore size, which may be caused by the decomposition of one biomass that may cover the pores of the other biochar, resulting in pore blockage [227]. According to the BET values, three biochar samples (WH, SCB and T_0_SWY) are recommended as impregnation media based on their higher surface area and pore volume.

3.5.3.2 FESEM analysis

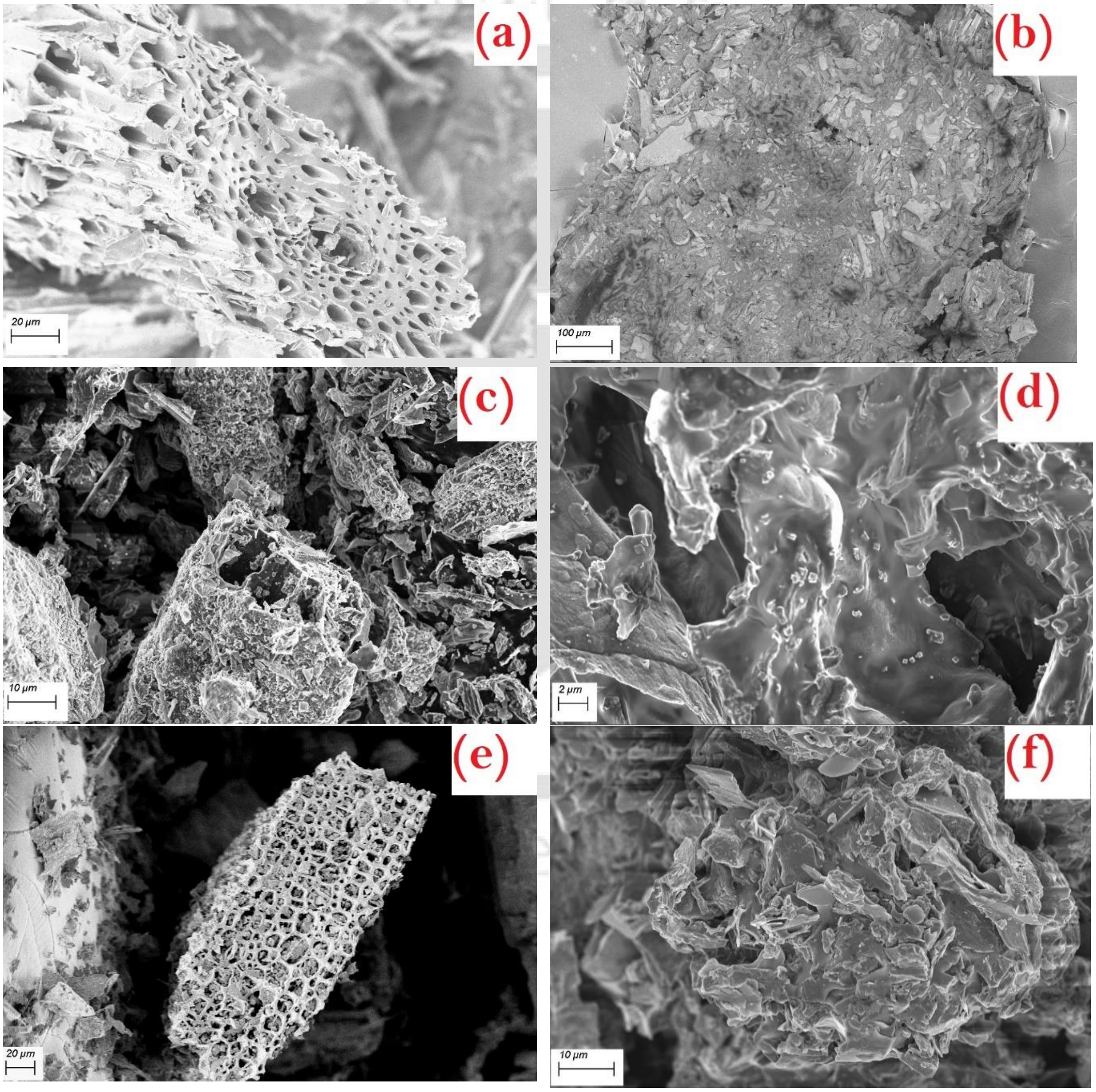

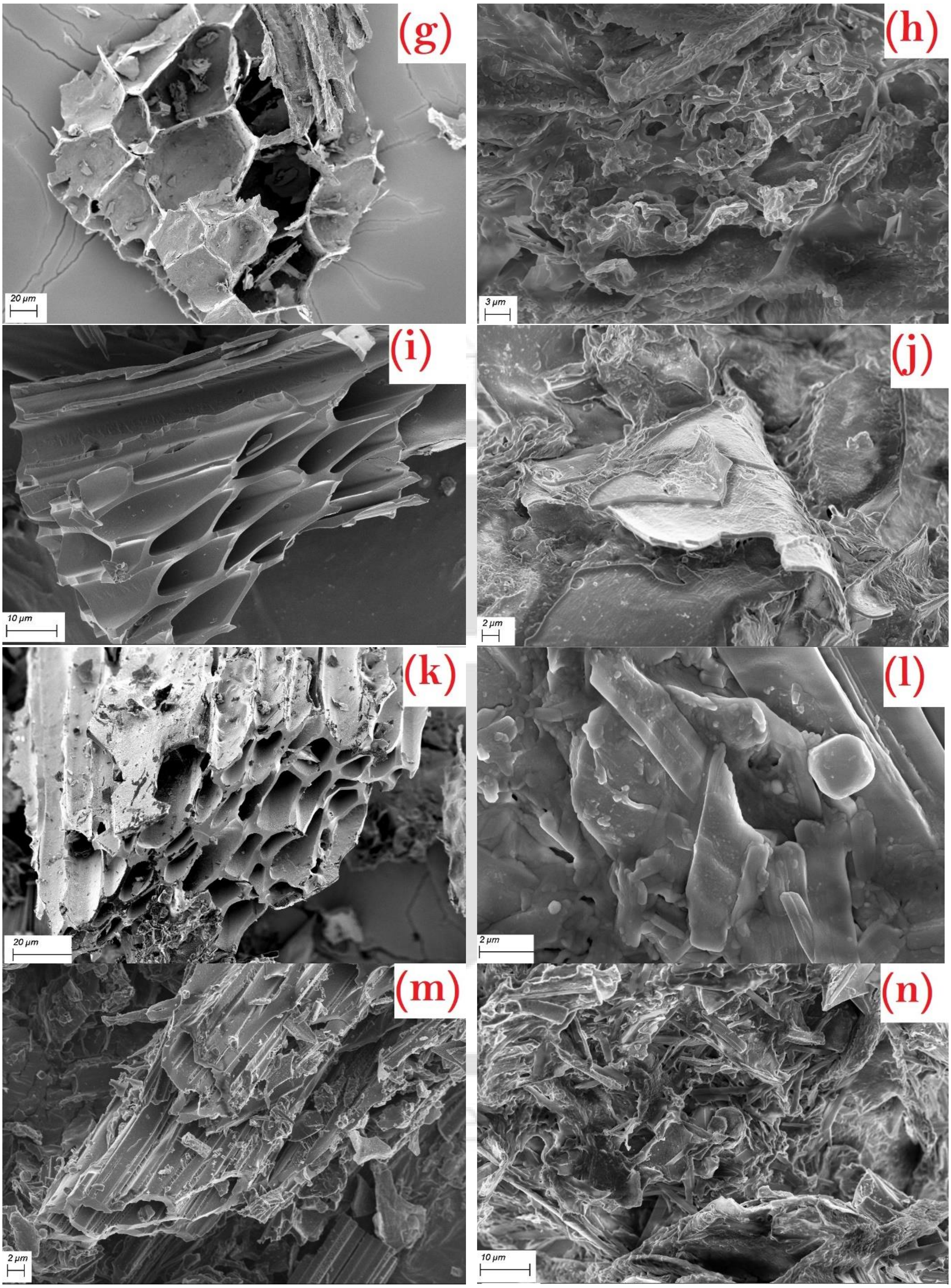

Fig. 3.9 FESEM images of different biochar and their respective composite PCMs, (a) SCB, (b)SCB-PCM, (c)WH, (d) WH-PCM,(e) YO, (f) YO-PCM, (g) B_1_SW, (h) B_1_SW -PCM, (i) B_2_SY, (j) B_2_SY-PCM, (k) B_3_WY, (l) B_3_WY-PCM, (m) T_0_SWY, (n) T_0_SWY -PCM

The FESEM images of the biochar and biocomposite PCM are demonstrated in **Fig.3.9**. The morphological analysis of the samples gives an insight into the pore development of biochar when subjected to a higher temperature. The surface of all the biochar can be seen as porous. The thermal decomposition of cellulose and hemicellulose and the volatile matters at high temperatures (550^{o}C) lead to the highly porous structure of all the biochars. SCB is full of tiny pores, which are distributed homogeneously, as seen in **Fig.3.9 (a)**. The micrographs (**Fig.3.9 (c)**) of WH show uneven pores and irregular structure. **Fig.3.9 (e)** shows a highly porous structure for YO, and the pores seem to be nearly round. B_1_SW shows a honeycomb-like structure, as shown in **Fig.3.9 (g)**, which originated from the tubular plant cells present in SCB [228]. B_2_SY, as displayed in **Fig.3.9 (i),** is composed of oval-shaped pores extended in a tubular structure. **Fig.3.9 (k)** reveals that B_3_WY pores are not evenly shaped, but rectangular cross-sections can be seen, which are long in nature. The pores of T_0_SWY are not homogeneous, and a non-uniform structure can be observed in **Fig.3.9 (m)**. All the biochar composed of SCB shows a tubular structure because of the presence of vascular bundles in their feedstock [225]. FESEM images of all the biochars result in an extremely rough and lamellar structure consisting of vascular veins that are perfect for absorbing melted PCM through surface tension and capillary force. After absorption of PCM, all the rough surfaces of the biochar matrix become smooth in nature **Fig.3.9 (b,d,f,h,j,l,n)**. The pores are completely filled with a uniform dispersion of the melted PCM. Interconnected open pores provide the PCM to penetrate through capillary action. The dispersion looks very uniform with little agglomeration of the PCM on the porous matrix. Among the seven biochar matrices, the wider and systematic hexagonal long pores of SCB biochar and SCB blended biochars can be treated as the most suitable option as a supporting matrix.

3.5.4 Chemical property analysis

3.5.4.1 FTIR analysis

FTIR spectroscopy is used to characterize the physical and chemical interactions between PCM and the encapsulating matrix (biochar). **Fig.3.10** represents the individual comparison of biocomposite PCM and biochar for all the samples. FTIR analysis is performed to evaluate the intermolecular interactions between the molecules of PCM and the biochar. The spectra of all the composites without any new absorption peaks verify that the interaction between the two materials is purely physical. Thus, the chemical properties of the new biocomposite PCM will be identical to the parent PCM (OM 35). The visible range and its respective explanation are provided in **Table 3.6**. The presence of aliphatic (C-H) and Carbonyl groups (C-O) is predominantly visible for all the PCMs. Aliphatic functional groups confirm the composite material as a chain of alkane hydrocarbon material. YO-PCM shows some peculiar behavior compared to the others, implying a possibility of chemical interaction between the two materials. The intensity of peaks is observed to be decreased in the composite PCMs than in the parent PCM. According to the Beer-Lambert law, the phenomena of weak intensities are caused by decreases in the functional groups per unit volume present on that molecular bond with the composite formation.

Table 3.6 Visible wavelengths and their respective functional groups

Wavelength (cm^{-1})	**Visible range from this work (cm^{-1})**	**Band assignment**	**Functional group**	**Remarks**
3000–3400		O–H	Hydroxyl	
2700–2900	2750-3000	C–H	Aliphatic	$-CH_3$ and CH_2, C-H stretching vibration of CH_2[229]
	2918-2850			CH asymmetric and symmetric stretching vibration [230]
1400–1700	1700-1740	C=O, C=C	Carbonyl	C=O vibration
	1467			C–H bending vibration of CH_2 [229]
1200–1300	1250-1500	C–H	Phenols	Single and double bond O-H
	1373			C–H bending vibration of CH_3 [229]
1000–1200	900-1200	C–O	Cellulose, hemicellulose and lignin	
600–799	719	C–H	Pyridine	$-CH_2$ stretching vibration of PCM [230]

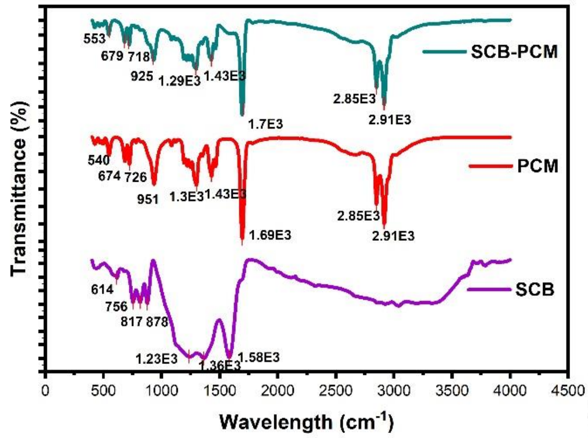
SCB-PCM
PCM
SCB
Transmittance (%)
Wavelength (cm-1)

(a)

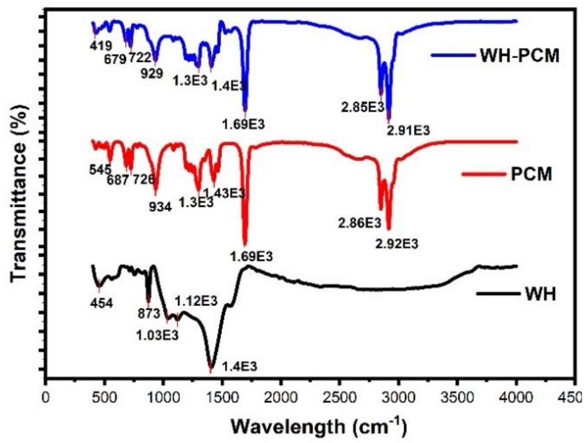
WH-PCM
PCM
WH
Transmittance (%)
Wavelength (cm-1)

(b)

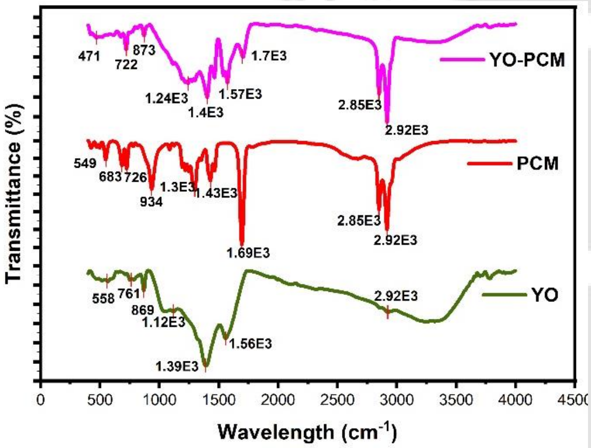
YO-PCM
PCM
YO
Transmittance (%)
Wavelength (cm-1)

(c)

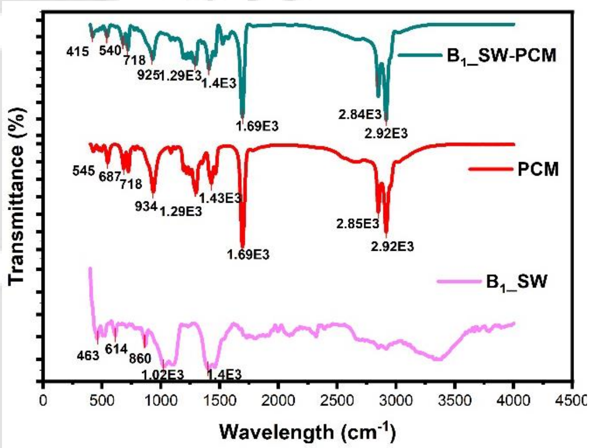
B1_SW-PCM
PCM
B1_SW
Transmittance (%)
Wavelength (cm-1)

(d)

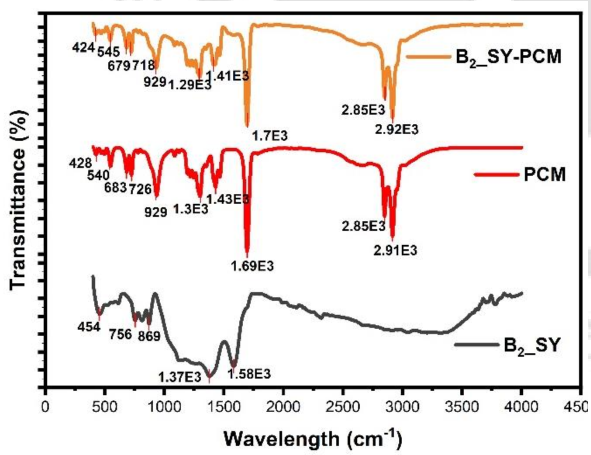
B2_SY-PCM
PCM
B2_SY
Transmittance (%)
Wavelength (cm-1)

(e)

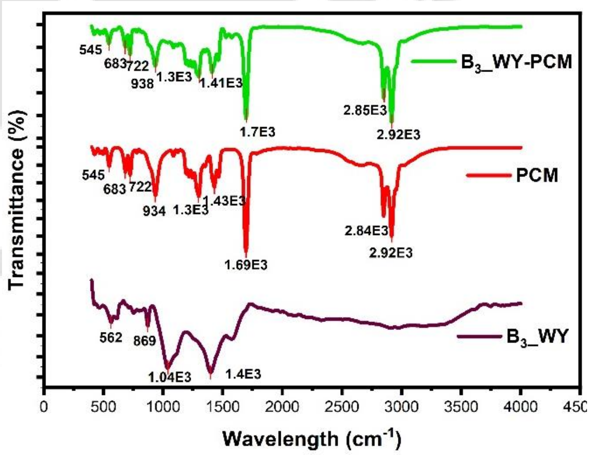
B3_WY-PCM
PCM
B3_WY
Transmittance (%)
Wavelength (cm-1)

(f)

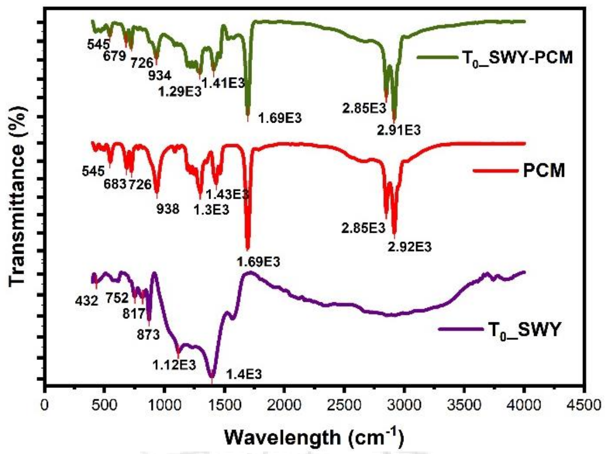

(g)

Fig. 3.10 FTIR characteristics curves of biocomposite PCMs, (a) SCB and SCB-PCM, (b) WH and WH-PCM, (c) YO and YO-PCM, (d) B_1_SW and B_1_SW-PCM, (e) B_2_SY and B_2_SY-PCM, (f)B_3_WY and B_3_WY-PCM, (g) T_0_SWY and T_0_SWY-PCM

3.5.4.2 XRD analysis

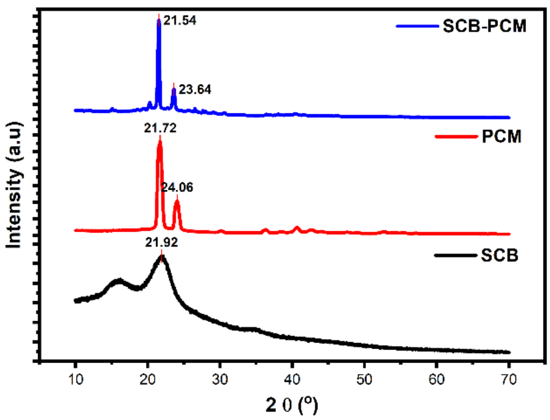

(a)

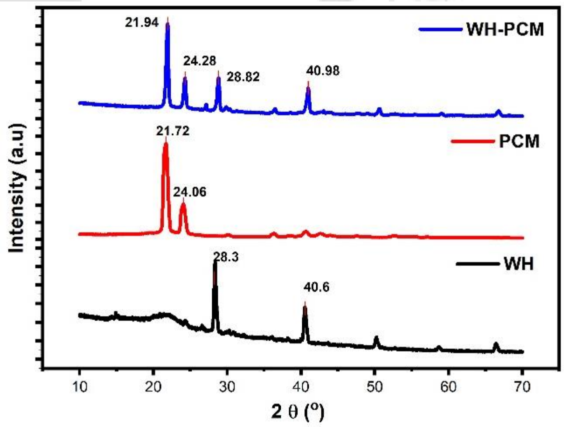

(b)

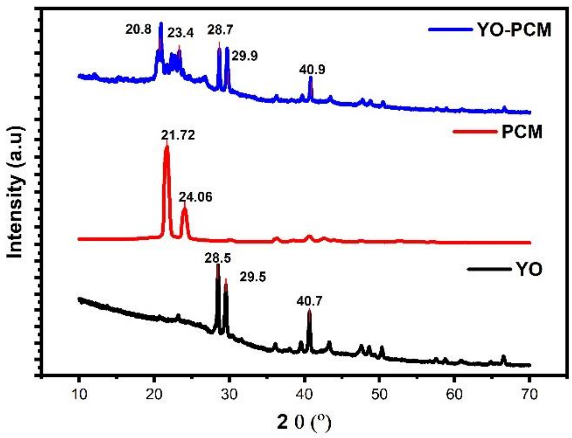

(c)

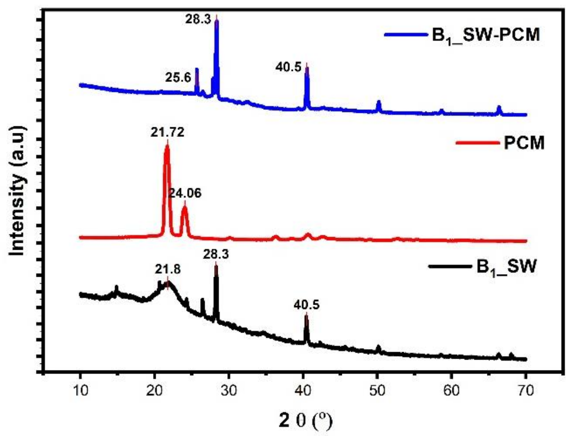

(d)

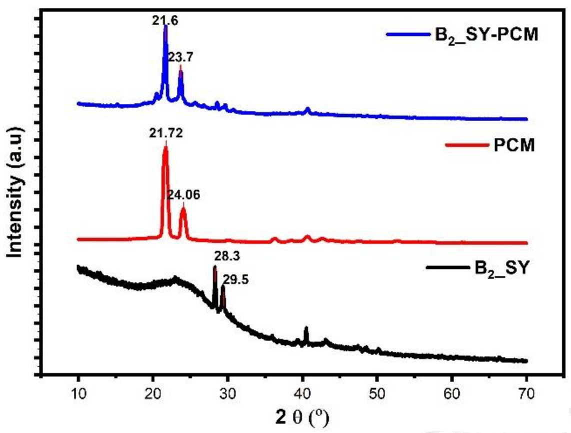

(e)

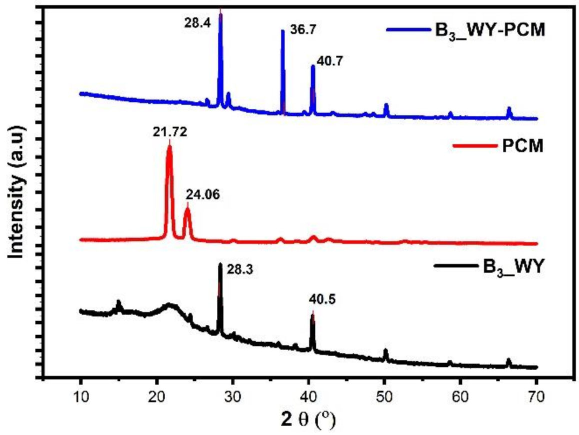

(f)

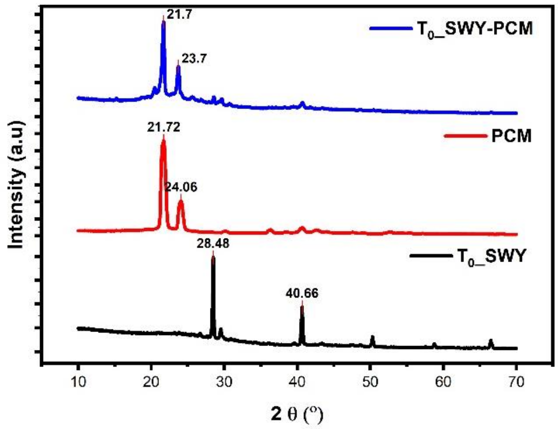

(g)

Fig. 3.11 XRD curves of biocomposite PCMs, (a) SCB and SCB-PCM, (b) WH and WH-PCM, (c) YO and YO-PCM, (d) B_1_SW and B_1_SW-PCM, (e) B_2_SY and B_2_SY-PCM, (f)B_3_WY and B_3_WY-PCM, (g) T_0_SWY and T_0_SWY-PCM

Fig.3.11 is the representation of all the XRD curves and their comparison of the biocomposite PCM and the original PCM. It is quite evident from the high-intensity peaks of XRD curves that OM35 and the newly developed composite possess extreme crystalline structures at an atomic level. The exact atomic planes specified by Miller indices (111) and (200) of OM35 can be observed with the samples T_0_SWY-PCM, SCB-PCM, and B_2_SY-PCM, confirming a similar atomic arrangement of the developed PCM. These results indicate that the crystal structure of OM35 is not affected by the addition of biochar and the fabrication process [231]. In the case of two samples, namely B_1_SW-PCM and B_3_WY PCM, one extra peak is found at an approximate angle of 40.5^o about the atomic plane (310) of their respective biochar sample. Similarly, the WH-PCM sample shows four distinctive peaks, which imply (111) and (200) planes of OM35 and (210) and (310) planes of WH biochar. In all the above three cases, the peaks of respective biochars get superimposed over the PCM, which does not affect the crystal structure of the composite PCM [232]. The XRD pattern of the YO-PCM sample has a peak at a 2θ angle of 23.4°, which is not present either in the supporting matrix or in the parent PCM. The unusual peaks detected for the YO-PCM sample imply a possibility of chemical interactions between biochar and OM35, and this developed PCM may lose the properties of the parent PCM. Other than YO-PCM, for all other composite PCM, weak hydrogen bonding or van der Waals forces may be the key attraction between the biochar and PCM [223]. A similar trend of decreasing diffraction peak intensity of composite PCM compared to the original PCM can be observed for all the XRD curves, which can result from the decrease in crystallite size with the influence of the biochar pores [233]. The biochar pores restrict the formation of big crystallite grains by promoting the development of small crystallite grains [234]. The analysis concludes that, other than the YO-PCM sample, no new diffraction peaks are observed for all the new PCM, and only physical interactions happen between OM35 and the biochar in the composite preparation process.

3.5.5 Thermal properties (TGA, DTG, DSC and Thermal Conductivity)

3.5.5.1 TGA analysis

The thermal stability of all the developed biocomposite PCMs is compared with the original PCM through TGA curves, as shown in **Fig.3.12**. Thermal stability is a critical parameter for energy-saving materials, and the graph ensures that the developed PCMs are thermally more stable than the original PCM. The higher stability is achieved through the strong confinement effect of the supporting matrix, which prevents the seepage of OM35 [235]. The mass loss percentage of OM35 is 99.98%, whereas it is 54.55% for YO-PCM. The differential thermogravimetric spectra (DTG), as shown in **Fig.3.13,** reveal that the peak degradation temperatures obtained with the composite PCM are higher, except for YO-PCM, than those of the original PCM. The physical affinity of biochar provides successful prevention of a discharge of vaporized n-alkane molecules from the PCM chain. The developed green PCMs show no thermal degradation at the desired operating temperature of building applications. It can be seen from the DTG curves that when blended with biochar, all the biocomposites are thermally stable up to approximately 110°C. This observation proves that biochar can be applied with commercial PCM for moderate solar temperature storage applications.

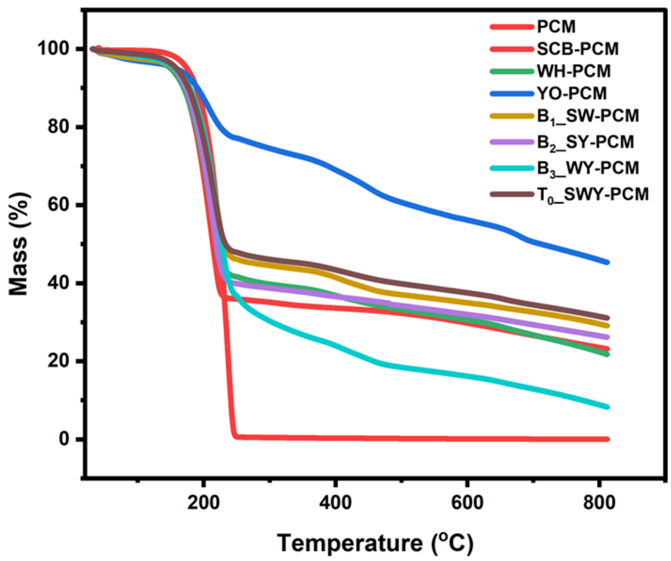

Sample	Mass Loss (%)
PCM	99.98
SCB-PCM	76.85
WH-PCM	78.24
YO-PCM	54.69
B_1_SW-PCM	70.91
B_2_SY-PCM	73.85
B_3_WY-PCM	91.72
T_0_SWY-PCM	68.93

Fig. 3.12 TGA comparison graphs for OM35 and developed biocomposite PCMs

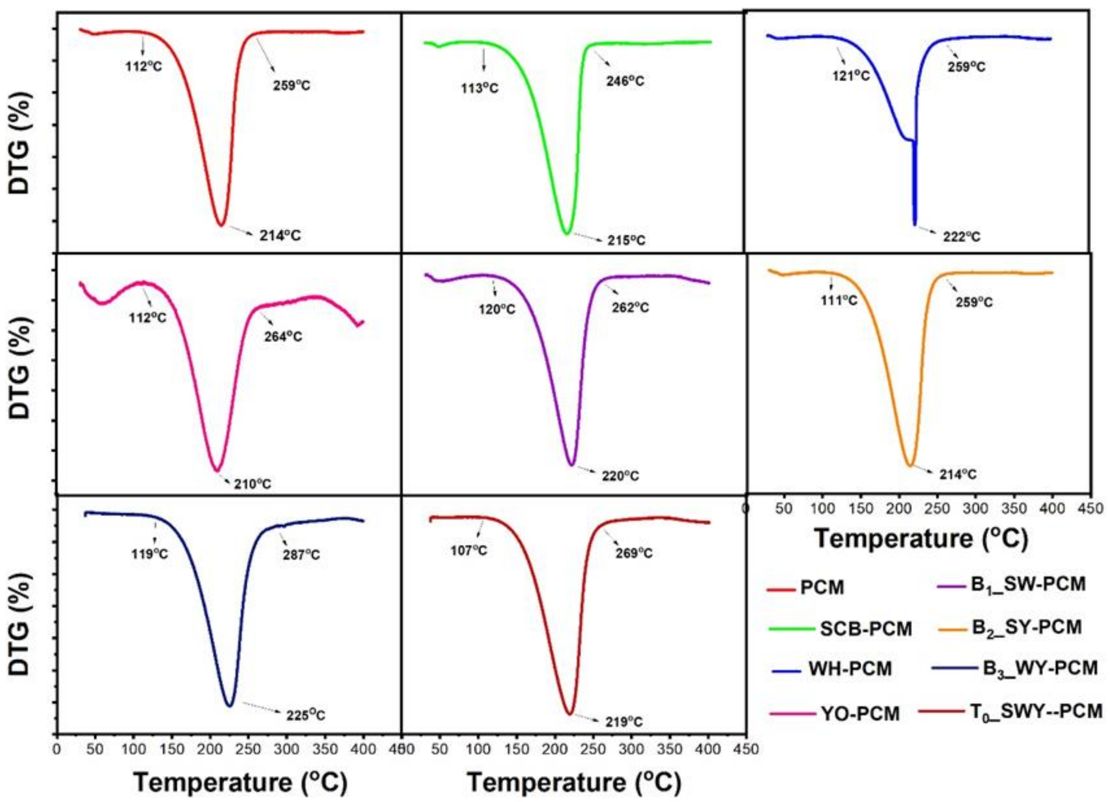

Fig. 3.13 DTG graphs for OM35 and developed biocomposite PCMs

3.5.5.2 DSC analysis

he DSC endothermic curves of all the materials are presented in **Fig.3.14.** The Melting point and heat of fusion for biocomposite PCM are calculated and mentioned in **Table 3.7**. T_{onset} from the DSC curve is used to represent the melting point for all the biocomposite PCM in **Table 3.7**. The encapsulation ratio (ER) of each biocomposite PCM is calculated as per **Eq. 3.2**.

$$ER = \frac{H_{m,biocomposite}}{H_{m,PCM}} \quad (3.2)$$

where $H_{m,biocomposite}$ is the melting enthalpy of the biocomposite PCM, and $H_{m,PCM}$ is the melting enthalpy of the PCM (OM35).

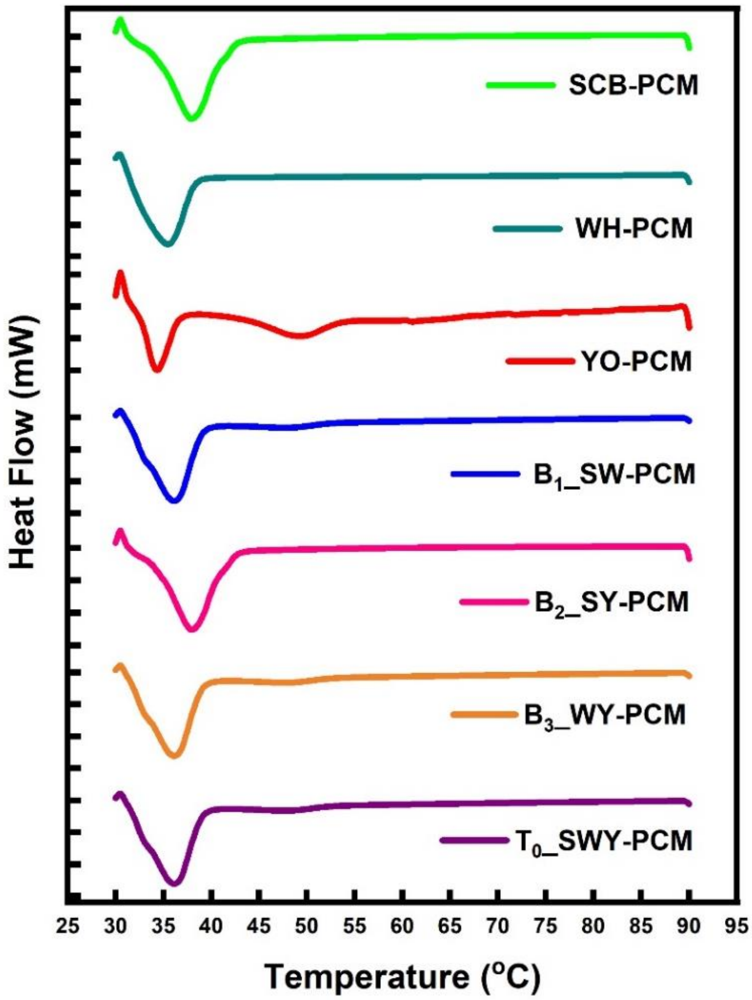

Fig. 3.14 DSC curves of different biocomposite PCM

Table 3.8 Melting point, heat of fusion and specific heat comparison for biocomposite PCM

Sample name	Melting point (°C)	The heat of fusion (J/g)	Encapsulation Ratio (ER)	References
SCB-PCM	31.50	91.50	0.53	This study
YO-PCM	31.83	51.39	0.30	This study
WH-PCM	31.50	66.63	0.39	This study
B_1_SW-PCM	31.50	98.82	0.58	This study
B_2_SY-PCM	31.83	91.26	0.53	This study
B_3_WY PCM	31.33	98.16	0.57	This study
T_0_SWY PCM	31.33	98.55	0.58	This study
PEG/Diatomite composite	27.80	87.09	Not given	[236]
FS PCM 3	27.90	85.80	Not given	[237]

Among the biocomposite PCMs, B_1_SW-PCM and T_0_SWY PCM exhibit the highest heat of fusion and maximum encapsulation ratio of 58%, while these two parameters are lowest for YO-PCM. T_0_SWY biochar shows much higher pore volume and specific surface area in comparison to YO biochar, which resulted in greater surface tension and capillary force exerted by the fluid media (PCM). This may possibly be the main reason for obtaining a higher heat of fusion and encapsulation ratio with T_0_SWY-PCM [238]**.** The chemical analysis (both XRD and FTIR analysis) in previous sections also confirms that YO-PCM loses the properties of the parent PCM on a molecular level. The DSC analysis of YO-PCM shows multiple blunt melting peaks, e.g., between 45°C and 55 55°C. A smaller and similar endothermic peak is also observed with B_1_SW, B_3_WY and T_0_SWY. These smaller, blunt peaks can result from different crystallographic forms and crystallites of various sizes. Another reason may be the melting of OM35 and biochar blends at two different temperatures. Though the melting point temperature is slightly lower than that of the parent PCM, all of them are in the same range. The range is very suitable for use in solar PV/T and building applications[29,143]. The melting point depression is caused due to several reasons, viz. (i) smaller crystal grains formed with the influence of biochar, (ii) the enhancement of surface to volume ratio in the composite material compared to bulk original PCM, (iii) the weak interaction of PCM and the inner surfaces of the supporting matrix, and (iv) increase irregularities in PCM crystals due to pores, thus increase in a lattice defect [235,239]. According to the simple mixing theory, the theoretical melting heat of fusion is calculated as **Eq. 3.3** [240]. The value is found to be 102.6

J/g, which is comparable with the experimental values of PCMs blended with binary and ternary biochar.

$$\Delta H_m^{theortical} = \Delta H_m^{PCM}(1-\phi) \tag{3.3}$$

where $H_m^{theoritical}$ is the theoretical enthalpy of biocomposite PCM, H_m^{PCM} is the measured enthalpy of PCM [211], ϕ is the weight fraction of supporting material.

The possibilities for the cause of the lower heat of fusion for the developed green composites compared to the original PCM are many. One possibility is that the decrease in mass fraction of PCM (60 wt.%) in the biocomposite is greater than that of pure PCM [230]. The non-melting enthalpy of added biochar significantly affects the melting enthalpy of PCM [241]. Another reason may be the difference in the specific heat of biochar and OM35, which affects the thermal absorbance of the composite [46]. The pore characteristics and surface tension also greatly influence the heat of fusion of the composite PCM. The decrease in enthalpy also results from the weak intermolecular forces that restrict the natural movement of the paraffin chain (the aliphatic functional groups share a major percentage in the biochar-based PCMs, as evident from the FTIR study, too) [219]. Based on the DSC analysis, binary blends and ternary blend biochar with PCM have a higher heat of fusion and are recommended for thermal energy storage in building applications. The calculated melting point and heat of fusion values show good agreement with the previous works [236,237].

Table 3.9 Average specific heat capacity of the biocomposite PCM

SCB-PCM (J/g/K)		**WH-PCM (J/g/K)**		**YO-PCM (J/g/K)**		**B_1_SW-PCM (J/g/K)**		**B_2_SY-PCM (J/g/K)**		**B_3_WY-PCM (J/g/K)**		**T_0_SWY-PCM (J/g/K)**	
C_{ps}	C_{pl}	C_{ps}	C_{pl}	C_{ps}	C_{pl}	C_{ps}	C_{pl}	C_{ps}	C_{pl}	C_{ps}	C_{pl}	C_{ps}	C_{pl}
0.33	0.89	1.63	3.86	0.16	0.47	1.67	3.04	1.97	2.89	2.22	3.57	1.01	1.97

Table 3.8 presents the values for the average specific heat capacity for all the biocomposite PCM, both in the solid and liquid states. The average specific heat is calculated for the temperature range of 31-32°C for all the biocomposite PCM. The specific heat capacity indicates the sensible heat storage capacity of the PCM, thus very useful for designing the volume of the storage system [242]. Since the specific heat capacity depends on the density of the material, it can be seen from **Table 3.4** that as the density increases, the specific heat of the material decreases for the current study.

3.5.5.3 Thermal conductivity test

Table 3.10 The thermal conductivities of the biochar

Sample Name	SCB	WH	YO	B_1_SW	B_2_SY	B_3_WY	T_0_SWY
Thermal Conductivity (W/mK)	0.103± 0.001	0.125± 0.001	0.069± 0.001	0.127± 0.001	0.096± 0.001	0.109± 0.001	0.124± 0.001

Based on the results obtained from the morphological, structural, chemical and thermal analysis, the best four biocomposite PCM are selected for the test. WH-PCM, SCB-PCM, B_1_SW-PCM and T_0_SWY-PCM are the PCMs chosen, and further analysis will be compared with the pristine PCM. As presented in **Fig.3.15**, the obtained value can be comparable with the previous results for lauric acid/ activated carbon shape stabilized composite and n-octadecane activated carbon nanocomposite [243,244]. The thermal conductivities for the WH-PCM and T_0_SWY-PCM samples are found to be 50.55% and 23.01% higher than OM35, respectively. The higher thermal conductivity may be a reason for the carbon network of biochar, which provides heat conduction channels [245]. The phonon motion in the matrix of PCM in a particular direction over a long distance can increase the thermal conductivity. An unexpected decrease in thermal conductivity can be observed with SCB-PCM and B_1_SW-PCM. Hekimoglu *et al.*[245] also revealed that sometimes higher porosity adversely affects the thermal conductivity, as higher porosity means more air voids, and air always provides thermal resistivity. The decrease in phonon transmission for PCM with a supporting matrix can also lead to low thermal conductivity. Another justification for reducing thermal conductivity may be the formation of turbostatic carbon of biochar, which forms during the pyrolysis of respective biomasses [246]. As the density of the SCB is the lowest among all biochars, the mass proportion of biochar in SCB-PCM is the highest. The low thermal conductivity of biochar may cause a reduction in the overall thermal conductivity in the SCB-PCM composite [245,247]. **Table 3.9** shows the values of thermal conductivities of all the biochars, which indicates that the value of thermal conductivity of biochar and the respective biocomposite PCM fall within the same range. Thus, the study of thermal conductivity of encapsulating material prior to composite formation can give an idea about the overall thermal conductivity of the composite, which will minimize the energy and time needed for composite formation. The present study highly recommends the addition of nanostructured metal powder for thermal conductivity enhancement. Hybrid nanoparticles have been reported to be successful in increasing thermal conductivity and enthalpy of solidification [248].

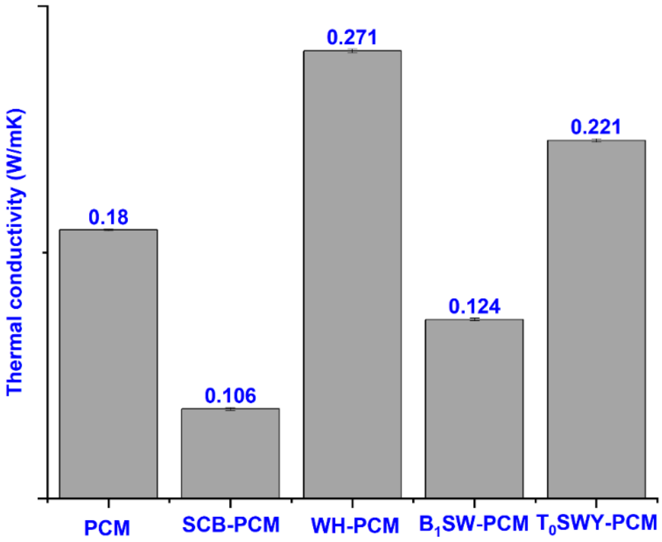

Fig. 3.15 Thermal conductivity comparison of PCM (OM 35), SCB-PCM, B_1_SW-PCM, WH-PCM and T_0_SWY PCM

3.6 Results and Discussion on thermal cycling stability of biocomposite PCM

3.6.1 Change in physical appearance

Fig. 3.16 Images of PCMs before and after thermal cycling test, (a) OM 35_0 (solid), (b) OM35_200 (solid), (c) OM 35_0 (liquid), (d) OM 35_200 (liquid), (e) WH-PCM_0, (f) WH-PCM_200, (g) T_0-SWY PCM_0, (h) T_0-SWY PCM_200

Fig.3.16 shows the visual appearance of OM35, WH-PCM and T_0-SWY PCM. The visual inspection reveals that there is a slight discoloration happening for OM35. A yellowish color can be observed for the melted OM35 after cycling, which was previously clear in color. For the biocomposite PCMs, no such discolouration can be observed in both the melted and solidified states. This appearance inspection proves that the developed PCMs are physically stable after cycling.

3.6.2 Leakage test result after thermal cycling

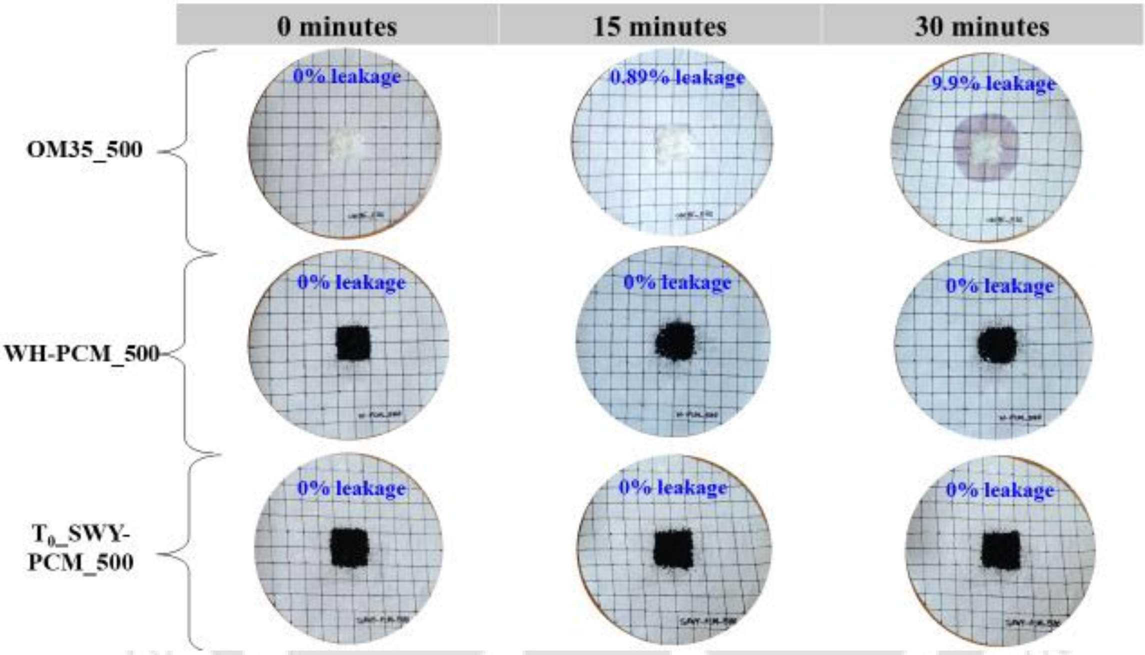

Fig. 3.17 Leakage test on filter paper

The matrix employed in the production of shape-stable PCM must exhibit thermal stability and chemical compatibility with the PCM it supports. Failure to meet these criteria could result in matrix degradation during thermal treatments, rendering it ineffective in its intended role of shielding against leakage. The leakage photographs, as shown in **Fig.3.17**, show that OM35 is strongly made leak-proof with the porous biochar matrix, which is not visible for the original PCM. The photographs of the leakage test after 15 minutes and 30 minutes show no leakage on the filter paper for WH-PCM and T_0_SWY-PCM. The leakage of OM35 after 15 minutes is also not very significant; a 0.89% change in the area has been observed compared to the area covered before the test.

On the other hand, after 30 minutes, the leakage is prominent, which covers 13.52% of the total area of the filter paper, which is 9.9% more area than the area before the test. The dense structure of biochar enhances the structural stability of OM35 due to the excellent degree of wettability of OM35 with both biochar matrices. The ability of molten PCM to wet the surface of the biochar matrix influences the capillary force, and this effect remains consistent after 500 cycles for both biocomposite PCMs [249]. Thermal cycling has not affected the wettability of the PCM with biochar, which is a good sign for use in buildings [204]. The mass loss $\phi_{leakage}$ for the leakage test has been calculated as per **Eq.3.1**.

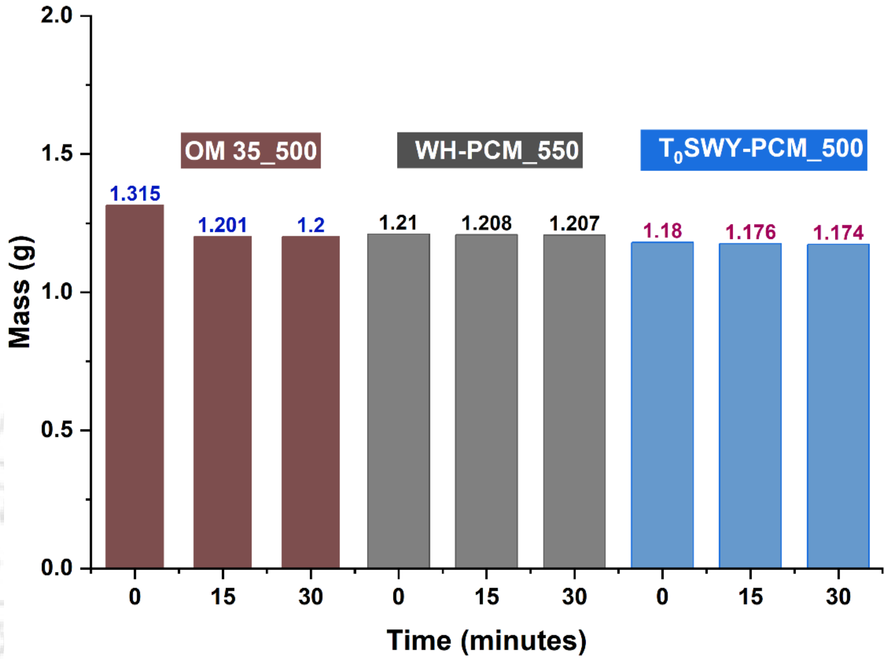

Fig. 3.18 Comparison of the mass loss of the PCMs during the leakage test

The loss of mass percentage in the leakage test after 500 thermal cycles is 8.74%, 0.24% and 0.49% for OM35, WH-PCM, and T_0_SWY-PCM, respectively, as shown in **Fig.3.18**. The mass loss of biocomposite PCMs can be negligible due to the flexible skeleton provided by the biochar matrix, which does not collapse due to thermal cycling. The biochar matrix is able to hold the volume expansion of PCM during melting, and the leakage problem has been completely taken care of. During composite formation, some of the pores of the biochar matrix should remain unfilled to provide the space for accommodating the melted PCM during phase transition. If all the pores get filled, then the volume expansion that happens during melting will leak and will be visible on the filter paper. The structure of the developed biocomposite PCM remains unchanged after thermal cycling. Satisfying this specific criterion demonstrates that the expansion in volume when biocomposite PCMs melt will not pose challenges regarding the dampening of building materials by the released PCM.

3.6.3 Surface morphology analysis after thermal cycling

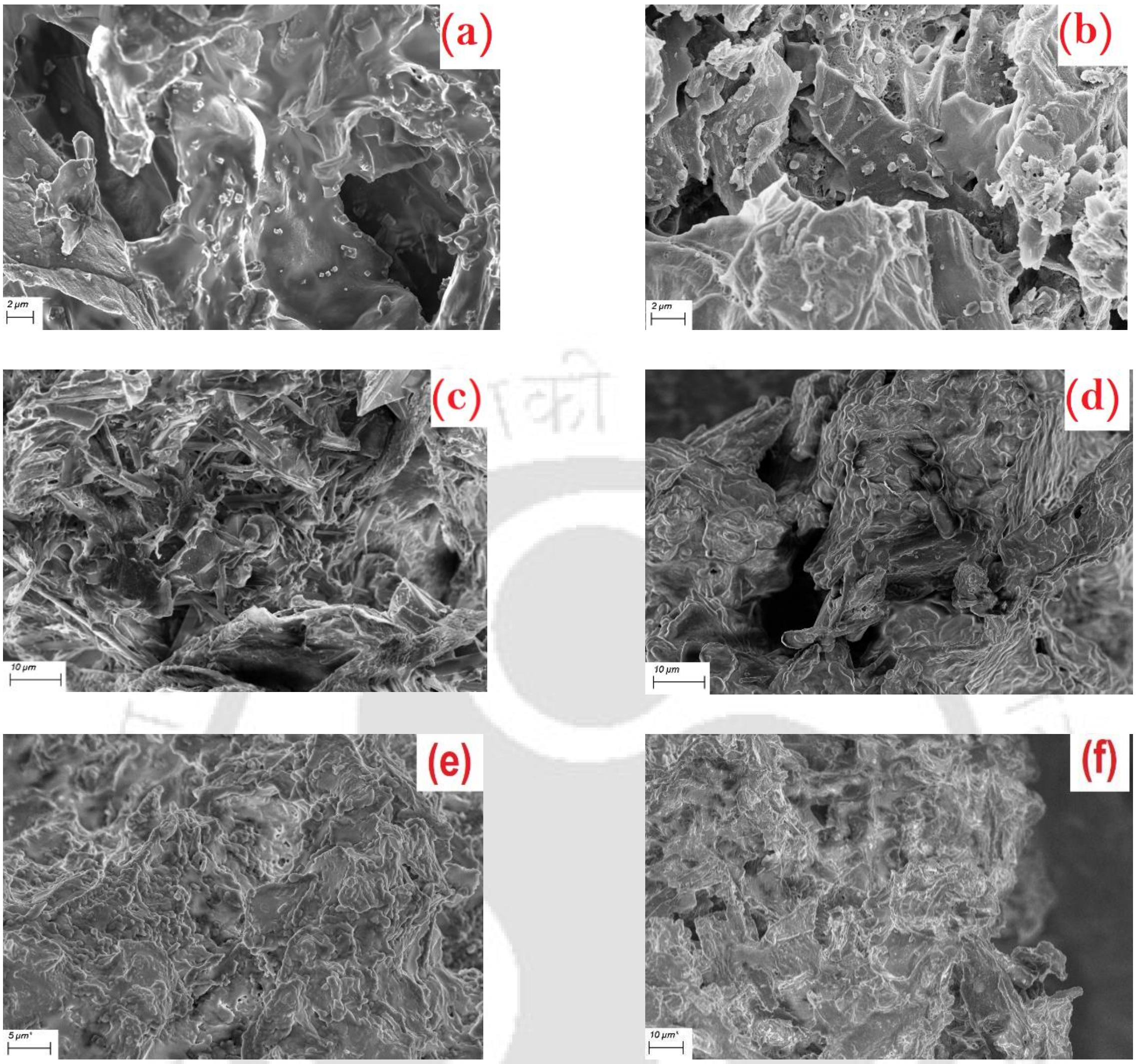

Fig. 3.19 FESEM images of (a) WH-PCM_0, (b) WH-PCM_200, (c) T_0_SWY-PCM_0, (d) T_0_SWY-PCM_200, (e) WH-PCM_500, (f) T_0_SWY-PCM_500

The FESEM images of the biocomposite PCMs are shown in **Fig.3.19**. It is clear from the figure that biochar is a 3D supporting matrix, which can provide enough porosity and a large specific surface area. As biochar is a porous carbon material, it is known as a lightweight 3D matrix, which is advantageous to provide structural stability [249].

The melted PCM fills the porous matrix of biochar, and the dispersion is homogeneous, which is confirmed by the FESEM images. There is no change in the structure after thermal cycling for both WH-PCM and T_0_SWY-PCM. The melted PCM penetrates through the pores of biochar due to capillary action and surface tension force. After thermal cycling, the impact of capillary action and surface tension force is still present. In application, PCM undergoes consecutive heating and cooling thermal cycles. Therefore, the supporting matrix should be able to resist the thermal shock and maintain structural rigidity. No cracks have been highlighted on the surface of the two biocomposite PCMs, implying that both biochar matrices are able to sustain thermal fatigue. These images confirm that the developed biocomposite PCMs maintain their structural integrity even after repeated freezing and melting cycles. Another important factor is that the supporting matrix should not decompose because of the repeated thermal cycling process. The consistent surface morphology observed in the developed PCMs before and after cycles suggests that there has been no decomposition of biochar within the temperature range relevant to building applications.

3.6.4 XRD analysis after thermal cycling

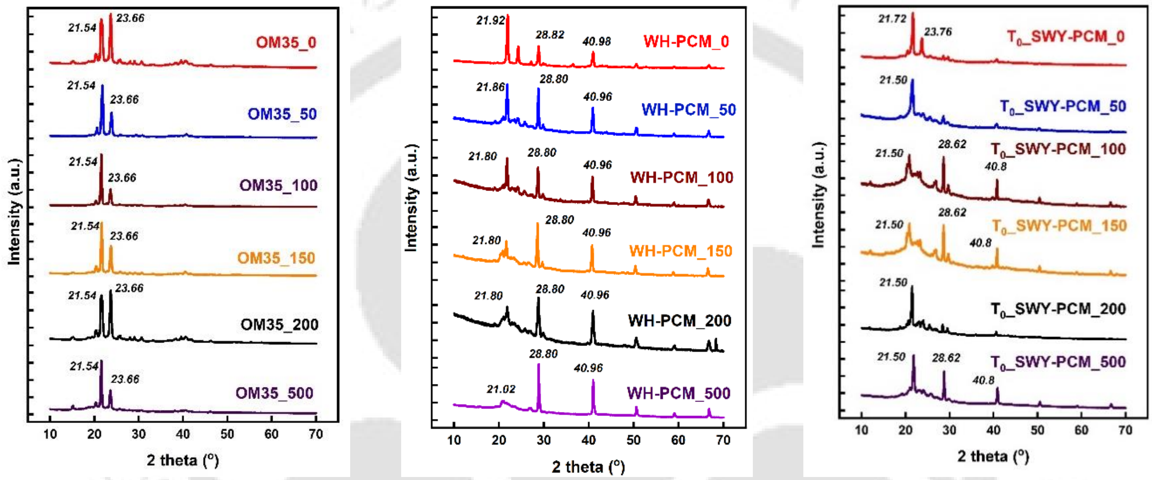

(a) **(b)** **(c)**

Fig. 3.20 XRD images of samples of (a) OM35, (b) WH-PCM, (c) T_0_SWY-PCM

The XRD graphs for the three samples after the 50^{th}, 100^{th}, 150^{th}, 200^{th}, and 500th cycles have been shown in **Fig.3.20**. The atomic arrangement and crystallinity of the uncycled and cycled OM35 are exactly the same, as confirmed by the XRD results. The two peak diffraction angles, i.e., 21.54^o and 23.66^o, represent the atomic miller indices of (111) and (200), respectively. The two atomic planes have not changed for all the samples of OM35. Similarly, the same atomic planes can be visible from T_0_SWY-PCM when the thermal cycles are not performed. After completing 100 cycles, another diffraction peak at 40.8^o has been found to exist for T_0_SWY-PCM, which appears for the atomic plane (310). The (310) plane is exactly matching with the biochar matrix, which was published earlier [250], and thus, it can be assured that no chemical structure change happens during the thermal cycles. Similarly, the planes specified by Miller indices (111), (200) and (310) can be found for all the samples of W-PCM.

Table 3.10 presents the crystallite size and lattice strain percentage for the three PCMs. The crystallite size has been calculated by using the Scherrer formula, as stated in **Eq.3.4** [251].

$$D = \frac{K \times \lambda}{\beta \times \cos\theta} \tag{3.4}$$

where D is the crystallite size (nm), K is the Scherrer constant, which is taken as 0.94 for this case, λ is the wavelength of the X-ray (1.5 Å), β is the full width at half maximum (FWHM) of the XRD peak in radians and θ is the Bragg angle.

The only visible difference is that the diffraction angle at around 21° broadens as more thermal cycles are performed. The broadening of the diffraction angle indicates that the crystallite size of the composite PCM may decrease, which is supported by the data provided in **Table 3.10** for WH-PCM_500. Another reason for the broadening of XRD peaks may be the inhomogeneous strain generated during thermal cycling.

Table 3.11 Comparison of Crystallite size of OM35 and biocomposite PCMs

Sample name	**Crystallite size (nm)**	**Lattice strain**
OM35	15.095	0.011
WH-PCM_0	22.120	0.006
WH-PCM_500	29.819	0.003
T_0_SWY-PCM_0	19.683	0.009
T_0_SWY-PCM_500	26.670	0.005

3.6.5 FTIR result after thermal cycling

The FTIR characterization has been performed to assess the chemical changes in functional groups after performing thermal cycles. **Fig.3.21** illustrates the comparison of FTIR graphs of uncycled and cycled OM35, WH-PCM and T_0_SWY-PCM, respectively. Hydroxyl groups are characterized by wavelengths falling within the range of 2800-3000, while aliphatic groups, indicated by stretching vibration of C-H bonds of CH_2, are observed in the 2700-2900 wavelength range. Carbonyl groups associated with the vibration of C=O and C=C double bonds are identifiable in all PCMs. Phenols are denoted by the bending vibration of the single bond C-H of CH_3 in the 1200-1300 range, and pyridine is represented in the 600-700 range [250]. No notable new absorption peaks are detected in the thermal cycling process for all three figures, confirming the stability of functional groups, primarily aliphatic and carbonyl, between uncycled and cycled materials. The thermal cycle comprises the sequential rupture and recombination of segments within the PCM, without any accompanying new chemical reactions [252]. The weakened intensity of peaks in cycled PCMs suggests a reduction in functional groups per unit volume compared to uncycled ones. Another reason for such a reduction may be the presence of weak hydrogen bonding that binds the biochar matrix with OM35 or particle agglomeration [253,254].

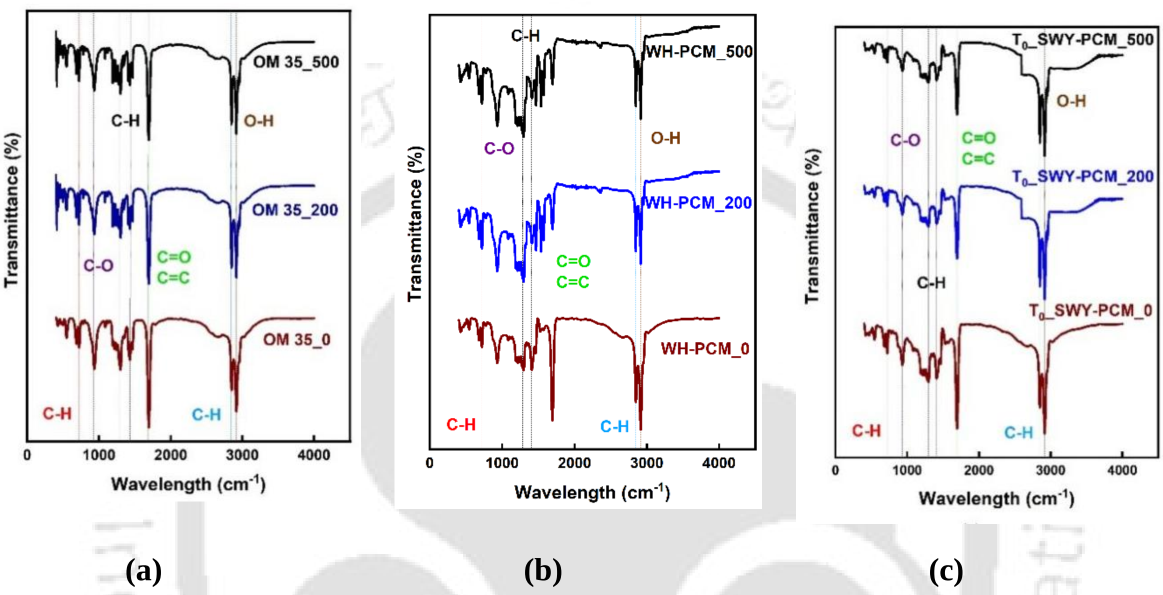

Fig. 3.21 FTIR graphs of cycled and uncycled PCMs (a) OM35, (b) WH-PCM, (c) T_0_SWY-PCM

3.6.6 DSC result after thermal cycling

The DSC graphs of WH-PCM and T_0_SWY-PCM are shown in **Fig.3.22**. A shift to a lower temperature range in the temperature-enthalpy curve after thermal cycling is evident in both **Fig.3.22 (a)** and **Fig.3.22 (b).** The details of the DSC results are represented in **Table 3.11**. The melting point for WH-PCM and T_0_SWY-PCM is decreased by 0.83°C and 0.46°C, respectively. The solidification temperature is reduced by 1.88°C and 2.13°C for both the biocomposite PCMs. The decrement in melting point and solidification temperature is caused by the effect of thermal stress caused by repeated thermal cycles [255]. It can be seen from **Table 3.10** that upon thermal cycling, the crystallite size increases for T_0_SWY-PCM. Smaller crystallites have a higher surface area per unit mass compared to larger ones [256]. The increased surface area results in higher surface energy, and this results in higher melting temperatures [29,257].

Table 3.12 DSC results of the uncycled and cycled biocomposite PCMs

Name	**Melting point (°C)**		**Heat of fusion (J/g)**		**Solidification temperature (°C)**		**Heat of solidification (J/g)**		**Degree of supercooling (°C)**	
	0 cycle	500 cycle	0 cycle	500 cycles	0 cycle	500 cycles	0 cycle	500 cycle	0 cycle	500 cycles
WH-PCM	31.5	30.67	66.63	73.52	29.67	27.79	42.9	43.98	1.83	2.88
T_0_SWY-PCM	31.33	30.87	98.55	113.52	29.83	27.7	63.84	85.44	1.5	3.17

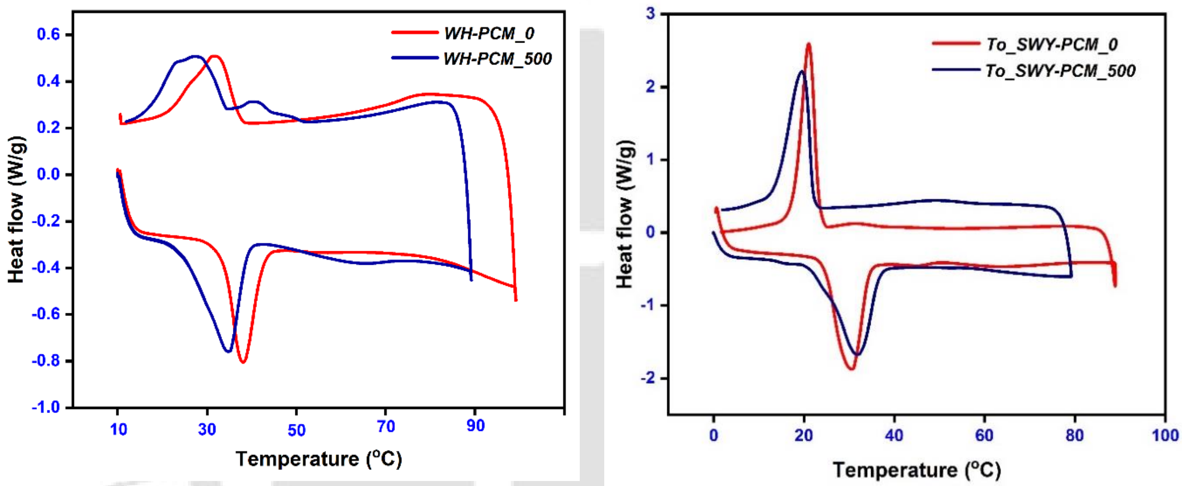

(a) (b)

Fig. 3.22 DSC graph of biocomposite PCMs before and after cycling, (a) W-PCM, (b) T_0_SWY-PCM

The thermal cycling of biocomposite PCM results in higher heat of fusion and higher heat of solidification than the uncycled PCM, similar to the results obtained with published literature [258,259]. The results confirmed that with thermal cycling, the storage capacity of the biocomposite PCMs increased. As studied by Anand *et al.* [259], the change in thermal properties is irregular in nature for PCM, which is also confirmed by the present study.

The degree of supercooling value of both the biocomposite PCMs has been determined using **Eq.3.5** by considering the peak melting and solidification temperature of the DSC curve [260].

$$\Delta T_s = T_m - T_f \qquad (3.5)$$

where is the degree of supercooling, T_m is the melting temperature and T_f freezing temperature.

Table 3.13 Comparison of DSC results with previous studies

References	**Name of PCM**	**Thermal cycles completed**	**% Change in melting point**	**% Change in heat of fusion**	**% Change in solidification temperature**	**% Change in heat of solidification**
Babar et al. [261]	Paraffin wax (PW_1)	500	+3.35	+3.86	-1.17	+11.66
	Paraffin wax (PW_4)	500	+9.86	+5.62	-4.35	-17.80
	Paraffin wax (PW_5)	500	-1.44	-33.93	-2.36	-7.41
Dheep et al. [262]	Benzamide	500	+0.02	-12.87		
Sharma et al. [263]	Binary mixture of capric acid and stearic acid	500	+0.64	-16.27		
	Binary mixture of capric acid and myristic acid (90:10 wt %)	500	+4.26	+9.23	Not mentioned	Not mentioned
	Binary mixture of capric acid and myristic acid (70:30 wt %)	500	+13.72	-9.95		
	Binary mixture of capric acid and lauric acid (40:60 wt %)	500	+9.07	-22.4		
Sari et al.[264]	Silica fume/capric acid-palmitic acid composite	1000	+5.21	-29.32		

	PCM with 5 wt% CNT					
	Silica fume/capric acid-palmitic acid composite PCM with 3 wt% CNT	1000	+13.95	-15.39	Not mentioned	Not mentioned
Present work	WH-PCM	500	-2.63	+10.34	-6.33	+2.4
	T_0_SWY-PCM	500	-1.46	+15.19	-7.14	+33.83

The results, as shown in **Table 3.11,** show that upon thermal cycling, the degree of supercooling increases. For WH-PCM, the enhancement is 1.05°C, whereas for T_0_SWY-PCM, the enhancement is 1.67°C. The enhancement may happen because of the presence of impurity, as described by Yang et al. [258], which results into heterogeneous nucleation. As minimum supercooling is a desired option for efficient use of PCM, WH-PCM is a preferable option for building out of the two selected PCMs. The DSC results have been compared with published literature and tabulated in **Table 3.12**.

3.7 Summary of the chapter

The current chapter explains the suitability of biochar as an efficient encapsulating medium to prevent the leakage of organic PCM, offering desirable chemical and thermal stability. The produced biochar pore size lies in the appropriate mesoporous range for PCM encapsulation. The seepage of liquid PCM during phase transition is prevented through weak physical affinity between biochar and OM35. Also, the enhancement of thermal conductivity of OM35 has been achieved with biochar addition. The thermal cycling test confirms the leakage stability of the developed biocomposite PCMs. Finally, considering the physical, chemical, and thermal stability, biocomposite PCM with water hyacinth biochar as a supporting matrix is recommended for further building applications. The next chapter discusses the methodology of incorporating selected biocomposite PCM into brick walls and its impact on the thermal performance of the wall.

Chapter 4

Development and thermal performance analysis of PCM-impregnated brick walls

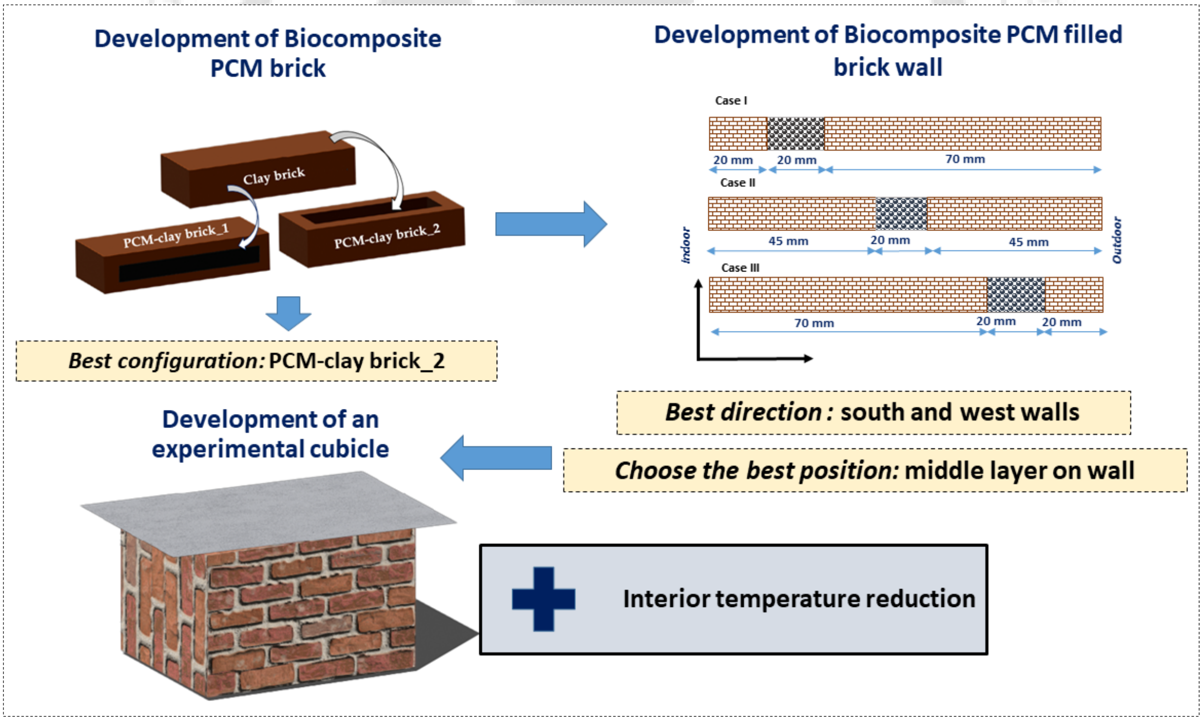

Outline

4.1 Introduction

4.2 Development of WH-PCM impregnated walls

4.3 Results and discussion on comparison of the temperature profile in the thermal chamber

4.4 Thermal performance test results in outdoor condition

4.5 Comparison of the quality of normal brick and PCM-incorporated brick

4.6 Thermal performance analysis of experimental cubicle

4.7 Summary of the chapter

4.1 Introduction

Brick is an integral construction component in most of the heavy-weight buildings due to their durability and strength. Bricks can withstand various environmental conditions and last for generations, and therefore, the current study selects the incorporation of biocomposite PCM into bricks as a viable approach. As mentioned in the last chapter, this chapter covers the detailed methodology of WH-PCM integration in bricks to increase their thermal mass. The chapter also discusses the experimental results of the effectiveness of WH-PCM on the regulation of indoor temperature in a scale-down building under outdoor conditions.

4.2 Development of WH-PCM impregnated walls

In the study, three different sets of experiments have been carried out to investigate the impact of incorporating WH-PCM in commercially available bricks on the thermo-mechanical performance. The three experimental schemes are briefly presented in **Fig. 4.1**.

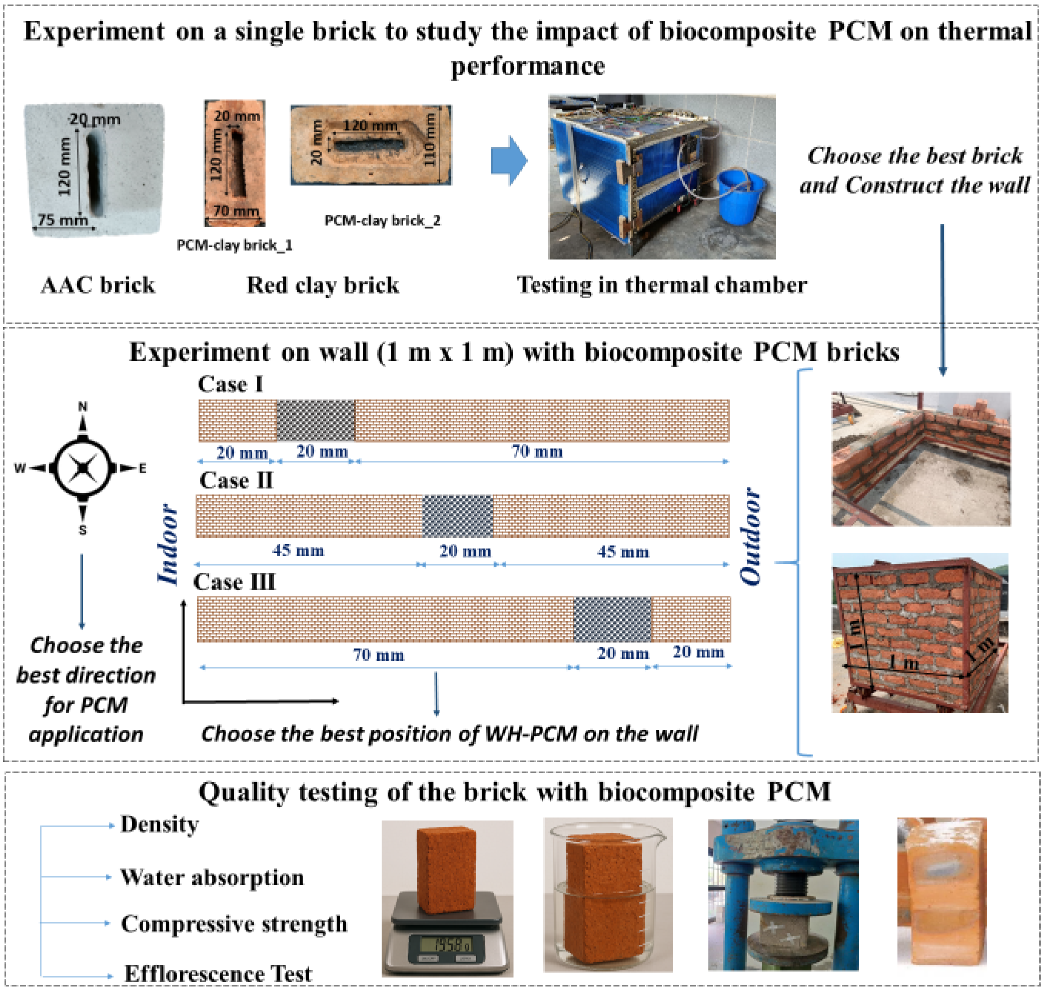

Fig. 4.1 Methodology of the study of WH-PCM incorporated bricks

4.2.1 Development of WH-PCM incorporated bricks for indoor experiment

Commercially available autoclaved aerated concrete (AAC) and red clay bricks have been purchased from local vendors for experimentation. Bricks from the same lot are selected for analysis to avoid any discrepancies for both types. The properties of the bricks are tabulated in **Table 4.1**. The AAC bricks are cut into three equal sizes (15cm x 15 cm x 15 cm) for ease of doing experiments.

Table 4.1 Properties of the selected brick [265]

Brick Name	Dry Density (kg/m^3)	Thermal conductivity (W/mK)	Specific heat (MJ/m^{3}K)
AAC brick	642	0.18	0.79
Red clay brick	1170	0.77	Not found

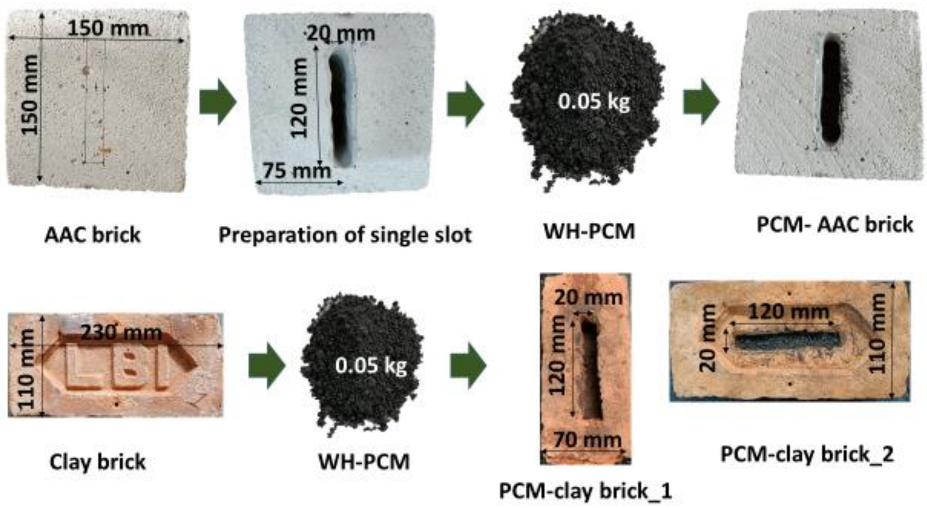

Fig. 4.2 Preparation of WH-PCM incorporated brick

The PCM bricks are prepared as shown in **Fig. 4.2**. The position and thickness of the PCM slot have been chosen based on published literature considering Indian climatic conditions [143,151]. An optimization study showed that the middle of a brick wall is most suitable for PCM application [82]. Also, it is recommended to use PCM in cavities inside the brick rather than use it as a separate component of the wall, which is both financially affordable and technically feasible[266]. The mass of powdered biocomposite PCM (50g) has been kept constant for all the brick configurations. As the red clay bricks are rectangular in shape, two different configurations for inserting WH-PCM have been developed, as shown in **Fig.4.2**. PCM_clay brick_1 represents the configuration where the hole is made through the thickness of the rectangular clay brick. The next configuration, named PCM_clay brick 2, specifies the hole position along the breadth of the rectangular brick. The reason behind making two slots on the same brick is that it is a common rural construction practice in India to lay the walls of residential buildings either along the thickness or the breadth of the brick, depending on the climatic conditions and affordability of the material.

4.2.2 Indoor experimental set-up

As room temperature is a major component for determining thermal comfort measurement, temperature fluctuation has been recorded for the preliminary study. The experiments have been performed under the controlled temperature range of 25-55°C in a thermal cycling chamber, as explained in **Chapter 3**. The temperature range is selected based on the typical ambient minimum and maximum temperatures observed during the summer season in a tropical climate. To ensure the robustness of the test and to account for extreme but realistic conditions, the upper limit was extended to 55 °C as a factor of safety.

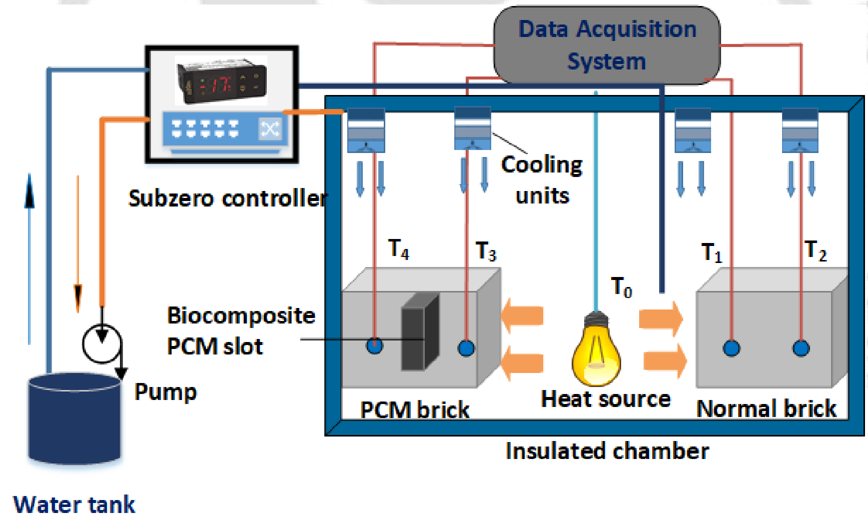

Fig. 4.3 Design of thermal performance test on the single brick in the controlled chamber

To measure the temperature of the blocks, two T-type thermocouples are attached to both the WH-PCM brick and reference brick at a distance of 120 mm and 170 mm from the heat source, respectively. T_1 and T_3 denote the temperature at measurement points located at 120 mm from the surface, whereas T_2 and T_4 represent the thermocouple measurements at a depth of 170 mm within the reference and the WH-PCM brick, respectively, as shown in **Fig. 4.3**. The standard bricks and PCM bricks are insulated with glass wool insulation of 3 cm thickness (except one face) so that one-directional heat transfer can be assumed throughout the indoor experiment. The uncertainty in measuring the temperature of the thermocouples is found to be ±0.25°C. A data acquisition system (Make: Keysight, Model: 34972A) is attached to record the temperature after a one-minute interval throughout the experiment. The heating and cooling have been performed simultaneously such that the maximum temperature of the chamber remains below 55°C for approximately 2.5 hours, and thereafter, the heating element is turned off and the chamber is cooled.

To assess the repeatability of the experiments, each configuration is experimented under the same conditions three times. The repeatability of the experiments ensures a similar temperature profile across three trials. Although the temperature profile presented in this study is one representative graph from one trial, a summary of three different trials for the same time interval is added in **Tables 4.2** and **4.3**. The tables show that the maximum standard deviation (SD) for the experiment is within 0.015 °C.

Table 4.2 Mean surface temperature and standard deviation for PCM-clay brick_1

Time (min)	**T_1 Mean ± SD (°C)**	**T_2 Mean ± SD (°C)**	**T_3 Mean ± SD (°C)**	**T_4 Mean ± SD (°C)**
1	26.83 ± 0.002	26.11 ± 0.010	26.45 ± 0.015	26.01 ± 0.005
150	41.86 ± 0.001	42.14 ± 0.015	41.48 ± 0.002	40.15 ± 0.006
300	39.58 ± 0.009	40.28 ± 0.010	39.21 ± 0.010	39.21 ± 0.008

Table 4.3 Mean surface temperature and standard deviation for PCM-clay brick_2

Time (min)	**T_1 Mean ± SD (°C)**	**T_2 Mean ± SD (°C)**	**T_3 Mean ± SD (°C)**	**T_4 Mean ± SD (°C)**
1	26.65 ± 0.002	26.75 ± 0.004	26.27 ± 0.004	26.01 ± 0.012
150	43.66 ± 0.002	40.86 ± 0.007	43.31 ± 0.004	35.30 ± 0.040
300	37.94 ± 0.004	38.70 ± 0.003	37.56 ± 0.005	36.27 0.004

4.2.3 Outdoor experimental set-up

After selecting the best configuration of brick with WH-PCM, the next set of thermal analysis has been carried out on walls constructed from WH-PCM clay bricks under actual outdoor conditions. Before constructing walls, a slot is cut, and a WH-PCM layer is inserted on each brick to facilitate easier assembly during wall construction. The slots in the clay bricks are cut based on ease of operation using an Electric Wall Chaser with Laser Guide Groove Cutting

Machine (Make: ElectroStop, Model: 133 B). Therefore, two different slot positions for WH-PCM incorporation are prepared, as shown in **Fig. 4.4,** with the slot cut either along the 110 mm side or the 70 mm thick side of the brick, respectively. A layer of 20 mm thick and 50 g powdered WH-PCM is then inserted within the prepared slot. Manual compression using a tamping bar is applied to each brick to ensure uniform material distribution. After the material is properly inserted, the brick is sealed with a layer of plaster to secure and protect the filled section.

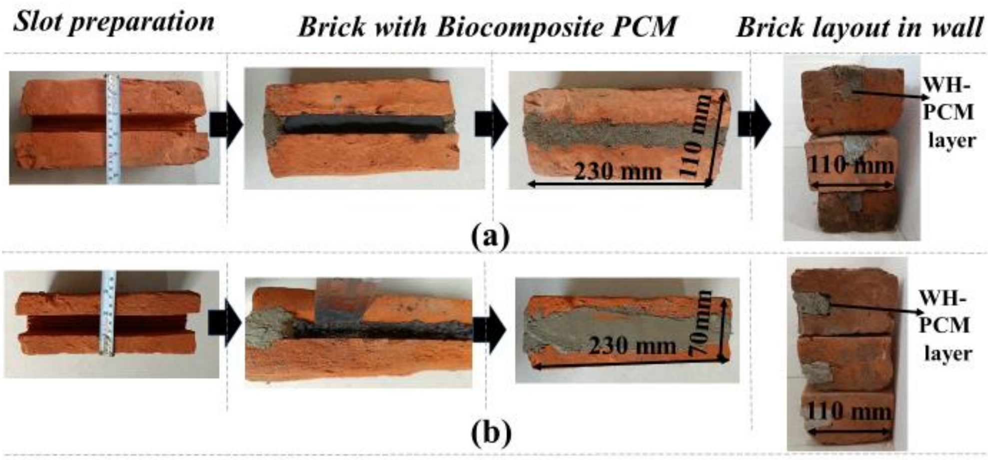

Fig. 4.4 (a) WH-PCM brick preparation for Case II, (b) WH-PCM brick preparation for Case I and Case III

After that, walls have been constructed with WH-PCM embedded red clay brick on a pre-fabricated cast iron structure, where provisions are given for wall fabrication, as shown in **Fig. 4.5 (a,b)**. While the slot configurations vary due to preparation convenience, all bricks are laid in the wall in a uniform orientation, maintaining a consistent wall thickness of 110 mm. The size of each wall is 1m x 1m. No plastering is applied to any surface of the wall. Three walls of the tested room have been constructed as mentioned in **Fig. 4.1**, i.e., Case I, Case II, and Case III, respectively, where the WH-PCM will be positioned along the thickness of the wall. In Case II, the WH-PCM layer is placed at the center of the wall thickness. For this configuration of wall, the bricks prepared as shown in **Fig. 4.4 (a)** are used. Case I and Case III refer to WH-PCM's position near the interior of the room and exterior of the environment, respectively. In these cases, the brick prepared as shown in **Fig. 4.4 (b)** is used. The bricks are then laid such that the WH-PCM layer faces the interior in Case I and the exterior in Case III, maintaining the wall thickness as 110 mm. The fourth wall of the tested room is constructed with normal clay bricks. The experimental setup involves rotating the test room weekly to align each PCM wall case (Case I, II, III) toward a specific cardinal direction (North, East, South, West). The structure is equipped with 6-inch nylon wheels so that rotation of the walls can be done according to the need for analysis in different directions. For each wall, four directions have been tested one by one.

The experimental matrix showing the directions for the three cases is mentioned in **Table 4.4.** For comparison, a similarly sized room is constructed with normal clay bricks. For each direction, case 0 represents a similar wall, faced in that direction, made up of normal clay bricks, kept under the same outdoor conditions. The floor and roof of both the test and reference rooms are made from wood and corrugated GI sheets, respectively.

Table 4.4 Matrix of Experimental Conditions for Outdoor Testing

Experimental period	**Direction**	**PCM position on the wall**
29.08.2024-04.09.2024	West	Case I
	South	Case II
	East	Case III
04.09.2024-10.09.2024	South	Case I
	East	Case II
	North	Case III
10.09.2024-16.09.2024	East	Case I
	North	Case II
	West	Case III
21.09.2024-27.09.2024	North	Case I
	West	Case II
	South	Case III

Two T-type thermocouples (accuracy: ±0.25°C) with a data acquisition system (Make: Keysight, Model: 34972A) are attached, on each of the walls, for both the reference and test room. The mean temperature recorded from the two thermocouples is calculated for each wall for the final calculation, with an uncertainty of ±0.17°C. The uncertainty of the temperature calculation is measured as per root-sum square-method, considering the independent readings of the thermocouple, as shown in **Eq. 4.1**.

$$u_{avg} = \sqrt{\left(\frac{\partial f}{\partial x_1}U_1\right)^2 + \left(\frac{\partial f}{\partial x_2}U_2\right)^2} \tag{4.1}$$

where U_1 and U_2 is the accuracy of each thermocouple, respectively, which is same in this particular case. x_1 and x_2 are the independent readings of both the thermocouple and f is the function, defining the average value of the two readings.

One heat flux sensor (Make: Hukseflux, Model: HFP01) is also positioned at the center of each wall to measure the heat flux across the wall (**Fig. 4.5 (c)**) for both rooms. The calibration uncertainty of the heat flux sensor is reported as $\pm 1.95\times10^{-6}$ W/m^2. The solar irradiation is measured with a pyranometer (Make: Apogee Instruments, Model: SP510), with an uncertainty of less than 3%. The output results are recorded at 30-minute intervals, and each wall has been exposed to a particular direction for a period of six days. The experiments are performed from 29th August 2024 to 27th September 2024 on the rooftop of the Solar Energy Laboratory at IIT Guwahati (26.1158° N, 91.7086° E). No thermal loads, such as internal heat generation units, are applied from the internal surface of the walls for both experimental cubicles.

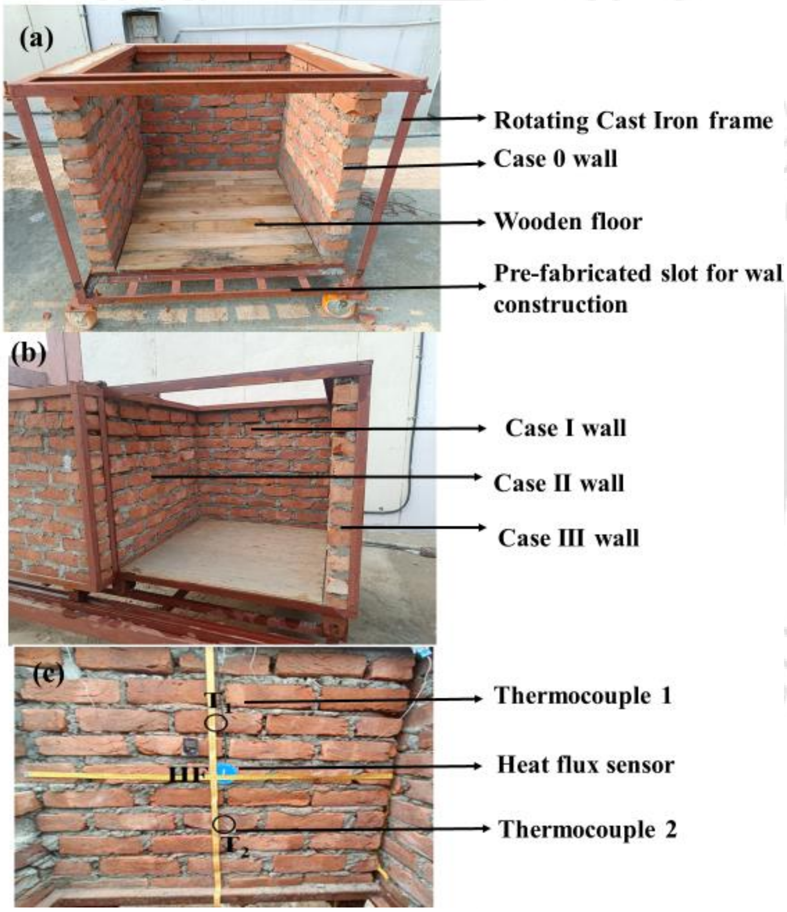

Fig. 4.5 (a) Wall construction on pre-fabricated cast iron frame (Case 0), (b) WH-PCM brick wall construction, (c) Thermocouple and heat flux sensor position on each wall

4.2.4 Quality testing of the modified bricks

The density of the red clay bricks has been determined according to BS EN 12390-7 standards [267]. The water absorption test has been conducted in accordance with BS 1881: 12 [268]. The brick samples have been put in a dry air oven (Make: Hamco, Model: 105 series) at

105±2°C for 24 hours to measure the dry weight. (m_d). The bricks are then cooled to room temperature and then immersed in water for another 24 hours. The weight of the wet bricks (m_w) has been recorded, and the percentage of water absorption has been calculated as per **Eq. 4.2**.

$$\text{Percentage of water absorption} = \frac{m_w - m_d}{m_d} \times 100 \tag{4.2}$$

The efflorescence test of bricks is done in accordance with IS 3495-Part 3 (1992) [269]. The compressive strength of the bricks is determined by ASTM C140-11a standards [270]. The test is done on a Compression Testing Machine (Make: Lawrence and Mayo, Model: 10913). The compressive strength has been determined using **Eq. 4.3**.

$$\text{Compressive strength} = \frac{P_{\max}}{A} \tag{4.3}$$

where $P_{\max}$ = Maximum compressive load (N) and

A = Average net area of specimen (mm^2)

4.2.5 Development of experimental cubicles

The section consists of the construction of an experimental cubicle with the best configuration of walls from the previous study. The subsection outlines the experimental methodology for the thermal performance study of the prototype experimental cubicle with walls made up of WH-PCM-filled bricks.

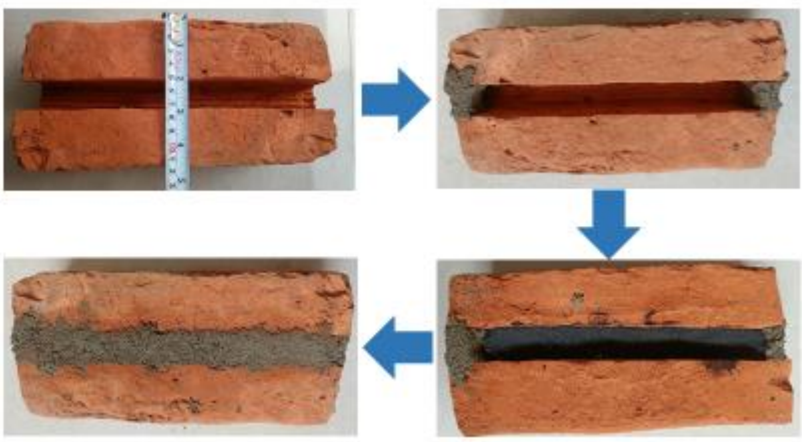

Fig. 4.6 Preparation of clay brick with WH-PCM slot

To construct the walls of the test cubicle, bricks are prepared in advance, as explained in **Section 4.2.3**. Case II of the previously explained configuration is selected for the wall construction of the experimental cubicle, as shown in **Fig.4.6**.

Fig. 4.7 Development of prototype buildings (a) Frame for reference cubicle, (b) Frame for PCM cubicle, (c) Sliding rail provision for PCM cubicle, (d) Interior of the developed PCM cubicle, (e) Reference cubicle outer view, (f) PCM cubicle outer view

Two outdoor experimental cubicles have been constructed to compare the thermal performance of walls made with PCM bricks versus those made with conventional bricks. The inner dimension of the cubicle is (1m x 1m x 1m). The two test cubicles are built on a movable cast-iron frame, where slots are provided for wall construction. One cubicle is referred to as the reference cubicle, where normal red clay bricks of size (23 cm x 11 cm x 7 cm) have been used for wall construction. The second cubicle is termed the PCM cubicle, where WH-PCM-enhanced brick walls have been constructed in all four directions. To build one wall, 50 bricks are needed, requiring a total of 10 kg of WH-PCM for the experimental cubicle. **Fig.4.7** demonstrates the different stages of construction of the experimental cubicles. A similar kind of portable room was already developed in published literature[271]. Finally, the thermal performance results have been compared with the published literature.

4.2.6 Experimental design for the thermal performance study

The experimental procedure includes the 24-hour recording of indoor and outdoor temperature fluctuation, along with the temperature variation on each wall for both cubicles. There are two main experimental schemes involved in the current study. The first set of experiments has been performed for one month from 8th October, 2024, to 8th November, 2024. The interior temperature has been recorded through a mini data logger (Make: Testo, Model: 174 H), placed in an identical position for both cubicles. The accuracy of the data logger is ±0.5^{o}C. The interior temperature has been further verified with the results of two thermocouples with an accuracy of ±0.25^{o}C, placed inside the cubicle. Also, the ambient temperature and solar radiation have been measured with a T-type thermocouple (accuracy ±0.25°C) and a pyranometer (uncertainty less than 3%), respectively. The second set of experiments involves a heat generation unit inside the cubicles. The experiment has been carried out for one week from 8th November to 13th November, 2024. The internal heat generation is achieved with an incandescent bulb of 200 W. The bulb is placed at the centre of the cubicle, as shown in **Fig.4.8**. The mini data logger and other thermocouple arrangements used for data generation are the same as those in the previous experiment. Beginning at 9:00 AM, the bulb has been operated in a cyclic on-off mode, with one hour of operation followed by one hour of shutdown. This cycle has been maintained continuously over a total duration of 12 hours. In both conditions, the outer and interior temperatures of each side wall have been measured with thermocouples.

Fig. 4.8 Experimental cubicle with heat generation unit

4.3 Results and discussion on comparison of the temperature profile in the thermal chamber

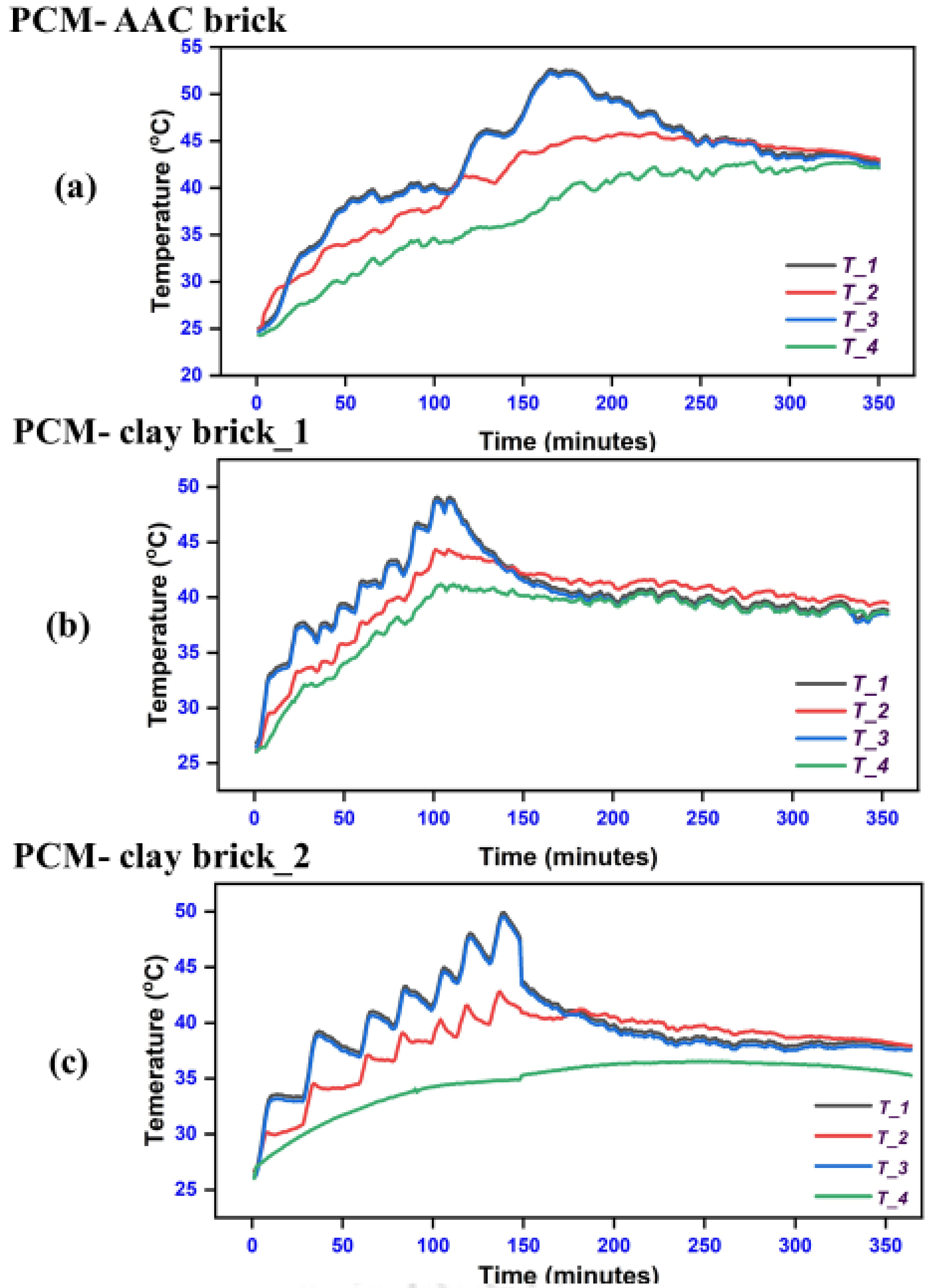

Fig. 4.9 Temperature profile of different reference and PCM bricks inside the thermal chamber (a) PCM-AAC brick, (b) PCM-clay brick_1, (c) PCM-clay brick_2

4.3.1 Autoclaved aerated concrete (AAC) brick

Figure 4.9 (a) illustrates a comparison of temperature patterns between regular AAC bricks and WH-PCM AAC bricks. The figure demonstrates that the temperature behavior near the heat source (T_1 and T_3) follows a similar pattern. In particular, the average temperature difference between the points (T_1 and T_2) and (T_3 and T_4) is 2.65°C for normal bricks and 6.5°C for WH-PCM bricks, respectively. These results indicate that the PCM melting occurs, resulting in heat absorption through fusion. Additionally, temperature fluctuation occurs steadily, which is crucial for comfortable indoor thermal environments, as rapid fluctuations can be highly discomforting. After both types of bricks are heated to 55°C in the thermal chamber, the heating element is turned off. As depicted in **Figure 4.9 (a)**, while the temperature near the heat source (T_1 and T_3) decreases, the interior temperatures of both normal bricks and WH-PCM bricks initially increase and then decrease. This phenomenon arises due to the high thermal resistance provided by the pores of the AAC bricks, which slows down heat penetration inside the bricks. Notably, the temperature at the point (T_4) of WH-PCM bricks remains lower than the temperature of normal AAC bricks throughout the experiment, with an average difference of 2.73°C during the cooling process.

4.3.2 PCM-clay brick_1

Fig. 4.9 (b) shows the temperature difference profile of normal and WH-PCM-clay brick_1. WH-PCM melts at 31.5^{o}C, so the WH-PCM brick is able to maintain an average temperature difference of 1.93^{o}C throughout for the thermocouple (T_4) compared to normal brick. The maximum temperature difference between (T_1 and T_2) and (T_3 and T_4) is found to be 4.8 and 7.8^{o}C for normal and WH-PCM brick, respectively. The surface near the heat source cools down rapidly after the heating source is turned off (T_1 and T_3), but an exception can be seen for the normal bricks for temperature T_2. The temperature T_2 increases for normal clay brick, and after 1 hour, the temperature is higher than T_1. The PCM-incorporated brick maintains the same temperature range throughout the cooling process. A maximum temperature difference of 3.5^{o}C can be achieved with the incorporation of WH-PCM in the clay brick. Thus, it is clear that PCM-clay brick_1 is suitable for maintaining a lower inside temperature in buildings day and night compared to normal clay bricks.

4.3.3 PCM-clay brick_2

Fig.4.9 (c) represents the temperature profile of the four thermocouples in the thermal chamber for PCM-clay brick_2. The temperature T_4 for WH-PCM brick in configuration 2 shows a smooth curve with an average temperature difference of 7.73^{o}C compared to T_3. A maximum temperature reduction of 7.98^{o}C has been found for PCM-clay brick_2 compared to the standard clay brick. When the heat source is turned off, the temperature T_2 increases, as explained in the case of PCM-clay brick_1. The curve showing temperature T_4 shows a smooth increment throughout the experiment. This behavior is very suitable for maintaining a steady comfort state in buildings without rapid temperature fluctuation. Also, it has been observed that no leakage of PCM happened throughout the experimental time, thereby confirming its stability and safety.

Based on the above discussion, it can be deduced that in real-world scenarios, the interior temperature of a building can be effectively regulated to a lower value using WH-PCM clay bricks during the daytime. However, it has been noticed that after the heating source is turned off, which partially resembles the setting of the sun, the temperature will rise for both regular bricks and PCM-clay brick_1. The indoor study also showed that PCM-clay brick_2 shows better results for temperature reduction and fluctuation than PCM-clay brick_1. In this regard, PCM-clay brick_2 is an exception, showing a smooth temperature variation and thus can be recommended for use in wall construction.

4.4 Thermal performance test results in outdoor conditions

Based on the above discussion, PCM-clay brick_2 is selected for wall construction, and WH-PCM is applied along the breadth of the wall in three different positional variations. This section describes the thermal performance of WH-PCM-incorporated walls compared to reference walls for the three different cases of PCM positions, as described in **Section 4.2.3**.

4.4.1 Calibration test

The calibration test is conducted to verify the proper functioning and consistency of the measurement instruments. The calibration tests are performed for each room without installing PCM, measuring the external and internal temperature and heat flux before the actual experimentation. Therefore, the east wall in the PCM room was constructed with normal bricks, so that an accurate comparison of the temperature and heat flux of the wall with the respective reference wall can be established. The calibration test was done on the 27th of August, 2024, from 9:30 hours to 17:00 hours. **Fig.4.10** depicts the results of the temperature and heat flux of the test walls in the calibration tests. The external temperature and heat flux of the reference room wall and the PCM room wall follow the same trend with little deviation. The maximum exterior and interior temperature deviation is 1.3° and 1.2°C, respectively, in the east wall, without any PCM layer. The maximum heat flux deviation is found to be 1.3 W/m^2.

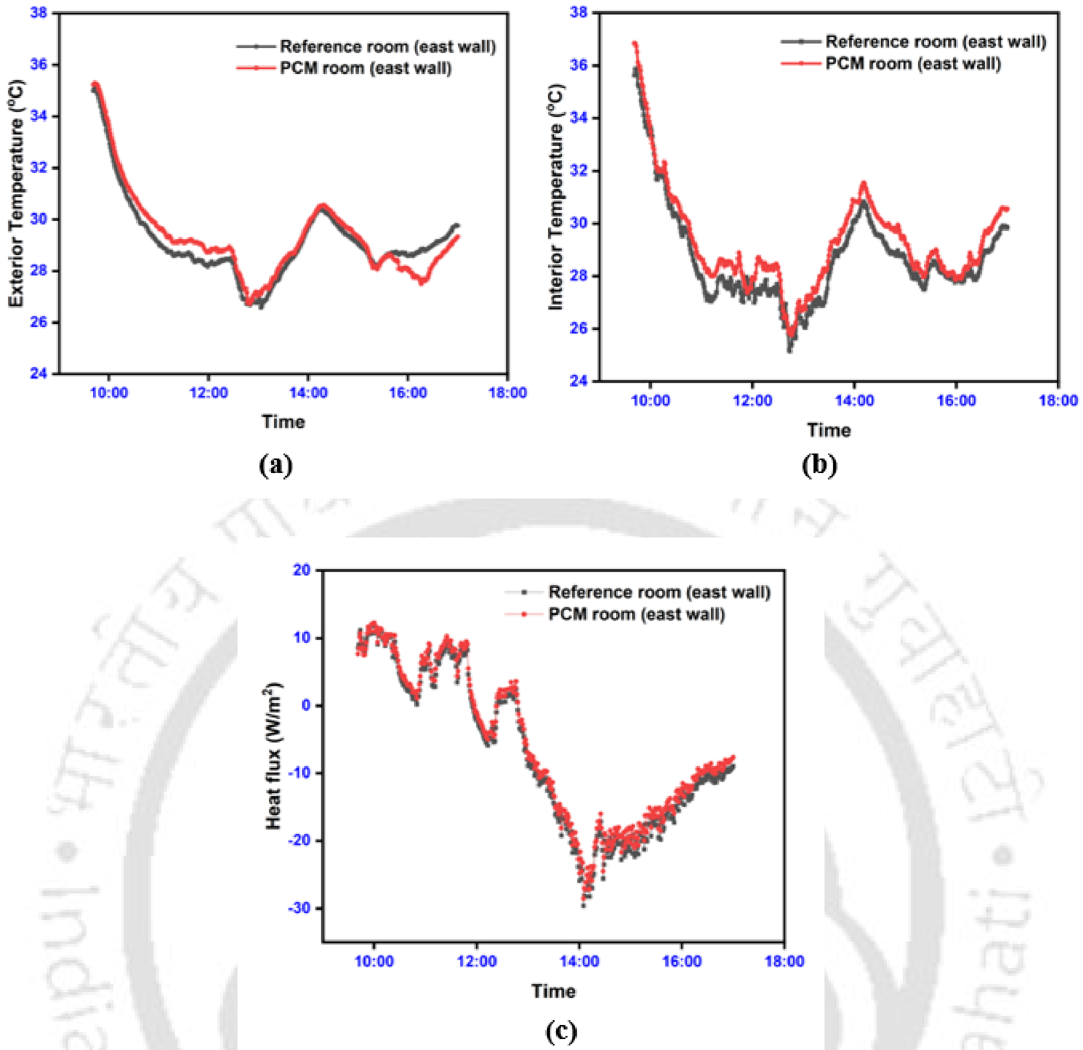

Fig. 4.10 Calibration test results (a) Exterior surface temperature, (b) Interior surface temperature, (c) Interior heat flux

4.4.2 Outdoor test results

4.4.2.1 Ambient temperature and solar irradiance

The ambient temperature and solar irradiance data of the experimental period are plotted in **Fig.4.11,** and **Fig.4.12**, respectively. Since the ambient temperature and solar irradiance during the four selected time periods are fairly comparable, as shown in **Table 4.5**, the results for each direction are analyzed and compared across the three different cases, with minor variations in ambient temperature being considered negligible. The term 'temperature difference' refers to the difference in temperature between the exterior and interior surface of the wall, either for the reference (case 0) or the test walls (case I, II or III).

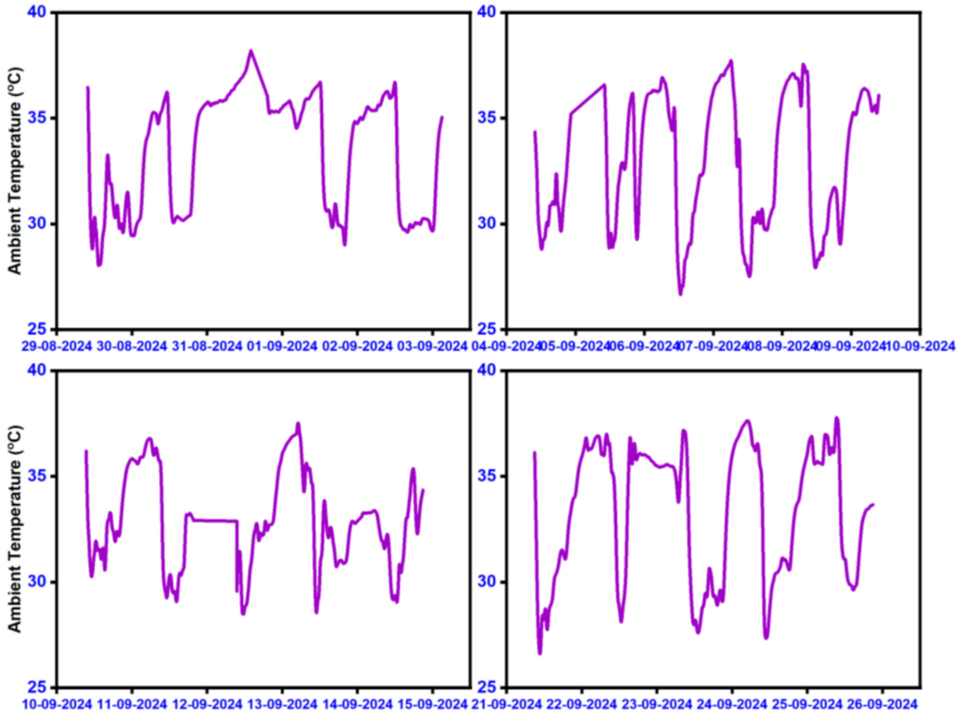

Fig. 4.11 Ambient temperature profile for the experimental period

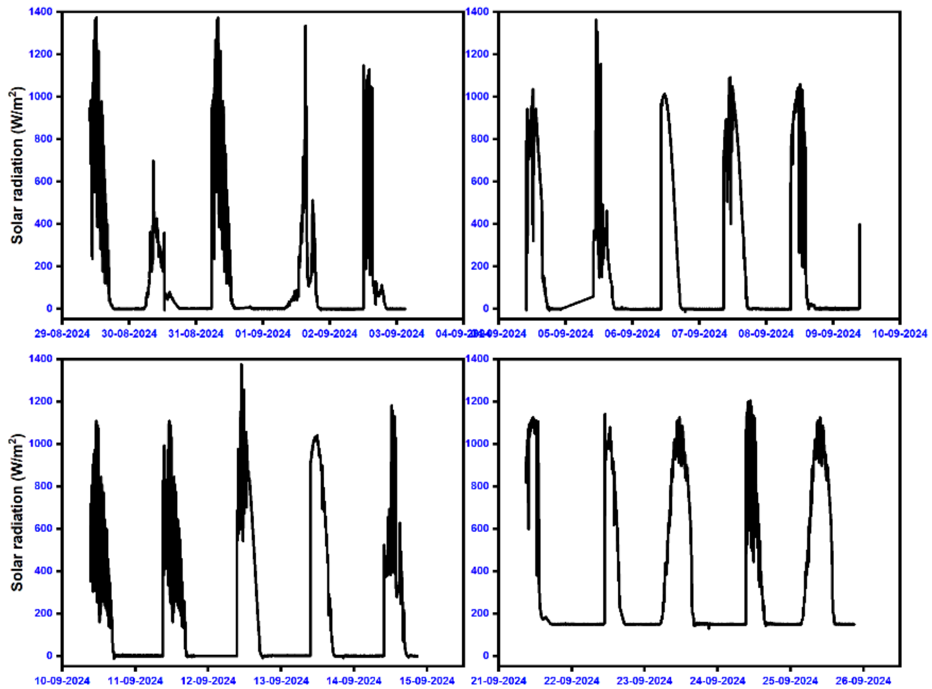

Fig. 4.12 Solar irradiance profile for the experimental period

Table 4.5 Temperature variation across different experimental period

	Ambient Temperature (°C)			Solar irradiance (W/m^2)	
	Minimum	Maximum	Average	Minimum	Maximum
29.8.2024-04.9.2024	25.6	38.2	33.3	0.001	1374.7
04.9.2024-10.9.2024	25.9	38.7	32.9	0.001	1363.7
10.9.2024-16.9.2024	25.7	38.2	32.6	0.003	1375.5
21.9.2024-27.9.2024	25.2	38.2	33.6	0.001	1204.5

4.4.2.2 East Wall

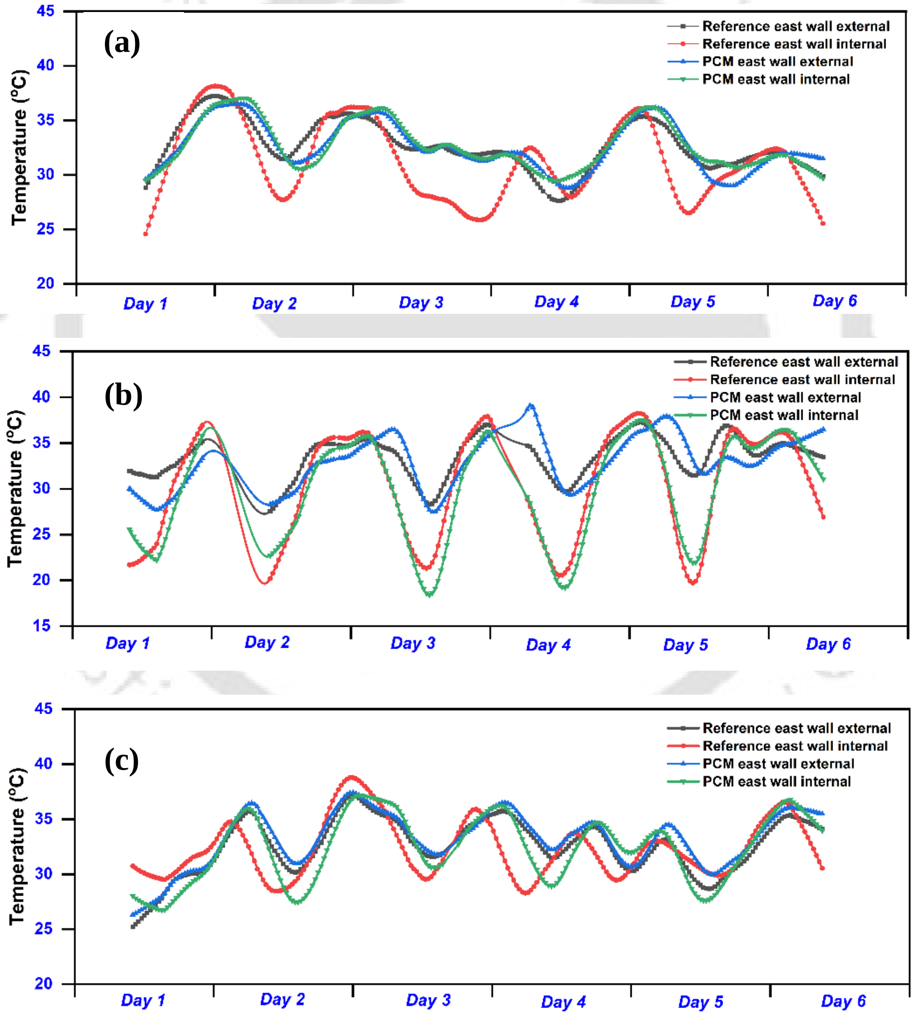

Fig. 4.13 Temperature profile in the east direction (a) Case I, (b) Case II, (c) Case III

The temperature profile for the east wall is represented in **Fig.4.13**. The curve shows that for case I in the east orientation, the inside surface temperature is higher than the outside surface temperature for the WH-PCM incorporated wall during the experimental period. In fact, the wall without WH-PCM behaves better in terms of temperature reduction The maximum observed temperature difference between the reference and WH-PCM wall is 6.2° and 2.74°C, respectively. Therefore, case I may not be an effective configuration for the PCM application on the east-facing wall. A similar effect has been observed in a previous study where the authors found that when the PCM layer is positioned on the interior side of a wall, the heat storage and heat release duration increase, which is beneficial for winter application for heating purposes. The slower charging and discharging of PCM leads to higher surface temperatures and an earlier onset of thermal stabilization [272]. Another reason for such a negative temperature profile trend may be due to the fact that the solar radiation hits the east wall and remains for a shorter period of time compared to the south and west walls, thus this time may not be enough to complete the full melting of WH-PCM, which is positioned on the interior side of the room.

Case II shows the best results in terms of temperature reduction out of the three cases, positioned in the east direction, specifically in the morning hours when direct solar radiation heats the east wall. The maximum temperature difference achieved for the WH-PCM wall is 11.8°C in the morning for case II, compared to 11.7°C for the reference wall. Case III is better in terms of temperature reduction compared to case I for the east direction, because the WH-PCM on the outer layer starts absorbing the latent heat quickly when the peak incident irradiation hits the wall in the morning, thereby reducing the temperature. Similar results were found for PCM placed at the outer surface, where the absorption of intense external heat led to the highest reduction in heat transfer, which was around 35% [273]. According to another study, the east wall demonstrated a reverse temperature trend compared to the other orientations. As the surface temperatures rise earlier in the day due to morning solar irradiance, the PCM completes its melting phase more quickly, thereby failing to maintain the reduced temperature difference for a longer time [274]. Although case II, the east direction, shows some potential in lowering the indoor surface temperature in the morning hours, the effectiveness of PCM is limited at other times of the day. Therefore, the use of WH-PCM in the east-facing wall is not recommended.

4.4.2.3 North wall

The temperature profile for the north wall is shown in **Fig.4.14.** For case I, the WH-PCM wall behaves almost similarly to the reference wall in most cases. But, the maximum temperature difference of the WH-PCM wall is 11°C, compared to 8.6°C of the reference wall. The middle position (case II) of WH-PCM in the north direction results in an overall temperature reduction, contrary to cases I and III, but the maximum temperature difference is around 7°C for both the reference and WH-PCM wall. For case III, it has been observed that the inside surface temperature of the reference wall is lower compared to the WH-PCM layer for a longer period during all days. It is reported that the north direction receives minimum direct solar radiation, and the only factor that affects the PCM charging or discharging is the ambient temperature; therefore, WH-PCM may merely act as a thermal insulator due to its low thermal conductivity. In such cases, the solidified PCM essentially behaves like a weak concrete layer with reduced structural rigidity and without contributing to thermal regulation through latent heat absorption. Therefore, it may be more effective to use a plain concrete wall without incorporating PCM on the outer layer in the north direction [275]. Comparing the results for the north direction, it can be concluded that the north direction is also not effective in terms of the reduction of inside surface temperature.

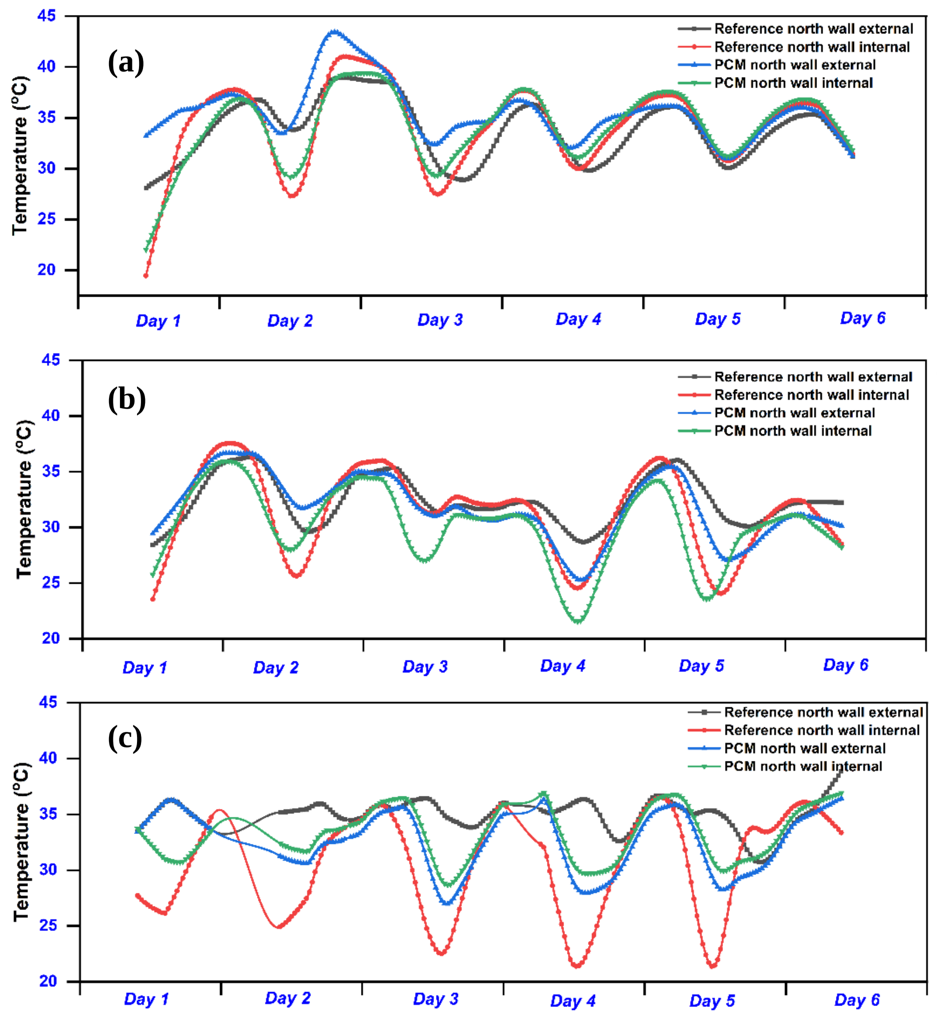

Fig. 4.14 Temperature profile in the north direction (a) Case I, (b) Case II, (c) Case III

4.4.2.4 South wall

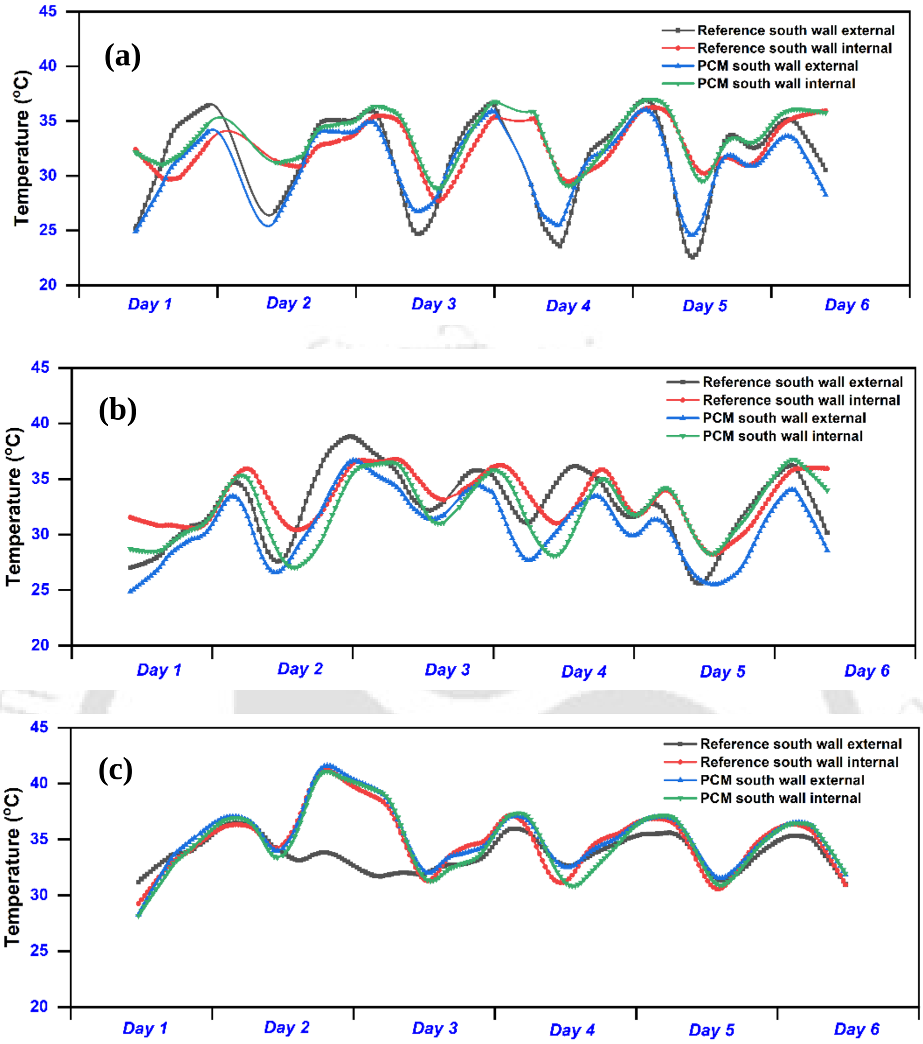

Fig. 4.15 Temperature profile in the south direction (a) Case I, (b) Case II, (c) Case III

Fig.4.15 shows the temperature profile of the three cases in the south direction. As no effect in terms of temperature reduction can be observed for Case I in the south direction, the position is not recommended for the south wall. In fact, the inside temperature of the reference wall is lower in this case. The intense solar incident radiation in the south direction throughout the day may be a reason for such a phenomenon, and WH-PCM may remain in the superheated liquid state most of the time. On the south wall with Case II, it is evident that WH-PCM effectively reduces the inside surface temperature compared to the reference wall. The maximum temperature difference of the WH-PCM wall is 2.7°C. The maximum temperature reduction observed across the WH-PCM wall is approximately 2°C, while that of the reference wall is about 1.94°C for case III. It can be seen from the temperature graph that the inside surface of the reference wall is occasionally higher than the outside surface. With the application of WH-

PCM as case III, the higher inside temperature can be reduced successfully, thereby showing better indoor thermal regulation. Previous study confirmed that on the south wall, a faster temperature rise led to quicker PCM phase change, resulting in a moderate temperature reduction and shorter delays [274]. It can be observed that WH-PCM on the outermost layer is suitable for temperature reduction compared to the other two positions in the south direction. One reason for the behavior is that the outer layer is affected by external convective cooling; thus, heat dissipation to the environment is greater compared to Case I. For Case I, heat is stored in the wall mass, as there is little scope for heat dissipation to the ambient. Thus, applying the WH-PCM layer in the walls of the south direction can be recommended for inside surface temperature reduction.

4.4.2.5 West wall

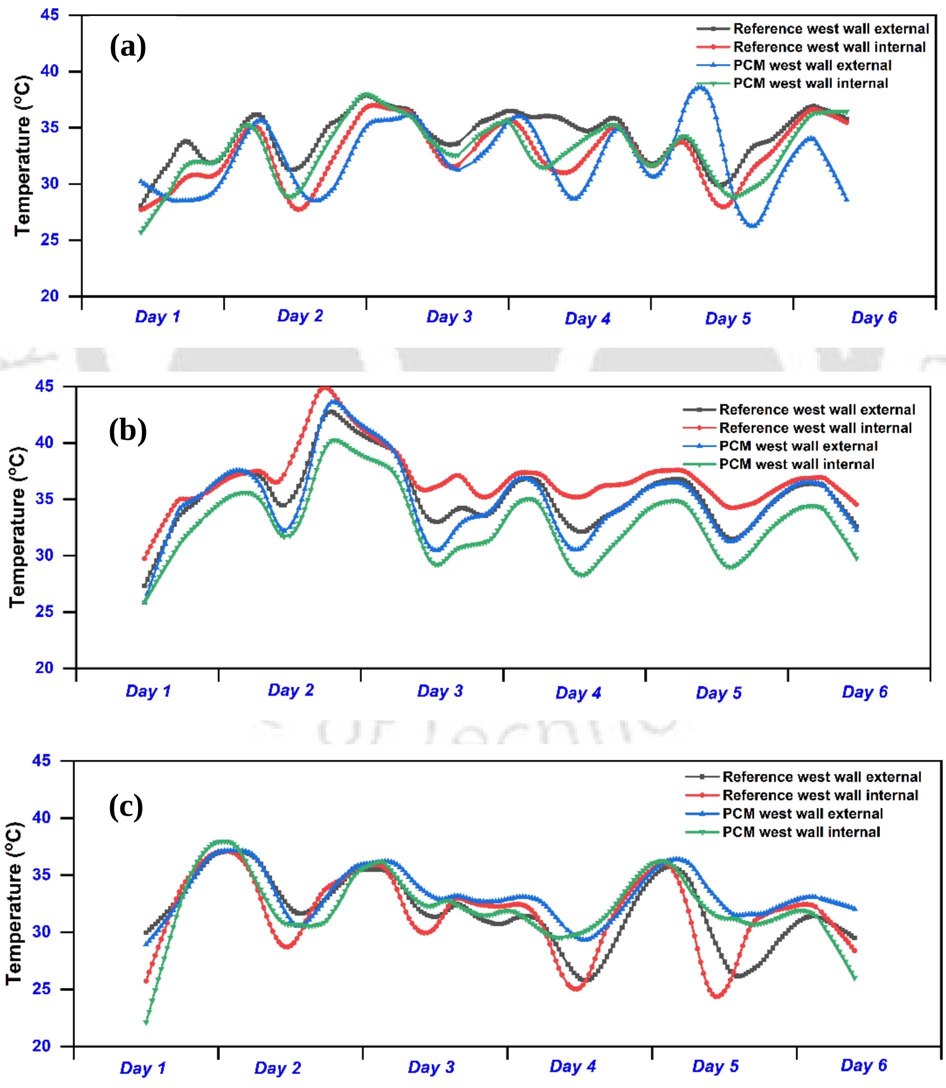

Fig. 4.16 Temperature profile in the west direction (a) Case I, (b) Case II, (c) Case III

Fig.4.16 represents the temperature profile of the west walls. The maximum recorded temperature difference across the case I wall is 6.7°C, which is 4.8°C for the reference wall. It is observed that when peak intensity hits the west wall in the afternoon, the temperature of the WH-PCM wall is lower than that of the reference wall, which will be beneficial in decreasing peak cooling demand. Earlier studies showed that the west wall showed the highest daily energy savings due to high afternoon solar loads that raised surface temperatures quickly, enabling full PCM melting [274]. Case II shows the best results in terms of indoor wall temperature reduction over the experimental time. In fact, the experimental data show that the inside temperature of the reference wall is more than the outside in most cases, but WH-PCM is able to keep the temperature near 35°C for peak daytime hours and an average minimum of 28°C in the off-peak night hours. The maximum temperature difference obtained for WH-PCM and the reference wall is 3.5°C. In the afternoon, at around 4 PM, when the outside temperature attains its maximum, the middle configuration on the west wall shows the maximum temperature difference. For Case III on the west wall, the maximum temperature difference between the exterior and interior surfaces of the PCM wall is 6.9 °C, compared to 5.3 °C for the reference wall.

The middle position is able to absorb heat from both sides and may make two distinct thermal zones. The absorption of heat from both sides reduces the heat gain through the wall, ultimately reducing the inside surface temperature. The PCM incorporation at the outside position in the west direction results in successful temperature reduction during the day. The nighttime shows a higher inside temperature than the outside wall, which indicates that the discharging of WH-PCM is not completely achieved. As the climatic condition of the studied site exhibits warmer nights, only night ventilation may not be sufficient for WH-PCM cooling. Discharging through an active system can assist in such cases. In nearly all cases, the indoor surface temperature showed unfavorable behavior at night due to the solidification phase of the PCM in the non-ventilated space, as previously noted [88]. Another study also showed that all elements of the PCM room exhibited increased temperatures at night due to the uncontrolled release of stored heat from the PCM [276]. The west direction is found to be more efficient in temperature reduction than the east direction because WH-PCM melting in the east direction occurs early in the morning and lasts for a shorter period of time than the west wall [277]. Overall, the application of WH-PCM on the west walls can be treated as the most effective direction for reducing the inside surface temperature, compared to the other three directions.

4.4.3 Comparison of peak temperature

After analyzing the overall temperature profile, a comparison is shown in **Table 4.6** in terms of peak temperature reduction through different configurations of the wall. When WH-PCM incorporated, a brick is placed next to the interior of the test room, and the effect of PCM in terms of peak temperature reduction is not very prominent. It has also been noticed from earlier research that applying PCM on interior surfaces has less effect on temperature reduction. All the walls behave satisfactorily in terms of peak temperature reduction when the PCM position is in the middle of the wall. The best peak temperature reduction result is found for the west-facing wall in case II, with a 10.47% reduction. The peak temperature reduction is suitable for reducing the electricity demand for peak power consumption. A similar peak temperature reduction (4.7 °C) is found for a room facing south direction when macroencapsulated PCM was used in the hollow brick of a small room, which is approximately half the size of the room used in the present study [149]

Table 4.6 Comparison of peak temperature reduction

Wall direction	PCM position	Reference wall peak temperature (ºC)	WH-PCM wall peak temperature (ºC)	Reduction in peak temperature (ºC)	Percentage reduction in peak temperature (%)
East	Case I	36.5	38.1	-1.6	-4.38
	Case II	38.2	37.5	0.7	1.83
	Case III	38.7	37.1	1.6	4.13
North	Case I	41.1	43.4	-2.4	-5.6
	Case II	37.5	35.9	1.6	4.27
	Case III	36.5	36.9	-0.4	-1.1
South	Case I	36.2	36.9	-0.7	-1.93
	Case II	36.7	36.7	0.01	0.05
	Case III	41.2	41.0	0.1	0.49
West	Case I	36.9	37.9	-0.9	-2.71
	Case II	44.9	40.2	4.6	10.47
	Case III	37.1	37.9	-0.8	0.49

Contrary to the results of Case I, the wall facing the east, west and south directions is successful in reducing peak temperature compared to normal walls for Case III. Based on the testing data, the best locations for peak temperature reduction, in decreasing order, are Case II, Case III, and

Case I. This is because the PCM position determines the starting time of PCM melting. Case III results in the early melting of WH-PCM; thus, thermal energy can be stored for a long time. Another possibility is that complete melting of WH-PCM may be ensured for Case III, compared to Case I. Also, the thermal resistance for heat flow is greater in Case I before reaching WH-PCM than in Cases II and III, as shown in **Fig.4.17.** Thus, the wall gets heated up before melting starts. On the other hand, placing WH-PCM in the middle of the wall may coincide with the peak heating hours, which may be earlier or later in Case III or Case I, respectively. The middle position may balance the charging and discharging of WH-PCM, thereby preventing a rapid temperature rise. Earlier studies also proposed placing PCM close to the exterior or in the middle position for maximum annual energy saving [278]. WH-PCM in the middle of the wall acts as a thermal buffer zone, reducing the overall thermal conductivity and dividing the wall section into two thermal zones. Therefore, the thermal conduction through the wall gets reduced. Applying the thermal resistance concept to a multilayer wall, the thermal resistance of the different configurations of WH-PCM walls has been calculated as per **Eq. 4.4.**

$$U_{overall} = R_{brick} + R_{WH-PCM} + R_{brick} = \left(\frac{L}{k}\right)_{brick} + \left(\frac{L}{k}\right)_{WH-PCM} + \left(\frac{L}{k}\right)_{brick} \tag{4.4}$$

where R is the thermal resistance, L and k are the thickness and thermal conductivity of each layer.

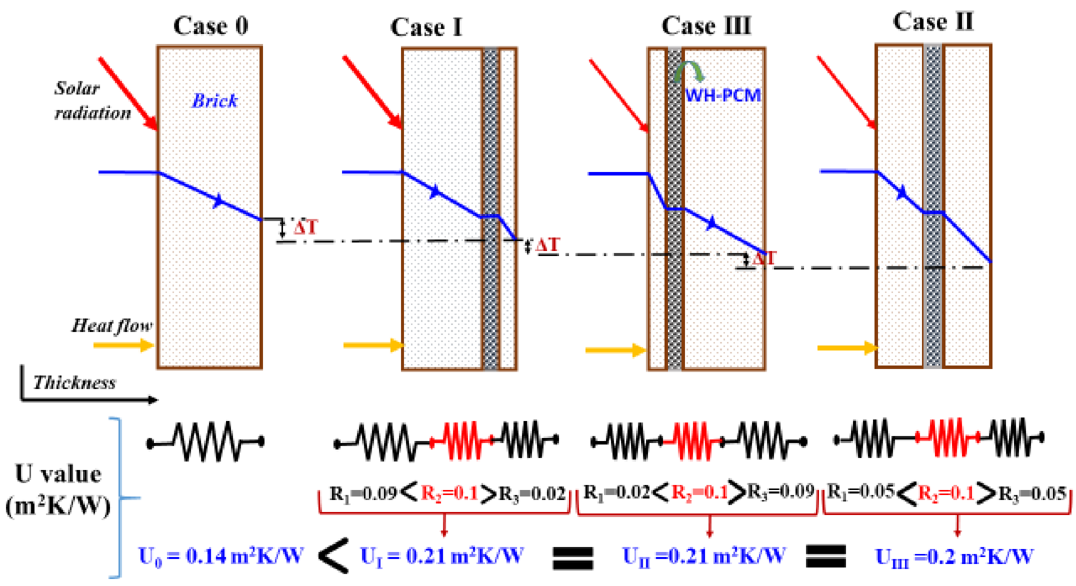

Fig. 4.17 The thermal resistance and heat flow analysis through WH-PCM walls

The overall thermal resistance values for Case I, Case II, and Case III are 0.21, 0.2, and 0.21 m^2K/W, respectively. Although the overall heat transfer coefficient value for the three cases is almost the same, a difference in inside temperature occurs due to the difference in thermal resistance value of the brick before reaching the WH-PCM layer.

Previous study on a test room of size 500 × 500 × 500 mm with PCM cladding on the outer wall resulted in peak surface temperature reductions of 6.75 °C (west), 6.50 °C (south), 5.00 °C (east), and 2.45 °C (north). Similar to the current study, the greatest reduction was observed on the west wall. On the south wall, extended solar exposure allowed full PCM melting, enhancing heat absorption. A moderate reduction was recorded on the east wall, and the lowest reduction occurred on the north wall, where limited solar input led to partial PCM activity [277].

Table 4.7 Peak temperature reduction comparison with earlier works

Reference	**Wall direction**	**PCM type**	**Peak temperature reduction (°C)**
Kong *et al.* [164]	South	A mixture of capric acid and 1-dodecanol	2.00
Mukram *et al.* [279]	Not mentioned	Micro-encapsulated PCM	8.91
Abbas *et al.* [149]	South	Encapsulated paraffin wax capsule	4.70
He *et al.* [278]	South	Rubitherm RT28HC	8.20
Absi et al. [277]	Not mentioned	Microencapsulated PCM	3.95
Ali et al. [280]	Not mentioned	Eutectic PCM	9.50
Present work	West	WH-PCM	4.66

The best results obtained from the present study have been compared with previous publications and presented in **Table 4.7**. Kong *et al.* [164]developed two configurations in which PCM was applied either to the outer surface and roof or to the inner wall and roof. Their findings aligned with the current study, showing that PCM placement on the east and west walls yielded better performance than on the east and north walls, particularly when applied to the outer surface, as in Case III. Similarly, Mukram *et al.*[281] recommended positioning PCM near the middle of the wall in commercial buildings. Their results indicated that placing PCM closer to the outer surface or heat source, combined with night ventilation, reduced the solidification time. Although many studies listed in **Table 4.7** report significant temperature reductions consistent with the present findings, most were conducted in rooms approximately half the size of the current test room. In several cases, only one PCM-modified wall was evaluated, with the remaining walls constructed from insulating materials and tested in controlled indoor setups. In contrast, the present study offers a more realistic representation of temperature reduction under actual conditions.

4.4.4 Thermal amplitude comparison

Table 4.8 presents the thermal amplitude values of the WH-PCM walls in comparison with the reference walls for each direction and position. The thermal amplitude value has been calculated by using **Eq. 4.5**.

$$\text{Thermal amplitude} = T_{peak} - T_{\min} \tag{4.5}$$

where and $T_{\min}$ represent the maximum and minimum inside surface temperature of the wall.

The middle position of PCM placement results in both reductions of maximum and minimum temperature, thus increasing the thermal amplitude values in all directions except the west direction.

Table 4.8 Thermal amplitude values for different directions and WH-PCM positions

Wall direction		Reference wall (°C)			WH-PCM wall (°C)			
		T_{peak}	T_{min}	Thermal amplitude	T_{peak}	T_{min}	Thermal amplitude	Reduction
East	Case I	36.5	28.8	7.7	38.1	24.5	13.5	-5.86
	Case II	38.2	19.7	18.55	37.5	18.4	19.1	-0.56
	Case III	38.7	28.2	10.5	37.1	26.7	10.4	0.07
North	Case I	41.1	19.4	21.55	43.4	22.0	21.4	0.15
	Case II	37.5	23.5	13.99	35.9	21.5	14.3	-0.4
	Case III	36.5	21.3	15.14	36.9	28.6	8.2	6.89
South	Case I	36.2	27.7	8.53	36.9	28.8	8.1	0.37
	Case II	36.7	28.2	8.58	36.7	27.0	9.7	-1.16
	Case III	41.2	29.2	12	41.0	28.1	12.9	-0.9
West	Case I	36.9	27.7	9.28	37.9	25.7	12.2	-2.97
	Case II	44.9	29.7	15.19	40.2	25.8	14.3	0.81
	Case III	37.1	24.3	12.73	37.9	22.1	15.8	-3.11

A negative value for thermal amplitude reduction indicates that PCM inclusion has undesirable thermal behavior in those particular directions. In another aspect, the WH-PCM layer can be seen as an insulator layer, compared to the reference wall in those directions, as the same amount of solar radiation is falling on both walls. According to the Fourier law of heat conduction, if the heat flux is constant, a higher value of temperature difference specifies lower thermal conductivity. Therefore, although the negative value of thermal amplitude reduction phenomena is not beneficial considering thermal comfort management, it may be helpful in reducing the peak heat gain value through the wall. The previous study also shows the same trend for Case I in stabilizing indoor thermal fluctuation [282]. Similar published work stated that positioning the PCM in the middle of the wall or nearer to the primary heat source resulted in better year-round thermal performance [278]. Another study also confirms that while PCM is positioned in the middle of the brick, overall thermal performance was found to be improved [281]. The main factor for which the effect of orientation on PCM behavior changes in each direction for the same position is the difference in the duration of incident solar radiation. The south wall receives solar radiation in a uniform manner compared to the east and west directions. Accordingly, the difference between peak and minimum temperature is very high compared to the north direction. The thermal amplitude in the north direction is good because the north wall does not get direct incident solar radiation. Thus, the outer surface temperature is reduced slowly due to convection. Earlier studies also concluded that the north wall, with minimal solar exposure, showed the lowest temperature fluctuations and indoor temperatures [274]. The WH-PCM application in the west direction leads to overall temperature reduction, and this trend is very beneficial in maintaining thermal comfort and peak power reduction. This is because the peak intensity of radiation falls in the west direction, and west-facing walls retain the heat for a longer period than the other three directions.

4.4.5 Comparison of the heat flux profiles

The temperature profile variation is supported by the heat flux variation curve for the experimental duration. Some representative curves are shown in **Fig.4.18,** selected from the whole experimental period. The positive heat flux refers to heat gain indoors, and the negative heat flux indicates heat dissipation to the environment.

For Case III in the west direction, a similar heat flux pattern is followed for the reference and the WH-PCM wall. The peak heat gain reduction is 4 W/m^2 with a time lag of 10 minutes for the WH-PCM wall compared to the reference wall. The heat loss through the WH-PCM wall from the outside position is almost 3 times more than the reference wall, as heat conduction is dominant in that position for the discharging of WH-PCM, as shown in **Fig.4.18.** The east direction shows peak heat gain value in the morning hours for both WH-PCM and reference walls, as solar radiation is at its peak during those hours. When WH-PCM is applied close to the interior, the peak heat gain value is delayed by 2 hours. This thermal lag is beneficial in reducing the morning cooling energy demand in the east direction.

The middle position of WH-PCM in the north direction results in a maximum heat gain and average daily heat gain reduction of 5.9 and 2.5 W/m^2, respectively. When WH-PCM is incorporated in the outside orientation of brick in the south direction, the wall results in lower heat gain than the reference wall from morning 6:00 AM to noon time, indicating storing heat through the melting of WH-PCM. The overall lower heat gain inside the room is beneficial for the reduction in cooling energy demand.

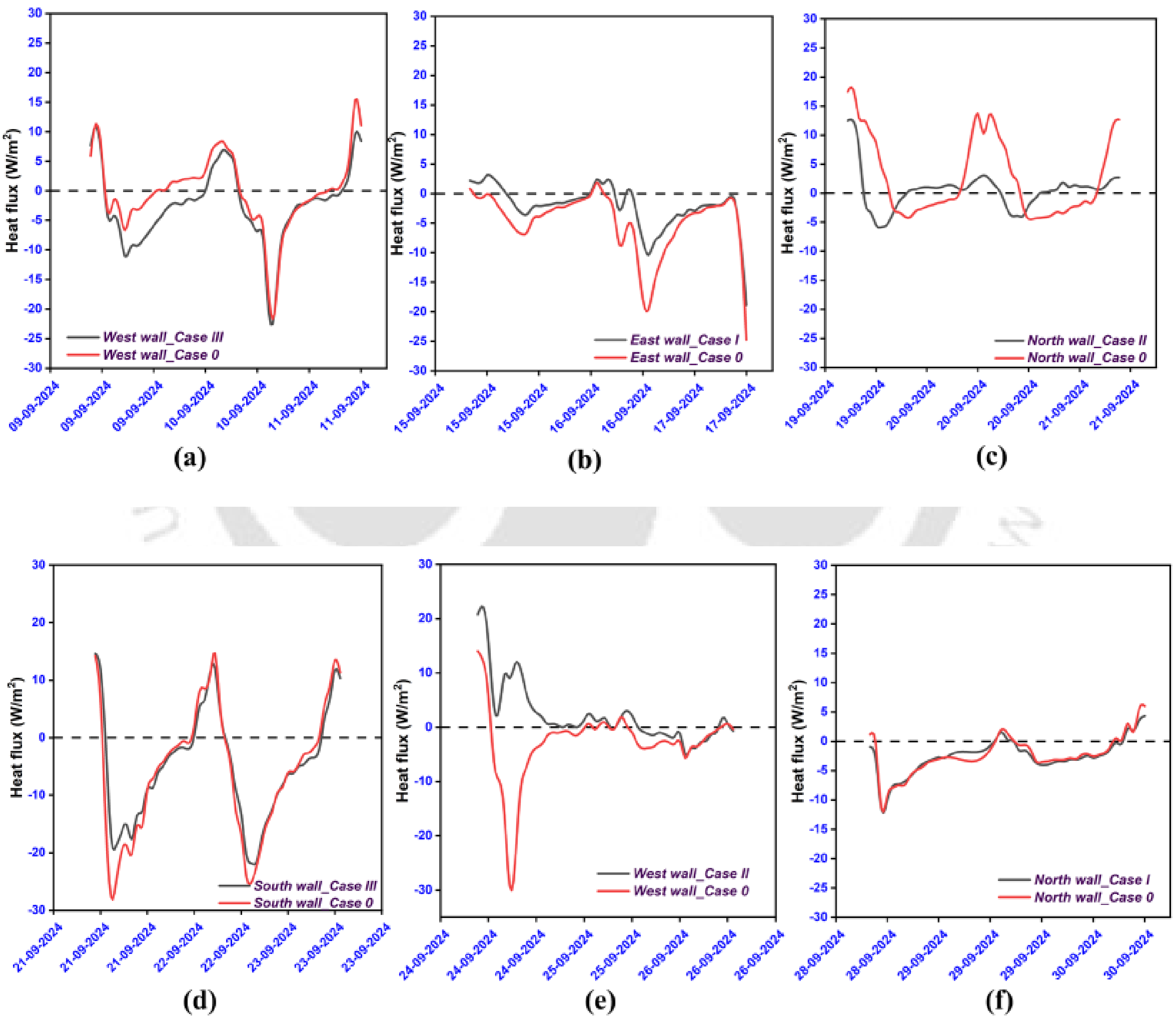

Fig. 4.18 Heat flux analysis through WH-PCM and reference wall, (a) West wall_Case III, (b) East wall_Case I, (c) North wall_Case II, (d) South wall_Case III, (e) West wall_Case II, (f) North wall_Case I

The daily average heat gain reduction using WH-PCM is 0.3 W/m^2 for Case III in the south direction. In the afternoon, due to increased inside temperature, both the reference and PCM wall start losing heat to the ambient until the next morning. At the early stage, the heat loss is more predominant in the reference wall till around 10:00 PM; after that, heat loss is more from the PCM wall, indicating less inside surface temperature of the PCM wall. Natural ventilation can be applied to the south wall from the afternoon to around 9:00 PM in the evening for the PCM wall to get the complete benefits of PCM incorporation in the south direction for Case III.

The average heat flux reduction is 2 W/m^2 for Case II in the west direction. When WH-PCM is applied on the interior side in the north direction, the heat flux profile follows exactly the same pattern for the two days. The orientation results in a 2.3 W/m^2 reduction in average daily heat gain and a 3.3 W/m^2 reduction in maximum heat gain value after WH-PCM incorporation. Also, the heat loss through this orientation is 14.5% more than the reference wall, which indicates the cooling of the PCM room. Previous literature showed that the heat gain decreased as the PCM position moved from the exterior toward the centre of the brick, from 11.62% to 32.05% [281].

The phenomenon of average and maximum heat flux reduction by using WH-PCM in walls can be explained through the thermal diffusivity, thermal conductivity and effective heat capacity concept. The thermal diffusivity of both WH-PCM and brick has been calculated by using **Eq. 4.6**.

$$\alpha = \frac{k}{\rho C_p} \tag{4.6}$$

where is the thermal diffusivity $\left(m^2/s\right)$, k is the thermal conductivity (W/mK), ρ is the density $\left(kg/m^3\right)$ and C_p is the specific heat capacity at constant pressure (J/kgK) of the material.

The values of C_P for WH-PCM vary, as mentioned in **Eq. 4.7**.

$$C_P = \begin{cases} C_{P,solid} & ;\text{WH} - \text{PCM is in solid state} \\ C_{P,effective} = C_{P,solid} + \left(\dfrac{\Delta H_m}{\Delta T}\right) & ;\text{WH} - \text{PCM is in phase transition} \\ C_{p,liquid} & ;\text{WH} - \text{PCM is in liquid state} \end{cases} \tag{4.7}$$

where ΔH_m and ΔT are the latent heat of fusion (J/kg) and the temperature range over which phase change occurs.

The thermal diffusivity value for the three states of WH-PCM is higher than that of the brick material in the wall. The higher thermal diffusivity value indicates that WH-PCM allows the heat to pass more quickly than the brick material and absorbs the heat as latent heat storage. As the effective heat capacity of the WH-PCM is more than the heat capacity in pure solid and liquid phases, WH-PCM absorbs significant heat and reduces the maximum heat gain through the walls. When WH-PCM is applied on the outer surface, its higher thermal diffusivity enables it to respond quickly by absorbing heat during the morning hours for the south-facing wall and in the afternoon for the west-facing wall, thereby reducing the maximum heat gain. The thermal lag observed in peak heat gain for Case I and Case II is attributed to the lower thermal diffusivity of the brick wall, which slows down heat penetration. As a result, the WH-PCM melts later compared to the outer placement, leading to a shift in the peak heat flux timing.

4.5 Comparison of the quality of normal brick and PCM-incorporated brick

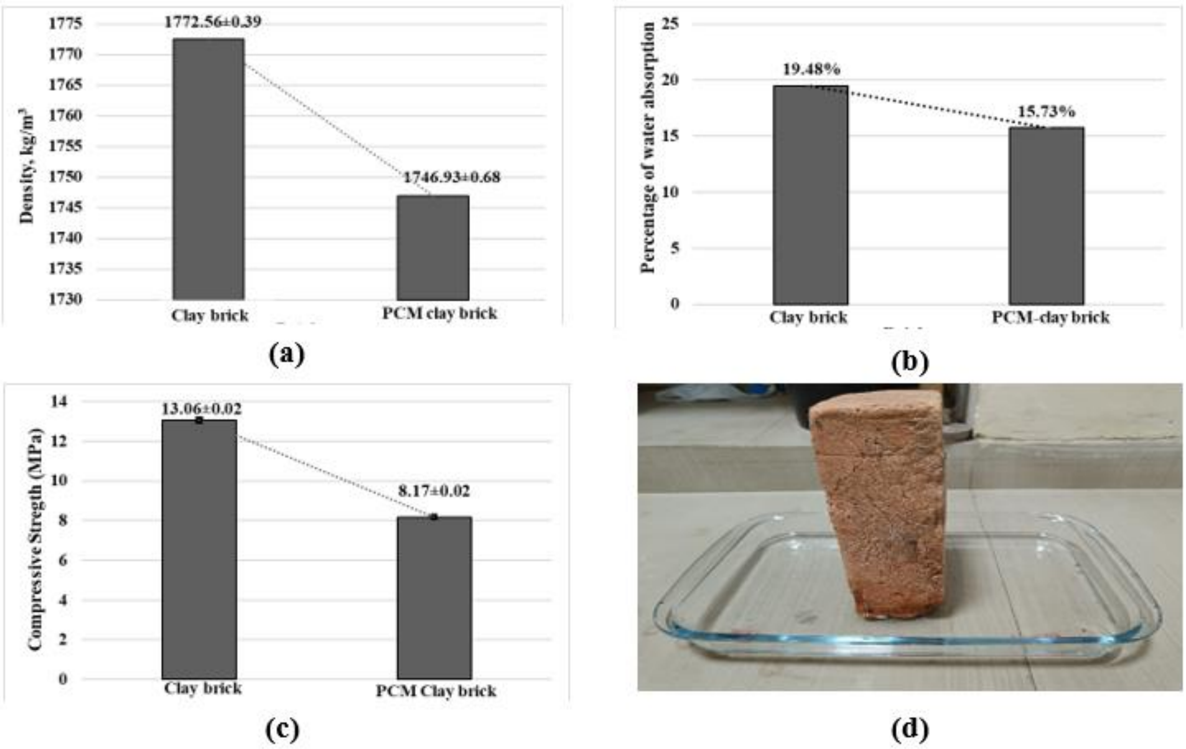

Fig. 4.19 Comparison of quality testing of WH-PCM clay bricks (a) dry density, (b) water absorption test, (c) compressive strength test, (d) efflorescence test of WH-PCM bricks

It is clear from **Fig.4.19 (a)** that the density decreases when PCM is incorporated into the bricks. It is obvious because when the PCM slot is created inside the brick, the mass of the brick reduces. The WH-PCM can not compensate for the mass loss of the brick material, as the density of WH-PCM is only 510 kg/m^3. The percentage change before and after PCM incorporation in clay bricks is found to be 1.45%. As per the ASTM C90-16a standards, the PCM clay bricks range in medium-weight density bricks, which can be used in practical applications [283]. **Fig.4.19 (b)** shows the comparative analysis of the water absorption test of clay bricks with and without PCM. The water absorption capacity of the clay brick after inserting WH-PCM decreases by 19.23%, which is desirable for building applications. The non-absorbent property of WH-PCM may be the reason for such a decrease in water absorption percentage.

Fig. 4.19 (c) shows the comparison of the compressive strength of clay bricks. It can be observed that the compressive strength is reduced for bricks when WH-PCM is introduced in the slot. The strength is reduced because the middle section of both bricks has been cut, and the brick material is replaced with the powdered WH-PCM. The reduction of compressive strength for clay brick before and after PCM insertion is 37.4%. According to IS 1077: 1992 standards, the PCM clay bricks come under grade 7.5, which is 12.5 for a normal clay brick [284]. The efflorescence test of the modified brick results in nil salt deposition on the surface of the brick, as shown in **Fig.4.19 (d).** The efflorescence test gives the idea of the presence of soluble salts, like potassium, sodium, magnesium, iron and calcium; silicate, or carbonates of calcium and sodium; or sodium bicarbonate, etc., inside the brick, which reacts with aluminate tricalcium in the cement, resulting in the fragmentation of joints and walls due to the volume expansion. As no white or yellow spots have been observed on the surface of the brick upon biocomposite PCM incorporation, the developed brick can be used in buildings without any risk of failure of the walls [269].

4.6 Thermal performance analysis of experimental cubicle

4.6.1 Solar irradiance and ambient temperature

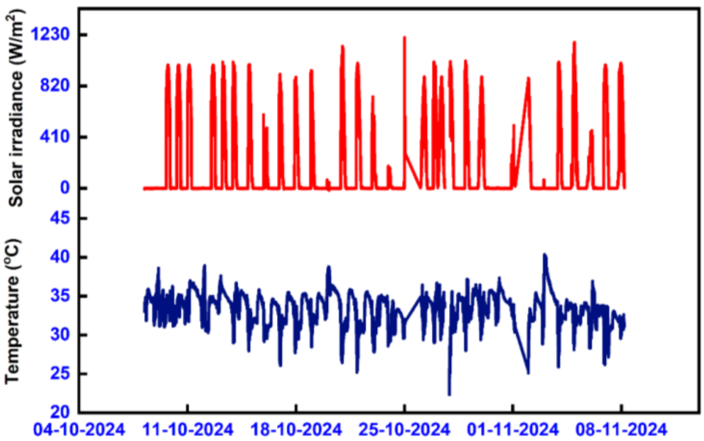

(a)

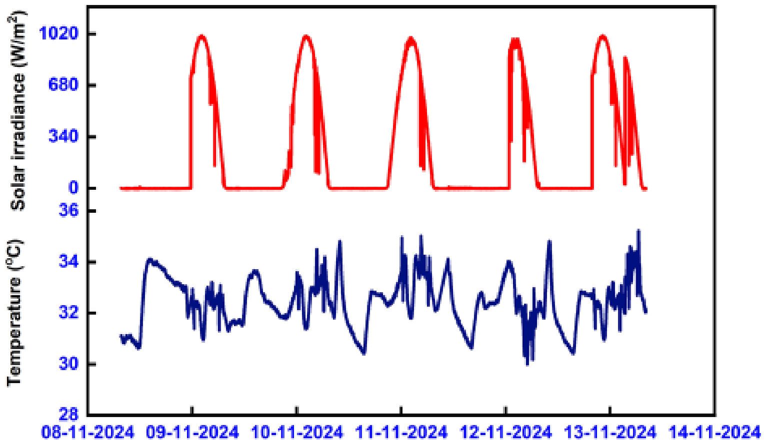

(b)

Fig. 4.20 Solar irradiance and temperature profile (a) for the period 8.10.2024 to 8.11.2024, (b) for the period 8.11.2024 to 14.11.2024

Fig.4.20 presents the daily solar irradiance and temperature profile of the experimental period as recorded by the pyranometer and thermocouples.

4.6.2 Comparison of the temperature profile of the experimental cubicles

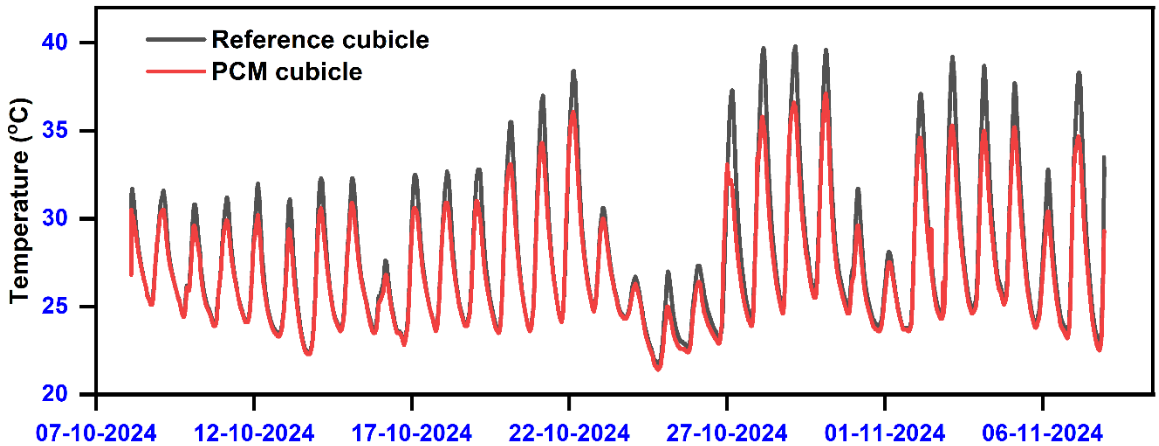

Fig. 4.21 The interior temperature of both rooms without any applied thermal load

The effect of WH-PCM integration on the walls of the test cubicle is compared with the reference cubicle and plotted in **Fig. 4.21.** The one-month temperature regulation study proves that WH-PCM is successful in the passive thermal management of experimental cubicles. During the daytime when the solar insolation is at its peak, WH-PCM walls store the heat, and thus the interior of the PCM cubicle remains cooler than the reference cubicle. The temperature difference is very prominent for the peak hours, i.e., from 12 AM to 12 PM at midnight. This reduction in temperature not only ensures occupant thermal comfort but also significantly contributes to the peak cooling load reduction of the building. The maximum temperature difference between the reference and the PCM cubicle is measured as 5.8°C on the 27th of October, 2024, at around 4:10 PM. A similar temperature reduction of 3.09 °C at peak hours was reported in a lab-scale experimental set-up incorporating microencapsulated PCM as a panel mixed with cement plaster and foamed concrete in the published literature [285]. After midnight, the temperature difference between the cubicles is not very significant. As the outside temperature is low at that particular time, a natural ventilation system can reduce the temperature inside the PCM cubicle, ensuring proper discharging of the PCM at night. As the WH-PCM discharging is a time-dependent phenomenon, in the morning hours when solar radiation heats the east and south walls, due to incomplete solidification of WH-PCM, the latent heat of solidification may discharge towards the interior side of the building. Thus, on some of the days from the experimental period, a slight increase in temperature has been observed in the PCM cubicle from around 9 AM to 11 AM. Thus, the discharging of WH-PCM should be completed before the day begins, and ventilation may be a good option for such conditions.

Table 4.9 Comparison of the present work with published literature

Reference	**Experimental cubicle dimensions (L×B×H) m^3**	**PCM integration technology**	**Wall orientation**	**Type of PCM**	**Temperature difference relative to the control cubicle (°C)**
Yasiri *et al.* [91]	(1×1×1)	Aluminium capsule compacted in bricks.	All walls and the roof	Macroencapsulated PCM (Paraffin)	4
Meng *et al.* [286]	(1×1×1)	Aluminium panels	Floor, ceiling, all walls	Macroencapsulated PCM (SP29 and RT18)	7.7
Rathore *et al.* [86]	(1.12×1.12×1.12)	Tubular container embedded in the walls	All walls and the roof	Macroencapsulated PCM (OM 37)	3.3
Shahcheraghian *et al.* [90]	(1×1×0.8)	Layer of PCM panel	All walls	PCM (Hydrated salt)	2.3
Present work	1 × 1× 1	Clay brick	All walls	Shape-stabilized PCM	5.8

Table 4.9 presents various published results from earlier studies where PCM was applied to experimental cubicles of similar sizes. The present work exhibits a peak temperature difference comparable to that reported in published studies for summer conditions.

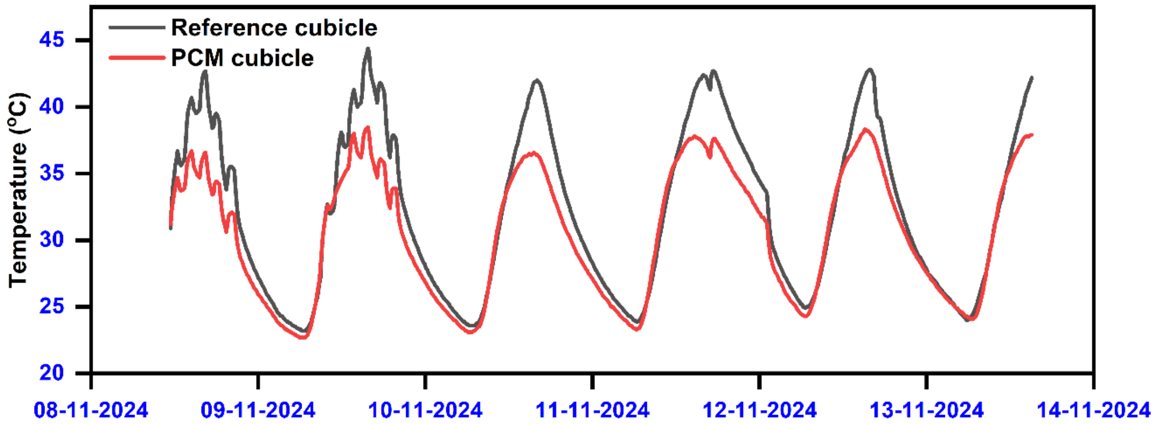

Fig. 4.22 The interior temperature of both rooms with applied internal thermal load

When internal thermal loads are applied to both cubicles, the resulting temperature profile is shown in **Fig.4.22**. The temperature profile appears similar to that observed in the absence of any applied loads. No negative effect of the internal heat generation has been observed on the interior temperature. The average temperature difference is around 1.74°C throughout the experimental period. The interior temperature of the PCM cubicle is lower than the reference room at the peak hours, and a slight increase in temperature has been measured for the period from 9 AM to 11 AM, as explained earlier. The average interior temperature of the PCM cubicle is more than 0.3°C than the reference cubicle for that particular morning hours. This may happen because the rate of discharge of PCM is slow and continues till the morning. A night ventilation system may improve the situation by completing the discharge of PCM during nighttime only. The maximum temperature difference of 6.2°C between the PCM cubicle and the reference cubicle was recorded on November 8, 2024, at 4:05 PM. The analysis with internal thermal load reflects real-world building conditions, where various internal heat-generating activities take place. The observed reduction in temperature under these conditions indicates that WH-PCM is a promising option for improving building envelope performance.

4.6.3 Comparison of the wall-wise temperature profile of the experimental cubicles

After analyzing the interior temperature of both rooms, the effect of each direction on the overall thermal performance of the room has been evaluated for one week starting from 17th October, 2024. The interior temperature of the WH-PCM embedded walls for the four directions has been shown in **Fig.4.23 (a).** Out of the four directions, the minimum temperature has been observed for the west wall at the peak hours. The north direction is not suitable for WH-PCM incorporation, as evident by the higher temperature profile throughout the experimental period. Similar observations can be seen with the east direction, where higher inside temperatures can be observed in the morning hours. Thus, it can be said that the east and north directions have a negative impact on the overall thermal performance of the room. Therefore, only the south and west walls are recommended for passive regulation of interior temperature for the prototype building/ experimental cubicle.

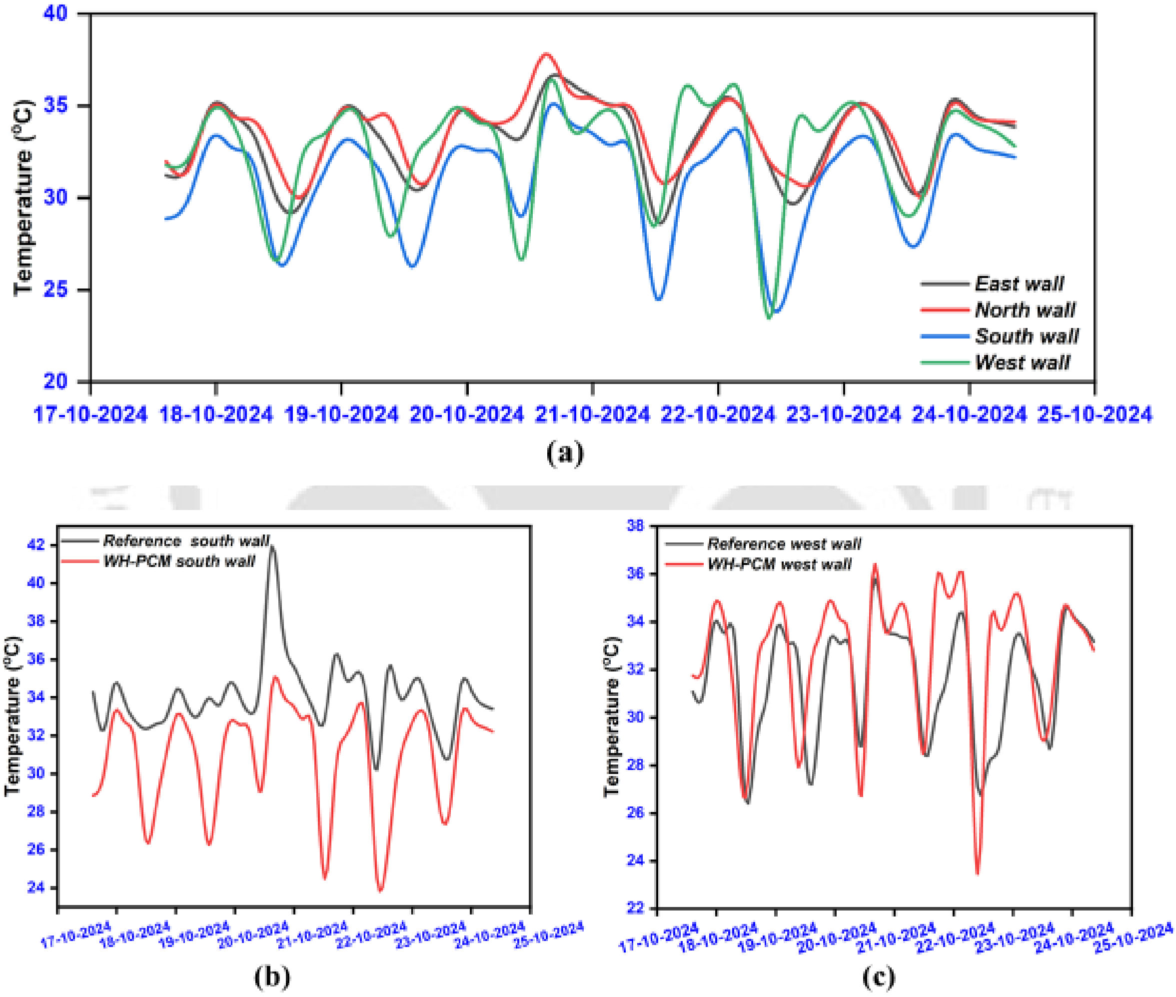

Fig. 4.23 Interior temperature (a) WH-PCM incorporated walls inside temperature, (b) reference and WH-PCM wall in the south direction, (c) reference and WH-PCM wall in the west direction

When the inside surface temperature of the south and west WH-PCM embedded walls is compared with their respective reference wall, the temperature profile shows a similar pattern, as shown in **Fig.4.23 (b) and (c)**, respectively. The noticeable difference in the temperature profile is that the WH-PCM incorporated walls result in a lower inside surface temperature.

The maximum temperature difference between the PCM and reference wall in the south and west directions is 10.45°C and 9.08°C, respectively, for around 1:15 PM in the afternoon. Solar radiation intensity peaks in the afternoon, and the passive integration of WH-PCM into building walls has proven effective in significantly reducing indoor temperatures. The west wall may get enough time for WH-PCM solidification from the night till noon, as no direct solar radiation is incident on the wall for that time. A similar trend was observed in a previous study, where the reference and PCM-enhanced west wall inside surface temperatures remain similar until noon, after which PCM activation started, and the temperature began to decrease. The temperature difference between the reference and encapsulated PCM-impregnated west wall was 3.6^{o}C [287]. Another study also confirmed that the south and west wall significanlty reduced temperature upto 5^{o}C, along with cooling energy savings up to 317 kWh [288]. But for the east wall, before the complete solidification of the WH-PCM, solar radiation hits the walls in the morning hours. Thus, WH-PCM may not be able to absorb the total latent heat of fusion.

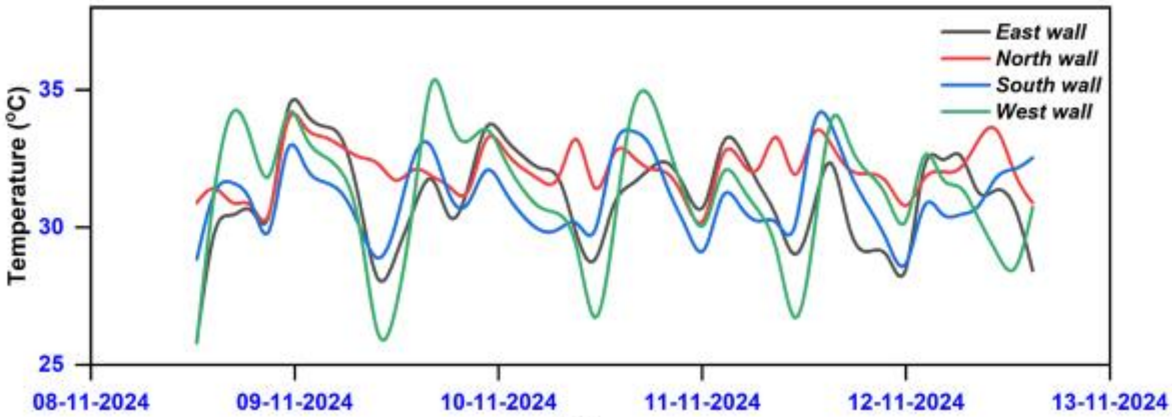

(a)

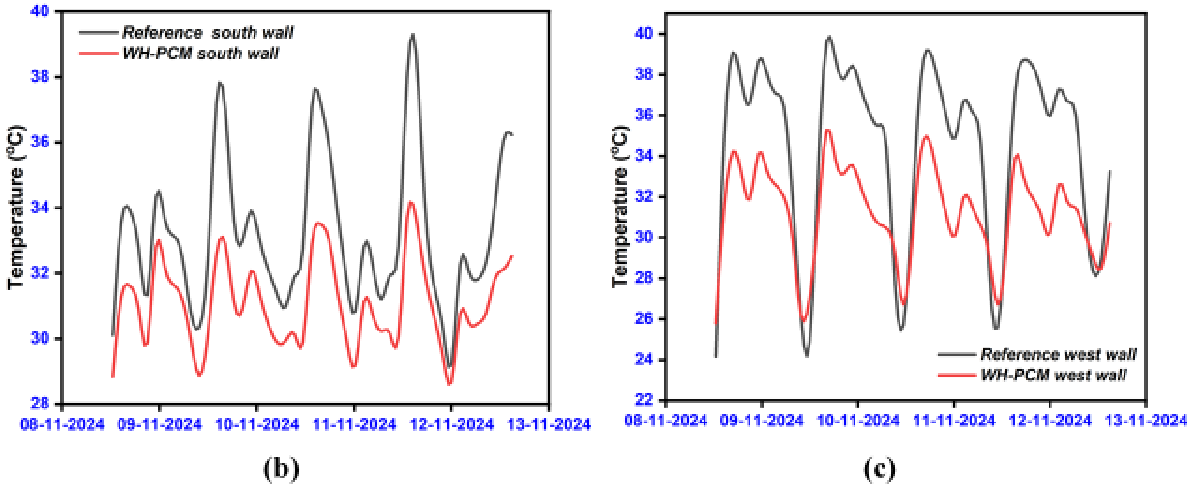

Fig. 4.24 Interior temperature with internal thermal load (a) WH-PCM walls, (b) reference and WH-PCM wall on south direction, (c) reference and WH-PCM wall on west direction

Similar observations can be made for the temperature profile for all the walls, with and without any applied internal load, as shown in **Fig.4.24**. In this case also, the WH-PCM east wall shows extreme temperature fluctuation during morning and afternoon hours, which is not desirable. The south wall shows a very smooth temperature profile compared to the other three walls, which is due to the uniform solar irradiance incident on the wall throughout the day. The maximum temperature difference between the reference and WH-PCM wall is 8.06^{o} and 8.92^{o}C, for the south and west wall, respectively. The wall temperature of the north side remains higher compared to all the other three walls during the peak hours throughout the experimental hours. This phenomenon may be attributed to the fact that the melting and solidification of WH-PCM rely solely on external convective heat transfer in that direction. Since the WH-PCM is embedded in the middle layer of the wall, an adequate temperature gradient may not develop on that side, as the north wall receives no direct solar radiation throughout the day, unlike the south wall.

4.7 Summary of the chapter

The current chapter describes the successful practical implementation of the developed biocomposite PCM for indoor temperature regulation in a hot and humid climate. Thermal performance tests have been conducted on an experimental cubicle, considering the financial constraints associated with experimentation on a real building. WH-PCM is inserted by making a slot in different positions of the brick, and the improved brick is then used for the wall construction of the experimental cubicle. The study highlights that when biocomposite PCM is applied at the middle of the wall thickness, consistent indoor temperature fluctuation can be observed throughout the experimental time for almost all four directions. The investigation revealed that placing the WH-PCM layer near the interior surface of the wall is not effective for the studied climatic zone. The WH-PCM incorporation in the south and west direction is recommended based on the study, for passive temperature regulation inside a building. The key findings of this chapter have been used to model a real building. A detailed techno-economic and environmental assessment study is presented in the next chapter.

Chapter 5

Techno-Economic and Life Cycle Analysis of biocomposite PCM-incorporated building

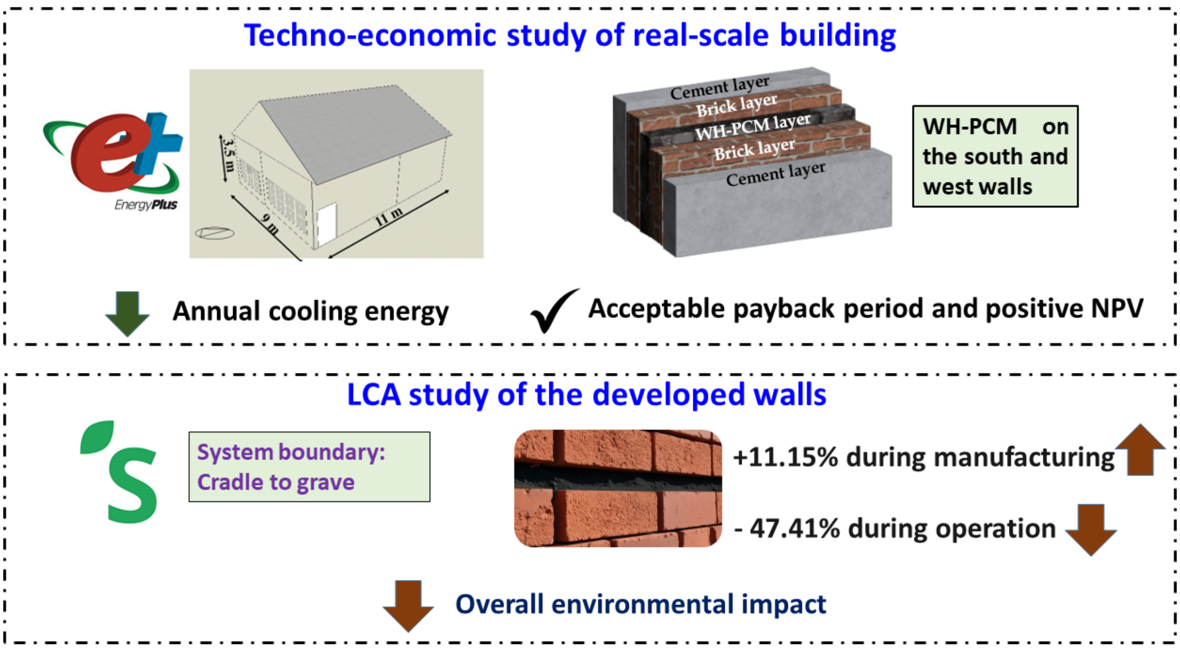

Outline

5.1 Introduction
5.2 Numerical Study on the Energy Saving Potential of WH-PCM Walls
5.3 Validation of numerical investigation with experimental study
5.4 Energy performance evaluation of the reference and PCM buildings
5.5 Economic analysis
5.6 Life cycle assessment (LCA)
5.7 Summary of the chapter

5.1 Introduction

Based on the experimental investigation it has been concluded in the last chapter that applying WH-PCM on the south and west walls gives the better results for thermal comfort. In order to investigate the economic feasibility and sustainability of the developed material, a comprehensive analysis has been carried out. The incorporation of biocomposite PCM on the walls of an existing real building for techno-economic evaluation involves significant practical challenges. Therefore, this chapter presents the study of a building model that is developed using the DesignBuilder interface and analyzed through EnergyPlus software. Additionally, the chapter includes economic and environmental studies based on the actual occupancy of the modelled building. For the techno-economic-environmental study, the same climatic zone as that of the experimental investigations has been assumed, as described in the previous chapter. This chapter discusses the Life Cycle Assessment (LCA) methodology and results, demonstrating the long-term environmental impact of applying WH-PCM in the building envelope. Some of the significant results are compared with those previously published.

5.2 Numerical Study on the Energy Saving Potential of WH-PCM Walls

5.2.1 Climatic background

The study area is Guwahati in India; the latitude, longitude and altitude of the place are 26.11° N, 91.70° E and 59 meters above sea level, respectively. According to Köppen–Geiger Climate Classification, the climatic zone of Guwahati is defined as a monsoon-influenced humid tropical climate, which includes warm temperature climate, dry winters and hot summer (Cwa) [289]. The reported maximum and minimum temperatures of the location are 30-35°C and 22-27°C in the summer, respectively [289]. The EPW weather dataset has been used for the simulation study [290].

5.2.2 Building Model Description

The current simulations are performed for a typical Assam-type house, which is a common residential building structure in the studied area, as shown in **Fig.5.1 (a) and 5.1 (c)**. The building is designed for three bedrooms, one living cum dining room and one kitchen (**Figure 5.1 (d)**). The inputs for the occupancy details and other appliances for all the rooms have been predefined. For comparison, a reference building with the same dimensions and design has also been simulated for the energy usage. Based on the analysis of the experimental results described in **Chapter 4**, the WH-PCM layer is inserted on the south and west walls of the building. Therefore, to study the impact of PCM application more accurately, no windows or openings are given on the south and west walls (except for a door on the south wall).

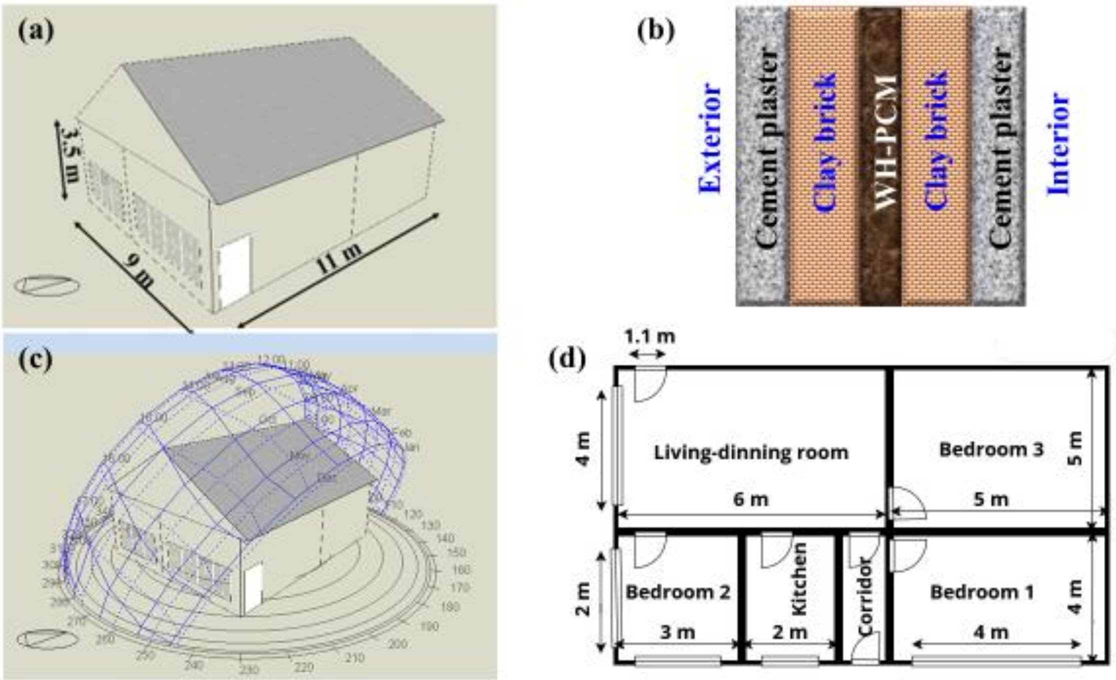

Fig. 5.1 (a) Building model, (b) WH-PCM position on wall, (c) Sun path diagram for the building model, (d) Detailed floor plan of the building model

Table 5.1 Thermo-physical properties of the construction materials

Building element	Materials	Thermal conductivity (W/mK)	Density (kg/m^3)	Specific heat (J/kgK)	Thickness (m)
Wall	Cement/plaster/mortar	0.72	1860	840	0.012
	Burned brick	0.85	1500	840	0.11
	WH-PCM	0.271	510	1630	0.02
Roof	Galvanized Corrugated Iron sheet	50	7850	0.470	0.0004
Ground floor	Rammed Earth	1.28	1460	880	0.3
	Sand	2	1950	1045	0.15
	Cement plaster	0.72	1860	840	0.75
	Cement screed	1.4	2100	650	0.04
Door	Painted Oak	0.19	700	2390	0.035

The walls of the reference room are constructed using the material listed in **Table 5.1**. All the construction materials for the reference room and PCM room are the same, except for the wall configuration as shown in **Fig.5.1 (b)**, where a WH-PCM layer is applied on the south and west walls for the PCM building. **Table 5.2** presents the WH-PCM properties that are used for the simulation study.

Table 5.2 Properties of WH-PCM

PCM name	**Density (kg/m^3)**	**Melting point (^oC)**	**Heat of fusion (J/g)**	**Specific heat-solid (J/kgK)**	**Specific heat-liquid (J/kgK)**	**Thermal conductivity (W/mK)**
WH-PCM	510	31.50	66.63	1.63	3.86	0.27

5.2.3 Mathematical formulation

The simulation has been performed in EnergyPlus V23-1-0 software using the DesignBuilder interface (Version 6.1.0.006). EnergyPlus is a flexible software for simulating building energy flows, including lighting, heating, and cooling. It enables detailed analysis of building performance, aiding in the design of energy-efficient systems. With its user-friendly tools for designing and assessing building designs, DesignBuilder, a graphical interface for EnergyPlus, considerably streamlines the modelling process [92,290].

The study is performed using a one-dimensional Conduction Finite Difference Method (CondFD) algorithm, as presented in **Eq. 5.1** [291]. The CondFD algorithm takes care of the changing thermal properties during the phase transition process of the WH-PCM during the simulation, as represented by **Eq. 5.2** [291].

$$C_p \rho \frac{\partial T}{\partial t} = \frac{\partial}{\partial x}\left(k \frac{\partial T}{\partial x}\right) \tag{5.1}$$

$$C_p \rho \frac{\partial T}{\partial t} = \frac{\partial}{\partial x}\left(k \frac{\partial T}{\partial x}\right) - \Delta H_m \rho \frac{\partial f}{\partial t} \tag{5.2}$$

$$f = \begin{cases} 0 & if \quad T \le T_s \\ \dfrac{T - T_s}{T_l - T_s} & if \quad T_s < T < T_l \\ 1 & if \quad T > T_l \end{cases} \tag{5.3}$$

The f mentioned in **Eq. 5.2** is used to describe the liquid phase of PCM, which varies according to **Eq. 5.3** [291].

where is the specific heat capacity in kJ/kgK, ρ is the density in kg/m^3, k is the thermal conductivity in W/mK, f is the melting fraction, ΔH_m is the latent heat of PCM in kJ/kg, T_s and T_l is the solidification and melting temperature in K, respectively.

EnergyPlus uses the finite difference method to solve the heat transfer equation, where the building envelopes are divided into nodes, as shown in **Fig. 5.2.**

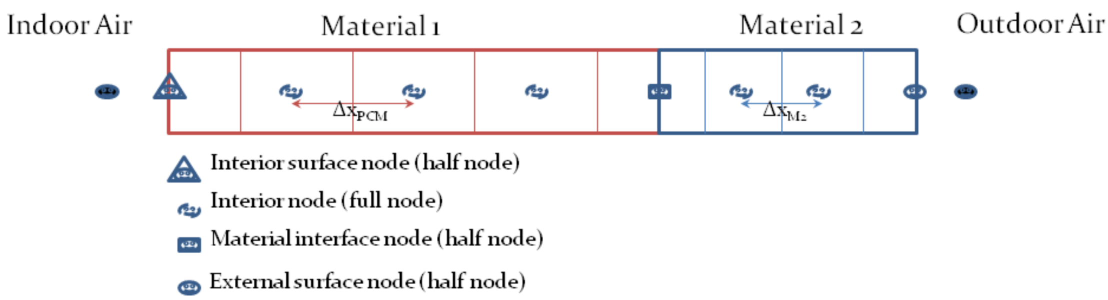

Fig. 5.2 Node depiction for the condFD model [292]

In this current study, the WH-PCM is modelled using the hysteresis method so that the actual building envelope scenario can be observed. **Eq. 5.4** is used for the discretization of all the elements of the building model [167]. To get better accuracy from the model, the timestep for the study is considered as 12, relaxation factor of 1, inside face surface temperature convergence criteria as 0.01, and space discretization constant as 3, which is equivalent to the Fourier number (F_o) of 1/3.

$$\Delta x = \sqrt{\alpha c \Delta t} = \sqrt{\frac{\alpha \Delta t}{F_o}} \tag{5.4}$$

where c is the spatial discretization constant, α is the thermal diffusivity and Δt is the time step.

The fully implicit scheme has been employed for the phase change energy calculations out of the two schemes available under the CondFD method. It incorporates specific heat-based enthalpy-temperature functions for enhanced precision. The fully implicit heat transfer model equation is shown in **Eq. 5.5** [167,290,293].

$$C_p \rho \Delta x \frac{T_i^{j+1} - T_i^j}{\Delta t} = \left(k_W \frac{\left(T_{i+1}^{j+1} - T_i^{j+1}\right)}{\Delta x} + k_E \frac{\left(T_{i-1}^{j+1} - T_i^{j+1}\right)}{\Delta x} \right) \tag{5.5}$$

where T_i^j is the temperature of the node i at time j, in K, i is the node that is being modelled, $i+1$ adjacent node to the interior of the construction, $i-1$ is the adjacent node to the exterior of the construction, $j+1$ is the new time step, j is the previous time step, Δx is the finite difference layer thickness, k_W is the thermal conductivity of the interface between the nodes i and $(i+1)$ in W/mK, and k_E is the thermal conductivity of the interface between nodes i and $(i-1)$ in W/mK.

The specific heat of PCM depends on temperature, as shown in **Eq. 5.6** [291].

$$C_p = \frac{H_i^{new} - H_i^{old}}{T_i^{new} - T_i^{old}} \tag{5.6}$$

where H_i is the node enthalpy.

The detailed input parameters used for the building simulation are described in **Table 5.3**.

Table 5.3 Input parameters for the building model used in the simulation

Total Building area	90.04 m^2	Net conditioned building area	79.67 m^2
Height of the floor	3.5 m	Gross roof area	124.48 m^2

Envelope: Window to wall ratio

	Total	North	East	South	West
Gross wall area	167.72	38.50	45.36	38.50	45.36
Window opening area	20.87	10.44	10.43	0.00	0.00
Gross window-wall ratio	12.44	27.12	22.99	0.00	0.00

Zone summary

	Area (m^2)	Conditioned (Y/N)	Volume (m^3)	Lighting Intensity (W/m^2)	Occupancy density (person/ m^2)	Plug and process (W/m^2)
Block 2:Zone 2	10.62	Yes	37.18	5	0.02	20.58
Block 3: Zone 3	7.08	No	24.79	15	0.02	30.28
Block 4: Zone 4	3.28	No	11.50	5	0.01	2.16
Block 5: Zone 6	18.22	Yes	63.76	5	0.02	3.58
Block 1: Zone 1	27.81	Yes	97.35	7.5	0.01	3.90
Block 6: Zone 2	23.02	Yes	80.56	5	0.02	3.58
Roof 1: Zone 5	84.27	No	95.52	NA	NA	NA

Boundary conditions			
Weather data	IND_Guwahati.424100_ISHRAE.epw		
Number of conditioned zones	4	Number of unconditioned zones	3
Cooling set-point (^{o}C)	25^{o}C	Natural ventilation	On for an unconditioned zone
Infiltration (ACH)	0.7	Indoor maximum temperature control	25^{o}C
Simulation parameters			
Simulated period: 12 months			
Solution algorithm	Conduction Finite Difference	Finite Difference scheme	Fully implicit first order
Time steps per hour	12	Space discretization constant	3
Inside surface convection algorithm	TARP	Outside surface convection algorithm	DOE-2
HVAC template	Split no fresh air		
Fuel: electricity from the grid	Seasonal COP: 1.8		
	Schedule type: 7/12 schedule		

5.3 Validation of numerical investigation with experimental study

In this study, the simulation study is validated against an experimental study conducted in the same climatic conditions, as explained in **Chapter 4.** An identical room, with the same inner dimensions, construction materials and operating conditions as the experimental set-up, has been simulated using EnergyPlus (DesignBuilder), as shown in **Fig.5.3**. The experiment has been carried out for 24 hours on 20th July 2024. The temperature profiles of the experimental and simulated rooms for the 24 hours have been compared and reported for validation.

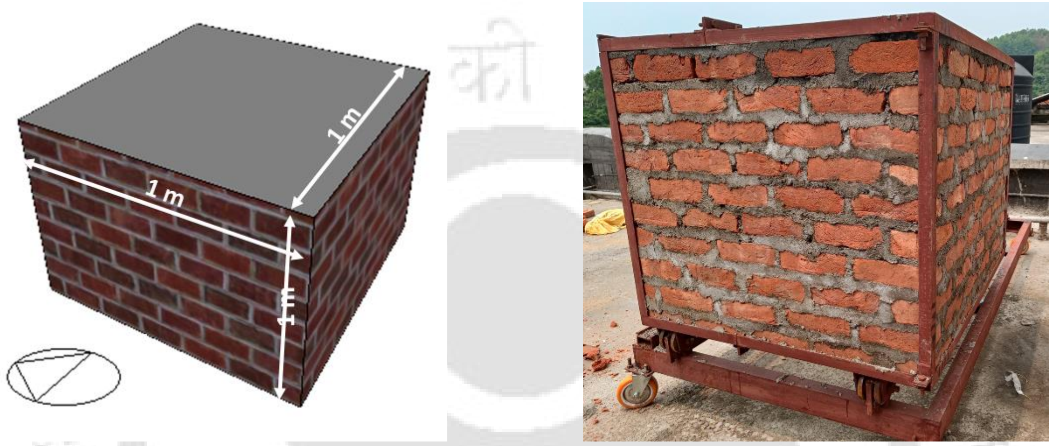

(a) **(b)**

Fig. 5.3 Building model for validation, (a) Numerical model, (b) Experimental set-up

As shown in **Fig. 5.4**, the temperature profile of both experimental and numerical investigations has been plotted over 24 hours. The trend in the temperature variation in both the experimental and numerical investigations is similar. A standard error of 2.88% can be observed between the experimental and the numerical study. The root-mean-square-error of the numerical and experimental analysis is found as around 1.72%, which implies numerical model is accurately represents the experimental data. In the case of the simulated WH-PCM room, all the walls of the room have been constructed with a WH-PCM layer, sandwiched between bricks. On the contrary, in the experimental study, the WH-PCM is inserted into the slot of the brick and then used for wall fabrication. The dissimilarity in construction of wall layers between the experimental set-up and numerical analysis causes a higher experimental indoor temperature than the simulated indoor temperature for the selected period of study. A similar type of variation between experimental and numerical studies has also been published in other literature [96,291].

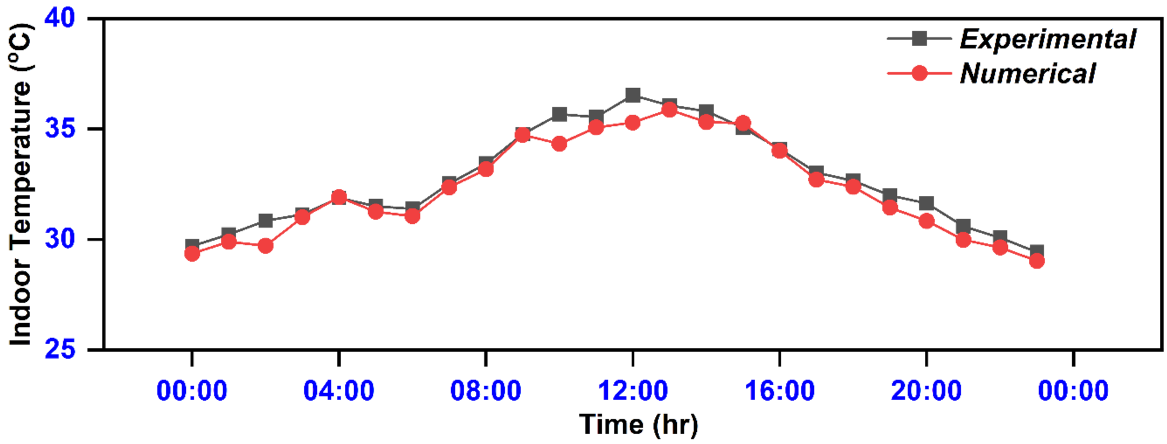

Fig. 5.4 Validation between experimental and numerical analysis

5.4 Energy performance evaluation of the reference and PCM buildings

Figures 5.5 and **5.6** present the comparative results obtained from real Assam-type buildings with the application of WH-PCM on the south and west walls, as mentioned in **Section 5.2.2**. **Fig.5.5** shows the comparison between the annual cooling energy demand and the energy required per total building area for both buildings. The annual cooling energy demand for the reference building is found to be 8780.12 kWh, whereas the same is 6018.07 kWh for the building with WH-PCM enhanced walls. Here, the cooling energy refers to the HVAC system applied in the living and dining room and the three bedrooms. Accordingly, the energy required per total building area for the reference and PCM building is 99.57 and 66.84 kWh/m^2, respectively. The results indicate that the biocomposite PCM is not only useful in interior temperature regulation, as obtained from experimental results, but also enhances the energy efficiency of the building. The energy consumption reduction (ECR) is calculated with the help of **Eq. 5.7** [200].

$$\mathrm{ECR} = \frac{\mathrm{EC}(\mathrm{No\ PCM}) - \mathrm{EC}(\mathrm{PCM})}{\mathrm{EC}(\mathrm{No\ PCM})} \times 100 \tag{5.7}$$

The ECR for the WH-PCM building is calculated as 31.4%, which implies that the WH-PCM enhanced wall cuts down the operational hours of the HVAC system by efficiently storing and releasing heat.

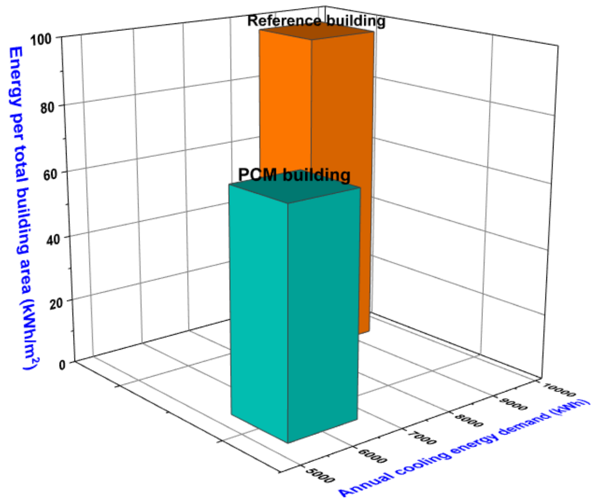

Fig. 5.5 Comparison of annual cooling energy and energy per total building area

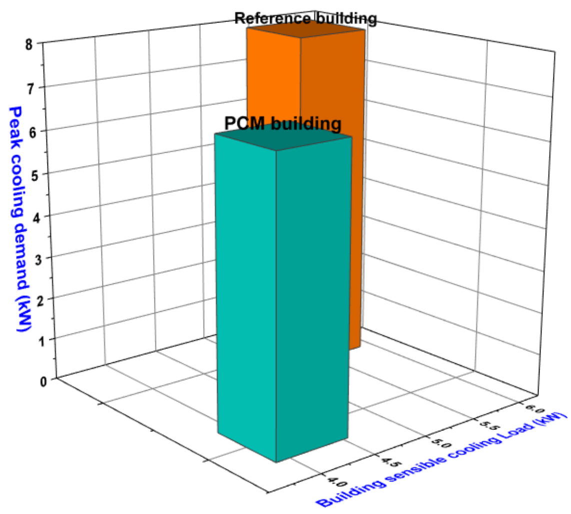

Fig. 5.6 Comparison of the building sensible cooling load and peak cooling load

The annual cooling consumption reduction with the WH-PCM enhanced wall is also supported by peak cooling demand reduction compared to the normal building. The EnergyPlus output report showed that the peak cooling demand occurs both for the reference and the PCM building in the month of June at the peak afternoon hours, corresponding to the summer season. But the peak cooling demand is reduced by 1.33 kW, as shown in **Fig. 5.6.** The WH-PCM-enhanced wall is thus capable of reducing peak cooling demand, thereby lowering energy costs, easing HVAC sizing, and enhancing grid efficiency, making the choice more economical and sustainable. As the southern and western walls with WH-PCM reduce the heat gain, the sensible cooling load of the building also decreased by 24.14%, as shown in **Fig. 5.6**. A simulation study conducted by Anter *et al*.[294] also reported a reduction of 66% energy gain during summer for Aswan City, Egypt (latitude 24.09° N, longitude 32.9° E). They used a 1.5 cm layer of PCM on both inner and outer surfaces, which reduced the wall temperature by 3.4^{o}C. Similarly, another study showed a total energy savings of 822.9 kJ/m^2 for maintaining thermal comfort while using a layer of PCM of 40 mm thickness near the interior surface of a wall in a south-facing room [295].

5.5 Economic analysis

Based on the simulation study, it is evident that the installation of WH-PCM enhanced walls leads to a reduction in the cooling energy demand of air-conditioning systems in an Assam-type residential house. However, before implementing these walls in real buildings, it is crucial to assess their economic feasibility. In the present study, three fundamental economic parameters have been evaluated to gain insights into this aspect. The cost of WH-PCM and electricity is taken as INR600/kg and INR8.15/unit, respectively, as per the current Indian market, for calculating the economic parameters. The cost of the WH-PCM is evaluated, including all the expenses related to biomass collection, electricity cost for biochar production and other expenses during production, transportation, procurement of OM35, etc.

5.5.1 Static/simple payback period (SPP)

The simple payback period is the amount of time required for an investment to generate cash flows sufficient to recover its initial cost. It is calculated by dividing the initial investment by the annual cash inflow, or by summing annual cash flows until the cumulative amount equals the original investment [296]. In this particular case, the initial cost includes the cost of WH-PCM that is required for the modification of the west and south walls. The SPP is estimated as per **Eq. 5.8** [194]. As per the design that is adopted in the current study, the weight of WH-PCM to provide a layer between the bricks is approximately 302 kg for the two walls in the specified building. When WH-PCM is manufactured on a laboratory scale, the total cost of WH-PCM is estimated to be around INR181200. This amount is considered the initial cost $\left(C_{PCM}\right)$ for calculating the simple payback period. In this case, the annual savings (S) refer to the total yearly electricity cost savings resulting from the use of passive walls in south and west direction, specifically the reduction of 2762 kWh in cooling energy consumption.

$$\text{SPP} = \frac{C_{PCM}}{S} \tag{5.8}$$

The calculated SPP is 8.03 years. Thus, the payback period falls within a favourable range for building structures and is considered financially secure. A study conducted by Sahili *et al.*[288] showed that using three layers of PCM with different melting temperatures reduced the annual cooling energy demand by 15.21%, resulting in a lowest SPP of 12.94 years.

5.5.2 Dynamic/discounted payback period (DPP)

The dynamic payback period, also known as the discounted payback period, is the time it takes for the present value of an investment's cash inflows to recover the initial investment, considering the time value of money. Each future cash flow is discounted back to its present value using a specified discount rate, and the period is determined when the cumulative discounted cash flows equal the initial outlay. This method provides a more accurate assessment than the simple payback period, as it reflects the reduced value of future cash flows [194]. The dynamic payback period is calculated as per **Eq. 5.9** [198].

$$\text{DPP} = \frac{\ln\left(\frac{S}{S - C_{PCM} \times I}\right)}{\ln(1+I)} \quad (5.9)$$

where I is the modified discount rate, which is calculated using the discount rate for the time value of money i_t and the annual inflation in the electricity tariff r, as described in **Eq. 5.10** [198].

$$I = \frac{(1+i)}{(1+r)} - 1 \quad (5.10)$$

For the present study, the i and r values are assumed to be 6% and 4%, respectively, as per the Indian economy [297].

The estimated DPP is around 9.16 years, which is greater than the simple payback period. As it has been reported that the service life of a normal PCM is about 35 years [198], the energy savings achieved through the incorporation of WH-PCM will offset the initial investment costs before the end of its service life based on both SPP and DPP. As DPP more accurately reflects real-world energy management, the lower value of DPP makes the system economically more viable. The present payback periods are compared with different already published works, as shown in **Table 5.4.**

5.5.3 Net Present Value (NPV)

Net Present Value (NPV) is defined as a financial parameter that determines the potential future profits of a project. NPV calculates the difference between the existing value of the inflow of cash and the current value of the outflow of funds over the period of an investment, using a specified discount rate. NPV incorporates the time value of money by converting all future cash flows into their present value through discounting. The NPV is calculated using **Eq. 5.11** [198]. The N value, representing the life span, is assumed to be 30 years[194].

$$\text{NPV} = \frac{S\left[(1+I)^N - 1\right]}{i\left[(1+I)^N\right]} \quad (5.11)$$

NPV should always be in the positive range for a project to be economically viable. Negative NPV results in a loss, indicating that the studied project will generate less value than the cost of the project. The NPV for the incorporation of biocomposite PCM on the building wall is positive, and the value is INR 162685.19, indicating the profitability of the option.

Table 5.4 SPP and DPP values for PCM-integrated buildings under different climatic conditions

References	**Type of study**	**Type of building**	**Type of climate**	**SPP (years)**	***i* value (%)**	**DPP (years)**
Imafidon *et al.*[198]	Simulation	Typical Canadian residential building	Tropical	15.63	1	8.28
					3	8.85
					5	9.52
Raheim et al. [195]	Simulation	One room with a heavyweight envelope	Hot and dry	44.2	Not given	Not given
Mi *et al.* [194]	Simulation	Multi-story office building	Subhumid warm	5.91	6	7.52
			Humid subtropical	5.99		7.64
			Subtropical monsoon	7.07		9.48
			Subtropical plateau monsoon	19.91		NA
			Tropical monsoon	30.09		NA
M'hamdi *et al.*[200]	Simulation	Residential house	Mediterranean climate (hot summer)	32.98	Not given	Not given
			Semi-arid climate with warm winter	34.49		
			Arid climate with warm winter	54.45		
Present study	Simulation	Residential Assam-type house	Tropical hot and humid	8.04	6	9.16

5.6 Life cycle assessment (LCA)

As described in the previous section, the techno-economic analysis shows the economic viability of using WH-PCM on the south and west walls of a real Assam-type building model. In addition, it is essential to evaluate the environmental sustainability of this developed material before implementation in real buildings. Therefore, an LCA study has been conducted and presented in the next sections. The current LCA evaluates the environmental impacts associated with constructing a WH-PCM brick wall throughout the entire service life of a building. To simplify the analysis, the same building model and associated design parameters assumed for techno-economic analysis have been adopted to assess the environmental assessment. The current analysis is based on the energy saving results of the Assam-type building after WH-PCM incorporation (described in **Section 5.4**).

Life cycle assessment comprises the compilation and evaluation of the inputs, outputs and the potential environmental impact of a product system throughout its life. LCA methodology is based on the standards of ISO 14040 and ISO 14044 [298]. The present LCA has been performed through SimaPro software (Version 9.0). The details of the LCA study have been highlighted in the subsequent sections.

5.6.1 Goal and scope definition

The objective of the LCA is to study the environmental impacts of using WH-PCM incorporated bricks on the south and west walls of a building, with the aim of energy savings of air conditioning systems. The methodology of this study follows a cradle-to-grave analysis. A comparative LCA analysis is carried out for the model buildings outlined earlier in **Section 5.2.2.**

5.6.1.1 Functional unit

In this study, the functional unit is defined as the energy savings potential of 1 m² of WH-PCM incorporated brick wall compared to a normal wall over a 30-year lifespan of the building. Thirty years of building lifespan is selected based on previous literature [201][202].

5.6.1.2 System boundaries

The phases considered for this LCA are raw material extraction, manufacturing, transportation, on-site construction, operation and end of life. The initial process starts with the manufacturing phase, which comprises raw material extraction for different construction materials, transportation and on-site construction. For WH-PCM incorporated bricks, the manufacturing phase consists of making biochar from water hyacinth biomass through pyrolysis, preparation of WH-PCM by simple impregnation method, and inserting PCM onto the clay bricks by making a slot. The other inputs related to wall manufacturing are the same for both the tested buildings. The operational phase of both buildings is similar as the same type of air-conditioning system is assumed to run for the building lifespan of 30 years. The end-of-life process includes the disposal of the construction material to the landfill or incineration, based on the type of materials.

5.6.1.3 Assumptions

To simplify the analysis, the following assumptions are assumed throughout the study [204].

1. As for both the test houses, an air-conditioning system has been used; therefore, the manufacturing phase of the air-conditioner has not been included in the study.
2. The useful lifespan of the building is taken as 30 years.
3. The energy mix is assumed to be constant for the studied lifespan.
4. The energy consumption by the air-conditioning system has been obtained from the EnergyPlus study as explained in the previous sections.
5. No information is available for the disposal of the biocomposite PCM. Therefore, the disposal method used for organic material is taken as a database for the same.
6. The WH-PCM layer is constructed as a layer, rather than as a slotted brick, maintaining the same thermal properties of the experimental wall.
7. The thermal, chemical and physical properties of WH-PCM are assumed to remain the same throughout the lifespan of the building.
8. Material properties obtained under laboratory conditions were assumed to be applicable under actual building operating conditions.

5.6.2 Life cycle inventory (LCI)

The Ecoinvent 3 life cycle inventory database integrated within SimaPro 9 software has been used to assess the overall scores and impacts of the components. The Ecoinvent database covers most sectors, including energy supply, agriculture, transport, biomaterials, construction materials, metals, electronics, and waste treatment. The ecoinvent database is known for its consistency and timely updates, and extensive online documentation. All the impacts are measured per kg of material for the calculations. For all the material and processes, the unit process is selected, which includes the inputs and outputs of the smallest element in the life cycle inventory analysis. Regarding the geographic origins of materials, the GLO (Global) option, which represents activities applicable worldwide, has been applied. In some cases, the ROW (Rest of the World) and the IN (India) options have been selected. Some particular data, such as water hyacinth biochar, the pyrolysis process is missing in the database of Ecoinvent 3; therefore, direct measurement values from experimental data are taken for analysis. The mass and properties of the material used in this LCA are tabulated in Tables **5.5** to **5.9**. For WH-PCM incorporated walls, all the material and quantity remain the same except for WH-PCM. At the end of the building's life cycle, construction materials are assumed to be landfilled, recycled, or incinerated in accordance with the Ecoinvent database and the adopted methodology, as summarized in **Table 5.10**. As no established disposal routes currently exist for the bio-based PCM, municipal solid waste incineration is assumed for the same.

Table 5.5 LCI for 1m^2 normal wall

Material	**Quantity**
Cement {IN}|market| Allocation, cut off by classification, Unit	10.8 kg
Sand {IN}|market| Cut off by classification, Unit	36 kg
Cement mortar {IN}|transformation, hand mixed| Cut off by classification, Unit	1 cm thickness (52.74 kg)
Clay brick {GLO}|market for| Cut off by classification, Unit	50 bricks (175 kg)
Water supply{IN}| Tap water production-conventional treatment| Cut off by classification, Unit	5.94 kg

Table 5.6 LCI for 1m^2 WH-PCM wall

Material	**Quantity**
WH-PCM incorporated bricks| Experimental data	50 bricks (159 kg)

Table 5.7 LCI for 1 kg of WH-PCM brick manufacturing

Material	**Quantity**
WH-PCM (direct measurement)| Experimental data	0.01667 kg
Cement plaster {IN}|transformation, hand mixed| Cut off by classification, Unit	0.000092 m^3
Electricity, medium voltage {IN: North-Eastern grid}|| Cut-off by classification, Unit (Electricity for brick cutting)	0.0174 kWh

Table 5.8 LCI for 1 kg of WH-PCM production

Material	**Quantity**

Biochar (direct measurement)|Experimental data	0.6 kg
Paraffin wax| Experimental measurement	0.4 kg
Electricity, medium voltage {IN: North-Eastern grid}|| Cut-off by classification, Unit (Electricity for PCM preparation)	0.32 kWh
Electricity, low voltage {IN: North-Eastern grid}|| Cut-off by classification, Unit (Electricity for biochar grinding)	0.3 kWh

Table 5.9 LCI for 1 kg of biochar production

Input Material	**Quantity**
Biomass| Experimental data	3.3 kg
Electricity, medium voltage {IN: North-Eastern grid}|| Cut-off by classification, Unit (Electricity for pyrolysis)	8 kWh
Electricity, low voltage {IN: North-Eastern grid}|| Cut-off by classification, Unit (Electricity for water pump)	2.33 kWh
Argon gas| Experimental data	1.02 kg
Freight, light commercial vehicle {RoW}, market for transport, freight, light commercial vehicle, Cut-off, Unit	0.005 tkm

Table 5.10 Waste disposal mythology of the construction materials

Waste treatment method	**Quantity**
Waste brick {GLO}|market for| Cut-off, U	175 kg
Waste cement in concrete and mortar {GLO}|market for| Cut-off, U	10.8 kg
Municipal solid waste (waste scenario) {ROW}| treatment of municipal solid waste, incineration| Cut-off, U (for WH-PCM)	2.5 kg
Transport, freight, lorry 16-32 metric ton, euro3 {ROW}|market for transport| Cut-off, U	50 km

5.6.3 Life cycle impact assessment and interpretation

The following assessment indicators have been used to quantify the environmental impacts of WH-PCM incorporated buildings over conventional buildings.

i. IPCC 2021 GWP20 V1.01 (with characterization)

ii. IPCC 2021 GWP100 V1.01 (with characterization)

iii. ReCiPe 2016 Midpoint (H) V1.07 (with normalization)

iv. ReCiPe 2016 Endpoint (H) V1.07 (single score)

v. Cumulative energy demand V1.07 (single score)

vi. Cumulative exergy demand V1.07 (single score)

Table 5.11 Impact categories description

Impact category indices	**Impact category name**	**Assessment step**	**Unit**	**Description**
IPCC 2021	Global warming potential GWP 20,100	Characterization	kg CO_2 eq	Climate change impact
ReCiPe Midpoint	Particulate matter, ionizing radiation, ozone depletion, human toxicity (cancer), human toxicity (non-cancer), global warming, water use, ozone formation, freshwater ecotoxicity, freshwater eutrophication, terrestrial ecotoxicity, terrestrial acidification, land use, marine ecotoxicity, marine eutrophication, mineral resources, fossil resources	Normalization	Points (Pts)	Early-stage cause-and-effect chain of environmental damage
ReCipe Endpoint	Resource, Ecosystems, Human Health	Single-score	Points (Pts)	Aggregates the midpoint impacts into overall damage indicators
Cumulative Energy Demand	Cumulative Energy Demand	Characterization	MWh	Total primary energy extracted from nature
Cumulative Exergy demand	Cumulative Exergy demand	Characterization	MWh	Total exergy extracted from nature

The details of each indicator are explained in **Table 5.11.** The characterization, normalization and single score, mentioned in the **Table 5.11,** are the successive assessment steps through which the inventory data are converted to quantified environmental impact indicators. Characterization involves multiplying each inventory flow by its corresponding characterization factor, which is defined for the specific elementary flow and impact category. Normalization gives a dimensionless number, where the characterized results are normalized with a reference value. Single score is the overall environmental indicator, where the normalized score is multiplied with weighting factor, based on subjective weighting of each category [299].

5.6.4 Global warming potential (GWP)

The International Panel of Climate Change (IPCC) has been issuing the global warming potential (GWP) of different gases for more than 35 years. Global warming potential is defined as the amount of heat trapped by the emission of 1 ton of a gas compared to the emission of 1 ton of CO_2 over a specified period. The GWP of CO_2 is considered to be 1 for reference. The time period for GWP calculation is usually taken as 100 years, which is termed as GWP100. A 20-year GWP (GWP20) is another alternative for GWP100, which is basically used for shorter life-span gases [300]. Emissions of non-CO_2 greenhouse gases are commonly expressed as carbon dioxide equivalents by multiplying their mass by the corresponding GWP. Total global warming potential (GWP) is calculated as the sum of three indicators: fossil GWP, biogenic GWP, and GWP from land transformation (land-use change). GWP fossil indicates the emissions related to the burning of fossil sources, either for thermal work or for electricity generation. GWP biogenic refers to CO_2 absorption and release originating from the biological carbon cycle. The land transformation indicates the emissions caused by activities like deforestation and conversion of agricultural land [301].

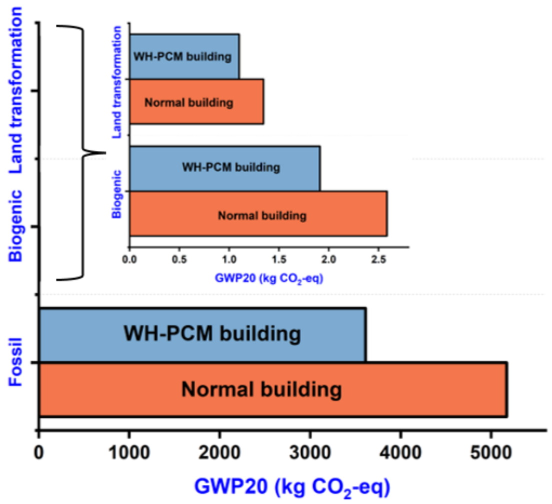

Fig. 5.7 GWP 20 comparison

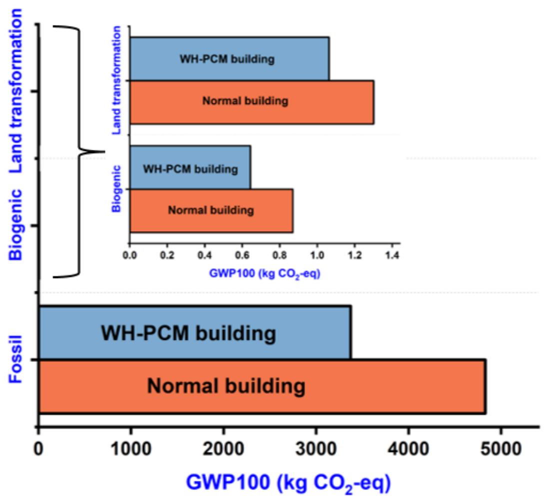

Fig. 5.8 GWP 100 comparison

In the case of the current analysis, the WH-PCM impregnated building shows lower values for both GWP20 and GWP100 compared to the normal building, as depicted in **Figures 5.7 and 5.8**. The higher values of GWP20 over GWP100 indicate that the short-lived climate pollutants have a stronger warming effect over the short time horizon. If the time frame is considered as 100 years, most of the pollutants decay and the related warming potential is reduced. The integration of WH-PCM results in a reduction of approximately 30% for both GWP20 and GWP100. The lower GWP value is obtained due to the operational energy savings throughout the lifespan. The emission associated with the construction phase is offset during the use phase of the buildings.

5.6.5 Cumulative energy and exergy demand

Cumulative energy demand (CED) is an indicator that signifies total primary energy consumed throughout the entire life cycle of the building from cradle to grave. CED primarily quantifies the energy extracted from nature, both from renewable and non-renewable sources. Cumulative exergy demand (CED_X) is a tool to measure the quality of energy throughout its life span. As exergy is related to useful energy potential, the same concept is applied for the LCA study. CED deals with the energy efficiency of buildings, whereas CED_X is concerned with the thermodynamic sustainability of the building.

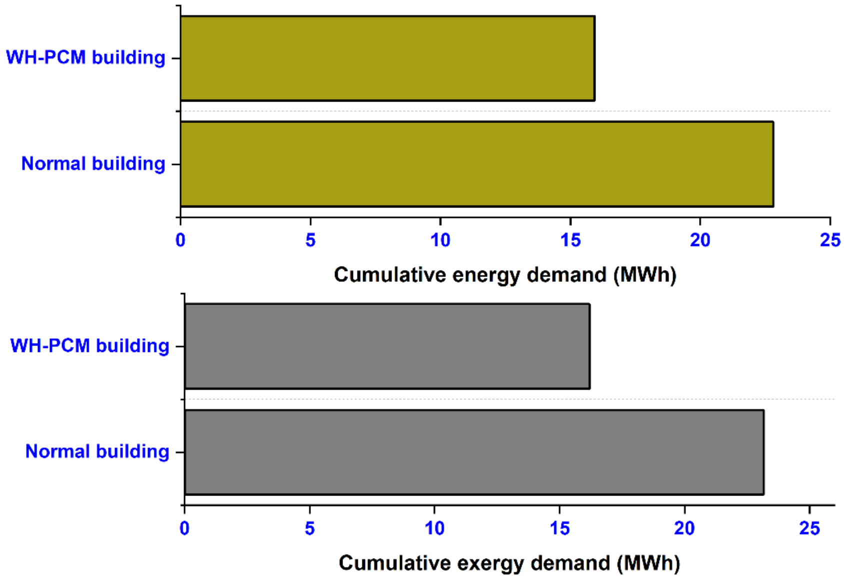

Fig. 5.9 Cumulative energy and exergy demand (single score)

The WH-PCM integrated building shows lower values both for energy and exergy demand compared to the normal building by 30.14% and 30%, respectively, as shown in **Fig.5.9**. The operational energy demand dominates the total value, and operational energy savings occur through load shifting, peak reduction and reduced HVAC run time. WH-PCM also make the building thermodynamically more efficient than the considered normal building. The building cooling demand is a low-grade energy demand, which is supplied with high-grade energy using electrical appliances. The use of the WH-PCM layer traps heat, which is a form of low-grade energy, and thus the exergy efficiency gets improved over the operational phase of the building. The environmental penalty caused during the manufacturing phase is negligible compared to the operational phase.

5.6.6 ReCiPe 2016 midpoint

Midpoint categories represent the environmental impact at an intermediate stage. The 18 different categories are already mentioned in **Table 5.11**. From **Fig.5.10**, it can be concluded that a WH-PCM impregnated building is environmentally less harmful than a normal building for all 18 categories. The range of reduction across various categories varies from around 22 to 30% between the normal and the WH-PCM integrated building. The highest impact can be seen from the human carcinogenic toxicity. This particular category quantifies the potential health damage to human health due to exposure to carcinogenic substances. The higher value may be attributed to the building construction phase, during which substantial emissions of carcinogenic substances occur. Similar observations were made when ester has been used as

PCM for an experimental cubicle set-up where the highest impact was shown for human health and fossil fuel category [207].

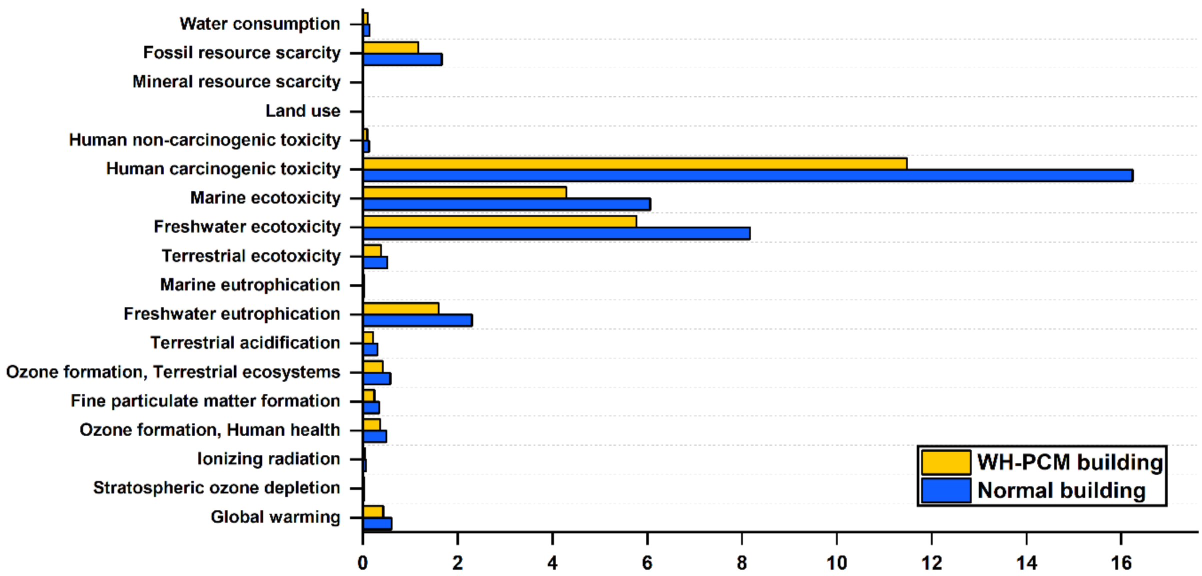

Fig. 5.10 ReCiPe 2016 midpoint categories (with normalization)

5.6.7 ReCiPe 2016 endpoint

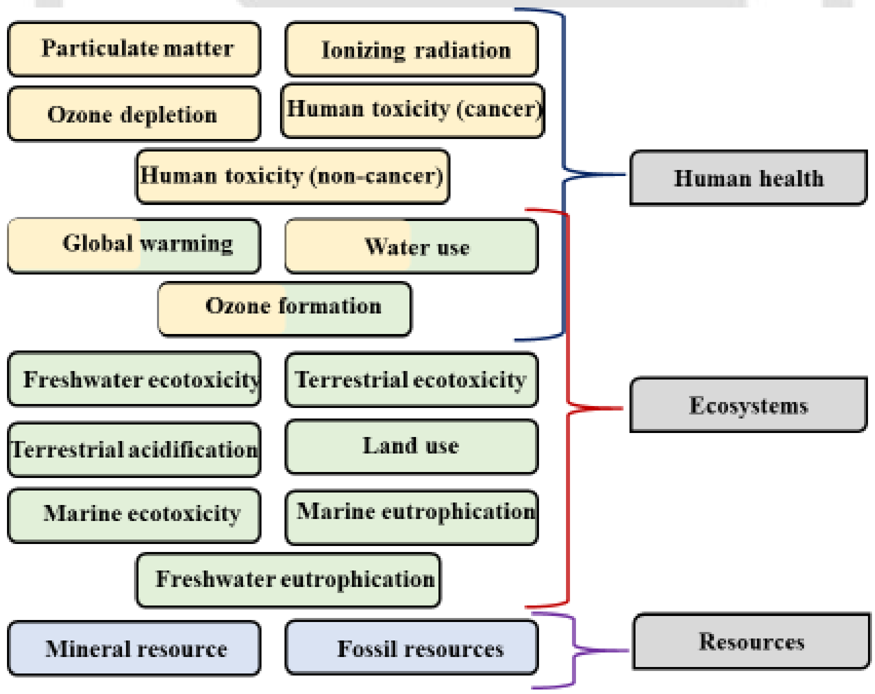

Fig. 5.11 ReCiPe method midpoint and endpoint categories relation

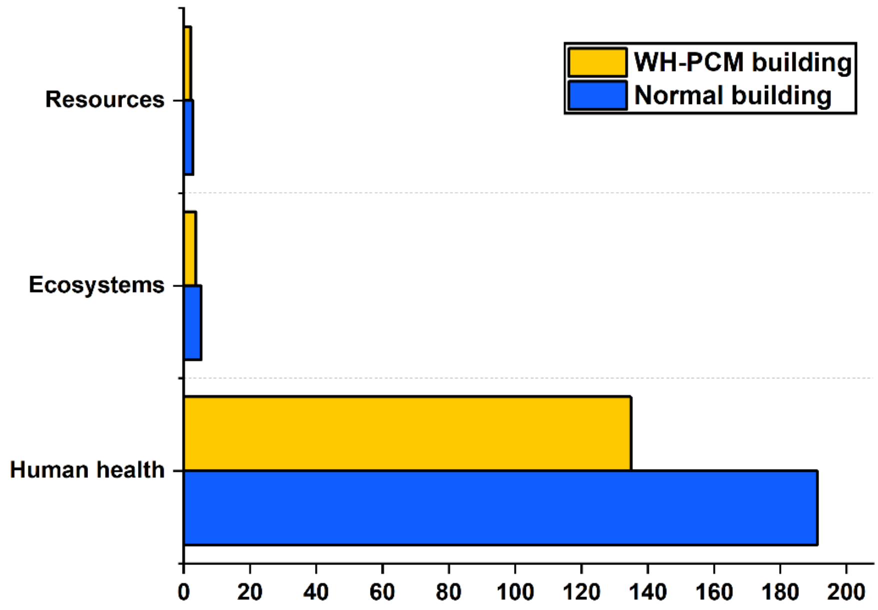

Fig. 5.12 ReCiPe 2016 endpoint categories (single score)

In ReCiPe endpoint method, all the 18 impact categories are summarized in three damage categories, as shown in **Fig.5.11**. In ReCiPe endpoint method, the parameters are expressed in "Point (Pt) unit, which is a single score, combining characterization, damage assessment and normalization [206]. As the endpoint analysis is based on the midpoint analysis, human health is showing the highest impact among the three categories. The total analysis shows that the use of a PCM wall is 29.4% more environmentally friendly than the conventional wall. The endpoint analysis is shown in **Fig. 5.12.**

5.6.8 Embodied and operational impact

Fig.5.13 represents the comparison of total environmental impact (ReCipe Endpoint single score) between the embodied and operational impacts. As explained earlier, the embodied impacts of a WH-PCM impregnated building are higher compared to a normal building. The reason for such a higher impact is because of the extra processes involved in the preparation of WH-PCM, which consists of pyrolysis of biomass, preparation of WH-PCM, PCM impregnated bricks and wall construction, which are additional to the construction of a normal building. WH-PCM building operational impact is much lower than normal building. The analysis shows that the manufacturing phase of the PCM wall is 11.15% more environmentally impactful than the manufacturing of a normal wall. But the operational phase is showing a 47.41% reduction in environmental impact compared to the normal building.

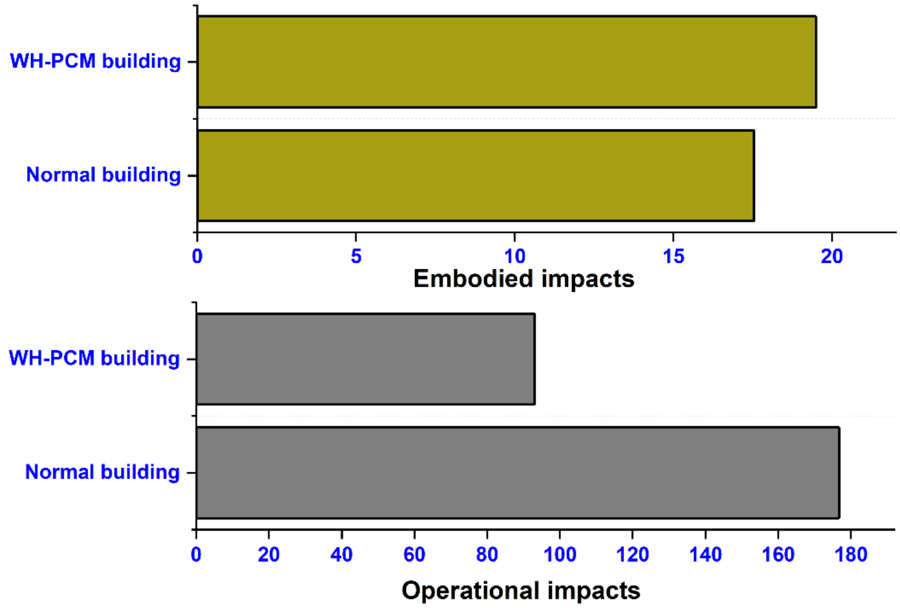

Fig. 5.13 Embodied and operational impacts comparison of ReCiPe 2016 endpoint (single score)

5.7 Summary of the chapter

The current chapter describes the techno-economic and LCA analysis of a WH-PCM-impregnated Assam-type building model. The integration of WH-PCM on the south and west walls of the modelled building shows considerable potential in annual cooling energy savings, also indicating strong economic feasibility. The LCA analysis indicates that the incorporation of WH-PCM has an overall positive environmental impact. The study confirms that the significant energy savings during the operational phase offset the environmental burden associated with the manufacturing of WH-PCM incorporated bricks. Based on the findings, it has been found that the developed biocomposite PCM, when used in buildings, gives a major beneficial impact in the environment compared to the reference building, by reducing approximately 30% impacts in GWP100, 29.4% in key endpoint impact categories, and 30.14% in cumulative energy demand throughout the building life span. The next chapter summarizes the findings of the present research and outlines the scope for future research.

Chapter 6

Conclusions and scope for future research

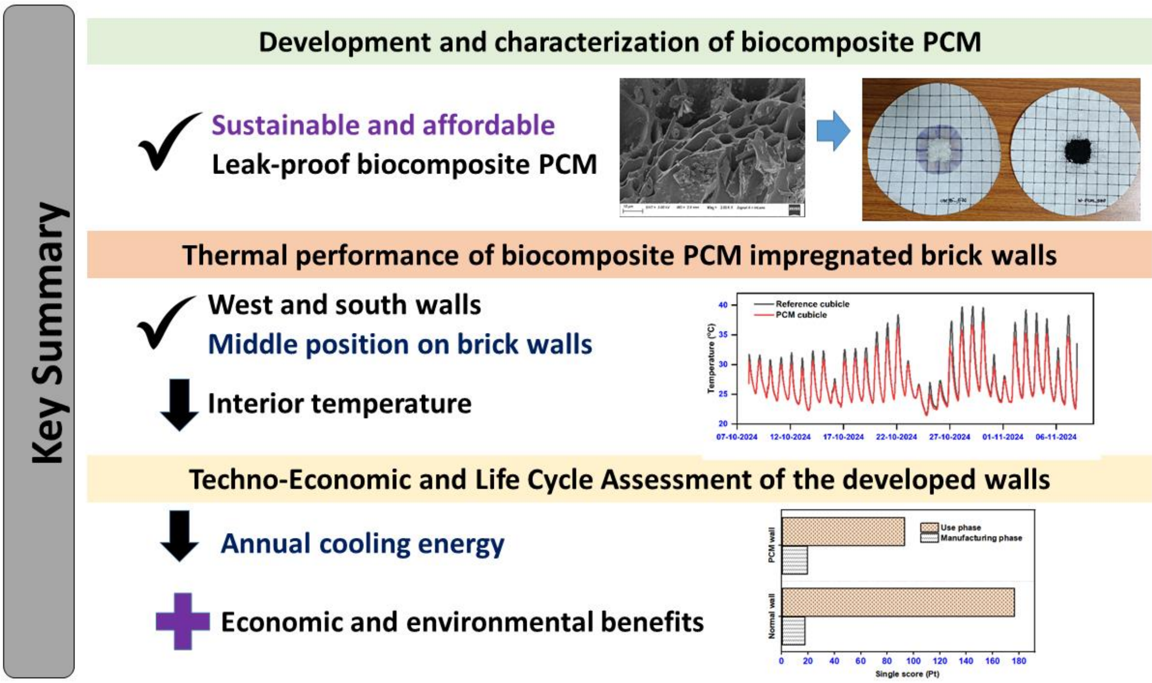

Outline

6.1 Conclusions and key findings
6.2 Scope for future research

6.1 Conclusions and key findings

The current study addresses the development of an alternative, passive and affordable building cooling solution for rural households. The study comprises the preparation of a novel biocomposite PCM using abundantly available biomass in the rural areas and directly applies the developed material onto the building wall. The key findings of the present study are highlighted in the following section.

Although organic PCM is widely used among all the commercially available PCMs due to numerous desirable qualities for building thermal management, the inherent disadvantages of leakage and low thermal conductivity are two critical challenges. To attenuate the challenges, seven different porous biochar materials are developed from three different biomasses, namely water hyacinth (WH), sugarcane bagasse (SCB) and yellow oleander (YO). Mesoporous biochar has been used as an encapsulating scaffold for incorporating OM35 (PCM) through simple impregnation method. The seepage of liquid PCM during phase transition is prevented through weak physical affinity between biochar and OM35. The chemical n-alkane chain of PCM remains intact after composite formation. The leakage stability test, conducted after 500 thermal cycles, confirms the excellent performance of the biochar matrix in maintaining the structural integrity of the biocomposite PCM. A thermal conductivity enhancement of 50.55% is observed for the biocomposite PCM with water hyacinth biochar. The suitable melting temperature range of 31-32°C makes the developed PCMs perfect for use as a building cooling material in tropical climates. Considering the physical, chemical, and thermal stability, biocomposite PCM with water hyacinth biochar as a supporting matrix (WH-PCM) is recommended for further building applications.

The study also extensively represents the feasibility of using biocomposite PCM on grooved bricks for passive thermal management in building walls. A mass of 50 g of WH-PCM has been inserted into a 20 mm thick groove in a red clay brick commonly used in rural construction. Walls have been constructed with WH-PCM embedded brick on a pre-fabricated cast iron structure. Directional analysis in the outdoor environment revealed that the orientation of PCM integrated walls has a significant impact on their thermal performance. For a hot and humid climate, it has been noticed that the WH-PCM-impregnated wall behaves best in the west direction, followed by the south direction, during the experimental period in terms of inside temperature reduction. The maximum peak temperature reduction is 10.47% on the west side wall. Along with the directions of the WH-PCM incorporated walls, three different positions of the WH-PCM layer within the wall thickness have been investigated. The study highlights that when biocomposite PCM is applied in the middle of the wall thickness, consistent indoor temperature fluctuation has been observed throughout the experimental time for almost all four directions. The investigation revealed that placing the WH-PCM layer near the interior surface of the wall is not effective for the studied climatic zone. The quality testing of the grooved brick with WH-PCM has been carried out, revealing that the water absorption capacity of clay bricks decreased by 19.23% after the insertion of WH-PCM, an improvement that is desirable for building applications. The compressive strength analysis shows that the brick with WH-PCM on the middle layer comes under grade 7.5 according to IS 1077: 1992 standards, which falls within the range for building construction.

The modified bricks with WH-PCM on the middle layer have been then used to construct an outdoor experimental cubicle (inner dimension of $1m^3$) to analyse the interior thermal performance. The effect of the walls on the interior temperature reduction has been observed for one summer month. During the daytime, when the solar insolation is at its peak, WH-PCM walls store the heat, and thus the interior of the PCM cubicle remains cooler than the reference cubicle. It has been found that the interior temperature of the cubicle with WH-PCM enhanced wall is lower at the peak hours for the summer months, with a peak temperature difference of around 6^oC, compared to the identical reference cubicle. Similar to the previous results, the maximum temperature difference between the WH-PCM and reference wall in the south and west directions is found to be 10.45°C and 9.08°C, respectively, for around 1:15 PM in the afternoon. In conclusion, the incorporation of WH-PCM on the south and west-facing walls is recommended for passive indoor temperature regulation.

The techno-economic and life cycle analysis have also been conducted in the current study. An Assam-type building with WH-PCM impregnated south and west walls has been modelled and evaluated for cooling energy consumption. The annual energy consumption reduction for the WH-PCM building is calculated as 31.4%, compared to a normal identical building, under the same environmental conditions. Techno-economic analysis shows the feasibility of applying WH-PCM in real buildings with positive net present value and acceptable payback periods. The cradle-to-grave LCA study for a building lifetime of 30 years shows that the use of a WH-PCM wall is 29.4% more environmentally friendly than the conventional wall due to the reduction in the electricity demand for the air conditioning system.

6.2 Scope for future research

The present work involves the development of new and affordable PCM, using locally available biomass materials in rural areas. The developed material can passively control indoor temperature when embedded in bricks, providing a cost-effective solution for houses in remote locations with limited access to grid electricity. However, the scope for future research in this particular domain is very promising, and some of them are listed below.

- It has been found that relative humidity plays a significant role in determining thermal comfort in buildings, along with the other three primary environmental parameters, Viz. air temperature, radiant temperature, and air velocity. Therefore, in addition to temperature, the effect of incorporating PCM into walls on indoor humidity can be experimentally investigated for a more comprehensive analysis. In addition, the development of hygrothermal PCMs at the material level for building applications remains a largely unexplored area and offers significant potential for future research.
- Before using as a green building material, the issue of the flammability of organic PCM needs proper attention. A comprehensive investigation of the fire safety performance of the developed PCMs is an important area for future research. If fire safety requirements are not met, incorporating suitable fire-retardant additives into biocomposite PCMs may offer another promising research direction.
- The long-term stability of the developed PCM through durability testing over thousands of thermal cycles can be performed under real environmental conditions to comprehensively understand their long-term behaviour and performance.
- Thermal management evaluation of PCM walls on a real-scale building throughout different climatic areas can be a scope of research, focusing on practical applicability, constructability, and economic feasibility. Such studies could explore and compare various methodologies for PCM incorporation in buildings, including use as a wall layer, integration within cement mortars, or fabrication of fully biocomposite PCM-based bricks, rather than limiting the approach to embedding PCMs into commercially available bricks.

- The thermal regulation performance of the biocomposite PCM envelope for alternative applications, such as cold storage and similar temperature-controlled environments, can be investigated in future. For every application, the selection of parent PCM may differ according to the required operating temperature; however, the potential of such systems can be systematically investigated through appropriate material development following the methodology adopted in the present study.
- Future studies may investigate the integration of PCM storage systems with active heat pump systems, sourced from renewable energy, for reducing demand for heating energy in buildings. The study may focus on the optimum design and development of a PCM heat exchanger to meet the daily heating requirement in buildings for the high-altitude regions of India.

References

[1] Space cooling, Int. Energy Agency. (2025). https://www.iea.org/energy-system/buildings/space-cooling (accessed April 25, 2025).

[2] International Energy Agency (IEA) and United Nations Environment Programme (UNEP), Global Alliance for Buildings and Construction: 2019 global status report for buildings and construction: Towards a zero-emission, efficient and resilient buildings and construction sector, 2019.

[3] World Economic Forum, Transforming Energy Demand W H I T E P A P E R J A N U A R Y 2 0 2 4 In collaboration with PwC, (2024).

[4] S. Zhou, Energy efficiency, Dict. Ecol. Econ. Terms New Millenn. (2023) 186. https://doi.org/10.4337/9781788974912.E.94.

[5] India Energy Outlook 2021, India Energy Outlook 2021. (2021). https://doi.org/10.1787/ec2fd78d-en.

[6] T.S. Cooling, INDIA ' S JOURNEY, (n.d.).

[7] T. Abergel, Chiara Delmastro, Is cooling the future of heating?, IEA. (2020). https://www.iea.org/commentaries/is-cooling-the-future-of-heating.

[8] India Cooling Action Plan (ICAP), (2024).

[9] V. Anand, V.L. Kadiri, C. Putcha, Passive buildings: a state-of-the-art review, J. Infrastruct. Preserv. Resil. 4 (2023). https://doi.org/10.1186/s43065-022-00068-z.

[10] J. Chai, J. Fan, Advanced thermal regulating materials and systems for energy saving and thermal comfort in buildings, Mater. Today Energy. 24 (2022) 100925. https://doi.org/10.1016/j.mtener.2021.100925.

[11] J. Lizana, R. Chacartegui, A. Barrios-padura, J. Manuel, Advances in thermal energy storage materials and their applications towards zero energy buildings : A critical review, 203 (2017) 219–239. https://doi.org/10.1016/j.apenergy.2017.06.008.

[12] Y. Zhang, G. Zhou, K. Lin, Q. Zhang, H. Di, Application of latent heat thermal energy storage in buildings: State-of-the-art and outlook, Build. Environ. 42 (2007) 2197–2209. https://doi.org/10.1016/j.buildenv.2006.07.023.

[13] N. Soares, J.J. Costa, A.R. Gaspar, P. Santos, Review of passive PCM latent heat thermal energy storage systems towards buildings' energy efficiency, Energy Build. 59 (2013) 82–103. https://doi.org/10.1016/j.enbuild.2012.12.042.

[14] M. Tao, L. Zhenpeng, Z. Jiaxin, Photovoltaic panel integrated with phase change materials (PV-PCM): technology overview and materials selection, Renew. Sustain. Energy Rev. 116 (2019) 109406. https://doi.org/10.1016/j.rser.2019.109406.

[15] P. Tatsidjodoung, N. Le Pierrès, L. Luo, A review of potential materials for thermal energy storage in building applications, Renew. Sustain. Energy Rev. 18 (2013) 327–349. https://doi.org/10.1016/j.rser.2012.10.025.

[16] K. Faraj, M. Khaled, J. Faraj, F. Hachem, C. Castelain, A review on phase change materials for thermal energy storage in buildings: Heating and hybrid applications, J. Energy Storage. 33 (2021) 101913. https://doi.org/10.1016/j.est.2020.101913.

[17] A. Benhorma, A. Bensenouci, M. Teggar, K.A.R. Ismail, M. Arıcı, E. Mezaache, Prospects and challenges of bio-based phase change materials : An up to date review, J. Energy Storage. 90 (2024) 111713. https://doi.org/10.1016/j.est.2024.111713.

[18] S. Riffat, B. Mempouo, W. Fang, Phase change material developments : a review, 0750 (2018). https://doi.org/10.1080/01430750.2013.823106.

[19] J. Tao, J. Luan, Y. Liu, D. Qu, Z. Yan, X. Ke, Technology development and application prospects of organic-based phase change materials : An overview, Renew. Sustain. Energy Rev. 159 (2022) 112175. https://doi.org/10.1016/j.rser.2022.112175.

[20] X. Wang, W. Li, Z. Luo, K. Wang, S.P. Shah, Energy & Buildings A critical review on phase change materials (PCM) for sustainable and energy efficient building : Design , characteristic , performance and application, Energy Build. 260 (2022) 111923. https://doi.org/10.1016/j.enbuild.2022.111923.

[21] C. Jakub, Energy & Buildings Inorganic phase change materials in thermal energy storage : A review on perspectives and technological advances in building applications, 252 (2021). https://doi.org/10.1016/j.enbuild.2021.111443.

[22] X. Wang, W. Li, Z. Luo, K. Wang, S.P. Shah, A critical review on phase change materials (PCM) for sustainable and energy efficient building: Design, characteristic, performance and application, Energy Build. 260 (2022) 111923. https://doi.org/10.1016/j.enbuild.2022.111923.

[23] K. Ghasemi, S. Tasnim, S. Mahmud, PCM , nano / microencapsulation and slurries : A review of fundamentals , categories , fabrication , numerical models and applications, Sustain. Energy Technol. Assessments. 52 (2022) 102084. https://doi.org/10.1016/j.seta.2022.102084.

[24] S.S. Magendran, F. Saleem, A. Khan, N.M. Mubarak, M. Vaka, Nano-Structures & Nano-Objects Synthesis of organic phase change materials (PCM) for energy storage applications : A review, Nano-Structures & Nano-Objects. 20 (2019) 100399. https://doi.org/10.1016/j.nanoso.2019.100399.

[25] N. Kumar, S. Kumar, V. Kumar, Materials Today : Proceedings Application of phase change material for thermal energy storage : An overview of recent advances, Mater. Today Proc. 44 (2021) 368–375. https://doi.org/10.1016/j.matpr.2020.09.745.

[26] B. Gupta, J. Bhalavi, S. Sharma, A. Bisen, Materials Today : Proceedings Phase change materials in solar energy applications : A review, Mater. Today Proc. 46 (2021) 5550–5554. https://doi.org/10.1016/j.matpr.2020.09.343.

[27] K. Pielichowska, K. Pielichowski, Phase change materials for thermal energy storage, Prog. Mater. Sci. 65 (2014) 67–123. https://doi.org/10.1016/j.pmatsci.2014.03.005.

[28] Y. Galazutdinova, S. Ushak, M. Farid, S. Al-hallaj, Development of the inorganic composite phase change materials for passive thermal management of Li-ion batteries : Application, 491 (2021). https://doi.org/10.1016/j.jpowsour.2021.229624.

[29] D. Das, U. Bordoloi, A.D. Kamble, H.H. Muigai, R.K. Pai, P. Kalita, Performance investigation of a rectangular spiral flow PV/T collector with a novel form-stable composite material, Appl. Therm. Eng. 182 (2021) 116035. https://doi.org/10.1016/j.applthermaleng.2020.116035.

[30] H. Liu, X. Wang, Sustainable Energy & Fuels change materials for thermal energy storage and versatile applications : a review, (2019) 1091–1149. https://doi.org/10.1039/c9se00019d.

[31] P. Kumar, S. Rathore, S.K. Shukla, Potential of macroencapsulated PCM for thermal energy storage in buildings : A comprehensive review, Constr. Build. Mater. 225 (2019) 723–744. https://doi.org/10.1016/j.conbuildmat.2019.07.221.

[32] I. Ait Laasri, N. Es-sakali, M. Charai, M.O. Mghazli, A. Outzourhit, Recent progress, limitations, and future directions of macro-encapsulated phase change materials for building applications, Renew. Sustain. Energy Rev. 199 (2024) 114481. https://doi.org/10.1016/j.rser.2024.114481.

[33] M. Gandhi, A. Kumar, R. Elangovan, C.S. Meena, K.S. Kulkarni, A. Kumar, G. Bhanot, N.R. Kapoor, A review on shape-stabilized phase change materials for latent energy storage in buildings, Sustain. 12 (2020) 1–17. https://doi.org/10.3390/su12229481.

[34] L. Boussaba, S. Makhlouf, A. Foufa, G. Lefebvre, L. Royon, vegetable fat: A low-cost bio-based phase change material for thermal energy storage in buildings, J. Build. Eng. 21 (2019) 222–229. https://doi.org/10.1016/j.jobe.2018.10.022.

[35] M. Iten, S. Liu, A. Shukla, A review on the air-PCM-TES application for free cooling and heating in the buildings, Renew. Sustain. Energy Rev. 61 (2016) 175–186. https://doi.org/10.1016/j.rser.2016.03.007.

[36] L. Navarro, A. de Gracia, S. Colclough, M. Browne, S.J. McCormack, P. Griffiths, L.F. Cabeza, Thermal energy storage in building integrated thermal systems: A review. Part 1. active storage systems, Renew. Energy. 88 (2016) 526–547. https://doi.org/10.1016/j.renene.2015.11.040.

[37] P.K. Latha, Y. Darshana, V. Venugopal, Role of building material in thermal comfort in tropical climates - A review, J. Build. Eng. 3 (2015) 104–113. https://doi.org/10.1016/j.jobe.2015.06.003.

[38] Y. Alassaf, Challenges , and Design Integration of Energy-Efficient Materials, (2024).

[39] Q. Al-Yasiri, M. Szabó, Incorporation of phase change materials into building envelope for thermal comfort and energy saving: A comprehensive analysis, J. Build. Eng. 36 (2021). https://doi.org/10.1016/j.jobe.2020.102122.

[40] Y. Li, N. Nord, Q. Xiao, T. Tereshchenko, Building heating applications with phase change material: A comprehensive review, J. Energy Storage. 31 (2020). https://doi.org/10.1016/j.est.2020.101634.

[41] M.K. Rathod, J. Banerjee, Thermal stability of phase change materials used in latent heat energy storage systems: A review, Renew. Sustain. Energy Rev. 18 (2013) 246–258. https://doi.org/10.1016/j.rser.2012.10.022.

[42] F. Souayfane, F. Fardoun, P.H. Biwole, Phase change materials (PCM) for cooling applications in buildings: A review, Energy Build. 129 (2016) 396–431. https://doi.org/10.1016/j.enbuild.2016.04.006.

[43] P.K.S. Rathore, S.K. Shukla, Enhanced thermophysical properties of organic PCM through shape stabilization for thermal energy storage in buildings: A state of the art review, Energy Build. 236 (2021) 110799. https://doi.org/10.1016/j.enbuild.2021.110799.

[44] Y. Wei, J. Li, F. Sun, J. Wu, L. Zhao, Leakage-proof phase change composites supported by biomass carbon aerogels from succulents, Green Chem. 20 (2018) 1858–1865. https://doi.org/10.1039/c7gc03595k.

[45] D. Das, O. Masek, M.C. Paul, Development of novel form-stable PCM-biochar composites and detailed characterization of their morphological, chemical and thermal properties, J. Energy Storage. 84 (2024) 110995. https://doi.org/10.1016/j.est.2024.110995.

[46] D. Das, U. Bordoloi, H.H. Muigai, P. Kalita, A novel form stable PCM based bio composite material for solar thermal energy storage applications, J. Energy Storage. 30 (2020) 101403. https://doi.org/10.1016/j.est.2020.101403.

[47] S. Wi, S.J. Chang, S. Kim, Improvement of thermal inertia effect in buildings using shape stabilized PCM wallboard based on the enthalpy-temperature function, Sustain. Cities Soc. 56 (2020) 102067. https://doi.org/10.1016/j.scs.2020.102067.

[48] S. Sharwan, P. Sikarwar, B. Mazumdar, Solar Energy Materials and Solar Cells Recent innovations in support materials for shape-stable organic composite phase change materials : A comprehensive review, Sol. Energy Mater. Sol. Cells. 272 (2025) 112910. https://doi.org/10.1016/j.solmat.2024.112910.

[49] Y. Zhang, Z. Jia, A. Moqeet, S. Zhang, B. Tang, Shape-stabilization micromechanisms of form-stable phase change materials-A review, Compos. Part A. 160 (2022) 107047. https://doi.org/10.1016/j.compositesa.2022.107047.

[50] D. Das, R. Crosby, M.C. Paul, A comprehensive review on the form stable phase change materials for storing renewable heat preparation , characterization and application, J. Energy Storage. 110 (2025) 115284. https://doi.org/10.1016/j.est.2024.115284.

[51] Y. chao Wan, Y. Chen, Z. xing Cui, H. Ding, S. feng Gao, Z. Han, J. kai Gao, A promising form-stable phase change material prepared using cost effective pinecone biochar as the matrix of palmitic acid for thermal energy storage, Sci. Rep. 9 (2019) 1–10. https://doi.org/10.1038/s41598-019-47877-z.

[52] R. Wen, X. Zhang, Z. Huang, M. Fang, Y. Liu, Solar Energy Materials and Solar Cells Preparation and thermal properties of fatty acid / diatomite form-stable composite phase change material for thermal energy storage, Sol. Energy Mater. Sol. Cells. 178 (2018) 273–279. https://doi.org/10.1016/j.solmat.2018.01.032.

[53] C. Li, H. Yu, Y. Song, M. Zhao, Synthesis and characterization of PEG / ZSM-5 composite phase change materials for latent heat storage, Renew. Energy. 121 (2018) 45–52. https://doi.org/10.1016/j.renene.2017.12.089.

[54] J. Liang, L. Zhimeng, Y. Ye, W. Yanjun, L. Jingxin, Z. Changlin, Fabrication and characterization of fatty acid/wood-flour composites as novel form-stable phase change materials for thermal energy storage, Energy Build. 171 (2018) 88–99. https://doi.org/10.1016/j.enbuild.2018.04.044.

[55] M. Muhammad, Y. Zhang, K. Iqbal, S. Zhang, B. Tang, Novel strategies and supporting materials applied to shape-stabilize organic phase change materials for thermal energy storage – A review, Appl. Energy. 235 (2019) 846–873. https://doi.org/10.1016/j.apenergy.2018.11.017.

[56] A. Sarı, A. Bicer, F.A. Al-sulaiman, A. Karaipekli, V. V Tyagi, Energy & Buildings Diatomite / CNTs / PEG composite PCMs with shape-stabilized and improved thermal conductivity : Preparation and thermal energy storage properties, 164 (2018) 166–175. https://doi.org/10.1016/j.enbuild.2018.01.009.

[57] D.G. Atinafu, W. Dong, C. Hou, R.S. Andriamitantsoa, J. Wang, X. Huang, H. Gao, G. Wang, A facile one-step synthesis of porous N-doped carbon from MOF for ef fi cient thermal energy storage capacity of shape-stabilized phase change materials, Mater. Today Energy. 12 (2019) 239–249. https://doi.org/10.1016/j.mtener.2019.01.011.

[58] J.A.C. Costa, A.E. Martinelli, R.M. do Nascimento, A.M. Mendes, Microstructural design and thermal characterization of composite diatomite-vermiculite paraffin-based form-stable PCM for cementitious mortars, Constr. Build. Mater. 232 (2020). https://doi.org/10.1016/j.conbuildmat.2019.117167.

[59] H. Abbasi Hattan, M. Madhkhan, A. Marani, Thermal and mechanical properties of building external walls plastered with cement mortar incorporating shape-stabilized phase change materials (SSPCMs), Constr. Build. Mater. 270 (2021) 121385. https://doi.org/10.1016/j.conbuildmat.2020.121385.

[60] A. Karaipekli, A. Sari, Development and thermal performance of pumice/organic PCM/gypsum composite plasters for thermal energy storage in buildings, Sol. Energy Mater. Sol. Cells. 149 (2016) 19–28. https://doi.org/10.1016/j.solmat.2015.12.034.

[61] J. Shi, M. Li, Lightweight mortar with paraffin/expanded vermiculite-diatomite composite phase change materials: Development, characterization and year-round thermoregulation performance, Sol. Energy. 220 (2021) 331–342. https://doi.org/10.1016/j.solener.2021.03.053.

[62] G. Hekimoğlu, M. Nas, M. Ouikhalfan, A. Sarı, V. V. Tyagi, R.K. Sharma, Ş. Kurbetci, T.A. Saleh, Silica fume/capric acid-stearic acid PCM included-cementitious composite for thermal controlling of buildings: Thermal energy storage and mechanical properties, Energy. 219 (2021). https://doi.org/10.1016/j.energy.2020.119588.

[63] G. Hekimoğlu, M. Nas, M. Ouikhalfan, A. Sarı, Ş. Kurbetci, V. V. Tyagi, R.K. Sharma, T.A. Saleh, Thermal management performance and mechanical properties of a novel cementitious composite containing fly ash/lauric acid-myristic acid as form-stable phase change material, Constr. Build. Mater. 274 (2021). https://doi.org/10.1016/j.conbuildmat.2020.122105.

[64] F.L. Rashid, M.A. Al-Obaidi, N.S. Dhaidan, A.K. Hussein, B. Ali, M.B. Ben Hamida, O. Younis, Bio-based phase change materials for thermal energy storage and release: A review, J. Energy Storage. 73 (2023) 109219. https://doi.org/10.1016/j.est.2023.109219.

[65] A.A. Mehrizi, H. Karimi-Maleh, M. Naddafi, F. Karimi, Application of bio-based phase change materials for effective heat management, J. Energy Storage. 61 (2023) 106859. https://doi.org/10.1016/j.est.2023.106859.

[66] M. Nazari, M. Jebrane, N. Terziev, Bio-based phase change materials incorporated in lignocellulose matrix for energy storage in buildings-a review, Energies. 13 (2020). https://doi.org/10.3390/en13123065.

[67] S. Palanti, A. Temiz, G.K. Demirel, G. Hekimoğlu, A. Sarı, M. Nazari, M. Jebrane, T. Schnabel, N. Terziev, Bio-Based Phase Change Materials for Wooden Building Applications, Forests. 13 (2022) 1–8. https://doi.org/10.3390/f13040603.

[68] A. Li, Y. Yang, Y. Ren, Y. Wan, W. Wu, H. Zhang, Bio-based composite phase change material utilizing wood fiber and coconut oil for thermal management in building envelopes, J. Clean. Prod. 469 (2024) 143177. https://doi.org/10.1016/j.jclepro.2024.143177.

[69] M. Nazari, M. Jebrane, N. Terziev, Solid wood impregnated with a bio-based phase change material for low temperature energy storage in building application, J. Therm. Anal. Calorim. 147 (2022) 10677–10692. https://doi.org/10.1007/s10973-022-11285-9.

[70] M. Sun, Q. Wang, H. Di, Review article A review of lignocellulosic biomass-based shape-stable composite phase change materials, J. Energy Storage. 73 (2023) 109114. https://doi.org/10.1016/j.est.2023.109114.

[71] J. Jeon, J.H. Park, S. Wi, S. Yang, Y.S. Ok, S. Kim, Latent heat storage biocomposites of phase change material-biochar as feasible eco-friendly building materials, Environ. Res. 172 (2019) 637–648. https://doi.org/10.1016/j.envres.2019.01.058.

[72] G. Ferrer, A. Solé, C. Barreneche, I. Martorell, L.F. Cabeza, Review on the methodology used in thermal stability characterization of phase change materials, Renew. Sustain. Energy Rev. 50 (2015) 665–685. https://doi.org/10.1016/j.rser.2015.04.187.

[73] T. Trisnadewi, E. Kusrini, D.M. Nurjaya, N. Putra, T.M.I. Mahlia, Experimental analysis of natural wax as phase change material by thermal cycling test using thermoelectric system, J. Energy Storage. 40 (2021) 102703. https://doi.org/10.1016/j.est.2021.102703.

[74] A. Shukla, D. Buddhi, R.L. Sawhney, Thermal cycling test of few selected inorganic and organic phase change materials, Renew. Energy. 33 (2008) 2606–2614. https://doi.org/10.1016/j.renene.2008.02.026.

[75] P.T. Saravanakumar, S.P. Arunkumar, B.B. Mansingh, P.M. Kumar, R. Subbiah, V.K. Eswarlal, Investigating the effect of thermal cycling on thermal characteristics of the nano-silica based phase changing material (PCM), Mater. Today Proc. 50 (2021) 1502–1507. https://doi.org/10.1016/j.matpr.2021.09.095.

[76] D. Gowthami, R.K. Sharma, V. V. Tyagi, P.K.S. Rathore, A. Sarı, Development of a novel form-stable phase change material based on alkali activated date seed biochar to harvest solar thermal energy, J. Energy Storage. 83 (2024) 110699. https://doi.org/10.1016/j.est.2024.110699.

[77] P. Singh, R.K. Sharma, R. Goyal, G. Hekimoğlu, A. Sarı, P.K.S. Rathore, V. V. Tyagi, Development and characterization a novel leakage-proof form stable composite of graphitic carbon nitride and fatty alcohol for thermal energy storage, J. Energy Storage. 55 (2022). https://doi.org/10.1016/j.est.2022.105761.

[78] K. Kumar, P. Kumar, S. Rathore, B. Singh, A.K. Pandey, Solar to thermal energy storage performance of composite phase change material supported by copper foam loaded with graphite and boron nitride, Sol. Energy. 272 (2024) 112459. https://doi.org/10.1016/j.solener.2024.112459.

[79] A. Kurdi, N. Almoatham, M. Mirza, T. Ballweg, B. Alkahlan, Potential phase change materials in building wall construction—a review, Materials (Basel). 14 (2021). https://doi.org/10.3390/ma14185328.

[80] J. Lizana, R. Chacartegui, A. Barrios-Padura, C. Ortiz, Advanced low-carbon energy measures based on thermal energy storage in buildings: A review, Renew. Sustain. Energy Rev. 82 (2018) 3705–3749. https://doi.org/10.1016/j.rser.2017.10.093.

[81] F. Kuznik, J. Virgone, J. Noel, Optimization of a phase change material wallboard for building use, Appl. Therm. Eng. 28 (2008) 1291–1298. https://doi.org/10.1016/j.applthermaleng.2007.10.012.

[82] C. Suresh, T. Kumar Hotta, S.K. Saha, Phase change material incorporation techniques in building envelopes for enhancing the building thermal Comfort-A review, Energy Build. 268 (2022) 112225. https://doi.org/10.1016/j.enbuild.2022.112225.

[83] B. Lamrani, K. Johannes, F. Kuznik, Phase change materials integrated into building walls: An updated review, Renew. Sustain. Energy Rev. 140 (2021) 110751. https://doi.org/10.1016/j.rser.2021.110751.

[84] R. Arivazhagan, N.B. Geetha, P. Sivasamy, P. Kumaran, M. Kumara Gnanamithra, S. Sankar, G.B. Loganathan, A. Arivarasan, Review on performance assessment of phase change materials in buildings for thermal management through passive approach, Mater. Today Proc. 22 (2020) 419–431. https://doi.org/10.1016/j.matpr.2019.07.616.

[85] X. Wang, H. Yu, L. Li, M. Zhao, Experimental assessment on the use of phase change materials (PCMs)-bricks in the exterior wall of a full-scale room, Energy Convers. Manag. 120 (2016) 81–89. https://doi.org/10.1016/j.enconman.2016.04.065.

[86] P.K.S. Rathore, S.K. Shukla, An experimental evaluation of thermal behavior of the building envelope using macroencapsulated PCM for energy savings, Renew. Energy. 149 (2020) 1300–1313. https://doi.org/10.1016/j.renene.2019.10.130.

[87] B. Nghana, F. Tariku, Phase change material's (PCM) impacts on the energy performance and thermal comfort of buildings in a mild climate, Build. Environ. 99 (2016) 221–238. https://doi.org/10.1016/j.buildenv.2016.01.023.

[88] Q. Al-Yasiri, M. Szabó, Experimental study of PCM-enhanced building envelope towards energy-saving and decarbonisation in a severe hot climate, Energy Build. 279 (2023) 112680. https://doi.org/10.1016/j.enbuild.2022.112680.

[89] A. Marani, M. Madhkhan, Thermal performance of concrete sandwich panels incorporating phase change materials : An experimental study, J. Mater. Res. Technol. 12 (2021) 760–775. https://doi.org/10.1016/j.jmrt.2021.03.022.

[90] A. Shahcheraghian, R. Ahmadi, A. Malekpour, Utilising Latent Thermal Energy Storage in Building Envelopes to Minimise Thermal Loads and Enhance Comfort, J. Energy Storage. 33 (2021) 102119. https://doi.org/10.1016/j.est.2020.102119.

[91] Q. Al-Yasiri, M. Szabó, Hourly analysis of temperature and heat gain reduction for building envelope-compacted phase change material in extremely hot conditions, J. Energy Storage. 68 (2023). https://doi.org/10.1016/j.est.2023.107838.

[92] P. Arumugam, V. Ramalingam, P. Vellaichamy, Optimal positioning of phase change material and insulation through numerical investigations to reduce cooling loads in office buildings, J. Energy Storage. 52 (2022) 104946. https://doi.org/10.1016/j.est.2022.104946.

[93] A.C. Rai, Energy performance of phase change materials integrated into brick masonry walls for cooling load management in residential buildings, Build. Environ. 199 (2021) 107930. https://doi.org/10.1016/j.buildenv.2021.107930.

[94] A. Kumar, B.M. Suman, Experimental evaluation of insulation materials for walls and roofs and their impact on indoor thermal comfort under composite climate, Build. Environ. 59 (2013) 635–643. https://doi.org/10.1016/j.buildenv.2012.09.023.

[95] C. Hema, A. Messan, A. Lawane, G. Van Moeseke, Impact of the Design of Walls Made of Compressed Earth Blocks on the Thermal Comfort of Housing in Hot Climate, Buildings. 10 (2020). https://doi.org/10.3390/BUILDINGS10090157.

[96] Q. Al-Yasiri, M. Szabó, Building envelope-combined phase change material and thermal insulation for energy-effective buildings during harsh summer: Simulation-based analysis, Energy Sustain. Dev. 72 (2023) 326–339. https://doi.org/10.1016/j.esd.2023.01.003.

[97] D. Kumar, M. Alam, P.X.W. Zou, J.G. Sanjayan, R.A. Memon, Comparative analysis of building insulation material properties and performance, Renew. Sustain. Energy Rev. 131 (2020) 110038. https://doi.org/10.1016/j.rser.2020.110038.

[98] Q. Al-Yasiri, M. Szabó, Experimental evaluation of the optimal position of a macroencapsulated phase change material incorporated composite roof under hot climate conditions, Sustain. Energy Technol. Assessments. 45 (2021). https://doi.org/10.1016/j.seta.2021.101121.

[99] H. Suehrcke, E.L. Peterson, N. Selby, Effect of roof solar reflectance on the building heat gain in a hot climate, Energy Build. 40 (2008) 2224–2235. https://doi.org/10.1016/j.enbuild.2008.06.015.

[100] M. Hou, X. Kong, H. Li, H. Yang, W. Chen, Experimental study on the thermal performance of composite phase change ventilated roof, J. Energy Storage. 33 (2021) 102060. https://doi.org/10.1016/j.est.2020.102060.

[101] A.L. Pisello, E. Fortunati, S. Mattioli, L.F. Cabeza, C. Barreneche, J.M. Kenny, F. Cotana, Innovative cool roofing membrane with integrated phase change materials: Experimental characterization of morphological, thermal and optic-energy behavior, Energy Build. 112 (2016) 40–48. https://doi.org/10.1016/j.enbuild.2015.11.061.

[102] S. Lu, Y. Chen, S. Liu, X. Kong, Experimental research on a novel energy efficiency roof coupled with PCM and cool materials, Energy Build. 127 (2016) 159–169. https://doi.org/10.1016/j.enbuild.2016.05.080.

[103] Q. Al-Yasiri, M. Szabó, Case study on the optimal thickness of phase change material incorporated composite roof under hot climate conditions, Case Stud. Constr. Mater. 14 (2021) 1–11. https://doi.org/10.1016/j.cscm.2021.e00522.

[104] N. Beemkumar, D. Yuvarajan, M. Arulprakasajothi, K. Elangovan, T. Arunkumar, Control of room temperature fluctuations in the building by incorporating PCM in the roof, J. Therm. Anal. Calorim. 143 (2021) 3039–3046. https://doi.org/10.1007/s10973-019-09226-0.

[105] A. Pasupathy, L. Athanasius, R. Velraj, R. V. Seeniraj, Experimental investigation and numerical simulation analysis on the thermal performance of a building roof incorporating phase change material (PCM) for thermal management, Appl. Therm. Eng. 28 (2008) 556–565. https://doi.org/10.1016/j.applthermaleng.2007.04.016.

[106] K.S. Reddy, V. Mudgal, T.K. Mallick, Thermal performance analysis of multi-phase change material layer-integrated building roofs for energy efficiency in built-environment, Energies. 10 (2017). https://doi.org/10.3390/en10091367.

[107] C. Mano, A. Thongtha, Enhanced thermal performance of roofing materials by integrating phase change materials to reduce energy consumption in buildings, J. Renew. Mater. 9 (2021) 495–506. https://doi.org/10.32604/jrm.2021.013201.

[108] H. Jamil, M. Alam, J. Sanjayan, J. Wilson, Investigation of PCM as retrofitting option to enhance occupant thermal comfort in a modern residential building, Energy Build. 133 (2016) 217–229. https://doi.org/10.1016/j.enbuild.2016.09.064.

[109] M. Saffari, C. Piselli, A. de Gracia, A.L. Pisello, F. Cotana, L.F. Cabeza, Thermal stress reduction in cool roof membranes using phase change materials (PCM), Energy Build. 158 (2018) 1097–1105. https://doi.org/10.1016/j.enbuild.2017.10.068.

[110] A. Jayalath, L. Aye, P. Mendis, T. Ngo, Effects of phase change material roof layers on thermal performance of a residential building in Melbourne and Sydney, Energy Build. 121 (2016) 152–158. https://doi.org/10.1016/j.enbuild.2016.04.007.

[111] C. Liu, Y. Zhou, D. Li, F. Meng, Y. Zheng, X. Liu, Numerical analysis on thermal performance of a PCM-filled double glazing roof, Energy Build. 125 (2016) 267–275. https://doi.org/10.1016/j.enbuild.2016.05.002.

[112] D. Li, Y. Zheng, C. Liu, G. Wu, Numerical analysis on thermal performance of roof contained PCM of a single residential building, Energy Convers. Manag. 100 (2015) 147–156. https://doi.org/10.1016/j.enconman.2015.05.014.

[113] J. Yu, K. Leng, F. Wang, H. Ye, Y. Luo, Simulation study on dynamic thermal performance of a new ventilated roof with form-stable pcm in Southern China, Sustain. 12 (2020) 1–21. https://doi.org/10.3390/su12229315.

[114] D.K. Bhamare, M.K. Rathod, J. Banerjee, Numerical model for evaluating thermal performance of residential building roof integrated with inclined phase change material (PCM) layer, J. Build. Eng. 28 (2020) 101018. https://doi.org/10.1016/j.jobe.2019.101018.

[115] H.J. Alqallaf, E.M. Alawadhi, Concrete roof with cylindrical holes containing PCM to reduce the heat gain, Energy Build. 61 (2013) 73–80. https://doi.org/10.1016/j.enbuild.2013.01.041.

[116] A. Pasupathy, R. Velraj, Effect of double layer phase change material in building roof for year round thermal management, Energy Build. 40 (2008) 193–203. https://doi.org/10.1016/j.enbuild.2007.02.016.

[117] R. Elghamry, H. Hassan, Impact of window parameters on the building envelope on the thermal comfort, energy consumption and cost and environment, Int. J. Vent. 19 (2020) 233–259. https://doi.org/10.1080/14733315.2019.1665784.

[118] S. Grynning, F. Goia, E. Rognvik, B. Time, Possibilities for characterization of a PCM window system using large scale measurements, Int. J. Sustain. Built Environ. 2 (2013) 56–64. https://doi.org/10.1016/j.ijsbe.2013.09.003.

[119] C. Li, H. Tang, Phase change material window for dynamic energy flow regulation : Review, Renew. Sustain. Energy Rev. 189 (2024) 113937. https://doi.org/10.1016/j.rser.2023.113937.

[120] W. Jiang, B. Liu, X. Zhang, T. Zhang, D. Li, L. Ma, Energy performance of window with PCM frame, Sustain. Energy Technol. Assessments. 45 (2021) 101109. https://doi.org/10.1016/j.seta.2021.101109.

[121] Y. Li, J. Darkwa, G. Kokogiannakis, W. Su, Phase change material blind system for double skin façade integration: System development and thermal performance evaluation, Appl. Energy. 252 (2019) 113376. https://doi.org/10.1016/j.apenergy.2019.113376.

[122] T. El Rhafiki, T. Kousksou, A. Allouhi, W. Benomar, H. Zennouhi, A. Jamil, Y. Zeraouli, Numerical analysis of a micro-encapsulated PCM wallboard: Fluxmeter applications, J. Build. Eng. 14 (2017) 127–133. https://doi.org/10.1016/j.jobe.2017.10.008.

[123] X. Kong, C. Yao, P. Jie, Y. Liu, C. Qi, X. Rong, Development and thermal performance of an expanded perlite-based phase change material wallboard for passive cooling in building, Energy Build. 152 (2017) 547–557. https://doi.org/10.1016/j.enbuild.2017.06.067.

[124] Y. Zhang, K. Lin, Y. Jiang, G. Zhou, Thermal storage and nonlinear heat-transfer characteristics of PCM wallboard, Energy Build. 40 (2008) 1771–1779. https://doi.org/10.1016/j.enbuild.2008.03.005.

[125] R. Baetens, B.P. Jelle, A. Gustavsen, Phase change materials for building applications: A state-of-the-art review, Energy Build. 42 (2010) 1361–1368. https://doi.org/10.1016/j.enbuild.2010.03.026.

[126] K. Biswas, J. Lu, P. Soroushian, S. Shrestha, Combined experimental and numerical evaluation of a prototype nano-PCM enhanced wallboard, Appl. Energy. 131 (2014) 517–529. https://doi.org/10.1016/j.apenergy.2014.02.047.

[127] X. Kong, P. Jie, C. Yao, Y. Liu, Experimental study on thermal performance of phase change material passive and active combined using for building application in winter, Appl. Energy. 206 (2017) 293–302. https://doi.org/10.1016/j.apenergy.2017.08.176.

[128] K.O. Lee, M.A. Medina, X. Sun, On the use of plug-and-play walls (PPW) for evaluating thermal enhancement technologies for building enclosures: Evaluation of a thin phase change material (PCM) layer, Energy Build. 86 (2015) 86–92. https://doi.org/10.1016/j.enbuild.2014.10.020.

[129] R. Barzin, J.J.J. Chen, B.R. Young, M.M. Farid, Application of PCM energy storage in combination with night ventilation for space cooling, Appl. Energy. 158 (2015) 412–421. https://doi.org/10.1016/j.apenergy.2015.08.088.

[130] P. Santos, C. Martins, L. Simões Da Silva, Thermal performance of lightweight steel-framed construction systems, Metall. Res. Technol. 111 (2014) 329–338. https://doi.org/10.1051/metal/2014035.

[131] N. Soares, A.R. Gaspar, P. Santos, J.J. Costa, Multi-dimensional optimization of the incorporation of PCM-drywalls in lightweight steel-framed residential buildings in different climates, Energy Build. 70 (2014) 411–421. https://doi.org/10.1016/j.enbuild.2013.11.072.

[132] Z. Yu, R. Shao, J. Li, C. Wu, An in-depth review of phase change materials in concrete for enhancing building energy-efficient temperature control systems, J. Energy Storage. 104 (2024) 114533. https://doi.org/10.1016/j.est.2024.114533.

[133] X. Shi, S.A. Memon, W. Tang, H. Cui, F. Xing, Experimental assessment of position of macro encapsulated phase change material in concrete walls on indoor temperatures and humidity levels, Energy Build. 71 (2014) 80–87. https://doi.org/10.1016/j.enbuild.2013.12.001.

[134] C.P. Wall, Thermal Regulation Performance of Shape-Stabilized-Phase-, (2023).

[135] A. Castell, I. Martorell, M. Medrano, G. Pérez, L.F. Cabeza, Experimental study of using PCM in brick constructive solutions for passive cooling, Energy Build. 42 (2010) 534–540. https://doi.org/10.1016/j.enbuild.2009.10.022.

[136] A. Figueiredo, J. Lapa, R. Vicente, C. Cardoso, Mechanical and thermal characterization of concrete with incorporation of microencapsulated PCM for applications in thermally activated slabs, Constr. Build. Mater. 112 (2016) 639–647. https://doi.org/10.1016/j.conbuildmat.2016.02.225.

[137] Z.A. Al-Absi, M.I.M. Hafizal, M. Asif, A. Alabdullatief, M. Ismail, Impacts of installation methods on the thermal performance of lightweight exterior cladding panels incorporating PCM: An experimental evaluation, Build. Environ. 265 (2024). https://doi.org/10.1016/j.buildenv.2024.111964.

[138] Z.A. Al-Absi, M. Asif, M.I.M. Hafizal, Numerical investigation and parametric analysis of PCM-based lightweight panels for wall's exterior cladding, Case Stud. Therm. Eng. 65 (2025) 105654. https://doi.org/10.1016/j.csite.2024.105654.

[139] M.C. M'ziane, A. Grine, Z. Younsi, M.S.K. Touhami, Modelling and Numerical Simulation of a Passive Wall Incorporating a Phase Change Material, J. Adv. Res. Fluid Mech. Therm. Sci. 79 (2021) 169–181. https://doi.org/10.37934/arfmts.79.1.169181.

[140] E.M. Alawadhi, Thermal analysis of a building brick containing phase change material, Energy Build. 40 (2008) 351–357. https://doi.org/10.1016/j.enbuild.2007.03.001.

[141] A. Castell, K. Menoufi, A. de Gracia, L. Rincón, D. Boer, L.F. Cabeza, Life Cycle Assessment of alveolar brick construction system incorporating phase change materials (PCMs), Appl. Energy. 101 (2013) 600–608. https://doi.org/10.1016/j.apenergy.2012.06.066.

[142] N. Hichem, S. Noureddine, S. Nadia, D. Djamila, Experimental and numerical study of a usual brick filled with PCM to improve the thermal inertia of buildings, Energy Procedia. 36 (2013) 766–775. https://doi.org/10.1016/j.egypro.2013.07.089.

[143] R. Saxena, D. Rakshit, S.C. Kaushik, Experimental assessment of Phase Change Material (PCM) embedded bricks for passive conditioning in buildings, Renew. Energy. 149 (2020) 587–599. https://doi.org/10.1016/j.renene.2019.12.081.

[144] N.S. Bondareva, M.A. Sheremet, F.Y. Zhao, The Brick Thermal Performance Improvement using Phase Change Materials, J. Appl. Comput. Mech. 6 (2020) 1283–1292. https://doi.org/10.22055/JACM.2020.33496.2237.

[145] K. Kant, A. Shukla, A. Sharma, Heat transfer studies of building brick containing phase change materials, Sol. Energy. 155 (2017) 1233–1242. https://doi.org/10.1016/j.solener.2017.07.072.

[146] R. Saxena, D. Rakshit, S.C. Kaushik, Phase change material (PCM) incorporated bricks for energy conservation in composite climate: A sustainable building solution, Sol. Energy. 183 (2019) 276–284. https://doi.org/10.1016/j.solener.2019.03.035.

[147] S. Shaik, C. Arumugam, S.V. Shaik, M. Arıcı, A. Afzal, Z. Ma, Strategic design of PCM integrated burnt clay bricks: Potential for cost-cutting measures for air conditioning and carbon dioxide extenuation, J. Clean. Prod. 375 (2022) 134077. https://doi.org/10.1016/j.jclepro.2022.134077.

[148] Y. Gao, X. Meng, A comprehensive review of integrating phase change materials in building bricks: Methods, performance and applications, J. Energy Storage. 62 (2023) 106913. https://doi.org/10.1016/j.est.2023.106913.

[149] H.M. Abbas, J.M. Jalil, S.T. Ahmed, Experimental and numerical investigation of PCM capsules as insulation materials inserted into a hollow brick wall, Energy Build. 246 (2021) 111127. https://doi.org/10.1016/j.enbuild.2021.111127.

[150] Y. Hamidi, Z. Aketouane, M. Malha, D. Bruneau, A. Bah, R. Goiffon, Integrating PCM into hollow brick walls: Toward energy conservation in Mediterranean regions, Energy Build. 248 (2021) 111214. https://doi.org/10.1016/j.enbuild.2021.111214.

[151] R. Saxena, D. Rakshit, S.C. Kaushik, Phase change material (PCM) incorporated bricks for energy conservation in composite climate: A sustainable building solution, Sol. Energy. 183 (2019) 276–284. https://doi.org/10.1016/j.solener.2019.03.035.

[152] Q. Al-Yasiri, M. Szabó, Effect of encapsulation area on the thermal performance of PCM incorporated concrete bricks: A case study under Iraq summer conditions, Case Stud. Constr. Mater. 15 (2021). https://doi.org/10.1016/j.cscm.2021.e00686.

[153] M. Arif Kamal, Analysis of autoclaved aerated concrete (AAC) blocks with reference to its potential and sustainability, J. Build. Mater. Struct. 7 (2020) 76–86. https://doi.org/10.34118/jbms.v7i1.707.

[154] . A.K., Thermal Performance & Fire Resistance of Autoclaved Aerated Concrete Exposed Humidity Conditions, Int. J. Res. Eng. Technol. 03 (2014) 267–272. https://doi.org/10.15623/ijret.2014.0303050.

[155] K.S. and J.K. Saurabh, An Overview of Advantages and Disadvantages of Autoclaved Aerated Concrete Review of Autoclaved Aerated Concrete : - Advantages and Disadvantages, (2019) 14–19.

[156] C. Punlek, S. Maneewan, A. Thongtha, Phase change material coating on autoclaved aerated lightweight concrete for cooling load reduction, Medziagotyra. 23 (2017) 161–165. https://doi.org/10.5755/j01.ms.23.2.15451.

[157] C. Li, X. Wen, W. Cai, H. Yu, D. Liu, Phase change material for passive cooling in building envelopes: A comprehensive review, J. Build. Eng. 65 (2023) 105763. https://doi.org/10.1016/j.jobe.2022.105763.

[158] M. Mahdaoui, S. Hamdaoui, A. Ait Msaad, T. Kousksou, T. El Rhafiki, A. Jamil, M. Ahachad, Building bricks with phase change material (PCM): Thermal performances, Constr. Build. Mater. 269 (2021) 121315. https://doi.org/10.1016/j.conbuildmat.2020.121315.

[159] Z. Younsi, H. Naji, Numerical simulation and thermal performance of hybrid brick walls embedding a phase change material for passive building applications, J. Therm. Anal. Calorim. 140 (2020) 965–978. https://doi.org/10.1007/s10973-019-08950-x.

[160] Y. Gao, F. He, X. Meng, Z. Wang, M. Zhang, H. Yu, W. Gao, Thermal behavior analysis of hollow bricks filled with phase-change material (PCM), J. Build. Eng. 31 (2020) 101447. https://doi.org/10.1016/j.jobe.2020.101447.

[161] S. Dabiri, M. Mehrpooya, E.G. Nezhad, Latent and sensible heat analysis of PCM incorporated in a brick for cold and hot climatic conditions, utilizing computational fluid dynamics, Energy. 159 (2018) 160–171. https://doi.org/10.1016/j.energy.2018.06.074.

[162] L. Li, H. Yu, R. Liu, Research on composite-phase change materials (PCMs)-bricks in the west wall of room-scale cubicle: Mid-season and summer day cases, Build. Environ. 123 (2017) 494–503. https://doi.org/10.1016/j.buildenv.2017.07.019.

[163] P. Principi, R. Fioretti, Thermal analysis of the application of PCM and low emissivity coating in hollow bricks, Energy Build. 51 (2012) 131–142. https://doi.org/10.1016/j.enbuild.2012.04.022.

[164] X. Kong, S. Lu, J. Huang, Z. Cai, S. Wei, Experimental research on the use of phase change materials in perforated brick rooms for cooling storage, Energy Build. 62 (2013) 597–604. https://doi.org/10.1016/j.enbuild.2013.03.048.

[165] A. Chelliah, S. Saboor, A. Ghosh, K.J. Kontoleon, Thermal Behaviour Analysis and Cost-Saving Opportunities of PCM-Integrated Terracotta Brick Buildings, Adv. Civ. Eng. 2021 (2021). https://doi.org/10.1155/2021/6670930.

[166] Y. Gao, X. Meng, A comprehensive review of integrating phase change materials in building bricks: Methods, performance and applications, J. Energy Storage. 62 (2023) 106913. https://doi.org/10.1016/j.est.2023.106913.

[167] H. Wang, W. Lu, Z. Wu, G. Zhang, Parametric analysis of applying PCM wallboards for energy saving in high-rise lightweight buildings in Shanghai, Renew. Energy. 145 (2020) 52–64. https://doi.org/10.1016/j.renene.2019.05.124.

[168] H. Wang, W. Lu, Z. Wu, Numerical model of applying PCM boards for energy saving in lightweight buildings in Shanghai, IOP Conf. Ser. Mater. Sci. Eng. 556 (2019). https://doi.org/10.1088/1757-899X/556/1/012014.

[169] Y. Qu, D. Zhou, F. Xue, L. Cui, Multi-factor analysis on thermal comfort and energy saving potential for PCM-integrated buildings in summer, Energy Build. 241 (2021). https://doi.org/10.1016/j.enbuild.2021.110966.

[170] A.G. Anter, A.A. Sultan, A.A. Hegazi, M.A. El Bouz, Thermal performance and energy saving using phase change materials (PCM) integrated in building walls, J. Energy Storage. 67 (2023) 107568. https://doi.org/10.1016/j.est.2023.107568.

[171] T. Saeed, Influence of the number of holes and two types of PCM in brick on the heat flux passing through the wall of a building on a sunny day in Medina, Saudi Arabia, J. Build. Eng. 50 (2022) 104215. https://doi.org/10.1016/j.jobe.2022.104215.

[172] S. Haghshenaskashani, H. Pasdarshahri, Simulation of thermal storage phase change material in buildings, World Acad. Sci. Eng. Technol. 58 (2009) 1020–1024.

[173] Y. Chihab, R. Bouferra, M. Garoum, M. Essaleh, N. Laaroussi, Thermal inertia and energy efficiency enhancements of hollow clay bricks integrated with phase change materials, J. Build. Eng. 53 (2022) 104569. https://doi.org/10.1016/j.jobe.2022.104569.

[174] T. Anfas Mukram, J. Daniel, Building bricks with PCM inserts for Passive cooling applications, IOP Conf. Ser. Earth Environ. Sci. 573 (2020). https://doi.org/10.1088/1755-1315/573/1/012034.

[175] E. Tunçbilek, M. Arıcı, S. Bouadila, S. Wonorahardjo, Seasonal and annual performance analysis of PCM-integrated building brick under the climatic conditions of Marmara region, J. Therm. Anal. Calorim. 141 (2020) 613–624. https://doi.org/10.1007/s10973-020-09320-8.

[176] P. Arumugam, V. Ramalingam, P. Vellaichamy, Effective PCM, insulation, natural and/or night ventilation techniques to enhance the thermal performance of buildings located in various climates – A review, Energy Build. 258 (2022) 111840. https://doi.org/10.1016/j.enbuild.2022.111840.

[177] X. Jin, M.A. Medina, X. Zhang, Numerical analysis for the optimal location of a thin PCM layer in frame walls, Appl. Therm. Eng. 103 (2016) 1057–1063. https://doi.org/10.1016/j.applthermaleng.2016.04.056.

[178] Z.X. Li, A.A.A.A. Al-rashed, M. Rostamzadeh, R. Kalbasi, Heat transfer reduction in buildings by embedding phase change material in multi-layer walls : Effects of repositioning , thermophysical properties and thickness of PCM, 195 (2019) 43–56. https://doi.org/10.1016/j.enconman.2019.04.075.

[179] A.G. Anter, A.A. Sultan, A.A. Hegazi, M.A. El Bouz, Thermal performance and energy saving using phase change materials (PCM) integrated in building walls, J. Energy Storage. 67 (2023) 107568. https://doi.org/10.1016/j.est.2023.107568.

[180] J. Hou, X. Meng, B. Julien, Case Studies in Construction Materials A numerical study on the effect of phase-change material (PCM) parameters on the thermal performance of lightweight building walls, Case Stud. Constr. Mater. 15 (2021) e00758. https://doi.org/10.1016/j.cscm.2021.e00758.

[181] M. Ar, F. Bilgin, S. Ni, H. Karabay, PCM integrated to external building walls : An optimization study on maximum activation of latent heat, 165 (2020). https://doi.org/10.1016/j.applthermaleng.2019.114560.

[182] M. Salihi, M. El, Y. Harmen, Y. Chhiti, F. Bentiss, C. Jama, Case Studies in Construction Materials Evaluation of global energy performance of building walls integrating PCM : Numerical study in semi-arid climate in Morocco, 16 (2022). https://doi.org/10.1016/j.cscm.2022.e00979.

[183] X. Sun, Y. Zhang, K. Xie, M.A. Medina, A parametric study on the thermal response of a building wall with a phase change material (PCM) layer for passive space cooling, J. Energy Storage. 47 (2022) 103548. https://doi.org/10.1016/j.est.2021.103548.

[184] Z. Shi, J. Ren, T. Zhang, Y. Shen, The Effects of Thickness and Location of PCM on the Building ’ s Passive Temperature-Control – A Numerical Study, (2024). https://doi.org/10.32604/ee.2023.045238.

[185] B. Jamal, R. Hidki, M. Boukendil, L. El Moutaouakil, Z. Charqui, A. Abdelbaki, Thermal performance analysis of building walls incorporating phase change materials under hot climatic conditions in Morocco, Therm. Sci. Eng. Prog. 59 (2025) 103373. https://doi.org/10.1016/j.tsep.2025.103373.

[186] W. Li, M. Rahim, D. Wu, M. El, R. Bennacer, Experimental study of dynamic PCM integration in building walls for enhanced thermal performance in summer conditions, Renew. Energy. 237 (2024) 121891. https://doi.org/10.1016/j.renene.2024.121891.

[187] P. Kumar, S. Rathore, S.K. Shukla, An experimental evaluation of thermal behavior of the building envelope using macroencapsulated PCM for energy savings, Renew. Energy. 149 (2020) 1300–1313. https://doi.org/10.1016/j.renene.2019.10.130.

[188] X. Wang, H. Yu, L. Li, M. Zhao, Experimental assessment on the use of phase change materials (PCMs) -bricks in the exterior wall of a full-scale room, 120 (2016) 81–89. https://doi.org/10.1016/j.enconman.2016.04.065.

[189] A. Gounni, M. El Alami, The optimal allocation of the PCM within a composite wall for surface temperature and heat flux reduction : An experimental Approach, Appl. Therm. Eng. 127 (2017) 1488–1494. https://doi.org/10.1016/j.applthermaleng.2017.08.168.

[190] Y. Zhou, Phase change materials in energy-efficient buildings—from material selection, design to system application and assessment, Energy Build. (2025) 116630. https://doi.org/10.1016/j.enbuild.2025.116630.

[191] A. Ahmad, S. Ali, H. Dang, A. Sari, O. Gencel, Breaking new ground : A first-of-its-kind critical analysis of review articles on phase change materials for building applications, Appl. Energy. 392 (2025) 125984. https://doi.org/10.1016/j.apenergy.2025.125984.

[192] P. Agarwal, A. Prabhakar, Energy and thermo-economic analysis of PCM integrated brick in composite climatic condition of Jaipur - A numerical study, Sustain. Cities Soc. 88 (2023) 104294. https://doi.org/10.1016/j.scs.2022.104294.

[193] A. Ahmad, S.A. Memon, A novel method to evaluate phase change materials ' impact on buildings ' energy , economic , and environmental performance via controlled natural ventilation, Appl. Energy. 353 (2024) 122033. https://doi.org/10.1016/j.apenergy.2023.122033.

[194] X. Mi, R. Liu, H. Cui, S.A. Memon, F. Xing, Y. Lo, Energy and economic analysis of building integrated with PCM in different cities of China, Appl. Energy. 175 (2016) 324–336. https://doi.org/10.1016/j.apenergy.2016.05.032.

[195] D. Abd El-Raheim, A. Mohamed, M. Fatouh, H. Abou-Ziyan, Comfort and economic aspects of phase change materials integrated with heavy-structure buildings in hot climates, Appl. Therm. Eng. 213 (2022) 118785. https://doi.org/10.1016/j.applthermaleng.2022.118785.

[196] Z. Abilkhassenova, S.A. Memon, A. Ahmad, A. Saurbayeva, J. Kim, Utilizing the Fanger thermal comfort model to evaluate the thermal, energy, economic, and environmental performance of PCM-integrated buildings in various climate zones worldwide, Energy Build. 297 (2023) 113479. https://doi.org/10.1016/j.enbuild.2023.113479.

[197] J. Hou, Z. Liu, L. Zhang, T. Zhang, C. Hou, H. Fukuda, Parametric and economic analysis of incorporating phase change material (PCM) into exterior walls to reduce energy demand for traditional dwellings in northeast of Sichuan hills , China, Appl. Therm. Eng. 223 (2023) 119982. https://doi.org/10.1016/j.applthermaleng.2023.119982.

[198] O.J. Imafidon, D.S.K. Ting, Retrofitting buildings with Phase Change Materials (PCM) – The effects of PCM location and climatic condition, Build. Environ. 236 (2023) 110224. https://doi.org/10.1016/j.buildenv.2023.110224.

[199] R. Golchimard, L. Zhu, S. Defilla, Performance evaluation of different building envelopes integrated with phase change materials in tropical climates, Energy Built Environ. 6 (2025) 332–346. https://doi.org/10.1016/j.enbenv.2023.11.008.

[200] Y. M'hamdi, K. Baba, M. Tajayouti, A. Nounah, Energy, environmental, and economic analysis of different buildings envelope integrated with phase change materials in different climates, Sol. Energy. 243 (2022) 91–102. https://doi.org/10.1016/j.solener.2022.07.031.

[201] R. Ji, X. Li, C. Lv, Energy & Buildings Synthesis and evaluation of phase change material suitable for energy-saving and carbon reduction of building envelopes, 278 (2023). https://doi.org/10.1016/j.enbuild.2022.112603.

[202] L. Zhang, Q. Zhang, L. Jin, X. Cui, X. Yang, Energy , economic and environmental (3E) analysis of residential building walls enhanced with phase change materials, J. Build. Eng. 84 (2024) 108503. https://doi.org/10.1016/j.jobe.2024.108503.

[203] A. Kylili, P.A. Fokaides, Life Cycle Assessment (LCA) of Phase Change Materials (PCMs) for building applications : A review, J. Build. Eng. 6 (2016) 133–143. https://doi.org/10.1016/j.jobe.2016.02.008.

[204] M. Vega, N. Llantoy, M. Chafer, S. Ushak, L.F. Cabeza, Life cycle assessment of the inclusion of phase change materials in lightweight buildings, J. Energy Storage. 56 (2022) 105903. https://doi.org/10.1016/j.est.2022.105903.

[205] E. Kyriaki, C. Konstantinidou, E. Giama, A.M. Papadopoulos, Life cycle analysis (LCA) and life cycle cost analysis (LCCA) of phase change materials (PCM) for thermal applications : A review, (2018) 3068–3077. https://doi.org/10.1002/er.3945.

[206] C. Fabiani, A.L. Pisello, M. Barbanera, L.F. Cabeza, Palm oil-based bio-PCM for energy e ffi cient building applications : Multipurpose thermal investigation and life cycle assessment, 28 (2020). https://doi.org/10.1016/j.est.2019.101129.

[207] K. Menou, A. Castell, M.M. Farid, D. Boer, L.F. Cabeza, Life Cycle Assessment of experimental cubicles including PCM manufactured from natural resources (esters): A theoretical study, 51 (2013) 398–403. https://doi.org/10.1016/j.renene.2012.10.010.

[208] D. Antypa, F. Petrakli, A. Gkika, A. Ali, F. Pawelz, E. Kieseritzky, E.P. Koumoulos, Life Cycle Assessment of a PCM-Filled Compact Storage Module for Building Applications, (2025).

[209] A. Castell, K. Menoufi, A. De Gracia, L. Rincón, D. Boer, L.F. Cabeza, Life Cycle Assessment of alveolar brick construction system incorporating phase change materials (PCMs), Appl. Energy. 101 (2013) 600–608. https://doi.org/10.1016/j.apenergy.2012.06.066.

[210] Pluss Polymers, Technical Data Sheet of Save ® OM35 PLUSS ® Encapsulation, (2018) 1–2.

[211] Pluss Advanced Technologies, TECHNICAL DATA SHEET – savE® OM 35, 2015.

[212] J. Huang, S. Lu, X. Kong, S. Liu, Y. Li, Form-stable phase change materials based on eutectic mixture of tetradecanol and fatty acids for building energy storage: Preparation and performance analysis, Materials (Basel). 6 (2013) 4758–4775. https://doi.org/10.3390/ma6104758.

[213] L.K. Lazzari, D. Perondi, V.B. Zampieri, A.J. Zattera, R.M.C. Santana, Cellulose/biochar aerogels with excellent mechanical and thermal insulation properties, Cellulose. 26 (2019) 9071–9083. https://doi.org/10.1007/s10570-019-02696-3.

[214] D. Patwa, U. Bordoloi, A.A. Dubey, K. Ravi, S. Sekharan, P. Kalita, Energy-efficient biochar production for thermal backfill applications, Sci. Total Environ. (2022) 155253. https://doi.org/10.1016/j.scitotenv.2022.155253.

[215] I.C. Oven, F. Hood, Quotation: STRX/21-22/1363, (2022).

[216] S. Karaman, A. Karaipekli, A. Sar, A. Biçer, Polyethylene glycol (PEG)/diatomite composite as a novel form-stable phase change material for thermal energy storage, Sol. Energy Mater. Sol. Cells. 95 (2011) 1647–1653. https://doi.org/10.1016/j.solmat.2011.01.022.

[217] T. Khadiran, M.Z. Hussein, Z. Zainal, R. Rusli, Activated carbon derived from peat soil as a framework for the preparation of shape-stabilized phase change material, Energy. 82 (2015) 468–478. https://doi.org/10.1016/j.energy.2015.01.057.

[218] H.H. Muigai, U. Bordoloi, R. Hussain, K. Ravi, V.S. Moholkar, P. Kalita, A comparative study on synthesis and characterization of biochars derived from lignocellulosic biomass for their candidacy in agronomy and energy applications, Int. J. Energy Res. 45 (2021) 4765–4781. https://doi.org/10.1002/er.6092.

[219] D.G. Atinafu, B.Y. Yun, S. Wi, Y. Kang, S. Kim, A comparative analysis of biochar, activated carbon, expanded graphite, and multi-walled carbon nanotubes with respect to PCM loading and energy-storage capacities, Environ. Res. 195 (2021) 110853. https://doi.org/10.1016/j.envres.2021.110853.

[220] D.G. Atinafu, S. Jin Chang, K.H. Kim, S. Kim, Tuning surface functionality of standard biochars and the resulting uplift capacity of loading/energy storage for organic phase change materials, Chem. Eng. J. 394 (2020) 125049. https://doi.org/10.1016/j.cej.2020.125049.

[221] T. Khadiran, M.Z. Hussein, Z. Zainal, R. Rusli, Activated carbon derived from peat soil as a framework for the preparation of shape-stabilized phase change material, Energy. 82 (2015) 468–478. https://doi.org/10.1016/j.energy.2015.01.057.

[222] Y. Liu, K. Yu, S. Lu, C. Wang, X. Li, Y. Yang, Experimental research on an environment-friendly form-stable phase change material incorporating modified rice husk ash for thermal energy storage, J. Energy Storage. 31 (2020). https://doi.org/10.1016/j.est.2020.101599.

[223] J. Huang, B. Wu, S. Lyu, T. Li, H. Han, D. Li, J. Wang, J. Zhang, X. Lu, D. Sun, Solar Energy Materials and Solar Cells Improving the thermal energy storage capability of diatom-based biomass / polyethylene glycol composites phase change materials by artificial culture methods, Sol. Energy Mater. Sol. Cells. 219 (2021) 110797. https://doi.org/10.1016/j.solmat.2020.110797.

[224] Y. Luo, S. Xiong, J. Huang, F. Zhang, C. Li, Y. Min, Solar Energy Materials and Solar Cells Preparation , characterization and performance of paraffin / sepiolite composites as novel shape-stabilized phase change materials for thermal energy storage, Sol. Energy Mater. Sol. Cells. 231 (2021) 111300. https://doi.org/10.1016/j.solmat.2021.111300.

[225] L. Leng, Q. Xiong, L. Yang, H. Li, Y. Zhou, W. Zhang, S. Jiang, H. Li, H. Huang, An overview on engineering the surface area and porosity of biochar, Sci. Total Environ. 763 (2021) 144204. https://doi.org/10.1016/j.scitotenv.2020.144204.

[226] P. Sakulkit, A. Palamanit, R. Dejchanchaiwong, P. Reubroycharoen, Characteristics of pyrolysis products from pyrolysis and co-pyrolysis of rubber wood and oil palm trunk biomass for biofuel and value-added applications, J. Environ. Chem. Eng. 8 (2020) 104561. https://doi.org/10.1016/j.jece.2020.104561.

[227] Z. Wang, K.G. Burra, M. Zhang, X. Li, M. Policella, T. Lei, A.K. Gupta, Co-pyrolysis of waste tire and pine bark for syngas and char production, Fuel. 274 (2020) 117878. https://doi.org/10.1016/j.fuel.2020.117878.

[228] O.D. Nartey, B. Zhao, Biochar preparation, characterization, and adsorptive capacity and its effect on bioavailability of contaminants: An overview, Adv. Mater. Sci. Eng. 2014 (2014). https://doi.org/10.1155/2014/715398.

[229] C. Li, H. Yu, Y. Song, M. Wang, Z. Liu, A n-octadecane/hierarchically porous TiO2 form-stable PCM for thermal energy storage, Renew. Energy. 145 (2020) 1465–1473. https://doi.org/10.1016/j.renene.2019.06.070.

[230] S. Hasanabadi, S.M. Sadrameli, H. Soheili, H. Moharrami, M.M. Heyhat, A cost-effective form-stable PCM composite with modified paraffin and expanded perlite for thermal energy storage in concrete, J. Therm. Anal. Calorim. 136 (2019) 1201–1216. https://doi.org/10.1007/s10973-018-7731-8.

[231] D. Wu, W. Wen, S. Chen, H. Zhang, Preparation and properties of a novel form-stable phase change material based on a gelator, J. Mater. Chem. A. 3 (2015) 2589–2600. https://doi.org/10.1039/c4ta06508e.

[232] J. Liang, L. Zhimeng, Y. Ye, W. Yanjun, L. Jingxin, Z. Changlin, Fabrication and characterization of fatty acid/wood-flour composites as novel form-stable phase change materials for thermal energy storage, Energy Build. 171 (2018) 88–99. https://doi.org/10.1016/j.enbuild.2018.04.044.

[233] M. Mehrali, S.T. Latibari, M. Mehrali, T.M. Indra Mahlia, H.S. Cornelis Metselaar, Preparation and properties of highly conductive palmitic acid/graphene oxide composites as thermal energy storage materials, Energy. 58 (2013) 628–634. https://doi.org/10.1016/j.energy.2013.05.050.

[234] X. Fu, Z. Liu, B. Wu, J. Wang, J. Lei, Preparation and thermal properties of stearic acid/diatomite composites as form-stable phase change materials for thermal energy storage via direct impregnation method, J. Therm. Anal. Calorim. 123 (2016) 1173–1181. https://doi.org/10.1007/s10973-015-5030-1.

[235] D.G. Atinafu, W. Dong, X. Huang, H. Gao, G. Wang, Introduction of organic-organic eutectic PCM in mesoporous N-doped carbons for enhanced thermal conductivity and energy storage capacity, Appl. Energy. 211 (2018) 1203–1215. https://doi.org/10.1016/j.apenergy.2017.12.025.

[236] S. Karaman, A. Karaipekli, A. Sarı, A. Bic, Solar Energy Materials & Solar Cells Polyethylene glycol (PEG)/ diatomite composite as a novel form-stable phase change material for thermal energy storage, 95 (2011) 1647–1653. https://doi.org/10.1016/j.solmat.2011.01.022.

[237] C. Li, H. Yu, Y. Song, M. Wang, Z. Liu, A n-octadecane / hierarchically porous TiO 2 form-stable PCM for thermal energy storage, Renew. Energy. 145 (2020) 1465–1473. https://doi.org/10.1016/j.renene.2019.06.070.

[238] K. Yu, Y. Liu, Y. Yang, Enhanced thermal properties of polyethylene glycol / modified rice husk ash eco-friendly form-stable phase change material via optimizing support pore structure, J. Energy Storage. 43 (2021) 103172. https://doi.org/10.1016/j.est.2021.103172.

[239] B. Eanest Jebasingh, A. Valan Arasu, A comprehensive review on latent heat and thermal conductivity of nanoparticle dispersed phase change material for low-temperature applications, Energy Storage Mater. 24 (2020) 52–74. https://doi.org/10.1016/j.ensm.2019.07.031.

[240] D. Kim, J. Jung, Y. Kim, M. Lee, J. Seo, S.B. Khan, Structure and thermal properties of octadecane/expanded graphite composites as shape-stabilized phase change materials, Int. J. Heat Mass Transf. 95 (2016) 735–741. https://doi.org/10.1016/j.ijheatmasstransfer.2015.12.049.

[241] B. Eanest Jebasingh, A. Valan Arasu, A comprehensive review on latent heat and thermal conductivity of nanoparticle dispersed phase change material for low-temperature applications, Energy Storage Mater. (2019). https://doi.org/10.1016/j.ensm.2019.07.031.

[242] S.N. Nyamsi, M. Lototskyy, I. Tolj, Selection of metal hydrides-based thermal energy storage: Energy storage efficiency and density targets, Int. J. Hydrogen Energy. 43 (2018) 22568–22583. https://doi.org/10.1016/j.ijhydene.2018.10.100.

[243] Z. Chen, F. Shan, L. Cao, G. Fang, Solar Energy Materials & Solar Cells Synthesis and thermal properties of shape-stabilized lauric acid / activated carbon composites as phase change materials for thermal energy storage, Sol. Energy Mater. Sol. Cells. 102 (2012) 131–136. https://doi.org/10.1016/j.solmat.2012.03.013.

[244] T. Khadiran, M.Z. Hussein, Z. Zainal, R. Rusli, Shape-stabilised n-octadecane/activated carbon nanocomposite phase change material for thermal energy storage, J. Taiwan Inst. Chem. Eng. 55 (2015) 189–197. https://doi.org/10.1016/j.jtice.2015.03.028.

[245] G. Hekimoğlu, A. Sarı, S. Arunachalam, H. Arslanoğlu, O. Gencel, Porous biochar/heptadecane composite phase change material with leak-proof, high thermal energy storage capacity and enhanced thermal conductivity, Powder Technol. 394 (2021) 1017–1025. https://doi.org/10.1016/j.powtec.2021.09.030.

[246] J. Jeon, H. il Kim, J.H. Park, S. Wi, S. Kim, Evaluation of thermal properties and acetaldehyde adsorption performance of sustainable composites using waste wood and biochar, Environ. Res. 196 (2021) 110910. https://doi.org/10.1016/j.envres.2021.110910.

[247] D. Patwa, H.H. Muigai, K. Ravi, S. Sreedeep, P. Kalita, A Novel Application of Biochar Produced from Invasive Weeds and Industrial Waste in Thermal Backfill for Crude Oil Industries, Waste and Biomass Valorization. (2022). https://doi.org/10.1007/s12649-022-01694-0.

[248] X. Liu, J. Tie, Z. Wang, Y. Xia, C. Wang, Improved thermal conductivity and stability of Na 2 SO 4 , 10H 2 O PCMs system by incorporation of Al / C hybrid nanoparticles, J. Mater. Res. Technol. 12 (2021) 982–988. https://doi.org/10.1016/j.jmrt.2021.02.096.

[249] Y. Zhang, Z. Jia, A. Moqeet Hai, S. Zhang, B. Tang, Shape-stabilization micromechanisms of form-stable phase change materials-A review, Compos. Part A Appl. Sci. Manuf. 160 (2022) 107047. https://doi.org/10.1016/j.compositesa.2022.107047.

[250] U. Bordoloi, D. Das, D. Kashyap, D. Patwa, P. Bora, H.H. Muigai, P. Kalita, Synthesis and comparative analysis of biochar based form-stable phase change materials for thermal management of buildings, J. Energy Storage. 55 (2022) 105801. https://doi.org/10.1016/j.est.2022.105801.

[251] S. Fatimah, R. Ragadhita, D.F. Al Husaeni, A.B.D. Nandiyanto, How to Calculate Crystallite Size from X-Ray Diffraction (XRD) using Scherrer Method, ASEAN J. Sci. Eng. 2 (2022) 65–76. https://doi.org/10.17509/ajse.v2i1.37647.

[252] L. Ma, C. Guo, R. Ou, Q. Wang, L. Li, Synthesis and characterization of the n-butyl palmitate as an organic phase change material, J. Therm. Anal. Calorim. 136 (2019) 2033–2039. https://doi.org/10.1007/s10973-018-7846-y.

[253] C. Cárdenas-Ramírez, M.A. Gómez, F. Jaramillo, A.G. Fernández, L.F. Cabeza, Thermal reliability of organic-organic phase change materials and their shape-stabilized composites, J. Energy Storage. 40 (2021). https://doi.org/10.1016/j.est.2021.102661.

[254] I.A. Laghari, M. Samykano, A.K. Pandey, K. Kadirgama, Y.N. Mishra, Binary composite (TiO2-Gr) based nano-enhanced organic phase change material: Effect on thermophysical properties, J. Energy Storage. 51 (2022) 104526. https://doi.org/10.1016/j.est.2022.104526.

[255] D. Rahmalina, R.A. Rahman, Ismail, Increasing the rating performance of paraffin up to 5000 cycles for active latent heat storage by adding high-density polyethylene to form shape-stabilized phase change material, J. Energy Storage. 46 (2022). https://doi.org/10.1016/j.est.2021.103762.

[256] C.L. Hobday, S. Krause, S.M.J. Rogge, J.D. Evans, H. Bunzen, Perspectives on the Influence of Crystal Size and Morphology on the Properties of Porous Framework Materials, Front. Chem. 9 (2021) 1–10. https://doi.org/10.3389/fchem.2021.772059.

[257] P. Mandal, K. Stokes, G. Hernández, D. Brandell, J. Mindemark, Influence of Binder Crystallinity on the Performance of Si Electrodes with Poly(vinyl alcohol) Binders, ACS Appl. Energy Mater. 4 (2021) 3008–3016. https://doi.org/10.1021/acsaem.0c02051.

[258] L. Yang, X. Cao, N. Zhang, B. Xiang, Z. Zhang, B. Qian, Thermal reliability of typical fatty acids as phase change materials based on 10,000 accelerated thermal cycles, Sustain. Cities Soc. 46 (2019) 101380. https://doi.org/10.1016/j.scs.2018.12.008.

[259] A. Anand, A. Shukla, A. Kumar, D. Buddhi, A. Sharma, Cycle test stability and corrosion evaluation of phase change materials used in thermal energy storage systems, J. Energy Storage. 39 (2021) 102664. https://doi.org/10.1016/j.est.2021.102664.

[260] M.H. Zahir, M.M. Rahman, K.O. Mohaisen, A. Helal, M.N. Shaikh, M.M. Rahman, Clarification of the Supercooling and Heat Storage Efficiency Calculation Formula for Shape-Stabilized Phase Change Materials, ACS Omega. 7 (2022) 41096–41099. https://doi.org/10.1021/acsomega.2c04594.

[261] O.A. Babar, V.K. Arora, P.K. Nema, Experimental analysis for thermo-physical properties of phase change materials during accelerated thermal cycling, Aust. J. Mech. Eng. 20 (2020) 1–13. https://doi.org/10.1080/14484846.2020.1794503.

[262] G. Raam Dheep, A. Sreekumar, Influence of accelerated thermal charging and discharging cycles on thermo-physical properties of organic phase change materials for solar thermal energy storage applications, Energy Convers. Manag. 105 (2015) 13–19. https://doi.org/10.1016/j.enconman.2015.07.040.

[263] A. Sharma, A. Shukla, Thermal cycle test of binary mixtures of some fatty acids as phase change materials for building applications, Energy Build. 99 (2015) 196–203. https://doi.org/10.1016/j.enbuild.2015.04.028.

[264] A. Sarı, A. Bicer, A. Al-Ahmed, F.A. Al-Sulaiman, M.H. Zahir, S.A. Mohamed, Silica fume/capric acid-palmitic acid composite phase change material doped with CNTs for thermal energy storage, Sol. Energy Mater. Sol. Cells. 179 (2018) 353–361. https://doi.org/10.1016/j.solmat.2017.12.036.

[265] Y. Ansari, T. Ansari, M. Junaid, K. Iqbal, A. Khan, Thermal Energy Storage and use of Thermal Insulation Composite light weight block as a phase change material in RCC Building Thermal Energy Storage and use of Thermal Insulation Composite light weight block as a phase change material in RCC Building, (2021).

[266] T.A. Mukram, J. Daniel, A review of novel methods and current developments of phase change materials in the building walls for cooling applications, Sustain. Energy Technol. Assessments. 49 (2022) 101709. https://doi.org/10.1016/j.seta.2021.101709.

[267] British Standards Institute, BS EN 12390-7:2000 Testing hardened concrete — Part 7: Density of hardened concrete, BSI Stand. Publ. 3 (2000) 13.

[268] BS 1881-122, Testing concrete method for determination of water absorption, London, Br. Stand. (1983) 3.

[269] H.T. Nhabih, K.K. Arat, A.S. Haidi, Methods of Processing Efflorescence of Clay Brick, Int. J. Sci. Eng. Sci. 3 (2020) 48–56. http://ijses.com/.

[270] British Standards Institution, A. BAUER, R. SHINE, M. PREEST, A. PATERSON, ISO, N. Warning, C. Copyright, ASTM E119, American Society for Testing & Mater, BSi, Standard test methods for felt, ASTM Int. West Conshohocken, PA. 2005 (2005) 1–36. https://doi.org/10.1520/C0140-11A.

[271] A. Sedaghat, H. Salem, W.K. Hussam, A. Mahdizadeh, M.I. Al-Khiami, M.A. Malayer, S.M. Soleimani, M. Sabati, R. Narayanan, M. Rasul, M.M.K. Khan, Exploring energy-efficient building solutions in hot regions: A study on bio-phase change materials and cool roof coatings, J. Build. Eng. 76 (2023) 107258. https://doi.org/10.1016/j.jobe.2023.107258.

[272] J. Xie, W. Wang, P. Sang, J. Liu, Experimental and numerical study of thermal performance of the PCM wall with solar radiation, Constr. Build. Mater. 177 (2018) 443–456. https://doi.org/10.1016/j.conbuildmat.2018.05.123.

[273] Q. Wang, R. Wu, Y. Wu, C.Y. Zhao, Parametric analysis of using PCM walls for heating loads reduction, Energy Build. 172 (2018) 328–336. https://doi.org/10.1016/j.enbuild.2018.05.012.

[274] X. Sun, M.A. Medina, Y. Zhang, Potential thermal enhancement of lightweight building walls derived from using Phase Change Materials (PCMs), Front. Energy Res. 7 (2019) 1–10. https://doi.org/10.3389/fenrg.2019.00013.

[275] P. Saikia, A.S. Azad, D. Rakshit, Thermodynamic analysis of directionally influenced phase change material embedded building walls, Int. J. Therm. Sci. 126 (2018) 105–117. https://doi.org/10.1016/j.ijthermalsci.2017.12.029.

[276] Q. Al-Yasiri, M. Szabó, Phase change material coupled building envelope for thermal comfort and energy-saving: Effect of natural night ventilation under hot climate, J. Clean. Prod. 365 (2022). https://doi.org/10.1016/j.jclepro.2022.132839.

[277] Z.A. Al-Absi, M.I.M. Hafizal, M. Ismail, Innovative PCM-incorporated foamed concrete panels for walls' exterior cladding: An experimental assessment in real-weather conditions, Energy Build. 288 (2023) 113003. https://doi.org/10.1016/j.enbuild.2023.113003.

[278] W. He, C. Yu, J. Yang, B. Yu, Z. Hu, D. Shen, X. Liu, M. Qin, H. Chen, Experimental study on the performance of a novel RC-PCM-wall, Energy Build. 199 (2019) 297–310. https://doi.org/10.1016/j.enbuild.2019.07.001.

[279] S. Mirrahimi, M.F. Mohamed, L.C. Haw, N.L.N. Ibrahim, W.F.M. Yusoff, A. Aflaki, The effect of building envelope on the thermal comfort and energy saving for high-rise buildings in hot-humid climate, Renew. Sustain. Energy Rev. 53 (2016) 1508–1519. https://doi.org/10.1016/j.rser.2015.09.055.

[280] U.N. Nor Ali, N. Mohamad Nor, N.A. Misnon, S.A. Mohd Noor, M. Othman, M.A.A. Alias, A. Syamsir, Integration of PCM as an external wall layer in reducing excessive heat of building walls, Funct. Compos. Struct. 4 (2022). https://doi.org/10.1088/2631-6331/ac826b.

[281] T.A. Mukram, J. Daniel, Performance evaluation of a novel cement brick filled with micro-PCM used as a thermal energy storage system in building walls, J. Energy Storage. 77 (2024) 109910. https://doi.org/10.1016/j.est.2023.109910.

[282] N.S. Bondareva, M.A. Sheremet, Influence of phase change material melting point and its location on heat and mass transfer in a brick, J. Energy Storage. 42 (2021) 103122. https://doi.org/10.1016/j.est.2021.103122.

[283] T. Concrete, M. Units, R. Units, M. Units, M. Units, Standardl Specification for Loadbearing Concrete Masonry Units 1 cO C90-14, (2015) 1–4. https://doi.org/10.1520/C0090-16A.2.

[284] I. 1077:1992, Building Common Burnt Clay Building Bricks- Specificatins, Bur. Indian Stand. (1992).

[285] Z.A. Al-Absi, M.I.M. Hafizal, M. Ismail, Experimental study on the thermal performance of PCM-based panels developed for exterior finishes of building walls, J. Build. Eng. 52 (2022) 104379. https://doi.org/10.1016/j.jobe.2022.104379.

[286] E. Meng, H. Yu, B. Zhou, Study of the thermal behavior of the composite phase change material (PCM) room in summer and winter, Appl. Therm. Eng. 126 (2017) 212–225. https://doi.org/10.1016/j.applthermaleng.2017.07.110.

[287] Z. Fan, Y. Zhao, Y. Shi, X. Liu, D. Jiang, Thermal performance evaluation of a novel building wall for lightweight building containing phase change materials and interlayer ventilation: An experimental study, Energy Build. 278 (2023) 112677. https://doi.org/10.1016/j.enbuild.2022.112677.

[288] M. Salihi, M. El Fiti, Y. Harmen, Y. Chhiti, A. Chebak, F.E. M'Hamdi Alaoui, M. Achak, F. Bentiss, C. Jama, Evaluation of global energy performance of building walls integrating PCM: Numerical study in semi-arid climate in Morocco, Case Stud. Constr. Mater. 16 (2022). https://doi.org/10.1016/j.cscm.2022.e00979.

[289] India - Summary | Climate Change Knowledge Portal, World Bank Gr. (n.d.). https://climateknowledgeportal.worldbank.org/country/india (accessed June 13, 2025).

[290] W. Li, M. Jing, R. Li, J. Gao, J. Zhu, R. Li, Study of the optimal placement of phase change materials in existing buildings for cooling load reduction - Take the Central Plain of China as an example, Renew. Energy. 209 (2023) 71–84. https://doi.org/10.1016/j.renene.2023.03.106.

[291] M. Salihi, Y. Chhiti, M. El, Y. Harmen, A. Chebak, Energy & Buildings Enhancement of buildings energy efficiency using passive PCM coupled with natural ventilation in the Moroccan climate zones Air Changes per Hour, Energy Build. 315 (2024) 114322. https://doi.org/10.1016/j.enbuild.2024.114322.

[292] Y. M'hamdi, K. Baba, M. Tajayouti, A. Nounah, Energy, environmental, and economic analysis of different buildings envelope integrated with phase change materials in different climates, Sol. Energy. 243 (2022) 91–102. https://doi.org/10.1016/j.solener.2022.07.031.

[293] A. Al-Janabi, M. Kavgic, Application and sensitivity analysis of the phase change material hysteresis method in EnergyPlus: A case study, Appl. Therm. Eng. 162 (2019) 114222. https://doi.org/10.1016/j.applthermaleng.2019.114222.

[294] A.G. Anter, A.A. Sultan, A.A. Hegazi, M.A. El Bouz, Thermal performance and energy saving using phase change materials (PCM) integrated in building walls, J. Energy Storage. 67 (2023). https://doi.org/10.1016/j.est.2023.107568.

[295] E. Tunçbilek, M. Arıcı, M. Krajčík, D. Li, S. Nižetić, A.M. Papadopoulos, Enhancing building wall thermal performance with phase change material and insulation: A comparative and synergistic assessment, Renew. Energy. 218 (2023). https://doi.org/10.1016/j.renene.2023.119270.

[296] X. Sun, Q. Zhang, M.A. Medina, K.O. Lee, Energy and economic analysis of a building enclosure outfitted with a phase change material board (PCMB), Energy Convers. Manag. 83 (2014) 73–78. https://doi.org/10.1016/j.enconman.2014.03.035.

[297] V. Sharma, A.C. Rai, Performance assessment of residential building envelopes enhanced with phase change materials, Energy Build. 208 (2020) 109664. https://doi.org/10.1016/j.enbuild.2019.109664.

[298] K. Struhala, M. Ostrý, Life-Cycle Assessment of phase-change materials in buildings : A review, J. Clean. Prod. 336 (2022) 130359. https://doi.org/10.1016/j.jclepro.2022.130359.

[299] R. Zelm, T. Hennequin, M.A.J. Huijbregts, Performing life cycle impact assessment with the midpoint and endpoint method ReCiPe, Nat. Protoc. 20 (2025). https://doi.org/10.1038/s41596-025-01207-y.

[300] Understanding Global Warming Potentials, United States Environ. Prot. Agency. (2025). https://www.epa.gov/ghgemissions/understanding-global-warming-potentials.

[301] Understanding the Climate Change Indicators GWP-total, -fossil, -biogenic and -luluc, ORIS Mater. Intell. (2025). https://knowledge.oris-connect.com/en/understanding-the-climate-change-indicators-gwp.

Appendix I

Design of thermal cycling chamber

The heating and cooling load requirement of the thermal cycling chamber is calculated as per the following section.

1) Total volume of the chamber = 0.18 m^3 (as per the pre-decided dimension of chamber as tabulated in Table 3.1)
2) Since, the thermal conductivity of polyethylene twin wall sheet and glasswool thermal conductivity is 0.4 W/mK and 0.04 W/mK, respectively. The overall thermal resistance provided by the surface of the wall will be 0.775 m^2K/W (considering the thickness as tabulated in Table 3.1). Thermal resistance provided by polyethylene sheet and glasswool will be 0.025 m^2K/W and 0.75 m^2K/W respectively.
3) Since the chamber lower surface is made up of plywood, the heat loss is assumed to happen through the other 5 surfaces including the door.
4) Total surface area = 1.68 m^2
5) The design temperature of the chamber is 15-50^{o}C.
6) The conductive heat transfer loss will be 45.16 W/m^2.
7) Assuming, the density and specific heat of air to be 1.2kg/m^3 and 1.005 kJ/kgK at atmospheric pressure, to heat the air of the chamber from 15 to 50^{o}C, the heating load requirement will be 7.59 kJ.
8) Considering 20% loss of the system, the heat load requirement will be 9.11 kJ.
9) As rapid heating is needed for performing thermal cycling test, it is assumed to meet the temperature requirement in 5 minutes.
10) Power requirement to meet the heat load in 5 minutes will be 30.37 W. Considering the heat losses, the actual power requirement will be 75.86 W.
11) Therefore, it is required to provide 106.23 W of power to heat the system. Thus, a 150 W incandescent bulb will be installed in the system considering the heat gain from the bulb is 90% of the rated power.
12) After heating, the cooling of the chamber needs to perform in the same temperature range and again the time is assumed to be 5 minutes. Therefore, the cooling load requirement will be 106.23 W. Since, Peltier cooling system is less costly than refrigeration unit, so it is proposed to use Peltier cooling element of 12 V.

13) Considering maximum current provided as 8 A, one Peltier cooling element rated power will be 96W. Assuming, the temperature difference of 30°C between the hot and cold side, the COP of the element will be 0.5.Therefore, practically one element cooling capacity will be approximately 48 W. Considering the other system losses as 15%, one Peltier element can give approximately 40W. Therefore, to meet the cooling requirement, 3 Peltier cooling module will be sufficient. But, as a factor of safety 4 cooling module will be installed.
14) As the chamber volume is 0.18 m^3, to distribute the cooling load, 8 Peltier cooling modules are installed at different positions at shown in Figure 3.2, so that at one time 4 module can be operated as per the requirement. Alternatively, the four modules are operated.

List of publications

Journal publications

1) **Bordoloi, U.**, Kalita, P., Experimental and numerical study of brick walls integrated with bio-composite phase change material for energy-efficient thermal management in buildings, Applied Thermal Engineering, 300, 131427, 2026, doi: https://doi.org/10.1016/j.applthermaleng.2026.131427.
2) **Bordoloi, U.**, Das, B., Kalita, P., Experimental investigation on biocomposite phase change material-filled bricks for passive temperature regulation in buildings in a hot and humid climate, Journal of Energy Storage, 139, 118761, 2025, doi: https://doi.org/10.1016/j.est.2025.118761.
3) **Bordoloi, U.**, Kalita, P., Experimental investigation of thermal cycling stability of biochar-based phase change materials for building applications, International Journal of Green Energy, 137-147, 2024, doi: https://doi.org/10.1080/15435075.2024.2394480.
4) **Bordoloi, U.**, Das, D., Kashyap, D., Patwa, D., Bora, P., Muigai, H., Kalita, P., Synthesis and comparative analysis of biochar based form-stable phase change materials for thermal management of buildings, Journal of Energy Storage, 55,105801, 2022, doi: https://doi.org/10.1016/j.est.2022.105801.

Conference publications

1) **Bordoloi, U.,** Kalita, P., Experimental Investigation on the Stability of Biocomposite Phase Change Materials for Building Applications. In: 15th International Green Energy Conference, Glasgow, UK, Springer Nature Switzerland, 137-147,2023.
2) **Bordoloi, U.,** Das,B., Kalita, P., Enhancing thermal comfort in buildings through the integration of phase change material on the building envelope: a simulation study. In: International Conference on Sustainable Energy and Green Technology, Vietnam, IOP Conference Series: Earth and Environmental Science (EES),2023.
3) **Bordoloi, U.,** Das,B., Kalita, P., Thermal performance investigation of biocomposite phase change material incorporated autoclaved aerated concrete bricks in a simulated environment. In: 2nd International Conference on Innovations in Clean Energy Technologies, Springer conference proceeding, Bhopal, 2023.

Patent filed

1) Development of novel biocomposite form-stable phase change material from locally available biomass for thermal energy storage applications (Reference no. 202331021892), status: published (4/10/2024)

Other Publications

1) Das,B., **Bordoloi,U.**, Singh, P., Kalita, P., Integration of bio-composite phase change materials in autoclaved aerated concrete bricks for enhanced thermal energy storage performance, Journal of Energy Storage, 148, 2026, https://doi.org/10.1016/j.est.2025.120324.
2) Patwa, D., **Bordoloi, U.,** Dubey, AA., Ravi, K., Sekharan, S., Kalita, P., Energy-efficient biochar production for thermal backfill applications, Science of The Total Environment, 833, 155253,2022, doi: https://doi.org/10.1016/j.scitotenv.2022.155253.
3) Das, B., **Bordoloi. U.**, Kalita, P., Thermal Analysis of Calcium Silicate Brick Wall with Bio-Composite PCM Numerically in ANSYS Software, Current Progress in Interdisciplinary Research, Springer Nature, 127-135, 2026. (Conference paper)
4) Banik, R.K., Das,S., **Bordoloi,U**., Das,H.J., Das,B., Basumatary,S., Das,B., Kalita,P., The Promising Role of Thermochemical Conversion in Sustainable Power Generation, Challenges and Opportunities of Distributed Renewable Power, Springer Nature Singapore, 101-140, 2024. (Book chapter)
5) Kamble,A.D., Das,S., Vijaya, Das,B., **Bordoloi,U**., Hazarika,P., Kalita,P., Role of Solar Energy in the Development of the Indian Economy, Challenges and Opportunities of Distributed Renewable Power, Springer Nature Singapore, 489-535, 2024. (Book chapter)
6) Kalita, P., Kashyap, D., **Bordoloi, U.**, Thermal Energy Storage Systems for Cooling and Heating Applications, Energy Storage, 149-199, 2021. (Book chapter)
7) Kalita, P., Das D., Das S., Banik RK., **Bordoloi U**., Heat Transfer Analysis in Solar Thermal Collectors, Advances in Sustainable Energy, 251-277,2021. (Book chapter)